A NONLINEAR AND INELASTIC CONSTITUTIVE EQUATION FOR HUMAN CEREBRAL ARTERIAL AND ANEURYSM WALLS

by

Rachmadian Wulandana

B.Sc., Bandung Institute of Technology,Indonesia,1992

M.Sc., University of Pittsburgh, 1996

Submitted to the Graduate Faculty of

the School of Engineering in partial fulfillment

of the requirements for the degree of

Doctor of Philosophy

University of Pittsburgh

2003

UNIVERSITY OF PITTSBURGH

SCHOOL OF ENGINEERING

This dissertation was presented

by

Rachmadian Wulandana

It was defended on

June 18, 2003

and approved by

A.M. Robertson, Assoc. Professor,Mechanical Engineering Dept.

G.P. Galdi, Professor, Mechanical Engineering Dept.

M.S. Sacks, Assoc. Professor, Bioengineering Dept.

W.S. Slaughter, Assoc. Professor, Mechanical Engineering Dept.

D.A. Vorp, Assoc. Professor, Surgery and Bioengineering Dept.

H. Yonas, Professor, Dept. of Neurological Surgery

Dissertation Advisor: A.M. Robertson, Assoc. Professor,Mechanical Engineering Dept.

A NONLINEAR AND INELASTIC CONSTITUTIVE EQUATION FOR HUMAN CEREBRAL ARTERIAL AND ANEURYSM WALLS

Rachmadian Wulandana, Ph.D.

University of Pittsburgh, 2003

The underlying motivation of this work is the desire to understand better the formation and development of cerebral saccular aneurysm, lesions frequently found at the apex of bifurcations in and near the Circle of Willis. Degradation of elastin, which is one important passive mechanical component of arterial walls, has been hypothesized to play a role in aneurysm formation. This hypothesis has been motivated by the aneurysm wall histology that always displays fragmented elastin.

Currently there is no single appropriate constitutive equation for both cerebral arterial and aneurysm walls. Available constitutive equations are directed at modeling the nonlinear behavior of cerebral arterial tissue that is hypothesized to arise from recruitment of collagen (another important passive biomechanical component of arterial wall) but not the inelastic behavior that is hypothesized to be due to elastin fragmentation.

In this work, we propose a constitutive equation that is capable of handling both the nonlinearity and inelasticity. This constitutive equation, unlike the classical single mechanism elastic constitutive relation, employs two mechanisms. The first and second mechanisms represent the mechanical response of elastin and collagen, respectively. The collagen recruitment is modelled by introducing the second mechanism at a specified deformed state, while the elastin breakage is modelled by deactivating the first mechanism at a later deformed state.

Moreover, we discuss applications of the new constitutive equation in some relevant problems. For example, we discuss the inflation of a cylindrical membrane and compare

analytical results to existing experimental data that demonstrates both the nonlinear and inelastic behavior of cerebral arterial walls and use the data to obtain material constants for the new constitutive equation.

The presentation of this work is intended to introduce a new approach that can be used to incorporate various biological mechanisms that have been hypothesized to be involved in aneurysm formation and development. Indeed the current work involves only two important mechanisms, but theoretically the current model can be generalized easily to include more mechanisms if necessary to represent gradual recruitment and breakage.

TABLE OF CONTENTS

LIST OF TABLES

LIST OF FIGURES

PREFACE

"*Praise be to Allah, The Cherisher and Sustainer of the worlds.*" [1]. I found a great pleasure for being engaged in this work. This work certainly has increased my understanding in the nonlinear mechanics particularly in its application for solving problems in living tissues. More importantly, this work has given me a chance to study many amazing natural phenomenon in the mechanics of living tissues. Also as a muslim what I have learned has always reminded me of the mercy of Allah, the Creator of this universe.

This work has been made possible partly by the support of many persons. Some of them I would like to acknowledge here.

First, I'd like to express my deep gratitude to my academic advisor, Dr. Robertson. She has been patiently giving me guidance in my graduate academic studies and in my preparation to enter professional life. My thanks to her are endless.

Special thanks to Dr. Galdi and Dr. Slaughter, whose courses on nonlinear mechanics and elasticity are truly essential in the conceptual development of the constitutive model. Their advice are also greatly appreciated. I also thank Dr. Slaughter for his help in preparing this dissertation.

Many thanks to Dr. Sacks whose course on tissue mechanics definitely has helped me in understanding biological aspects of cerebral aneurysmal and arterial walls.

A part of this project is to construct an experimental protocol potentially needed for future experimental works. I gratefully thank Dr. Vorp for allowing me to use his laboratory, equipments and supplies for the preliminary experimental works. I thank his group members, especially 'brother' Mohammad el Kurdi, who many times helped me and shared their expertise with me. Furthermore, I have learned many important both professional and technical aspects in biomedical research from the Vascular group meetings.

I thank Dr. David Peters from the Department of Human Genetics who supplied frozen samples from cadavers and allowed me to use his lab and also thank to Dr. Howard Yonas who provided appropriate tools for handling the tissue samples. That was a real experience.

I would like to express my thanks to many of my colleagues who provided supports, inspiration, ideas and most importantly, kindness. They, in alphabetical order, are: Mr. Khaled Bataineh, Mr. Fernando Carapau, Mr. Bong Jae Chung, Ms. Peggy Meinhardt, Mr. Clint Morrow, Mr. Dharma Nursani, Mr. Ashuwin Vaidya, Mr. David Volcheck, and Mr. Hasballah Zakariya. For me, it is a special blessing to be accompanied by these people.

I certainly have to thank Mr. Federico Gracia who worked very hard in preparing the pittetd class file that produces this 'beautiful' manuscript.

Nevertheless, this work probably would have taken a harder journey without continuous moral supports from my beloved wife, Yuni and my children, Athif and Afina. I thank for their love, kindness, patient, and help. May Allah reward them with paradise.

I also want to thank my families in Indonesia. They are my parents in law Mr. H. Wassil and his family and my sister Dita and her family. Remotely, they have supplied supports and prayers. I thank their prayers that might have protected me from difficulties in this life.

I also pray to Allah that He would credit my worldly accomplishment to both of my parents in their after life. May Allah reunite me and them in His garden in the days after.

Ultimately, I must sincerely acknowledge that none of this work is made possible without the permission from Allah the Almighty. Only due to His mercy that I can finish this work. The degree that I obtained is nothing but a trust from Him that I must carry and utilize for the benefit of the human kind.

I dedicate this manuscript to my wife and my children and the rest of the family !!

This work was supported in part by grants from the Whitaker Foundation and the National Science Foundation to Prof. Anne Robertson.

1.0 INTRODUCTION

1.1 MOTIVATION

This work is motivated by the mechanics of the initiation, development and rupture of human intracranial aneurysms or saccular aneurysms. In this work we refer to saccular aneurysm as a saccular or roughly spherical dilatation of cerebral arterial wall that measures two mm or more in diameter and shows a clear neck region that differentiates it from fusiform aneurysms that dilate rather laterally leading to an appearance of an inflated cylinder. This work will focus more on saccular aneurysms rather than cerebral fusiform aneurysms. Saccular aneurysms are found at the bifurcation or curved segments of arteries in or near the Circle of Willis [2, 3, 4, 5]. Figure 1 shows how saccular aneurysms that grow at a bifurcation and a curved segment of cerebral arteries differ from cerebral fusiform aneurysms.

Between 70 to 90 % of aneurysms, are less than 10 mm in diameter [6, 7, 8, 9, 10, 5]. Giant aneurysms, of size greater than 25 mm, comprise about five % of all intracranial aneurysms [7, 11, 9]. A larger percentage (15 to 24 %) however is reported in more recent studies [4, 12]. A saccular aneurysm may be stable in size or grow at an unpredictable rate [13]. When aneurysms grow, the growth rate can exceed almost two mm/year [14]. It is hypothesized that the growth rate of aneurysms combined with the arterial geometry near the growing point determine the critical size of rupture [5, 14]. Rupture of aneurysms is the ultimate danger of this disease. It is hypothesized that aneurysms at the bifurcations are more likely to rupture compared to those that grow at the curved and branching points [5]. It is also suspected that aneurysms in patients with deficiency of type III collagen, a structural protein that is hypothesized to be responsible for the mechanical integrity of arterial walls, are more prone to rupture [15]. When aneurysms rupture, the blood typically floods into the

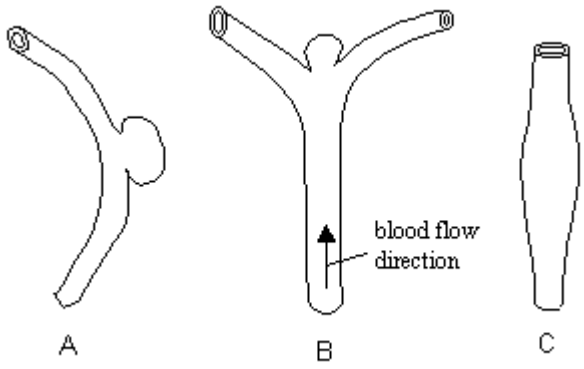

Figure 1: Typical appearances of (A) A saccular aneurysm at a curved section (B) A saccular aneurysm at a bifurcating artery and (C) A fusiform aneurysm.

subarachnoid space and causes a subarachnoid hemorrhage (SAH). Occasionally, the blood floods the brain parenchyma and causes an intracerebral hemorrhage (ICH).

Saccular aneurysms are common among the U.S. population. The incidence of saccular aneurysms have been investigated through both angiography and autopsy studies. However, many angiography studies have been performed on groups of patients who suffer diseases suspected to have association with the etiology of saccular aneurysms and therefore are not representative of the general population. The examples of such diseases include autosomal dominant polycystic kidney disease [16, 17, 18], spontaneous cervical artery dissection (SCAD) [19] , pituitary adenoma [20, 21], angina pectoris [22], carotid stenosis [23], and ischaemic cerebrovascular [24]. Other angiography studies have also been biased by data of relatives of patients who have experienced SAH [25, 26] or have experienced ICH [27] . One angiography study for the general population in the U.S. revealed an incidence of anterior circulation aneurysms of 1 % [28]. Autopsy studies report the incidence of saccular aneurysms in the range of 0.8 to 8.1 % among the population of the United States [29, 7, 30, 31, 32, 10]. Of these studies, the highest reported incidence of ruptured aneurysms is 3 % [7]. The International Study of Unruptured Intracranial Aneurysms Investigators reports that the rate of rupture of aneurysms smaller than 10 mm for patients who never suffered a SAH is approximately 0.05 % per year [33].

Rupture of an aneurysm can be fatal or disabling. Studies of the North America population found that the incidence of aneurysmal SAH has been in a constant range of 10 to 12 per 100,000 person per year over the last four decades [34, 35, 36]. Over 50 % of patients die following SAH, including death due to rebleeding of previously ruptured aneurysms [37, 36, 38]. Eleven percent of those died before getting medical attention or reaching the hospital [39, 34, 37]. Approximately 36 to 40 % of patients survived with either minor or no neurologic deficit and could return to normal lives [39, 37, 40, 36]. The remaining 14 to 20 % of the patients became moderately or severely disabled [37, 36, 39].

Aneurysmal SAH has a significant financial impact on the U.S. It was estimated that 513.1 million dollars annually were spent during the period between 1979 to 1989 to cover the cost of hospital and surgery for patients with aneurysmal SAH. In the same period, the loss of income based on annual mortality was approximately 827.1 million dollars [41]. This significant loss of income may be due to the high incidence (38 %) of aneurysmal SAH in the population with productive ages between 45 to 64 years old [41].

1.2 HISTOLOGY OF CEREBRAL ARTERIAL WALLS AND ANEURYSMS

Saccular aneurysms are characterized by a typical wall morphology that more closely resembles a modified cerebral arterial wall rather than a newly developed entity [42]. The following brief description of the histology of the wall of healthy cerebral arterial segments, walls of the cerebral arterial bifurcations and walls of the cerebral saccular aneurysms underlines the structural changes. Figure 2 illustrates a typical normal/healthy cross sectional area of an artery and the layers that make up the wall. The structure of healthy cerebral arterial walls and those of extracranial arteries with similar diameter are somewhat different. It has been hypothesized that these differences predispose cerebral arteries to the formation of saccular aneurysms [43]. The internal elastic lamina (IEL), which lies between the tunica intima and tunica media, of cerebral arteries are more prominent than the IEL of extracranial arteries [44, 45, 46]. The external elastic lamina, which presents between the tunica media and tunica adventitia of extracranial arterial walls, is absent in cerebral arterial walls [47]. The thickness of the media and adventitia of cerebral arteries are typically less than those of

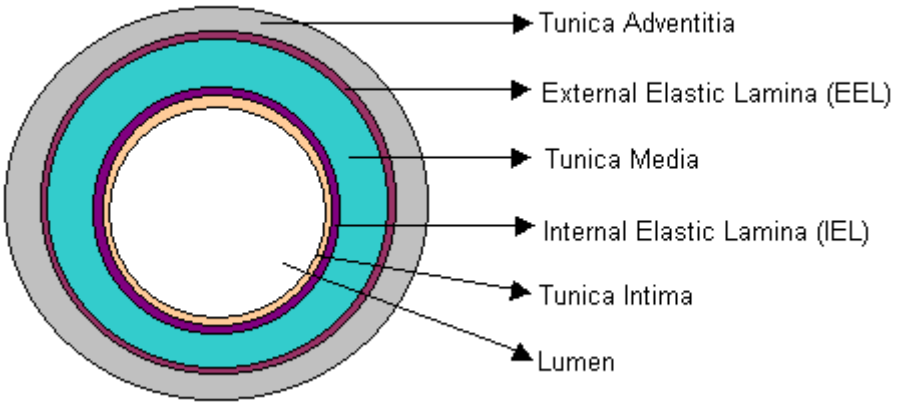

Figure 2: Typical cross section area of an artery. Cerebral arteries do not have external elastic lamina.

extracranial arteries with similar diameter [45, 48]. The cerebral arterial wall usually is thin and more transparent than walls of extracerebral arteries of similar caliber[48].

This work focuses on elastin and collagen, the two important passive components of arterial wall [49]. They are contained in different proportions in the layers in the arterial wall. Elastin in cerebral arterial walls is concentrated in the IEL and also can be found in small amounts in the media and adventitia [50]. The amount of elastin in the cerebral arterial media is less than that in extracranial arterial media [48]. The amount of reticular fibers, which are composed of type III collagen, are less in the cerebral arterial media of aneurysms patients compared to normal subjects [51]. Collagen fibers are mainly concentrated in the adventitia of cerebral arteries [48]. There is no difference in appearance and content of elastin fibers in the IEL of cerebral arteries of both aneurysms patients and normal subjects [51]. The intima of the cerebral arterial wall consists of an endothelial layer and a thin collagenous layer [44]. The morphology of cerebral arterial bifurcations is somewhat different from nonbifurcating arteries. Figure 3 depicts a typical cerebral arterial bifurcation with a saccular aneurysm. Arterial bifurcations display two morphological features: intimal pads and medial gaps or medial raphes, that distinguish them from nonbifurcating arteries. Intimal pad refers to a thickened region of the tunica intima [52, 53, 44, 47, 54, 55], while medial gap refers to a

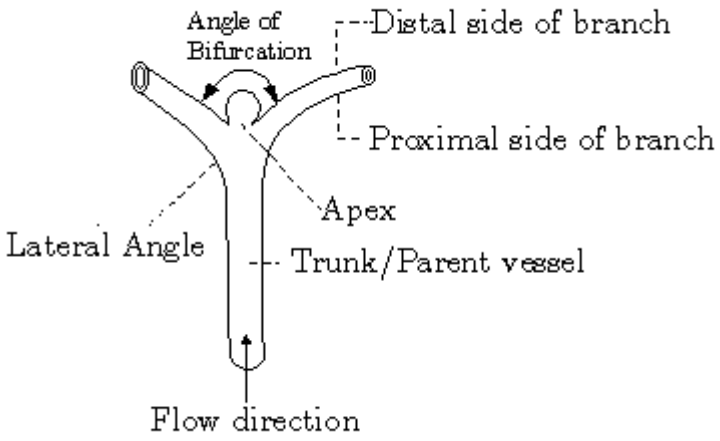

Figure 3: Typical arterial bifurcation region with a saccular aneurysm at the apex.

thinning or a disappearance of the media [55]. Researchers have hypothesized that either intimal pad or medial gap is a factor in aneurysm formation. All around the bifurcation area the intima thickens. However, the intimal pad at the apical region is thinner than in other regions [53, 44]. In infants, the intimal thickening consists of smooth muscle and elastic tissue and it appears stratified due to a layer of newly formed elastin beneath the endothelium lining and layer containing degenerated elastin [52]. The hypothesis that there is a relationship between the intimal pad and aneurysms formation is due to the frequent occurrence of aneurysms near to the intimal pad site [56, 42]. At the apical region, the medial gap, in the form of either media thinning or total disappearance, causes the adventitia and intima layers to coalesce [55, 57, 45, 54, 44, 48]. Within the gap, collagen fibers are observed to run from one arterial branch to another branch and the elastin ends abruptly [48]. Forbes, who observed the medial gap for the first time, regarded the gap as a local vascular weakening that plays an important role in aneurysms formation [55]. Stehbens expressed strong disagreement arguing that, for instance, the occurrence of the medial gap is more frequent than the occurrence of saccular aneurysms (other arguments can be found in Stehbens [58]). Figure 4 represent a schematic of layers that constitute the wall of a simple aneurysms. It is hypothesized that such a well developed simple aneurysm is a

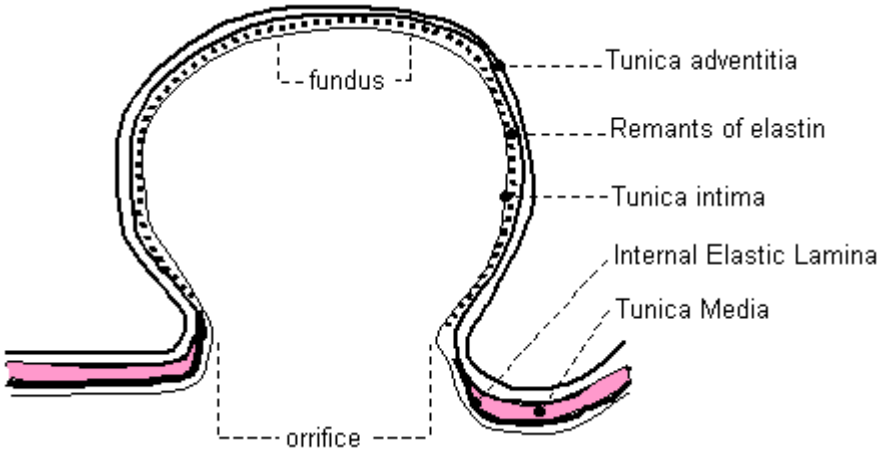

Figure 4: A sketch of a saccular aneurysm cross section.

product of progression from a small outpounching, sometimes referred as 'bleb' [59] or 'minute aneurysm' [60]. Figure 29 depicts the schema of the hypothesized progression. Furthermore, it is commonly believed that during their formation aneurysms draw in the adjacent arterial wall from both branches and parent arteries [60, 46]. The tissue of the saccular aneurysmal wall however is structurally different from both the cerebral arterial wall and the bifurcation region tissue from which it develops. The difference however can be viewed as a modification of the arterial wall and not necessarily as an emergence of a totally different/new tissue [61, 62]. The aneurysms may originate eccentrically to the apex of the bifurcation or in the axis of the parent vessel [46]. At the orifice of the sack, the media terminates or at most slightly extends into the aneurysm neck region while the elastic tissue, presumably of the IEL, may be fragmented [63] or slightly extended [45, 60, 64, 65]. Away from the orifice, the media layer is completely absent from aneurysmal wall. Remnants of elastic tissue can be found at the inner wall of aneurysms [53, 66, 67, 55, 47, 68]. The elastic fragments can be found also as early as in the 'bleb' but in lesser degree [60]. According to Suzuki [69], the aneurysm wall becomes collagenous when the aneurysms size is larger than four mm. Generally, type III collagen can be found in the arterial media and adventitia while type IV is found in the intima of arteries [70]. However, the aneurysm wall contains collagen type IV instead of type III [71].

The intima of parent arteries however doesn't end at the aneurysmal orifice. In fact, it also covers the inner aneurysmal wall [2]. The endothelial cells have been reported to be missing at the orifice [64] but Kataoka *et al.* reported that the walls of unruptured aneurysm are fully covered with these cells [71]. Suzuki [69] reported the appearance of endothelial cells on the wall of small (less than three mm in diameter) aneurysms. The adventitia is detected at the outer wall of aneurysms and appears stretched [2]. The composition of the aneurysmal wall may change during rupture. Kataoka *et al.* reported that the wall of ruptured aneurysms, unlike those of unruptured aneurysms, show evidence of a disrupted endothelial cells layer [71]. Rupture of aneurysms can occur either at the fundus, side or base of aneurysms. The greatest occurrence of the rupture, 64 to 84 %, is at the fundus [45, 72].

1.3 HYPOTHESIS REGARDING ANEURYSM FORMATION

The cause of the initiation, development and rupture of cerebral aneurysms is still unresolved. Several theories on the initiation and development have been proposed (some extensive reviews can be found in Connoly and Solomon [13] and Krex *et al.* [42]). Most or even all of the theories on the initiation of saccular aneurysms underline the vascular weakening of the arterial wall as a prelude to aneurysm formation. The degenerative theory, for example, suggests that the weakening of the wall, mostly manifested as elastin and media degradation, is due to hemodynamics forces [73]. Another theory is the congenital theory that is based on statistical findings of the coincidence of cerebral aneurysms and some inheritable connective disorders that may promote cerebral aneurysms (see the review in Schievink [74]). Examples of the associated diseases include Ehlers-Danlos Syndrome Type IV (EDS Type IV) and α_1-Antitrypsin Deficiency. In patients with EDS type IV, the arterial wall integrity may be altered due to deficiency of collagen type III. On the other hand, in patients with α_1-Antitrypsin Deficiency, the elastin is defective causing the loss of integrity of the arterial wall.

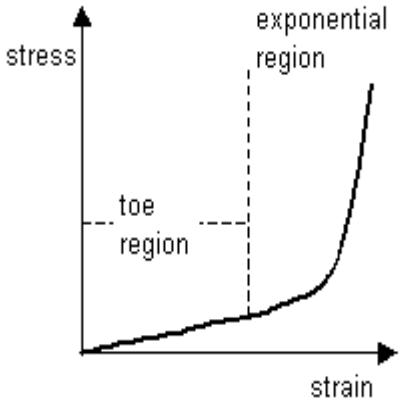

Figure 5: Representative nonlinear stress versus strain curve of cerebral and extracerebral arterial tissues.

1.4 THE NONLINEAR AND INELASTIC BEHAVIOR OF ARTERIAL WALLS

In order to test hypothesis on aneurysm etiology, mathematical modeling is often utilized instead of performing costly experiments to artificially produce in vivo aneurysms in animals (examples can be found by Hashimoto *et al.* [75] and Miskolczi *et al.* [76]). Mathematical modeling of the initiation, development and rupture of cerebral aneurysms requires a material description of the human cerebral arterial walls and saccular walls (A constitutive equation of blood and study of its flow in cerebral circulation are required if hemodynamics factors are considered). This work will focus on two important mechanical characteristics displayed by human arterial walls: the nonlinearity exhibited by both cerebral and extracerebral arterial walls and the inelasticity, exhibited by cerebral arterial walls. The meaning of the two features will be clear in the following paragraphs.

In the stress versus strain loading curves resulting from, for example, a uniaxial test, the nonlinearity of arterial walls is typically characterized by a toe region at low strain and an exponential region at high strain. A typical representative figure of the nonlinearity is depicted in Figure 5. Busby and Burton [49] hypothesized the nonlinearity is due to elastin and collagen fibers, the two important passive mechanical components of arterial wall. It is

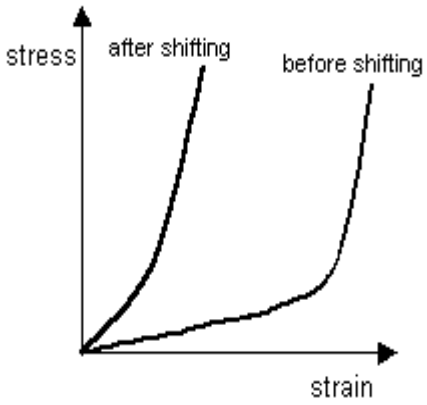

Figure 6: Representative stress versus strain curves before and after the shifting.

hypothesized that the initial toe region of the stress versus strain curves must be due to elastin load bearing, while the exponential region is produced by collagen fibers that are recruited gradually as the deformation progresses [49]. A similar hypothesis was also presented by Roach and Burton [77]. The collagen fibers however contribute more load bearing at large strain than the elastin does [77]. It was also observed that arterial tissues with artificially depleted elastin (presumably leaving the collagen fibers in the load bearing system) are much stiffer than tissue with depleted collagen fibers [77]. The phenomenon of collagen recruitment was shown by Samila *et al.* who morphologically observed the gradual unfolding of crimped collagen fibers in human carotid artery strips that were stretched uniaxially [78].

In addition to the nonlinear behavior, it was also observed that cerebral arterial walls exhibit inelastic behavior under sufficiently high loads. The most relevant mechanical testing in which the inelastic behavior was revealed is that by Scott *et al.* [79] who investigated the properties of cerebral arterial walls by means of inflation of cylindrical arterial segments. In the experiments by Scott *et al.* [79] the typical repeatable nonlinear stress versus strain curves immediately were recovered during repeated loading and unloading test indicating the nonlinear yet elastic behavior. The inelastic behavior emerged as an abrupt change of the stress versus strain curves after the cyclic loading went up to above a critical load level. It was reported that the curves after the shifting lost the toe region and became steeper. Moreover, it was clear that after unloading the original diameters of the segments

were not recovered. Instead the segments possessed larger diameters. The newly shaped curves however remain repeatable indicating that the material was in a new elastic regime. Figure 6 depicts representative stress versus strain curves before and after the shifting. The curves after the shifting are produced using the newly unloaded configuration as the reference configuration. A more detailed description on the experiments by Scott *et al.* and the observed inelastic behavior will be provided in Section 3.3. Scott *et al.* hypothesized that rupture of the elastin, probably caused by an excessive mechanical loading, was the source of the inelastic phenomenon. A morphology study to investigate the remnants of the damaged elastin in the tissues after the irreversible change however were not performed in this study [79]. A related hypothesis is that stated that elastin fragmentation may play a role in aneurysm formation since elastin is commonly fragmented or absent in the wall of aneurysms. It was known that elastin degradation can occur as a result of chemical treatment as was done by Roach and Burton [77] on segments of human iliac arteries. Significantly they found that the unloaded diameters of segments with depleted elastin are enlarged as well.

Significantly, Holzapfel *et al.* [80] observed similar inelastic phenomena in the media of extracranial arteries. In their experiments, they found repeated uniaxial loading and unloading on a circumferential strip of arterial tunica media exhibited a jump or shift of the stress versus strain curves similar to that reported by Roach *et al.* [79]. The shift occurred after over stretching the strip beyond a critical strain level (unlike Scott *et al.* who considered the shifting after a critical pressure level). After the shift, the strip also exhibited permanent strain. The inelastic (and nonlinear) behavior of the media of extracerebral arteries certainly can be modeled using the new constitutive equation that will be proposed in this work.

1.5 CLASSICAL VERSUS MULTI-MECHANISM CONSTITUTIVE EQUATIONS

The nonlinear and inelastic characteristics described above must be mathematically formulated in the material description of the arterial and aneurysms walls. Early attempts to describe the nonlinearity include some sort of linearization of the stress versus strain rela-

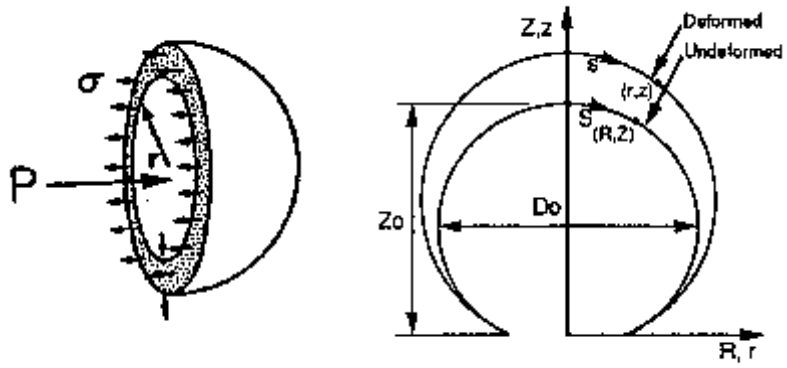

Figure 7: Frequently used models of undeformed shapes of well developed aneurysms: sphere (from Canham and Ferguson [91]) and truncated sphere (from Kyriacou and Humphrey [92]).

tions that produce stiffness parameters; such as elastance [77], incremental elastic modulus [81, 82, 83, 84], vascular compliance [85], and wall stiffness (β) [81, 82, 86]. Stiffness parameters are often chosen for convenience and they provide quantitative information about material elasticity for limited clinical applications [82, 85]. The nonlinearity of the arterial wall however cannot be adequately described using such parameters. Instead, nonlinear constitutive equations derived from strain energy functions: including exponential type [87, 88], polynomial type [89] or logarithmic type [90] are used. These classical elastic equations can successfully model the material nonlinearity, however they cannot be used to describe structural phenomena exhibited by material components that occur during the deformation of arterial walls, *i.e* collagen recruitment and elastin breakage, since they assume that the components do not experience microstructural changes, which sometimes is irreversible, during deformation.

The need for an appropriate constitutive equation that can handle both the nonlinearity and inelasticity of cerebral arterial walls is now clear. Clearly, the early development or initiation of cerebral aneurysms from a section of healthy arterial segment that involves collagen recruitment and elastin breakage cannot be modelled using classical hyperelastic constitutive equations. Investigators can mathematically model only the deformation of saccular aneurysms and not the development of saccular aneurysms from segments of arterial

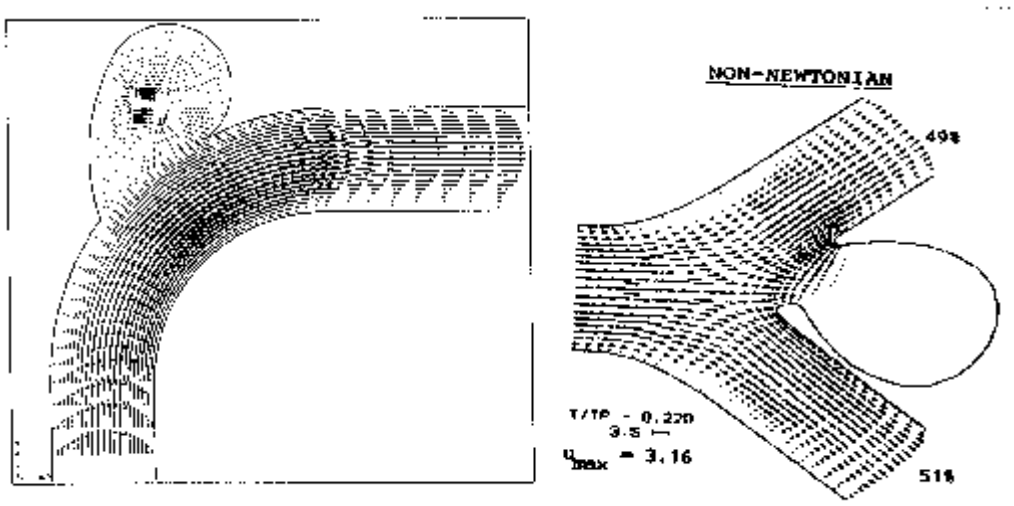

Figure 8: Typical assumed shapes of saccular aneurysms used in hemodynamic studies of blood flow inside aneurysms at curved segments (from Foutrakis *et al.* [59]) and bifurcations (from Perktold *et al.* [96]).

walls with these equations. In studies using classical hyperelastic equations, the unloaded reference configuration of the aneurysm was modelled either as a sphere [79, 91, 93, 94] or a truncated sphere [95, 92]. Figure 7 shows two commonly selected undeformed shapes of saccular aneurysm (from Canham and Ferguson [91] and Kyriacou and Humphrey [92]). It's clear that in these studies, the aneurysm tissue is treated as a different entity than the arterial tissue from which it developed. Also here, the material properties of the aneurysms are uncoupled from those of the arterial wall from which it developed.

The lack of appropriate constitutive equations for aneurysms walls also produces limitations on relevant hemodynamic studies. Since the shape of the sacs supposedly produced by hemodynamic forces cannot be computed, the shape has to be assumed. The studies therefore are limited to studying flow inside sacs of assumed shape on either curved cerebral arteries [97, 98], apices of arterial bifurcation [96, 59] or straight segments [99, 98, 100]. Figure 8, from Foutrakis *et al.* [59] and Perktold *et al.* [96], displays examples of assumed shapes of saccular aneurysms used in hemodynamic studies. Most studies assume that the wall of arteries and sacs, are fixed. Low *et al.* [98] however assume a flexible walled aneurysm

model whose displacement is linearly proportional to the transmural pressure where the external pressure is constant. Even the flexible wall studies are limited to small deformations about a presumed aneurysm shape. They are not appropriate for studying the large inelastic deformation involved in aneurysm formation and growth.

Modeling the development of a section of normal cerebral arterial wall into a simple saccular aneurysm requires a constitutive relation that can handle more than one mechanism of material components during deformation history. The proposed constitutive relation will include the participation of collagen and elastin as two separate mechanisms. Note that in the sense of Humphrey [101], the current approach may not be considered phenomenological due to the consideration of the individual constituents. However, the current approach clearly is not microstructural either since the detailed architecture of the cerebral arterial wall constituents is not used as the basis of the proposed equation.

In the current formulation, the usage of the structural information of elastin and collagen fibers is solely as a motivation to separate the mechanics of aneurysm formation into two mechanisms. The mathematical formulation of the two mechanisms therefore can be considered phenomenological. These mechanisms therefore are used to represent the gross mechanical response of elastin and collagen fibers and are not to be used to individually quantify the material characteristics of these structural components. The current approach is used so that the material identification of elastin and collagen fibers, which can become a challenging task considering the fine size of cerebral arterial walls, can be avoided.

The incorporation of the first and second mechanisms in the equation can be described as follows. At the early stage of deformation, only elastin is load bearing and its participation is regarded as the first mechanism. The material response at this deformation level is similar to the response of a single mechanism material. At some threshold deformation level, we suppose that collagen fibers are recruited and begin load bearing. The participation of collagen fibers is regarded as the second mechanism. When both mechanism are involved, the Cauchy stress of material points is generated based on the contribution of both the first and second mechanisms. At some larger deformation level, the elastin is damaged and its structural contribution to the material stiffness is terminated. This damage phenomenon is modelled by eliminating the contribution of the first mechanism from the material response.

The idea that more than one mechanism may be involved in the mechanical response of a material was introduced by Tobolsky *et al.* [102], as a way to describe the change in mechanical response due to breaking and reforming of cross links in polymeric solids under increasing loads. Wineman and Rajagopal [103, 104] developed the theoretical framework for multi-mechanism constitutive models in the early 1990s. Since then, multi-mechanism constitutive equations have been used to model numerous complex physical phenomena including damage induced softening of rubber materials [104, 105, 106], inelastic processes in metals due to twinning during impact [107], irreversible cyclic extension of human patellar tendons [108, 109], recovery process of reference shapes after heating ('shape memory effect') of deformed intermetallic alloys [110], and the viscoelastic response of isotropic [111] and anisotropic fluids [112].

1.6 CEREBRAL FUSIFORM ANEURYSMS AND ABDOMINAL AORTIC ANEURYSMS

Not all of aneurysms are saccular. Non saccular aneurysms occur both in intracranial and extracranial arteries. Here, we briefly discuss two examples of non saccular aneurysms of intracranial and extracranial arteries: cerebral fusiform aneurysms and abdominal aortic aneurysm (AAA). We will see that beside the shape, the etiology and histology of these aneurysms are different from that of saccular aneurysms.

Cerebral fusiform aneurysms are non saccular aneurysms that occur in the cerebral arteries. The following brief information on cerebral fusiform aneurysms is summarized from Stehbens [56]. Figure 1 depicts the difference in appearance between a typical cerebral fusiform aneurysm (C) and typical saccular aneurysms (A and B). Clearly, a cerebral fusiform aneurysm manifests as a whole wall dilatation of a mostly short straight segment of artery segment. The dilatation can be either bilateral, cylindrical or saccular. The last shape however is very rare. Cerebral fusiform aneurysms can be caused by severe atherosclerosis. The atherosclerotic nature of cerebral fusiform aneurysms distinguishes these aneurysms from saccular aneurysms. Due to the atherosclerosis, the dilatation however is not always accompanied by lumen enlargement. In fact, the lumen may be narrowed. Ruptures of cerebral

fusiform aneurysms are rare. The histology of cerebral fusiform aneurysms generally is similar to those of saccular aneurysms, except for the plaque deposition that is not found in saccular aneurysms. This histology includes thinning of the media, thickening of the intima, fragmentation of the elastic tissues and fibrosis of the wall.

The abdominal aortic aneurysms clearly are extracranial aneurysms. The following brief explanation on the AAA is summarized from Zarins and Glagov [113]. The AAA are type of fusiform aneurysm that manifest as dilatation of abdominal aorta. The formation of AAA has been strongly hypothesized to be associated with general atherosclerosis. Therefore, AAA are also atherosclerotic in nature, as cerebral fusiform aneurysms are.

Atherosclerosis process includes plaque deposition and vascular degeneration. The plaque deposition on the arterial walls does not always result in stenosis in particular when it is accompanied by compensatory vascular enlargement to maintain cross sectional area of arterial lumen. However, the process of vascular enlargement during atherosclerosis is an open question. One possible explanation begins with the alteration of local hemodynamics forces due to the narrowing of the lumen. It is hypothesized that elevated wall shear stress and blood flow velocity may induce lumen enlargement in order to return the level of wall shear stress into normal level. This possible process however is limited to cases where only part of the wall circumference is covered by plaque. When the entire wall is covered by plaque, the vascular enlargement may not accompany atherosclerosis process especially in the late phase of deposition.

It is hypothesized that in the AAA cases, the arterial enlargement is a result of vascular degeneration which is commonly associated with the atherosclerotic process. The degeneration process manifests mostly as the damage of the components of the tunica media such as collagen and elastin. Most hypothesis on the medial degradation generally agree that the degradation is due to some enzymatic process [114, 115]. Medial degradation results in reduction of total wall tensile strength. Stable or progressing plaque deposition however may provide tensile strength to the wall and thus may compensate the loss of elasticity resulted from the disintegration process of the wall. The support from the plaque however is temporary. It is hypothesized that the late process of atherosclerosis may involve plaque regression or erosion. The structural support may become insufficient if the plaque is eroded

or altered in its composition. The atherosclerotic artery then is enlarged causing the AAA to form. The histology of AAA therefore generally includes plaque deposition, fragments of both elastin and collagen fibers in the arterial walls and intraluminal thrombus (ILT). The mechanics of AAA walls has been an important subject of investigation. Constitutive modeling of AAA walls [116, 117] and of ILT [118], for example, can lead to understanding the rupture of AAA, the ultimate danger of this disease, and can help in improving surgical methods. Noting the complexity of the mechanisms that are involved in the formation of AAA, the multi-mechanism constitutive equation could be applied though the influence of the plaque need to be accounted for.

1.7 CENTRAL OBJECTIVE OF THE RESEARCH

The central objective of this work is to develop a suitable constitutive model for human cerebral arterial walls through inclusion of known phenomenological properties, especially collagen recruitment and elastin degradation, and to apply the proposed equation in model problems to predict clinically observed phenomena and experimentally induced passive mechanical behavior of segments of cerebral arterial walls.

2.0 THEORY AND PROPOSED CONSTITUTIVE EQUATION

2.1 QUALITATIVE DESCRIPTION OF ARTERIAL WALL TISSUE

In the Introduction, the elastin and collagen have been described as passive mechanical components that have been hypothesized to cause the mechanical nonlinearity and inelasticity of cerebral and extracerebral arterial wall tissues. The proposed contribution of the elastin and collagen fibers to the nonlinearity and inelasticity may be illustrated by considering an idealized model of an arterial wall strip with undeformed length L_o that experiences uniaxial stretch with stretch ratio λ defined as $\lambda = L/L_o$, where L is the deformed length. The diagram of the idealization is depicted in Figure 9.

Note however that as is mentioned briefly in the Introduction (Section 1.4) , the structural consideration of the elastin and collagen fibers is used only to motivate the separation of the mechanics of aneurysm formation into two mechanisms. The overall approach therefore is phenomenological. Yet, unlike previous phenomenological classical elastic constitutive equations, the current approach can capture mechanical responses that are produced by either individual or collective behavior of the constituents. More importantly, different mechanisms can be introduced in the equilibrium system at different configurations and not necessarily at the same reference configuration. This approach therefore recognizes the importance of the individual mechanical response produced by the constituents of tissues without requiring detailed architectural structure, for example collagen fibers orientation and waviness, and the interaction of the constituents, for example the interaction between the collagen fibers and surrounding ground matrix, as would be necessary if the structural approach is taken. Measurements of cerebral arterial tissue architecture that may require both complex experimental protocols and sophisticated devices therefore can be avoided.

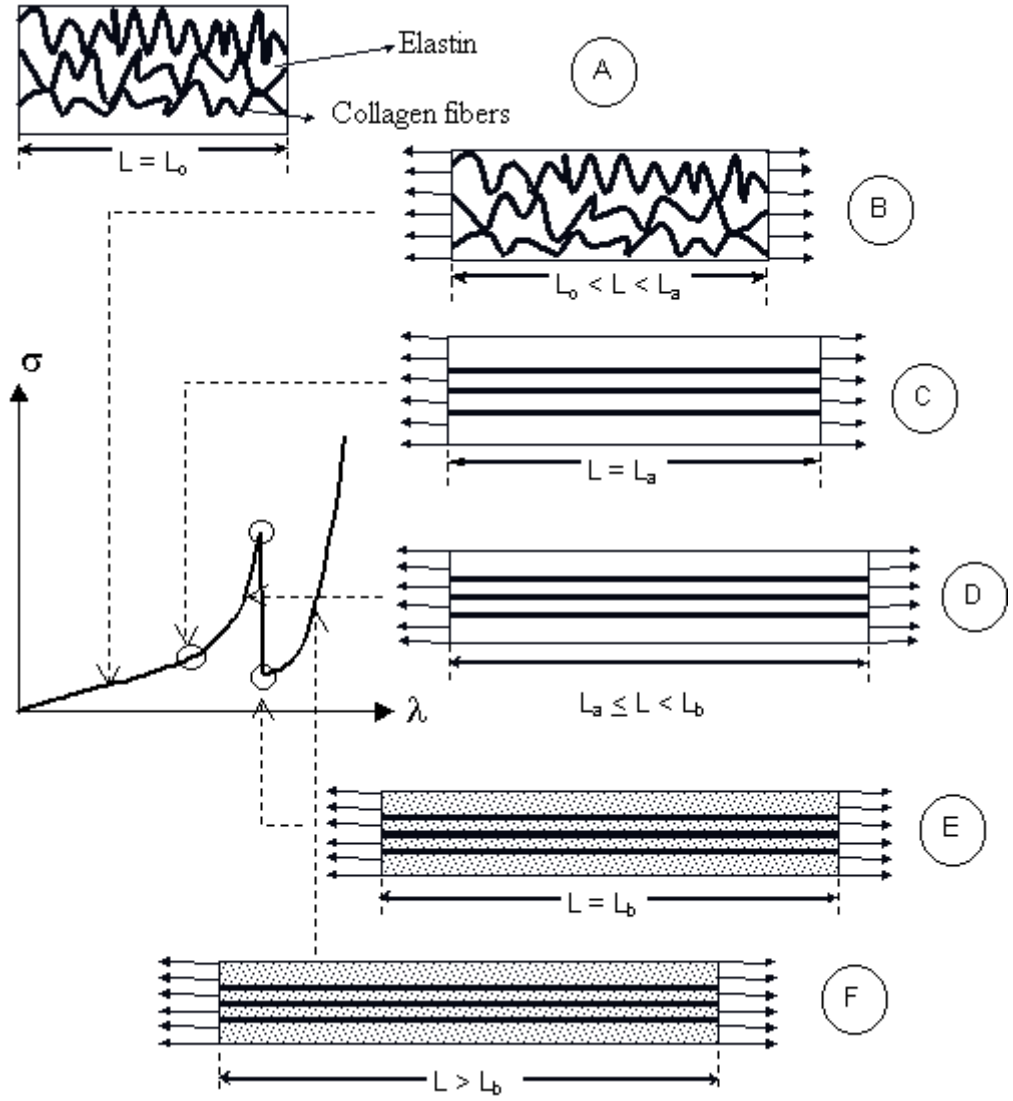

Figure 9: Proposed mechanisms of an idealized arterial wall tissue under uniaxial loading.

Note also that the following idealization inherits assumptions regarding the microstructure of the cerebral arterial tissues. It is assumed that the cerebral tissues are composed of elastin and noninteracting collagen fibers and ground substance matrix and extracellular fluids. Considering only the significance of elastin and collagen fibers in the cerebral arterial deformation and aneurysm formation, the remaining components are assumed to be non structural. It is assumed that the force to straighten the wavy collagen fibers is negligible. The histology of elastin and collagen fibers will be discussed further in Section 2.4.

The following description refers to Figure 9 that depicts the deformed states of an idealized arterial wall tissue and their corresponding regimes in a typical stress vs. strain curve. In the figure, the Greek letters λ and σ represent the stretch ratio and the applied traction at the ends of the strip, respectively.

- Figure 9 (A) illustrates the strip in its unloaded configuration with 'crimped' collagen fibers represented by zigzag lines. Experiments on human carotid arterial circumferential strips suggested collagen fibers were 'crimped' or 'folded' when the strips were unloaded [78].
- Figure 9 (B) shows the strip that is stretched due to the applied traction at the ends and the crimped collagen fibers partially unfolded. Unfolding of collagen fibers was observed in the stretched human carotid arterial circumferential strips [78]. Assuming the crimped collagen fibers do not bear the load, one should expect that the elastin fibers will dominate the mechanical response at this low strain deformation stage. This hypothesis gains support from experimental results on human iliac arterial segments [77]. The experimental results show the initial slope (slope in low strain region) of stress vs. strain curves of normal samples are qualitatively similar to those from segments with depleted collagen fibers. This supports the hypothesis that elastin is primarily responsible for the load bearing in the low strain region.
- In Figure 9 (C), the unfolding collagen fibers reach their critical length $L = L_a$ at which they start to participate in the load bearing. This critical stage will be referred to as the collagen recruitment stage. Here, it is only an assumption introduced for simplicity that the collagen fibers reached their critical length at the same single deformation stage. Busby [49] hypothesizes that collagen fibers are recruited gradually, in a sense that

collagen fibers at a material point reach their critical length at different deformation levels. The gradual recruitment results in, as is seen in Figure 5, gradual change of the slope of stress versus strain curve from small values at low strain to significantly high values at large strain. We denote λ_a stretch ratio corresponding to the critical length L_a.

- Figure 9 (D) shows the extension from the previous stage. In this stage, both the elastin and collagen fibers participate in the load bearing. As will be explained later, if the loading terminates at this stage and the stretch is gradually removed (unloaded), the strip will return to the reference configuration upon full unloading. Here we would consider that the stages A, B, C, and D constitute an elastic regime.
- As illustrated in Figure 9 (E), we also suppose that the elastin may fail, say at another critical stretch $\lambda_b > \lambda_a$. The elastin breakage becomes an important issue in this work because this phenomenon has been associated with early aneurysms formation. As in the collagen recruitment case, it is only an assumption that the elastin breakage occurs at a single deformation stage. The causes and the mechanisms of the failure of elastin and the deformation stages associated with it remain an open question. Scott *et al.* hypothesized that the shifting of the stress versus strain curve is due to purely mechanical loading [79]. Unfortunately the hypothesis was not accompanied by a morphological evidence. Elastin degradation can also be produced by chemical treatment. Roach and Busby [77] depleted the elastin of human iliac arterial segment samples and showed that the toe region at low strain region was missing or disappeared from the typical stress versus strain curve. In this work, we assume that the elastin degradation can be associated with some measure of strain level, as will be described later on.
- Figure 9 (F) corresponds to stretch beyond λ_b. In this particular stage, only collagen fibers contribute to the mechanical response. It will be seen later that when the unloading is initiated at this deformation stage, the strip will return to the configuration that is shown in stage C. Moreover, loading stages after total elastin breakage, for example the stages shown by C, D and E that are not accompanied by elastin contribution, constitute the second (new) elastic regime. That is, the loading and unloading cycles use the configuration shown by C, which is a new unloaded configuration, as the new reference configuration.

This inelastic feature is particularly clear when the strip experiences unloading. The behavior of the strip during unloading however depends on the maximum loading. The following list of cases occurs when the deformation is homogeneous. It will be shown in later sections that more cases must be considered in nonhomogeneous deformations. In the following list, λ^* denotes the maximum stretch experienced by the strip.

- Case 1: $\lambda^* < \lambda_a$

  In this case, the loading terminates at a deformation stage at which none of the collagen fibers were recruited. Such a deformation stage is depicted in Figure 9(B). As expected the behavior will be similar to that of materials with only a single mechanism. That is, after complete unloading, the body will return to its reference configuration.

- Case 2: $\lambda_a \leq \lambda^* < \lambda_b$

  In this case, the unloading initiates at a deformation level at which collagen fibers are recruited but the elastin is not damaged yet. Such a deformation stage corresponds to Figure 9 (D). Two unloading phases must be considered here. In the first unloading phase, the collagen fibers will be unloaded until they reach their critical stretch ratio λ_a. However, this configuration is not the fully unloaded configuration of the strip. When the unloading continues and enters its second phase, the elastin can further unload to its reference configuration causing the strip to return to its unloaded configuration. On the other hand, the collagen fibers will be 'recrimped' to their original fully crimped configuration and stop contributing .

- Case 3: $\lambda_b \leq \lambda^*$

  In this case, the unloading takes place after the elastin is damaged at $\lambda = \lambda_b$. Figure 9 (F) illustrates this deformation level. When $\lambda < \lambda_b$, it is assumed that the damaged elastin is not repaired. As is in the previous case, the unloading will cause the collagen fibers to contract to the reference configuration $\lambda = \lambda_a > 1$. However in this case, the unloading will terminate here, since it is assumed that the collagen fibers cannot contract further. In this case, the strip obtains a new unloaded configuration. The unloaded strip exhibits larger unloaded length $L_a = L_o * \lambda_a$ than the initial strip $L = L_o$. A relevant example was observed in the experiment on human iliac arterial segments in which the strips with depleted elastin showed larger diameters after complete unloading [77].

Classical constitutive equations for elastic solids in which the stress is generated from an unchanged single mechanism cannot be used to capture this type of behavior. The recently proposed multi-mechanism constitutive model can be used to model new mechanisms, for example in the form of recruitment of new material components, that are introduced during the deformation history.

The current approach clearly is different from the structural approach used for example by Lanir [119] and Sacks [120, 121] for modeling planar collagenous tissues. Structural modeling takes into account comprehensive structural information of the tissues components. Lanir for example [119] assumes that the total material response is due to collective contribution of the fluid matrix, elastin fibers and the collagen fibers. In his work, the elastin and collagen fibers are assumed to be linear materials. The model requires information regarding the volume fractions, distribution of fiber waviness, fiber orientations and the interaction between these three components. This information can be supplied by both histological data and data on the microstructural behavior of the tissue components during deformation. To quantify tissues architecture and interactions between the components sometimes requires sophisticated experimental devices. Sacks [122, 121] for example uses a Small Angle Light Scattering (SALS) device to obtain orientation of collagen fibers in planar collagenous tissues. Structural modeling therefore yields constitutive relations in terms of physically meaningful material parameters [101]. The resulting mathematical formulation however usually is complex and the required experimental measurements cannot always be made.

The idealized model shown in Figure 9 assumes that only fully taut collagen fibers are considered load bearing. It has been hypothesized that collagen fibers may already participate in the mechanical response even when they are not fully straight [123, 124]. When a structural approach is taken, the involvement of corrugated collagen fibers makes it necessary to find both the appropriate reference configuration of each fiber, which may be different for each fiber, and the stress versus strain relationship of both wavy and straight collagen fibers. Kwan and Woo [124], for example, assume that the reference configuration of at least one group of parallel collagen fibers contained in a tissue is the same as the stress free configuration of the tissue. This assumption may be acceptable for tissues predominated by collagen fibers where the participation of elastin at low strain can be neglected. Roach and

Burton [77] showed that during the inflation of human iliac arterial segments, only elastin is load bearing at low strain and the collagen fibers do not contribute up to a certain inflated state. Kwan and Woo also assume that the behavior of both wavy and taut collagen fibers can be considered linear with different elastic moduli.

The phenomenological approach that we take does not require a distinction between the contribution made by corrugated and straight fibers as long as the gross behavior of the deformed embedded body during the fiber straightening and stretching can be quantified. The incorporation of wavy collagen fibers in the current constitutive equation can be easily performed. Recall that the reference configuration of the second mechanism representing collagen fibers response can be associated with the permanent deformation remaining after unloading. In principle, there is no restriction that the non zero strain state must be associated with unloaded straight collagen fibers as long as the body is in a stress free configuration. The current approach does not make a distinction between whether the permanent set configuration of the body is occupied by wavy or straight collagen fibers. The fiber waviness is immaterial to the determination of the reference configuration of the second mechanism.

Moreover in general, from the phenomenological point of view, the mechanics of a deformed tissue embedded with straightening and stretching fibers can be considered simply as a continuously deforming body disregarding its microstructural changes. However, if necessary, the mechanism representing straightening fibers can be considered as separate mechanism from that representing stretching of already straightened fibers (provided that supporting experimental data is available).

2.2 KINEMATICS OF A MULTI-MECHANISM CONSTITUTIVE MODEL

The main kinematical feature that differs between the multiple mechanism constitutive equation used here and a classical hyperelastic material is that the stress response of multi-mechanism materials depends on deformation gradients relative to more than one reference configuration. Discussions regarding the more general kinematics necessary for the multi-mechanism theory can be found in Rajagopal and Wineman [103, 104] and Huntley and Wineman [105]. A brief discussion regarding a dual mechanism material, which includes

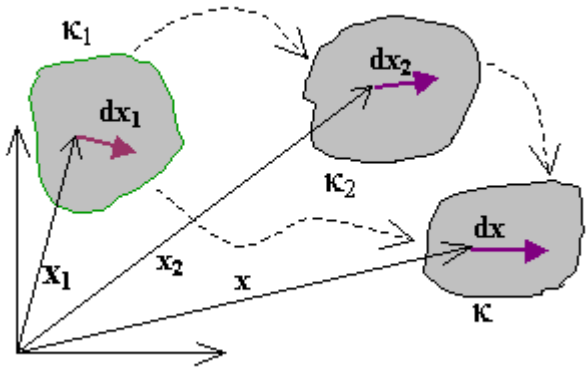

Figure 10: Kinematics of dual mechanism.

only two mechanisms, will be given below using Figure 10 as a reference. Let $\mathfrak{B}$ denote a three-dimensional body which at some time $t = t_1$ occupies a region that is referred as the reference configuration κ_1 and is chosen as the initial unloaded configuration of $\mathfrak{B}$. We suppose that the body is continuously deforming and at time $t > t_1$ it occupies a region referred to as the current configuration and denoted by $\kappa(t) = \kappa$. A motion of the body assigns a material position $\mathbf{X_1}$ of $\mathfrak{B}$ in the undeformed configuration κ_1 to $\mathbf{x}$ in the current configuration as follows:

$$\mathbf{x} = \chi_{\kappa_1}(\mathbf{X}_1, t), \tag{2.1}$$

where χ_{κ_1} is assumed to be single-valued, invertible and continuously differentiable with respect to its arguments as many times as required in the subsequent analysis. The subscript κ_1 is used to emphasize the dependence of the function on κ_1 as the reference configuration. The deformation gradient $\mathbf{F}_1$ at time t for an arbitrary material point $\mathbf{X}_1$, relative to the reference configuration κ_1 is given by

$$\mathbf{F}_1 = \mathbf{F}_{\kappa_1}(\mathbf{X}_1, t) = \nabla\chi_{\kappa_1}(\mathbf{X}_1, t) \qquad \text{or} \qquad F_{1iJ} = \frac{\partial x_i}{\partial X_{1J}}, \tag{2.2}$$

where $\nabla\chi_{\kappa_1}$ is the gradient operator with respect to $\mathbf{X}_1$, holding t fixed. As is in the case of classical single mechanism elastic materials, up to this deformation level, the Cauchy stress tensor $\mathbf{T}$ of elastic material will depend solely on $\mathbf{F}_1$. The following function is a general

representation of that dependency. A specific relation will be specified later on in Section 2.4 when the proposed constitutive equation is presented. The function is given as follows:

$$\mathbf{T} = \mathfrak{F}_1[\mathbf{F}_1]. \tag{2.3}$$

We now suppose that the body continuously deforms and that at some later state of deformation or time, say at time $t = t_2 > t_1$, a microstructural change occurs inside the material. The change under consideration may manifest itself in the form of conversion to a new microstructure or recruitment of a new material. The microstructural change could occur gradually or instantaneously. In the case of material conversion, a portion or all of material could convert to a new microstructure. Similarly in the case of material recruitment, a portion or all new material could be recruited gradually or simultaneously.

The initiation of the microstructural change may be related to some state of deformation through a function of the deformation parameters [105]. The parameter t that has been used to describe states of deformation may be used as a deformation parameter. However, its usage is limited to deformations which can be defined by a single kinematic parameter: such as uniaxial tension (where longitudinal stretch is the parameter) or inflation of long cylindrical membrane (where circumferential stretch is the parameter). When the deformation involves more than one parameter, such as biaxial extension, a scalar kinematic parameter s which is associated with configuration $\kappa(t)$ through the following relation:

$$s = A(\mathbf{F}_1), \tag{2.4}$$

is used as function of deformation parameters. For simplicity, at time $t = t_1$, when the body is undeformed, s is set to be 0. When the material is isotropic and incompressible, without loss in generality, relation (2.4) may be rewritten as a function of the invariants of $\mathbf{F_1}$ [105], as

$$s = s(I_1, II_1), \tag{2.5}$$

where the principal of material frame indifference has been used in obtaining (2.5). Here I_1 and II_1 are the first and second invariants of the Left Cauchy Green strain tensor $\mathbf{B_1} = \mathbf{F_1}\mathbf{F_1}^T$, respectively and they are defined as follows:

$$I_1 = \mathrm{tr}(\mathbf{B_1}) = B_{1ii} \qquad II_1 = \frac{1}{2}((\mathrm{tr}\mathbf{B_1})^2 - \mathrm{tr}\mathbf{B_1}^2) = \frac{1}{2}(B_{1ij}B_{1ij} - B_{1ij}B_{1ji}). \tag{2.6}$$

The initiation of the microstructural change, or specifically in our case the collagen fibers recruitment process, can be defined to depend on s through a criterion as follows:

$$A_a = s(I_1, II_1) - s_a, \tag{2.7}$$

where s_a is a scalar material parameter to be associated with the activation of collagen recruitment. We will refer to this criterion as the activation criterion. In then follows that the activation of the new mechanism (for example collagen recruitment) corresponds to

$$A_a = 0. \tag{2.8}$$

After the new mechanism is initiated, depending on the homogeneity of the material and the deformation under consideration, it is assumed that some or all material points that satisfy (2.8) are occupied simultaneously by two material particles or material elements: one represents the original material and the other represents the new (recruited) material [103]. Within the scope of collagen recruitment as the new mechanism, we shall also assume that prior to the recruitment, the collagen fibers are in a stress-free state. The new mechanisms generally can take any configurations, not necessarily those that are possessed by $\mathfrak{B}$ during the deformation history, as the reference configurations. However, it will be seen in this work that configurations occupied by the deformed body $\mathfrak{B}$ are often used as the reference configurations of the recruited collagen fibers. Moreover, as is emphasized in Wineman and Rajagopal [103] , we will see that a set of reference configurations each of which corresponds to (2.8), must be considered when spatial material recruitment occurs due to nonhomogeneous deformations.

Let's denote κ_2 the configuration that is occupied by the deformed body $\mathfrak{B}$ at $t = t_2$. We suppose that at this deformation level, the recruitment occurs and takes configuration κ_2 as the reference configuration. The recruitment occurs at material points whose deformation gradients satisfy the activation criterion (2.8). Depending on the deformation under consideration, such material points belong either to the entire or some parts of the body.

When the deformation is homogeneous, the deformation gradient $\mathbf{F_1}$ is space independent (constant) and therefore at $t = t_2$ the entire body will simultaneously satisfies the activation

criterion (2.8) (provided that s_a is also space independent). In this case, no more collagen fibers recruitment will occur when the deformation level (and therefore s) are increased.

In the case of nonhomogeneous deformations, the deformation gradient $\mathbf{F_1}$ is space dependent. Therefore, at $t = t_2$, the activation criterion (2.8) will be satisfied at only some parts of the body, say P_1. When the deformation level is increased, some other parts of the body, say $P_2 \neq P_1$, may eventually satisfy the activation criterion (2.8). Here, the body will occupy a new configuration, say κ_{2b}. The recruitment that occurs in P_2 will take κ_{2b} as its reference configuration. When the body continues deforming, more body parts will satisfy the activation criterion (2.8) and more reference configurations come into consideration. In further discussion we shall use κ_2 to denote all configurations of the body at which the new or second mechanism is introduced in any part of the body. Similarly, we use t_2 to denote all times $t_2 > t_1$ at which the second mechanism is introduced in any part or all of the body.

We shall now discuss the deformation gradient of the second mechanism representing the material recruitment relative to the reference configurations κ_2 . Let $\mathbf{X}_2$ denote the coordinates of the particle Y in κ_2 that was in the position $\mathbf{X}_1$ in configuration κ_1, then according to (2.1),

$$\mathbf{X}_2 = \chi_{\kappa_1}(\mathbf{X}_1, t_2). \tag{2.9}$$

We suppose that the body continues deforming so that at the present time $t > t_2$ a typical material point which in configuration κ_2 was at the place $\mathbf{X}_2$, moves to the place $\mathbf{x}$ in the present configuration. A motion that refers to configuration κ_2 is written as follows:

$$\mathbf{x} = \chi_{\kappa_2}(\mathbf{X}_2, t). \tag{2.10}$$

Similar to (2.2), the deformation gradient $\mathbf{F}_2$ at $\mathbf{X}_2$, relative to the reference configurations κ_2 is

$$\mathbf{F}_2 = \mathbf{F}_{\kappa_2}(\mathbf{X}_2, t) = \nabla\chi_{\kappa_2}(\mathbf{X}_2, t) \qquad \text{or} \qquad F_{2iJ} = \frac{\partial x_i}{\partial X_{2J}}, \tag{2.11}$$

where $\nabla\chi_{\kappa_2}$ is the gradient operator with respect to $\mathbf{X}_2$ holding t fixed. Using a change of variables for (2.11) and making use of (2.2) and its inverse evaluated at $t = t_2$, the relation between $\mathbf{F}_1$ and $\mathbf{F}_2$ can be established as follows:

$$\mathbf{F}_2 = \mathbf{F}_{\kappa_1}(\mathbf{X}_1, t)\mathbf{F}^{-1}_{\kappa_1}(\mathbf{X}_1, t_2). \tag{2.12}$$

It is then assumed that at some later time $t > t_2$, the Cauchy stress of material points at which the activation criterion (2.8) is satisfied depends on the deformation gradient of both the material possessing the original microstructure and a new material which either is recruited or contains newly formed microstructure as follows:

$$\mathbf{T}(t) = \mathfrak{F}_2[\mathbf{F}_1, \mathbf{F}_2]. \tag{2.13}$$

The Cauchy stress at the remaining material points will still be given by (2.3).

In the present work, in addition to material recruitment, the theory was adapted to model material degradation or deactivation. It is assumed that material degradation at a material point always begins after the initial material recruitment of that point. In the case of gradual recruitment, the degradation doesn't have to occur after the recruitment is completed. Here, we suppose that at a time $t = t_3 > t_2$, the first or original material starts to degrade. Similar to the activation of the material recruitment, we suppose that the initiation of the deactivation can be related to the deformation parameter, s. The relation is similar to (2.7), but a different scalar value s_b will be used as the criterion for degradation. The criterion that is referred to as the deactivation criterion will be defined as follows:

$$A_b = s(I_1, II_1) - s_b, \tag{2.14}$$

where the initiation of the degradation of the original material corresponds to

$$A_b = 0. \tag{2.15}$$

The Cauchy stress of material points that satisfy the deactivation criterion (2.15) will depend only on the deformation gradient of the recruited material, $\mathbf{F}_2$, as follows:

$$\mathbf{T} = \mathfrak{F}_{\mathbf{3}}[\mathbf{F}_{\mathbf{2}}]. \tag{2.16}$$

At the remaining material points at which the activation criterion (2.8) is satisfied, the Cauchy stress will still be given by (2.13), while at points at which (2.8) is not satisfied, the Cauchy stress will still be given by (2.3).

Generally, a multi-mechanism model may employ more than two reference configurations. The gradual recruitment of collagen fibers, for example, can be considered as recruitment

of each fiber or group of fibers which may be recruited at different configurations. Stress generated by a series of continuous microstructural changes can be presented in the form of integration of local stresses generated by each new mechanisms. This has been found useful to model damaged induced softening in polymeric materials under homogeneous deformation [104] and under non-homogeneous deformation [105].

2.3 APPLICATION OF MULTI-MECHANISM CONSTITUTIVE EQUATIONS FOR MODELING CEREBRAL ARTERIAL WALLS

In the present application, we are interested in modeling the observed nonlinear and inelastic behavior of cerebral arterial and aneurysms walls which are believed to be related to collagen recruitment and elastin breakage. The mechanisms produced by elastin and collagen fibers during the deformation of cerebral arterial walls will be considered as two separate mechanisms, each of which possesses different unloaded reference configuration and material response. The separation allows either activation or deactivation of each mechanism independently. As was discussed in Section 2.1, the mechanism produced by elastin is responsible for the initial (low strain) loading Figure 9 (B). In later sections, this mechanism is referred to as the first mechanism. Clearly, the reference configuration of the first mechanism coincides with the initial reference configuration. As was described in Section 2.1 at some later deformation stage, the collagen fibers recruitment is introduced (Figure 9 (C)). The mechanism produced by recruited collagen fibers will be referred to as the second mechanism. The second mechanism uses the configuration occupied by the body at the onset of collagen recruitment as the reference configuration. The association of the onset of collagen recruitment with some measurable quantity has not been explored experimentally and it subjects for further work. It is assumed that the onset is associated with the deformation history by means of the activation criterion (2.8). In this work, it is also assumed for simplicity that all of the collagen fibers occupying material points that satisfy the activation criterion (2.8) will be recruited at once. Moreover, as was described in Section 2.1, it is important to include elastin failure in the modeling (Figure 9 (D)). However, as was explained before, similar to collagen recruitment, the causes and mechanisms of elastin breakage remain to be resolved.

In this work, it as assumed that the failure of elastin can be associated with a deformation level by means of the deactivation criterion (2.15) that occurs at some later deformation level after collagen recruitment. Similar to collagen recruitment, for simplicity, it is assumed that all of the elastin material points satisfying criterion (2.15) break simultaneously. Scott *et al.* [79] hypothesized that elastin breakage in cerebral segments is due to intramural pressure that is above a critical pressure level.

Making use of the deformation parameter s described previously, the application of the multi-mechanism theory can be described briefly as follows. The unloaded arterial walls are assumed to have $s = 0$ everywhere in the body. When the arterial wall deforms, s increases from 0. As suggested before, at initial loading stages, only elastin, represented by the first mechanism, contributes to the mechanical response and therefore the Cauchy stress tensor for all of the material points is given by (2.3). In this stage, the crimped collagen fibers unfold but do not participate in the load bearing. As was assumed, the participation of collagen fibers is initiated when s reaches s_a at any parts or all of the body. On such occasion, it is assumed that all of the collagen fibers occupying material points which values of s satisfy the activation criterion (2.8) are recruited. Material points satisfying the activation criterion will be occupied by active elastin and collagen simultaneously and the Cauchy stress tensor of those points is given by (2.13). The stress in the remainder of the body (where the activation criterion is not satisfied) will still have the form of (2.3).

As was discussed before (Section 2.1), it is important to include the elastin breakage in the constitutive equation. We suppose that the breakage phenomenon is modelled by deactivating the first mechanism representing elastin response. As is assumed, the deactivation of the first mechanism occurs at material points at which the deactivation criterion (2.15) is satisfied. Therefore, when the deformation continues such that at some or all material points s reaches s_b, the Cauchy stress of such points will take the form of (2.16) where the Cauchy stress depends solely on the deformation gradient of the second mechanism $\mathbf{F_2}$.

When the process is reversed due to unloading, say at $s = s^*$, the value of s decreases and the stresses at material points will be determined by the values of s^* relative to s_a and s_b critical values. When the deformation is *homogeneous*, the following three cases of values of s^* must be considered:

- Case 1: $s^* < s_a$

  In this case, the unloading begins before the onset of collagen fibers recruitment. It is clear that only elastin is active during unloading. Therefore, the material response resembles those of classical elastic material. The Cauchy stress during unloading is governed solely by (2.3) and the zero stress will correspond to the original reference configuration.

- Case 2: $s_a \leq s^* < s_b$

  In this case, the unloading begins after the onset of the new material recruitment but before the initiation of elastin breakage. The unloading process consits of two unloading phases. In the first phase, s reduces from s^* to s_a. In this phase, both collagen fibers and elastin are active, so the Cauchy stress tensor will be given by (2.13). During this unloading phase, the collagen fibers will return to their unloaded configuration denoted by κ_2 at which $s = s_a$. As the unloading continues and enters the second phase, s reduces from s_a to $s = 0$. In this phase, the collagen fibers are assumed to recrimp and therefore become inactive, leaving elastin as the only active mechanical component. In this phase, the Cauchy stress tensor then is given by (2.3). The material response in the second unloading phase is similar to those of the first case.

- Case 3: $s_b \leq s^*$ This the case in which the unloading occurs after elastin breakage. In this case, elastin is inactive when the unloading is initiated and cannot be reactivated since it assumed that elastin regeneration does not occur even when $s < s_b$. Thus in this unloading case, only collagen fibers contribute to mechanical load bearing. The Cauchy stress is given by (2.16). The same equation is used when s is reduced below s_b. Since (2.16) depends on the deformation gradient relative to reference configuration κ_2 of which $s = s_a$, the body reaches zero stress when $s = s_a$. Since the elastin is deactivated, there are no forces contributing to further deformation. The body will not return to its initial reference configuration but possesses a new unloaded configuration.

We will see in Chapter 3 (particularly in Sections 3.4 and 3.5) that when the deformation is nonhomogeneous, s is space dependent and more unloading cases need to be considered.

2.4 THE PROPOSED CONSTITUTIVE RELATION

So far, no specific functional forms of (2.3), (2.13), and (2.16) have been imposed. We now suppose that each of the two material components performs as a hyperelastic material, which under quasi static loading exhibits no hysteresis. Moreover, it is assumed here that the elastin and collagen embedded body can be modelled as homogeneous and isotropic at the reference states κ_1 and κ_2, respectively. In the internal elastic lamina of cerebral arterial walls, elastin appears as fairly homogenous lamina [67, 48]. In the media and adventitia, collagen appears as bundles of fibers [48]. Collagen fibers in an undeformed tissue are known to be 'crimped' [121] and gradually become straight as the tissue is stretched [78]. Straightened collagen fibers may induce anisotropy [80]. A morphology study by Finlay *et al.* [54] however shows that the collagen fibers at the apex of bifurcations of cerebral arteries, the most common region for saccular aneurysms, are arranged in a complex net that possesses no specific fiber orientation. We then assume that the isotropy assumption for the apical region of bifurcation is an acceptable approximation. It is important here to point out that the isotropy of the body (or part of the body) containing the collagen is relative to the reference configurations corresponding to $s = s_a$.

We propose that the Cauchy stress tensor can be derived from a strain energy function W that involves both the first mechanism and second mechanism in the form that depends on s as follows:

$$\mathbf{T} = -p\mathbf{I} + 2\frac{\partial W}{\partial I_1}\mathbf{B}_1 - 2\frac{\partial W}{\partial II_1}\mathbf{B}_1^{-1} + 2\frac{\partial W}{\partial I_2}\mathbf{B}_2 - 2\frac{\partial W}{\partial II_2}\mathbf{B}_2^{-1}, \tag{2.17}$$

$$W = \begin{cases} W_1(I_1, II_1), & \text{when} \quad 0 \le s < s_a; \\ W_1(I_1, II_1) + W_2(I_2, II_2), & \text{when} \quad s_a \le s < s_b; \\ W_2(I_2, II_2), & \text{when} \quad s_b \le s. \end{cases} \tag{2.18}$$

Here, the total stress at each stage of deformation is defined to be the superposition of contributions of the original material and the recruited material represented by W_1 and W_2, respectively. We consider the constitutive equation suitable for hyperelastic, incompressible, and isotropic material for both of the material responses. Subscript '1' indicates that the

Left Cauchy Green Strain tensor and its inverse $\mathbf{B}_1$ and $\mathbf{B}_1^{-1}$, are calculated from the gradient of deformation $\mathbf{F}_1$ that refers to reference configuration κ_1 while subscript '2' indicates that $\mathbf{B}_2$ and $\mathbf{B}_2^{-1}$ are calculated with respect to configuration κ_2 at which material recruitment occurs. They are calculated as follow :

$$\mathbf{B}_1 = \mathbf{F}_1\mathbf{F}_1^T \qquad \text{or} \qquad B_{1ij} = F_{1ik}F_{1jk} \tag{2.19}$$

$$\mathbf{B}_2 = \mathbf{F}_2\mathbf{F}_2^T \qquad \text{or} \qquad B_{2ij} = F_{2ik}F_{2jk}. \tag{2.20}$$

Due to material incompressibility and isotropy, the dependency of W on the deformation gradients $\mathbf{F}_1$ and $\mathbf{F}_2$ has been reduced to a dependence on I_1 and I_2, the first invariants of $\mathbf{B_1}$ and $\mathbf{B_2}$, respectively and II_1 and II_2, the second invariants of $\mathbf{B_1}$ and $\mathbf{B_2}$, respectively. The invariants I_1 and I_2 are the trace of $\mathbf{B}_1$ and $\mathbf{B}_2$, while II_1 and II_2 are the trace of $\mathbf{B}_1^{-1}$ and $\mathbf{B}_2^{-1}$ (due to incompressibility and isotropy).

2.4.1 The selection of the strain energy function and the function of deformation parameters

Generally, there are at least three functional forms of strain energy functions (in the classical sense) that have been proposed to describe the mechanical behavior of arterial tissue [85]: exponential type, logarithmic type and polynomial type. In this work, we suppose that exponential type is suitable to be used for both W_1 and W_2. The formulations are given as follows:

$$W_1 = \frac{\alpha_1}{2\gamma_1}e^{\gamma_1(I_1-3)} \qquad \text{and} \qquad W_2 = \frac{\alpha_2}{2\gamma_2}e^{\gamma_2(I_2-3)}, \tag{2.21}$$

where $\alpha_1, \alpha_2, \gamma_1$ and γ_2 are material parameters and I_1 and I_2 are invariants of the first and second mechanism, respectively, that have been described before. The form of the strain energy function W_1 is similar to that used by Demiray and Vito [125] for an artery, by Delfino *et al.* [126] for a human carotid artery and in fact by Beatty for general biological tissues [127]. The value of γ_1 in general has no restriction, but it is necessary that $\gamma_1 \geq 0$ in order that the strain energy (2.21.1) to increase with the deformation from a reference state [127]. Eventually, we must impose the same restriction for γ_2 in particular since the

strain energy must also increase with the deformation even in the states where the elastin has been inactive. It will be shown in Section 3.3 that (2.21) is in satisfactory agreement with real experimental data based on statistical analysis. In fact, the strain energy functions employing the well known Neo Hookean and Mooney Rivlin models perform less well than the proposed form.

The form of s as well as the values of s_a and s_b are part of material parameters that need to be determined via some experimental procedures. Such experimental work is the focus of future research, however suggested methods to obtain the form of s and the values of s_a and s_b will be discussed in Chapter 3. The following form of s is selected to be used in future illustrative applications:

$$s = I_1 - 3. \tag{2.22}$$

Here, s is assumed to depend linearly only on I_1 which consistent with the form for strain energy functions for biological tissues. The selected form of s ensures that the undeformed body corresponds to $s = 0$. The linear dependency is preferred for the sake of simplicity. An example of (2.5) that is more general than (2.22) is given by Wineman and Huntley [105]. In that work, s is a function of both I_1 and II_1.

2.4.2 Material objectivity

A constitutive equation must satisfy at least two important invariance restrictions: the principles of coordinate invariance and material indifference [128]. A list other principles that must be considered can be seen, for example, in Eringen [129]. The principle of coordinate invariance for instance requires that a constitutive relation must not depend on a specific coordinate system. The restriction is satisfied when the physical quantities in the formulation are expressed using scalars, vectors and tensors with no dependency on a coordinate system. Clearly, the constitutive relation (2.17) has satisfied this requirement.

The axiom of objectivity [129, 130] or frame indifference [131] requires that a constitutive relation involving relevant physical quantities must be independent of observers' stand points. In order to satisfy this principle, transformations of the physical quantities due the presence of the different observers must follow certain rules.

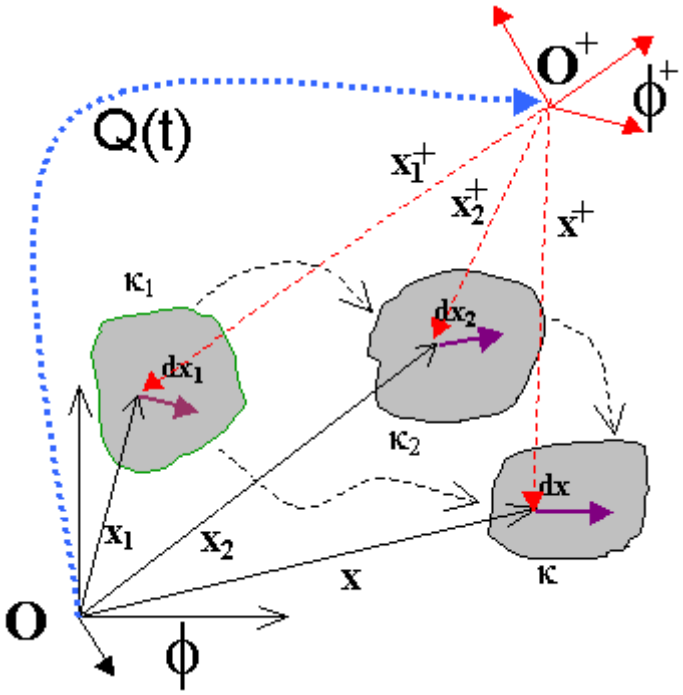

Figure 11: A sequence of motions evaluated by two different observers denoted by ϕ and ϕ^+.

The principle of material objectivity can be described by considering a motion that is monitored by two different observers that are moving relative to each other. Figure 11 depicts two different observers, denoted respectively by ϕ and ϕ^+, both monitor the motion given by (2.1). In order to describe physical quantities in the (three dimensional) Euclidian space, each of the two observers is equipped with a rectangular Cartesian coordinate system that is characterized by a set of fixed basis vectors and an origin point. We suppose that sets of basis vectors and origin points, or reference frames [127], $(O, \mathbf{e}_a)$ and $(O^+, \mathbf{e}_a^+)$ are assigned for observers ϕ and ϕ^+, respectively. The observers are also furnished with clocks to measure time differences, say t and t^+ [130]. Here, without loss of generality, we suppose that at a reference time, say $t = t_1$, the two reference frames are coincide and both observers use the same clock so that $t = t^+$.

Having these two reference frames we can analyze the objectivity of some relevant physical quantities. Quantities such as scalars s , vectors $\mathbf{v}$ and second order tensors $\mathbf{S}$ are objective if they satisfy the following relations [132, 133, 130]:

$$s^+ = s \qquad , \qquad \mathbf{v}^+ = \mathbf{Q}(t).\mathbf{v} \qquad \text{and} \qquad \mathbf{S}^+ = \mathbf{Q}(t).\mathbf{S}.\mathbf{Q}^T(t). \tag{2.23}$$

The derivations of the objectivity of these quantities can be found in, for example, Malvern [132] and Truesdell [131]. In (2.23), $\mathbf{Q}(t)$ is a proper orthogonal second order tensor, *i.e.*,

$$\mathbf{Q}(t)^T.\mathbf{Q}(t) = \mathbf{Q}(t).\mathbf{Q}^T(t) = \mathbf{I} \qquad \text{and} \qquad \det\mathbf{Q} = +1. \tag{2.24}$$

We suppose that the description of a motion (2.1) is given by observer ϕ. The other observer ϕ^+ will describe the same motion as:

$$\mathbf{x}^+ = \chi^+_{\kappa_1^+}(\mathbf{X}_1^+, t). \tag{2.25}$$

Recall however that the reference frames of the observers are coincide at the reference time so that

$$\kappa_1^+ = \kappa_1 \qquad \text{and} \qquad \mathbf{X}_1^+ = \mathbf{X}_1. \tag{2.26}$$

The most general form to relate (2.25) and (2.1) is given by [132, 133, 130]:

$$\mathbf{x}^+(t) = \chi^+_{\kappa_1}(\mathbf{X}_1, t) = \mathbf{c}(t) + \mathbf{Q}(t).\mathbf{x}(\mathbf{X}_1, t), \tag{2.27}$$

where $\mathbf{c}(t)$ is a vector that is independent of position and $\mathbf{X}_1 \in \kappa_1$ and $\mathbf{Q}(t)$ is given by (2.24). The deformation gradient of the first mechanism relative to reference configuration κ_1 described by observer ϕ and ϕ^+ are as follows:

$$\mathbf{F}_{\kappa_1}(t) = \mathbf{F}_1(t) = \frac{\partial \chi_1(\mathbf{X}_1, t)}{\partial \mathbf{X}_1} \qquad \text{and} \qquad \mathbf{F}^+_{\kappa_1}(t) = \mathbf{F}^+_1(t) = \frac{\partial \chi^+_1(\mathbf{X}_1, t)}{\partial \mathbf{X}_1}, \tag{2.28}$$

respectively. Substituting (2.27) into (2.28.2) and using (2.1) we can see that $\mathbf{F}_1$ transforms as follows:

$$\mathbf{F}^+_1(t) = \mathbf{Q}.\mathbf{F}_1(t). \tag{2.29}$$

In a sense of the objective definition set by (2.23.3) the deformation gradient of the first mechanism therefore is not objective.

During the motion described by (2.1), it is supposed that at $t = t_2$ the activation criterion of the second mechanism is satisfied. This material characteristic must be independent of observer's standpoint, so the activation criterion of the second mechanism is seen by the other observer to be satisfied at $t = t_2$. The position of a particle in body $\mathfrak{B}$ at $t = t_2$ is described by the first observer as (2.9), while those will be described by the second observer as:

$$\mathbf{x}^+_2 = \chi^+_{\kappa_1}(\mathbf{X}_1, t_2) = \mathbf{c}(t_2) + \mathbf{Q}(t_2).\mathbf{X}_2, \tag{2.30}$$

where the relation (2.27) has been used.

We suppose that the configurations occupied by body $\mathfrak{B}$ at $t = t_2$ due to the first mechanism of the first motion and the second motion be denoted by κ_2 and κ^+_2, respectively. The second mechanism of the first motion uses κ_2 as the reference configuration and is described using (2.10), while those of the second motion uses κ^+_2 as the reference configuration and is described as follows:

$$\mathbf{x}^+ = \chi^+_{\kappa_2}(\mathbf{X}^+_2, t). \tag{2.31}$$

The deformation gradient of the second mechanism relative to κ_2 is given as follows

$$\mathbf{F}_{\kappa_2}(t) = \mathbf{F}_2(t) = \frac{\partial \chi_{\kappa_2}(\mathbf{X}_2, t)}{\partial \mathbf{X}_2}, \tag{2.32}$$

which is analogous to (2.11). From observer ϕ^+ point of view, the deformation gradient of the second mechanism relative to κ_2^+ configuration is given as follows:

$$\mathbf{F}^+_{\kappa_2} = \mathbf{F}^+_2 = \frac{\partial \chi^+_{\kappa_2}(\mathbf{X}_2, t)}{\partial \mathbf{X}^+_2}. \tag{2.33}$$

Using chain rule for (2.33) and using the definitions given by (2.11),(2.27) and (2.30), we find that $\mathbf{F}^+_2(t)$ transforms as follows:

$$\begin{aligned} \mathbf{F}^+_2 &= \frac{\partial \chi^+_{\kappa_1}(\mathbf{X}_1, t)}{\partial \mathbf{x}} \frac{\partial \mathbf{x}}{\partial \mathbf{X}_2} \frac{\partial \mathbf{X}_2}{\partial \mathbf{X}^+_2} \\ &= \mathbf{Q}(t).\mathbf{F}_2(t).\mathbf{Q}^T(t_2). \end{aligned} \tag{2.34}$$

Similar result can be obtained by employing (2.29) in the relation similar to (2.12) that must be unaltered by superposed rigid body motion:

$$\begin{aligned} \mathbf{F}^+_2 &= \mathbf{F}^+_1.\mathbf{F}^+_1(t_2)^{-1} \\ &= (\mathbf{Q}.\mathbf{F}_1).(\mathbf{Q}(t_2).\mathbf{F}_1(t_2))^{-1} \\ &= \mathbf{Q}.\mathbf{F}_1.\mathbf{F}_1(t_2)^{-1}.\mathbf{Q}^T(t_2) \\ &= \mathbf{Q}.\mathbf{F}_2.\mathbf{Q}^T(t_2), \quad \text{since } \mathbf{Q}^{-1} = \mathbf{Q}^T. \end{aligned} \tag{2.35}$$

Clearly, the transformation (2.35) shows that $\mathbf{F}_2(t)$ is not objective (in a sense of the definition (2.23.3)).

The constitutive relations (2.3),(2.13), and (2.16) therefore must not depend on $\mathbf{F}_1(t)$ and $\mathbf{F}_2(t)$ but must depend on other restricted quantities that satisfy the objectivity. Here, however, we will show that the proposed constitutive equation (2.17) transforms according to (2.23.3) and therefore is an objective quantity. In other word, the components of the equation are objective. Using the definitions of (2.12),(2.34), and (2.29) , the objectivity of the quantities $\mathbf{B}_1$, $\mathbf{B}_2$, $\mathbf{B}_1^{-1}$ and $\mathbf{B}_2^{-1}$ can be verified as follows.

The Left Cauchy-Green deformation tensor of the first mechanism denoted by $\mathbf{B}_1$ is transformed as follows:

$$\begin{aligned} \mathbf{B}^+_1 &= (\mathbf{F}^+_1).(\mathbf{F}^+_1)^T \\ &= (\mathbf{Q}.\mathbf{F}_1).(\mathbf{Q}.\mathbf{F}_1)^T = \mathbf{Q}.\mathbf{F}_1.(\mathbf{F}_1)^T.\mathbf{Q}^T \\ &= \mathbf{Q}.\mathbf{B}_1\mathbf{Q}^T. \end{aligned} \tag{2.36}$$

The transformation of Left Cauchy-Green deformation tensor of the second mechanism $\mathbf{B}_2$ is given as follows:

$$\begin{aligned}\mathbf{B}_2^+ &= (\mathbf{F}_2^+).(\mathbf{F}_2^+)^T \\ &= (\mathbf{Q}.\mathbf{F}_2.\mathbf{Q}^T(t_2)).(\mathbf{Q}.\mathbf{F}_2.\mathbf{Q}^T(t_2))^T = \mathbf{Q}.\mathbf{F}_2.\mathbf{Q}^T(t_2).\mathbf{Q}(t_2).\mathbf{F}_2^T.\mathbf{Q}^T \\ &= \mathbf{Q}.\mathbf{F}_2.\mathbf{F}_2^T.\mathbf{Q}^T = \mathbf{Q}.\mathbf{B}_2.\mathbf{Q}^T. \end{aligned} \tag{2.37}$$

Recalling that $\mathbf{B}_1^{-1} = (\mathbf{F}_1.\mathbf{F}_1^T)^{-1}$, the transformation rule for $\mathbf{B}_1^{-1}$ is given as follows:

$$\begin{aligned}(\mathbf{B}_1^{-1})^+ &= ((\mathbf{F}_1^+).(\mathbf{F}_1^+)^T)^{-1} = (\mathbf{B}_1^+)^{-1} \\ &= (\mathbf{Q}.\mathbf{B}_1\mathbf{Q}^T)^{-1} = \mathbf{Q}.\mathbf{B}_1^{-1}\mathbf{Q}^T. \end{aligned} \tag{2.38}$$

Similarly for the objectivity of $\mathbf{B}_2^{-1}$ can be seen as follows:

$$\begin{aligned}(\mathbf{B}_2^{-1})^+ &= ((\mathbf{F}_2^+).(\mathbf{F}_2^+)^T)^{-1} = (\mathbf{B}_2^+)^{-1} \\ &= (\mathbf{Q}.\mathbf{B}_2\mathbf{Q}^T)^{-1} = \mathbf{Q}.\mathbf{B}_2^{-1}\mathbf{Q}^T. \end{aligned} \tag{2.39}$$

Clearly, in the sense of (2.23.3) the second order tensors $\mathbf{B}_1$ $\mathbf{B}_2$, $\mathbf{B}_1^{-1}$, and $\mathbf{B}_2^{-1}$ are all objective quantities. It is instructive that the resulting Cauchy stress tensors are also objective:

$$\mathbf{Q}.\mathbf{T}(\mathbf{B}_1, \mathbf{B}_2, \mathbf{B}_1^{-1}, \mathbf{B}_2^{-1}).\mathbf{Q}^T = \mathbf{T}(\mathbf{Q}.\mathbf{B}_1.\mathbf{Q}^T, \mathbf{Q}.\mathbf{B}_2.\mathbf{Q}^T, \mathbf{Q}.\mathbf{B}_1^{-1}.\mathbf{Q}^T, \mathbf{Q}.\mathbf{B}_2^{-1}.\mathbf{Q}^T). \tag{2.40}$$

We have shown that according to the objectivity restriction, the proposed formulation (2.17) are sufficient. Wineman and Rajagopal [103] show the necessity of the dependency of Cauchy stress $\mathbf{T}$ on the left stretch tensor of the first mechanism, $\mathbf{U}_1$ and the right stretch tensor of the second mechanism, $\mathbf{V}_2$. The formulation (2.17) may be too restrictive since it allows only isotropic materials to be involved in the mechanism. This formulation however can serve well in the current work. The activation and deactivation criteria introduced earlier must also objective. Their transformation must follow the relation (2.23.1) for they are scalar-valued functions. Since the deformation gradient $\mathbf{F}_1$ is not objective, the dependency of s on $\mathbf{F}_1$ needs to be reformulated. The choice of scalar invariants of $\mathbf{B}_1$ serves the objectivity requirement and satisfies (2.4).

3.0 ANALYTICAL AND NUMERICAL RESULTS FOR SOME MODEL PROBLEMS

In this section we wish to apply the dual mechanism model to some specific applications and present the results. We will consider three homogeneous deformations; uniaxial and biaxial loading of rectangular slabs and inflation of cylindrical membranes. In addition we will consider two nonhomogeneous deformations; inflation of a thick cylindrical shell and inflation of a circular membrane cap. In addition, we will also present results of unloading for each model problem.

In Section 3.1, 3.2 and 3.3, we present results for homogeneous deformations. These problems are simple in the sense that during the deformation the strain is uniform throughout the body and therefore both activation and deactivation criteria will be satisfied simultaneously throughout the body. Uniaxial loading employs only a single deformation parameter that will simplify the form of scalar parameter s. Biaxial loading requires two deformation parameters and therefore a scalar function of s is needed. In Section 3.3, we discuss the inflation of a cylindrical membrane and compare the results to the existing experimental data on inelastic behavior of cerebral tissue provided by Scott *et al.* [79]. Moreover, the experimental data is used to obtain the exponential type forms and their material constants of the proposed constitutive equation.

In Sections 3.4 and 3.5, we present results for nonhomogeneous deformations. Here, the strain during deformation is not uniform and therefore the activation and deactivation criteria are not satisfied simultaneously throughout the body. We will see in this section that nonhomogeneous deformations are characterized by, depending on the deformation level, the occurrences of fronts that divide the body into regions containing only active elastin, both active elastin and collagen, and only active collagen.

3.1 HOMOGENEOUS DEFORMATION: UNIAXIAL EXTENSION OF A RECTANGULAR SLAB

3.1.1 Loading

In this section, we consider a rectangular slab of an incompressible dual mechanisms material that is stretched in its longitudinal direction with a stretch ratio λ. As is well known, the exact and explicit solution of the same problem for classical hyperelastic material is available without prior specification of strain energy functions (see these solutions for examples in Rivlin and Saunders [134] and Leigh [135]). This feature is useful for experimenters interested in obtaining material parameters. It will be shown that such an exact solution is also available for materials that possess dual mechanisms. This problem is governed by a single parameter (in this case, λ) making it valuable for explaining the dual mechanism in a simple way.

With respect to the Cartesian coordinates (X, Y, Z) with the origin at the center of the slab and the X, Y, and Z axis parallel to the sides of the slab of length L_o, W_o and H_o, respectively, the undeformed slab occupies the following domain:

$$X \in [-\frac{L_o}{2}, \frac{L_o}{2}], \qquad Y \in [-\frac{W_o}{2}, \frac{W_o}{2}], \qquad Z \in [-\frac{H_o}{2}, \frac{H_o}{2}]. \tag{3.1}$$

In the current/deformed configuration κ, the deformed length of the slab becomes L. The stretch ratio λ is defined as L/L_o. When only extension is considered, $\lambda > 1$. Positive normal uniform traction $\mathbf{t} = \pm\sigma\mathbf{e}_x$ are applied at surfaces $X = \pm L_o/2$, respectively. The lateral surfaces are traction free. Figure 12 shows the rectangular slab with its traction in x direction. In the resulting deformation, the position of arbitrary material points in the deformed or current configuration κ, identified using rectangular coordinates (x, y, z), can be related to these position in the undeformed or initial reference configuration, κ_1, identified by rectangular coordinates (X, Y, Z), as follows:

$$x = \lambda X, \qquad y = \frac{1}{\sqrt{\lambda}}Y, \qquad \text{and} \qquad z = \frac{1}{\sqrt{\lambda}}Z, \tag{3.2}$$

where the incompressibility restriction has been imposed.

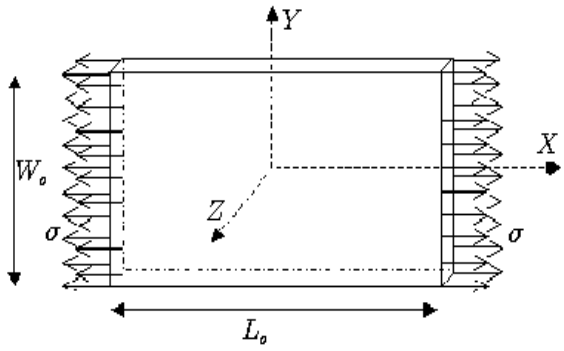

Figure 12: Uniaxial extension of a rectangular slab.

We suppose that the slab is being stretched according to (3.2) without causing the second mechanism to be activated. So here only the first mechanism, representing the response of elastin, is active. It follows from (3.2), that the deformation gradient $\mathbf{F_1}$ relative to original reference configuration κ_1 is:

$$\mathbf{F_1} = \text{DIAG}[\lambda, \frac{1}{\sqrt{\lambda}}, \frac{1}{\sqrt{\lambda}}], \tag{3.3}$$

where the notation $\text{DIAG}[\Lambda_1, \Lambda_2, \Lambda_3]$ is used to denote a three by three matrix with zero off diagonal components and nonzero Λ_1, Λ_2,and Λ_3 as the diagonal components. Using (3.3), the Left Cauchy Green strain tensor and its inverse: $\mathbf{B_1}$, and $\mathbf{B_1}^{-1}$ are:

$$\mathbf{B_1} = \text{DIAG}[\lambda^2, \frac{1}{\lambda}, \frac{1}{\lambda}], \qquad \mathbf{B_1}^{-1} = \text{DIAG}[\frac{1}{\lambda^2}, \lambda, \lambda]. \tag{3.4}$$

The first and second invariants of $\mathbf{B_1}$ denoted by I_1 and II_1 , respectively are

$$I_1 = \lambda^2 + \frac{2}{\lambda} \qquad \text{and} \qquad II_1 = \frac{1}{\lambda^2} + 2\lambda. \tag{3.5}$$

We suppose that the second mechanism representing the mechanical response by collagen fibers will be activated at some later level of deformation. As is discussed in previous section, we will employ scalar parameter s as defined in (2.4) to describe both the activation and later on the deactivation process. We suppose that the collagen recruitment and elastin breakage each occur at s satisfying the recruitment criterion (2.8) and deactivation criterion (2.15), respectively. However, according to (2.5), s is a function of invariants and so by (3.5),

$s = s(I_1, II_1) = \hat{s}(\lambda)$. Moreover, when s is a strictly monotonically increasing function of the invariants, then s is also a strictly monotonically increasing function of λ. This implies that for a given value of s_a, a root, say λ_a, for $A_a = 0$ in (2.7) can be found. Note that the value of s_a and the form of s must be constructed in a way to produce $\lambda_a > 1$. The progression of the deformation level can now be described simply by λ, with λ_a indicating the initiation of the second mechanism.

Furthermore we suppose that at some higher level deformation, the first mechanism is deactivated. In this case, a similar argument used before may be used to introduce λ_b that satisfies $s_b = s(\lambda_b)$ for $A_b = 0$ in (2.14) that indicates the occurrence of the deactivation. Here, we only consider that the deactivation occurs after the recruitment of the second material, so λ_b is always greater than λ_a. The activation and deactivation criteria introduced in (2.7) and (2.14), respectively then are reduced to

$$A_a = \lambda - \lambda_a \quad \text{and} \quad A_b = \lambda - \lambda_b. \tag{3.6}$$

The activation of the second mechanism and deactivation of the first mechanism correspond to $\lambda = \lambda_a$ and $\lambda = \lambda_b$, respectively.

We wish to obtain the relation between σ and λ during three stages of increasing λ:

- $\lambda < \lambda_a$: The stages before the recruitment of the second material,
- $\lambda_a \leq \lambda < \lambda_b$: The stages when the recruitment has occurred but before the deactivation of the first mechanism, and
- $\lambda_b \leq \lambda$: The stages after the deactivation.

Only three stages need to be evaluated since the nature of the deformation causes an instantaneous new material recruitment and instantaneous deactivation of the original material and so there is no partial process that needs to be considered.

When $\lambda < \lambda_a$, corresponding to $s < s_a$, the second mechanism is not activated and the strain energy function described by (2.18), is given by $W = W_1(I_1, II_1)$. The Cauchy stress at each material point depends only on the deformation gradient of the first mechanism, $\mathbf{F_1}$,

through the relation (2.3). Following (3.4) and (2.17) for $s < s_a$, the nonzero components of the Cauchy stress tensor are as follows:

$$T_{xx} = -p + 2\lambda^2 \frac{\partial W}{\partial I_1} - \frac{2}{\lambda^2} \frac{\partial W}{\partial I I_1} \quad , \tag{3.7}$$

$$T_{yy} = T_{zz} = -p + \frac{2}{\lambda} \frac{\partial W}{\partial I_1} - 2\lambda \frac{\partial W}{\partial I_2}, \tag{3.8}$$

where p is the Lagrangian multiplier arising from the incompressibility condition and the terms accompanying it are called the extra stress of T_{xx},T_{yy}, and T_{zz}. Since λ is independent of the material position, it follows that the extra stress terms in (3.7) and (3.8) are too. Moreover, in order that (3.7) and (3.8) satisfy the equilibrium, then ∇p must be zero, i.e, p must be a constant. This implies that the body experiences uniform stress. The zero traction on surfaces $Y = \pm H_o/2$ and $Z = \pm W_o/2$ imply that $T_{yy} = T_{zz} = 0$. While the nonzero traction vector $\pm\sigma e_x$ on surface $X = \pm L_o/2$ implies that $T_{xx} = \sigma$ throughout the body. The value of p then can be obtained from (3.8) and it can be substituted into (3.7) to obtain T_{xx}. The relation between σ and λ are therefore:

$$\sigma = 2(-\frac{1}{\lambda} + \lambda^2)(\frac{\partial W}{\partial I_1} + \frac{1}{\lambda} \frac{\partial W}{\partial I I_1}), \tag{3.9}$$

throughout the body. For classical hyperelastic materials the relation (3.9) is true for any λ greater than one. However, the second mechanism that will be introduced when $\lambda = \lambda_a$ will contribute to the stress generation in the body. The relation (3.9) then is true only when $1 \leq \lambda < \lambda_a$.

We suppose that the slab is stretched further to $\lambda = \lambda_a$. At this level of deformation, the material points in the body will occupy the following coordinate points:

$$\hat{x} = \lambda_a X, \qquad \hat{y} = \frac{1}{\sqrt{\lambda_a}} Y, \qquad \text{and} \qquad \hat{z} = \frac{1}{\sqrt{\lambda_a}} Z. \tag{3.10}$$

We denote this configuration as κ_2 and let the body be further stretched so that the activation criterion is satisfied but not the deactivation criterion. In other word, λ is increased so that $\lambda_a \leq \lambda < \lambda_b$. The relation (3.2) still holds for the original material (the first material). The second material will be activated with respect to the configuration κ_2. Following (3.2) and (3.10), the relationship between the position of arbitrary material points of the recruited

material in the current configuration κ relative to its position in reference configuration κ_2 can be written as follows:

$$x = \lambda X = \frac{\lambda}{\lambda_a}\hat{x}, \qquad y = \frac{1}{\sqrt{\lambda}}Y = \frac{\sqrt{\lambda_a}}{\sqrt{\lambda}}\hat{y}, \qquad \text{and} \qquad z = \frac{1}{\sqrt{\lambda}}Z = \frac{\sqrt{\lambda_a}}{\sqrt{\lambda}}\hat{z}. \tag{3.11}$$

It follows from (3.11) that the deformation gradient of the second mechanism relative to the reference configuration κ_2 , $(\mathbf{F_2})$, and the corresponding Left Cauchy Green strain tensor and its inverse, $\mathbf{B_2}$ and $\mathbf{B_2^{-1}}$, respectively, are:

$$\mathbf{F_2} = \text{DIAG}[\frac{\lambda}{\lambda_a}, \frac{\sqrt{\lambda_a}}{\sqrt{\lambda}}, \frac{\sqrt{\lambda_a}}{\sqrt{\lambda}}], \tag{3.12}$$

$$\mathbf{B_2} = \text{DIAG}[\frac{\lambda^2}{\lambda_a^2}, \frac{\lambda_a}{\lambda}, \frac{\lambda_a}{\lambda}], \qquad \mathbf{B_2}^{-1} = \text{DIAG}[\frac{\lambda_a^2}{\lambda^2}, \frac{\lambda}{\lambda_a}, \frac{\lambda}{\lambda_a}]. \tag{3.13}$$

Generally, the deformation gradient $\mathbf{F_2}$ can be obtained using (2.12) with $t = t_2$ corresponds to $\lambda = \lambda_a$.

After the second mechanism is activated, the strain energy function is composed of two contributions: W_1 and W_2 representing the original and the recruited materials, respectively, as is described in (2.18) for $s_a \leq s < s_b$. It follows from (2.17), (2.18),(3.4), and (3.13), that the nonzero components of Cauchy stress tensor are as follows :

$$T_{xx} = -p + 2\lambda^2\frac{\partial W}{\partial I_1} - \frac{2}{\lambda^2}\frac{\partial W}{\partial II_1} + 2\frac{\lambda^2}{\lambda_a^2}\frac{\partial W}{\partial I_2} - 2\frac{\lambda_a^2}{\lambda^2}\frac{\partial W}{\partial II_2} \quad , \tag{3.14}$$

$$T_{yy} = T_{zz} = -p + \frac{2}{\lambda}\frac{\partial W}{\partial I_1} - 2\lambda\frac{\partial W}{\partial II_1} + 2\frac{\lambda}{\lambda_a}\frac{\partial W}{\partial I_2} - 2\frac{\lambda_a}{\lambda}\frac{\partial W}{\partial II_2}. \tag{3.15}$$

The stress strain relations (3.14) and (3.15) can be solved so that they satisfy the equilibrium equation and the boundary conditions using the procedure previously described. It follows that relation between σ and λ, when $\lambda_a \leq \lambda < \lambda_b$ is:

$$\sigma = 2(-\frac{1}{\lambda} + \lambda^2)(\frac{\partial W}{\partial I_1} + \frac{1}{\lambda}\frac{\partial W}{\partial II_1}) + 2(-\frac{\lambda_a}{\lambda} + \frac{\lambda^2}{\lambda_a^2})(\frac{\partial W}{\partial I_2} + \frac{\lambda_a}{\lambda}\frac{\partial W}{\partial II_2}). \tag{3.16}$$

We now consider stretch with $\lambda \geq \lambda_b$, when the deactivation criterion of the first mechanism is satisfied throughout the body. At this state of deformation the original material is deactivated and so the strain energy function contributed by the first mechanism is disregarded. Therefore, for $\lambda_b \leq \lambda$:

$$W = W_2(I_2, II_2), \tag{3.17}$$

as is described in (2.18) for $s_b \leq s$. It follows from (2.17), (2.18), and (3.13) that the nonzero components of Cauchy stress tensor are:

$$T_{xx} = -p + 2\frac{\lambda^2}{\lambda_a^2}\frac{\partial W}{\partial I_2} - 2\frac{\lambda_a^2}{\lambda^2}\frac{\partial W}{\partial II_2} \quad , \tag{3.18}$$

$$T_{yy} = T_{zz} = -p + 2\frac{\lambda}{\lambda_a}\frac{\partial W}{\partial I_2} - 2\frac{\lambda_a}{\lambda}\frac{\partial W}{\partial II_2}. \tag{3.19}$$

The use of standard procedures previously employed for $\lambda < \lambda_b$ reveals the following relation between σ and λ:

$$\sigma = 2(-\frac{\lambda_a}{\lambda} + \frac{\lambda^2}{\lambda_a^2})(\frac{\partial W}{\partial I_2} + \frac{\lambda_a}{\lambda}\frac{\partial W}{\partial II_2}), \tag{3.20}$$

that can be obtained simply by removing the first term of (3.16).

3.1.2 Unloading

We shall now study the behavior of the relations between σ and λ during decreasing λ. We suppose that the maximum of the stretch ratio λ before unloading is denoted by λ^*. It follows from the loading cases that only three cases of λ^* must be considered:

- Case 1: $\lambda^* < \lambda_a$

  In this case, the unloading begins before the onset of collagen fibers recruitment. The unloading path will follow the curve of σ versus λ for $\lambda < \lambda_a$ (3.9). Here, the material response resembles that of classical hyperelastic materials. It can be seen from (3.9), the zero stress corresponds to $\lambda = 1$, the original reference configuration, κ_1.

- Case 2: $\lambda_a \leq \lambda^* < \lambda_b$

  In this case, the collagen fibers have been recruited when the unloading begins. However, the recruited material only contributes when $\lambda \geq \lambda_a$ and the contribution will be ceased

when the criterion is not satisfied, *i.e.* $\lambda < \lambda_a$. So during unloading, the relation for σ versus λ follows (3.16) when $\lambda \geq \lambda_a$ and it follows (3.9) when $\lambda < \lambda_a$. It is clear therefore that in this case, the slab will return to the original reference configuration for its zero stress condition.

- Case 3: $\lambda^* \geq \lambda_b$

  Here, the unloading begins after the elastin breakage at $\lambda = \lambda_b$. When λ is reduced so that $\lambda < \lambda_b$, the degraded elastin, cannot be reactivated. The path of the unloading curve therefore cannot follow (3.16) nor (3.9), instead it follows (3.20). However, it can be seen from (3.20) that the zero stress ($\sigma = 0$) corresponds to $\lambda = \lambda_a > 1$. This implies that the slab doesn't return to its original undeformed configuration but rather it occupies a new unloaded configuration. The unloaded configuration corresponds to the reference configuration of the second mechanism or recruited material.

3.1.3 Summary

The exact solution of a slab composed of dual mechanism material undergoing uniaxial extension has been presented. Clearly, the solution doesn't require specification of the strain energy function W *a priori*. Namely, the deformation is a controllable deformation for the dual mechanism material. It can be seen in (3.9), (3.16), and (3.20) that in this deformation, the deformation parameters s_a and s_b are simplified to the stretch ratios λ_a and λ_b, respectively.

The relation between σ and λ in (3.9) can be seen as a composition of a functional of stretch, denote $E(\Lambda)$, defined as

$$E(\Lambda) \equiv 2(-\frac{1}{\Lambda} + \Lambda^2) \tag{3.21}$$

and functional of derivatives of the strain energy function, denote w_1, defined as

$$w_1(\lambda) \equiv (\frac{\partial W}{\partial I_1} + \frac{1}{\lambda}\frac{\partial W}{\partial I I_1}) \tag{3.22}$$

that is commonly known as the response function (see Rivlin and Sanders [134]). The relation (3.9) can be written as follows;

$$\sigma = E(\lambda) w_1(\lambda). \tag{3.23}$$

Table 1: The relation between σ and λ during uniaxial loading. The definitions of $E(\Lambda), w_1, w_2$ are given by (3.21),(3.22),and (3.24), respectively.

Range of λ	σ vs. λ
$1 \leq \lambda < \lambda_a$	$\sigma = E(\lambda)w_1(\lambda)$
$\lambda_a < \lambda \leq \lambda_b$	$\sigma = E(\lambda)w_1(\lambda) + E(\frac{\lambda}{\lambda_a})w_2(\lambda)$
$\lambda_b \leq \lambda$	$\sigma = E(\frac{\lambda}{\lambda_a})w_2(\lambda)$

The same functional E but with different argument; $\Lambda = \lambda/\lambda_a$, can be seen in the second term of (3.16) and also in (3.20). Another response function is found in (3.16) and (3.20), denoted w_2, and defined as follows;

$$w_2(\lambda) \equiv (\frac{\partial W}{\partial I_2} + \frac{\lambda_a}{\lambda}\frac{\partial W}{\partial I I_2}). \tag{3.24}$$

Using the definitions of E, w_1 and w_2 above, the relationship between σ and λ during loading and unloading can be summarized in Tables 1 and 2. Generally, the two strain energy functions W_1 and W_2 for (2.18) can be of two different types. In Table 4, values of the response functions w_1 and w_2 used in (3.9),(3.16) and (3.20) for different types of strain energy functions are presented. In that table, α_1, β_1 and γ_1 are material parameters of the first mechanism, while α_2, β_2, and γ_2 are of the second mechanism. While the response functions: w_1 and w_2 are simply constants for Neo Hookean materials, w_1 for Mooney Rivlin materials is a linear function of stretch ratio, λ. For the second mechanism, w_2 for Mooney Rivlin materials still depends linearly on λ, since λ_a is merely a constant. Here, λ_a serves as an indirect material parameter that can be derived from the more general scalar parameter s_a that indicates the deformation level of the initiation of the second mechanism. For the exponential type strain energy, the first invariants of the first and second mechanisms denoted by I_1 and I_2, respectively, are included in the response functions. The first invariant of the second mechanism, I_2, for uniaxial stretching is:

$$I_2 = \frac{\lambda^2}{\lambda_a^2} + 2\frac{\lambda_a}{\lambda}. \tag{3.25}$$

Table 2: The relation between σ and λ during uniaxial unloading for three different possible maximum stretch λ^*. The definitions of $E(\Lambda), w_1, w_2$ are given by (3.21),(3.22),and (3.24), respectively.

Location of λ^*	Range of λ	σ vs. λ
$1 \le \lambda^* < \lambda_a$	$1 \le \lambda < \lambda_a$	$\sigma = E(\lambda)w_1(\lambda)$
$\lambda_a \le \lambda^* < \lambda_b$	$\lambda_a < \lambda \le \lambda_b$	$\sigma = E(\lambda)w_1(\lambda) + E(\frac{\lambda}{\lambda_a})w_2(\lambda)$
	$1 \le \lambda < \lambda_a$	$\sigma = E(\lambda)w_1(\lambda)$
$\lambda_b \le \lambda^*$	$1 \le \lambda$	$\sigma = E(\frac{\lambda}{\lambda_a})w_2(\lambda)$

Table 3: Examples of W_1 and W_2 from commonly used strain energy functions.

W	W_1	W_2
Neo Hookean	$\frac{\alpha_1}{2}(I_1 - 3)$	$\frac{\alpha_2}{2}(I_2 - 3)$
Mooney Rivlin	$\frac{\alpha_1}{2}(I_1 - 3) + \frac{\beta_1}{2}(II_1 - 3)$	$\frac{\alpha_2}{2}(I_2 - 3) + \frac{\beta_2}{2}(II_2 - 3)$
Exponential	$\frac{\alpha_1}{2\gamma_1}e^{\gamma_1(I_1-3)}$	$\frac{\alpha_2}{2\gamma_2}e^{\gamma_2(I_2-3)}$

Table 4: Some examples of w_1 and w_2 for uniaxial extension derived from the strain energy functions tabulated in Table 3. The definitions of w_1 and w_2 are given by (3.22) and (3.24), respectively.

W	$w_1(\lambda)$	$w_2(\lambda)$
Neo Hookean	$\frac{\alpha_1}{2}$	$\frac{\alpha_2}{2}$
Mooney Rivlin	$\frac{\alpha_1}{2} + \frac{\beta_1}{2}\frac{1}{\lambda}$	$\frac{\alpha_2}{2} + \frac{\beta_2}{2}\frac{\lambda_a}{\lambda}$
Exponential	$\frac{\alpha_1}{2}e^{\gamma_1(I_1-3)}$	$\frac{\alpha_2}{2}e^{\gamma_2(I_2-3)}$

Table 5: Material parameters for exponential type strain energy function (2.21) used as an example in this chapter. Parameters s_a and s_b indicate the activation and deactivation criteria, respectively.

Material parameters	
α_1 $(10^3 dynes/cm^2)$	71.21986
γ_1	0.6224785
α_2	312.6121
γ_2	1.867605
s_a	1.4237
s_b	3.479

3.1.4 An example and discussion

It will be useful to consider a specific example for the strain energy density function W and plot the curves of σ versus λ. We will present results for an exponential strain energy function (2.21), since this type is most relevant to this work. Table 5 displays values of the six material parameters used in this discussion. These values are obtained from a nonlinear regression analysis of real experimental data that will be discussed Section 3.3 where the inflation of a cylindrical membrane is discussed. The results of uniaxial extension of the dual mechanism material (2.21) with material constants given in Table 5 are presented in Figure 13. Four curves depicted in Figure 13. Curve OAB shows the relation $\sigma(\lambda)$ for selected W without activating the second mechanism, thus mimicking the response of a classical elastic material. Curve OAC shows the results of activating the second mechanism that represents the recruited material without considering the deactivation of the first material. Here, the second mechanism occurs when the deformation parameter s reaches s_a corresponding to $\lambda = \lambda_a = 1.8241$ indicated by point A. It can be seen that curve OAC deviates from curve OAB at point A to a stiffer relation as is expected when the second mechanism contributes to the load bearing. The two curves OAB and OAC represent the unloading paths as well as loading paths. When unloading occurs along three curves, the deformed body will return to

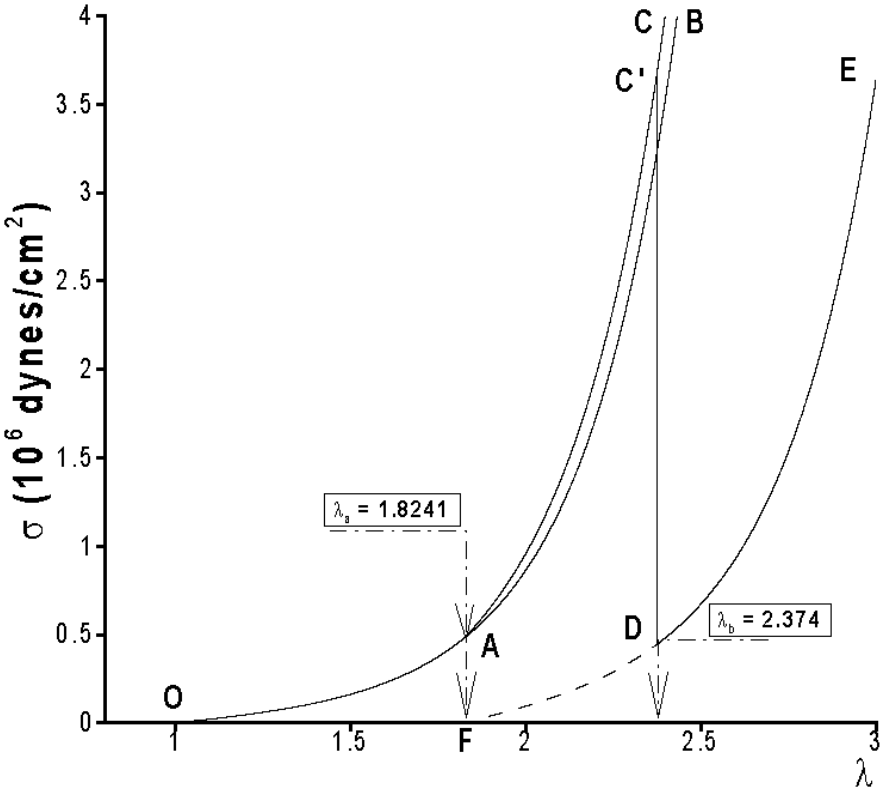

Figure 13: Resulting σ vs. λ curves of a material composed of two mechanisms both of which are represented by an exponential type strain energy function under uniaxial stretch (loading and unloading). The second mechanism is initiated at $\lambda = \lambda_a = 1.8241$ and the first mechanism is terminated at $\lambda = \lambda_b = 2.374$.

point O, the original reference configuration. Line OAC'DE represents the relation of $\sigma(\lambda)$ when the first mechanism is deactivated, which represents the elastin breakage, following the recruitment or the activation of the second mechanism. The deactivation occurs when the stretch ratio $\lambda = \lambda_b = 2.374$, indicated by point C', corresponds to deformation parameter $s = s_b$. The jump that occurs at C' clearly is caused by the termination of the participation of the first mechanism in the load bearing. This termination happens abruptly throughout the body at a single stretch ratio, $\lambda = \lambda_b$. Curve DE therefore shows the response of material to further load bearing when only the second mechanism is active. Since the reactivation of damaged elastin is not considered, the unloading that occurs after $\lambda = \lambda_b$ will not follow line EDC'AO. Instead, curve EDF indicates the path taken by such an unloading case. Clearly, the zero stress state corresponds to a value of $\lambda > 1$ indicated by point F. This stretch ratio, not surprisingly, corresponds to $\lambda = \lambda_a$, the stretch ratio at which the second mechanism is activated. Hence, the unloaded configuration is the reference configuration of the second mechanism that differs from the original reference configuration.

The last unloading case suggests one method for experimentally handling material parameter identification of λ_a, *i.e* to detect or obtain the level of deformation at which the second mechanism is activated. For a dual mechanism material of which each of the criterion, either the activation or deactivation, occurs abruptly, the values of λ_a and λ_b, in theory, can be discovered by performing unloading for increasing values of λ^* until a new unloaded configuration is revealed. The new unloaded configuration theoretically corresponds to $\lambda = \lambda_a$. The corresponding λ^* theoretically can give an approximation of the value of λ_b. The values of s_a and s_b can be determined from measuring λ_a and λ_b and using the form of $s(I_1, II_1)$ that is formulated through experiments.

The curve FDE can be viewed as a new loading and unloading curve for an elastic material with a reference configuration corresponding to $\lambda = \lambda_a$. The response therefore can be seen as classical elastic response with a single mechanism (the second mechanism). The overall response of the material however is inelastic in a sense that the material doesn't return to the original reference configuration. The very important feature of this model is the coupling of two elastic responses: before and after the breakage, in one deformation history. This allows us to model the transition of a normal nonaneurysmal arterial wall section to an

aneurysmal wall section. And this is particularly important for more complex deformations where the tissue cannot be merely treated as two different elastic materials.

3.2 HOMOGENEOUS DEFORMATION: BIAXIAL EXTENSION OF A RECTANGULAR SLAB

3.2.1 Loading

In this section, we will discuss biaxial extension of a dual mechanism rectangular slab, for which both mechanisms are hyperelastic, isotropic, and incompressible. As is known, an explicit solution of biaxial extension of classical hyperelastic materials is available even without prior specification of the strain energy function [134, 135]. The availability of such a solution and it's simple boundary conditions attract investigators to perform biaxial stretch experiments on both rubbery materials [134, 136] and biological tissue samples [120]. We will show here that within the framework of dual mechanism materials, an exact solution is also available. More importantly, the problem is presented to show the use of scalar parameter s defined in (2.4) for describing the deformation stages experienced by the slab. As is explained in the previous section, the parameter s is used to determine the initiation of the second mechanism and the termination of the first mechanism.

With respect to Cartesian coordinates (X, Y, Z) with the origin at the center of the slab and the X,Y, and Z axis parallel to the sides of length L_o, W_o, and H_o, respectively, the undeformed slab occupies the following domain:

$$X \in [-\frac{L_o}{2}, \frac{L_o}{2}], \qquad Y \in [-\frac{W_o}{2}, \frac{W_o}{2}], \qquad Z \in [-\frac{H_o}{2}, \frac{H_o}{2}]. \tag{3.26}$$

We first suppose that the slab is biaxially stretched without causing the second mechanism (collagen recruitment) to be activated. Therefore only one mechanism (representing elastin activity) is active during this process. In the deformed or current configuration κ, the deformed length and width of the slab are L and W, respectively. The extension ratios in the longitudinal (X) and lateral (Y) directions are given by $\lambda_x = L/L_o \geq 1$ and $\lambda_y = W/W_o \geq 1$, respectively. At surfaces $X = \pm L_o/2$ and $Y = \pm W_o/2$, we apply positive normal uniform

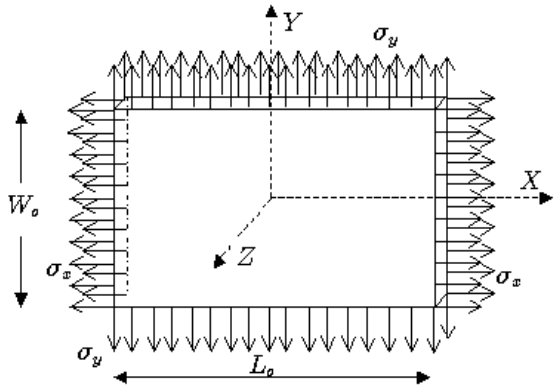

Figure 14: Biaxial stretch of a rectangular slab.

traction $\pm\sigma_x e_x$ and $\pm\sigma_y e_y$, respectively. The remaining surfaces are traction free. Figure (14) shows the rectangular slab with its traction in x and y directions. We wish to obtain the relations between σ_x and σ_y and λ_x and λ_y. The relationship between the position of arbitrary material points in the deformed or current configuration κ, identified by rectangular coordinates (x, y, z), relative to its position in the undeformed or reference configuration κ_1 identified by coordinates (X, Y, Z) is as follows:

$$x = \lambda_x X, \qquad y = \lambda_y Y, \qquad \text{and} \qquad z = \lambda_z Z = \frac{Z}{\lambda_x \lambda_y}, \tag{3.27}$$

where λ_x and λ_y are constants representing the stretch ratios in the longitudinal and lateral directions, respectively. It can be seen in (3.27) that the restriction of material incompressibility, $\lambda_x \lambda_y \lambda_z = 1$, has been implemented.

The body with active first mechanism (representing elastin) in κ_1 deforms according to (3.27). The deformation gradient of the first mechanism denote $\mathbf{F_1}$ relative to the original reference configuration κ_1 is obtained from (3.27) as follows:

$$\mathbf{F_1} = \text{DIAG}[\lambda_x, \lambda_y, \frac{1}{\lambda_x \lambda_y}]. \tag{3.28}$$

The Left Cauchy Green strain tensor and its inverse for the first mechanism, $\mathbf{B_1}$ and $\mathbf{B_1}^{-1}$, can be obtained from (3.28), and are as follows:

$$\mathbf{B_1} = \text{DIAG}[\lambda_x^2, \lambda_y^2, \frac{1}{\lambda_x^2 \lambda_y^2}], \qquad \mathbf{B_1}^{-1} = \text{DIAG}[\frac{1}{\lambda_x^2}, \frac{1}{\lambda_y^2}, \lambda_x^2 \lambda_y^2]. \tag{3.29}$$

The first and second invariants of $\mathbf{B_1}$ denote I_1 and II_1, respectively are:

$$I_1 = \lambda_x^2 + \lambda_y^2 + \frac{1}{\lambda_x^2 \lambda_y^2}, \qquad II_1 = \frac{1}{\lambda_x^2} + \frac{1}{\lambda_y^2} + \lambda_x^2 \lambda_y^2. \tag{3.30}$$

Here, since the deformation is described using two deformation parameters; λ_x and λ_y, it is convenient to employ the scalar parameter s as is defined in (2.4), with the invariants $I_1 = I_1(\lambda_x, \lambda_y)$ and $II_1 = II_1(\lambda_x, \lambda_y)$ given by (3.30) as the arguments.

We suppose that at this deformation level, the second mechanism is not activated yet. The Cauchy stress tensor therefore is generated based on the strain energy function $W = W_1$ as described in (2.18) for $s < s_a$. Therefore, the nonzero components of the Cauchy stress tensor obtained from (2.17),(2.18) and (3.29. 1 and 2) are as follows:

$$T_{\alpha\alpha} = -p + 2\lambda_\alpha^2 \frac{\partial W}{\partial I_1} - \frac{2}{\lambda_\alpha^2} \frac{\partial W}{\partial II_1}, \tag{3.31}$$

where $\alpha = x$ or y and no sum on α.

$$T_{zz} = -p + \frac{2}{\lambda_x^2 \lambda_y^2} \frac{\partial W}{\partial I_1} - 2\lambda_x^2 \lambda_y^2 \frac{\partial W}{\partial II_1}. \tag{3.32}$$

Clearly, (3.29) imply that the off diagonal components are zero. Moreover, since both λ_x and λ_y are constants, the extra stress tensor for each of the nonzero components are constant too. Moreover, the equilibrium equations $T_{ij,j} = 0$, implies that p is a constant and therefore the stresses are uniformly distributed throughout the body and the boundaries. Zero traction at the $Z = \pm H_o/2$ surfaces implies that $T_{zz} = 0$ throughout the body, while the nonzero traction applied at other surfaces imply that $T_{yy} = \sigma_y$ and $T_{xx} = \sigma_x$ throughout the body. The Lagrangian multiplier p can be obtained from (3.32) and can be substituted into (3.31), to obtain the following relations:

$$\sigma_\alpha = 2(\lambda_\alpha^2 - \lambda_z^2)\left(\frac{\partial W}{\partial I_1} + \frac{1}{\lambda_\alpha^2 \lambda_z^2} \frac{\partial W}{\partial II_1}\right), \tag{3.33}$$

where $\lambda_z = 1/(\lambda_x \lambda_y)$ and $\alpha = x$ or y.

We now suppose that the deformation continues and the second mechanism is activated. During loading, the deformation parameter s increases as the stretch progresses. We suppose that the activation criterion and the deactivation criterion given by (2.8) and (2.15), respectively, are used in this problem. As mentioned before, we will employ (2.5) to measure

the deformation level. More specifically, in this example we will use the formulation for s introduced in Chapter 2 (equation 2.22). Here, I_1 is given by (3.30) and the expanded s formulation for this case is given as follows:

$$s = \hat{s}(\lambda_x, \lambda_y) = \lambda_x^2 + \lambda_y^2 + \frac{1}{\lambda_x^2 \lambda_y^2} - 3. \tag{3.34}$$

We suppose that the activation criterion (2.8) is met when $\lambda_x = \lambda_{xa}$ and $\lambda_y = \lambda_{ya}$, where $s = \hat{s}(\lambda_{xa}, \lambda_{ya}) = s_a$. Generally, there is an infinite number of combinations of λ_{xa} and λ_{ya} that satisfy the criterion (2.8) (for all possible loading paths). So, unlike the uniaxial case, there is a set of configurations, say K_a, satisfying the activation criterion, (2.8). Similarly, there is a set of configurations, say K_b, satisfying the deactivation criterion (2.15). We denote the pairs of λ_x and λ_y satisfying (2.15) as λ_{xb} and λ_{yb}, respectively. Clearly, recalling (3.34), $\hat{s}(\lambda_{xb}, \lambda_{yb}) = s_b$. The pairs of λ_{xa} and λ_{ya} can be plotted on a 2D coordinate system with λ_x and λ_y as the axes. The pairs form a curve along which the s values equal to s_a ($s = s_a$ curve). Similarly, the plot of $(\lambda_{xb}, \lambda_{yb})$ form another curve along which $s = s_b$ ($s = s_b$ curve). Figure 15 shows curves PQ and RS representing $s = s_a$ and $s = s_b$ curves, respectively. Figure 15 also displays two examples of possible loading paths represented by lines OC and OD. The two paths represent loading paths for which λ_y are linearly dependent on λ_x. The loading path OC crosses the s_a curve at point A, while the loading path OD crosses the same curve at point F. Points A and F indicate two different configurations, yet they can equally function as the reference configuration of the activated second mechanism. Similarly, the two loading paths cross the s_b curve at two different locations (denoted by points B and E) representing two possible configurations at which the first mechanism is deactivated.

We suppose that we have reached a configuration at which $s = s_a$. Because the deformation is homogeneous, s will be uniform throughout the body and provided that s_a is space independent, the activation criterion will be satisfied simultaneously throughout the body. When $\lambda_x = \lambda_{xa}$ and $\lambda_y = \lambda_{ya}$, the body will take the following configuration, denoted by $\kappa_2 \in K_a$:

$$\hat{x} = \lambda_{xa} X, \qquad \hat{y} = \lambda_{ya} Y, \qquad \text{and} \qquad \hat{z} = \frac{1}{\lambda_{xa}\lambda_{ya}} Z. \tag{3.35}$$

At this deformation level, the second mechanism, representing the recruited material, is activated. When the body is further deformed, the original or old material will deform

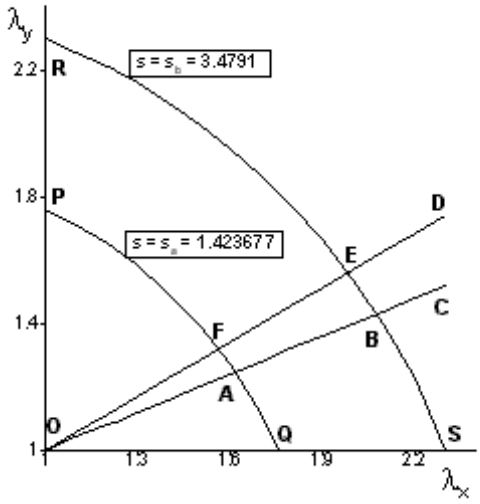

Figure 15: The curves of $s = s_a$ (PQ) and $s = s_b$ (RS) for the biaxial stretch case. The lines OC and OD show examples of two possible loading paths. The two lines cross $s = s_a$ and $s = s_b$ curves at two different locations for each curve, indicating that each criterion, activation or deactivation, can be satisfied at more than one configuration.

according to the first mechanism. The deformation gradient of the mechanism of the original material relative to reference configuration κ_1 is still given by (3.28). The recruited material, however, will take configuration κ_2 as its reference configuration. The deformation gradient relative to configuration κ_2 can be described using (3.27) and (3.35). The mapping can be written as follows:

$$x = \lambda_x X = \frac{\lambda_x}{\lambda_{xa}}\hat{x}, \qquad y = \lambda_y Y = \frac{\lambda_y}{\lambda_{ya}}\hat{y}, \qquad \text{and} \qquad z = \frac{Z}{\lambda_x\lambda_y} = \frac{\lambda_{xa}\lambda_{ya}}{\lambda_x\lambda_y}\hat{z}, \tag{3.36}$$

where the incompressibility restriction is used. The gradient of deformation of the second mechanism relative to reference configuration κ_2 and the Left Cauchy Green tensor of the second mechanism and its inverse are:

$$\mathbf{F_2} = \text{DIAG}[\frac{\lambda_x}{\lambda_{xa}}, \frac{\lambda_y}{\lambda_{ya}}, \frac{\lambda_{xa}\lambda_{ya}}{\lambda_x\lambda_y}]. \tag{3.37}$$

$$\mathbf{B_2} = \text{DIAG}[\frac{\lambda_x^2}{\lambda_{xa}^2}, \frac{\lambda_y^2}{\lambda_{ya}^2}, \frac{\lambda_{xa}^2\lambda_{ya}^2}{\lambda_x^2\lambda_y^2}], \qquad \mathbf{B_2}^{-1} = \text{DIAG}[\frac{\lambda_{xa}^2}{\lambda_x^2}, \frac{\lambda_{ya}^2}{\lambda_y^2}, \frac{\lambda_x^2\lambda_y^2}{\lambda_{xa}^2\lambda_{ya}^2}]. \tag{3.38}$$

The deformation gradient (3.37) can be recovered using relation (2.12) with $\mathbf{F_1}$ given by (3.28), to obtain:

$$\mathbf{F_2} = \mathbf{F_1}.\mathbf{F_1}^{-1}|_{(\lambda_{xa},\lambda_{ya})} \tag{3.39}$$

Therefore, the deformation gradient $\mathbf{F_2}$ is the product of the deformation gradient of the first mechanism and its inverse, evaluated at $s = s_a$.

The nonzero components of Cauchy stress tensor are obtained from (2.17), (2.18) for $s_a \leq s < s_b$, (3.29), and (3.38) as follows:

$$T_{\alpha\alpha} = -p + 2\lambda_\alpha^2\frac{\partial W}{\partial I_1} - \frac{2}{\lambda_\alpha^2}\frac{\partial W}{\partial II_1} + 2\frac{\lambda_\alpha^2}{\lambda_{\alpha a}^2}\frac{\partial W}{\partial I_2} - 2\frac{\lambda_{\alpha a}^2}{\lambda_x^2}\frac{\partial W}{\partial II_2}, \tag{3.40}$$

where $\alpha = x$ or y and

$$T_{zz} = -p + 2\frac{1}{\lambda_x^2\lambda_y^2}\frac{\partial W}{\partial I_1} - 2\lambda_x^2\lambda_y^2\frac{\partial W}{\partial II_1} + 2\frac{\lambda_{xa}^2\lambda_{ya}^2}{\lambda_x^2\lambda_y^2}\frac{\partial W}{\partial I_2} - 2\frac{\lambda_x^2\lambda_y^2}{\lambda_{xa}^2\lambda_{ya}^2}\frac{\partial W}{\partial II_2}. \tag{3.41}$$

The boundary conditions, equilibrium equations and previously used standard arguments will lead to the following relations:

$$\sigma_\alpha = 2(\lambda_\alpha^2 - \lambda_z^2)(\frac{\partial W}{\partial I_1} + \frac{1}{\lambda_\alpha^2\lambda_z^2}\frac{\partial W}{\partial II_1}) + 2(\frac{\lambda_\alpha^2}{\lambda_{\alpha a}^2} - \frac{\lambda_{za}^2}{\lambda_z^2})(\frac{\partial W}{\partial I_2} + \frac{\lambda_{\alpha a}^2\lambda_{za}^2}{\lambda_\alpha^2\lambda_z^2}\frac{\partial W}{\partial II_2}), \tag{3.42}$$

where $\alpha = x$ or y, so $\lambda_{\alpha a}$ is either λ_{xa} or λ_{ya}, and $\lambda_z = 1/(\lambda_x\lambda_y)$, $\lambda_{za} = 1/(\lambda_{xa}\lambda_{ya})$. We can see that (3.42) is composed of the stress contribution of the original material, shown in the first term, and the contribution of the recruited material, shown in the second term.

We will suppose that after the second mechanism is activated, s increases so that $s = s_b > s_a$. In any case, the deactivation is initiated when $\lambda_x = \lambda_{xb}$ and $\lambda_y = \lambda_{yb}$, where $s = \hat{s}(\lambda_{xb}, \lambda_{yb}) = s_b$. Similar to the activation case, there is a set of configurations, say K_b, satisfying deactivation criterion (2.15).

When the level of deformation is further increased until $s > s_b$, the contribution of the first mechanism in (3.42) is terminated. The strain energy function W now is composed of only the second mechanism, so that $W = W_2(I_2, II_2)$ as described in (2.18) for $s_b \leq s$. The stresses can be obtained from (2.17), (2.18) for $s_b \leq s$, and (3.38) as follows:

$$T_{\alpha\alpha} = -p + 2\frac{\lambda_\alpha^2}{\lambda_{\alpha a}^2}\frac{\partial W}{\partial I_2} - 2\frac{\lambda_{\alpha a}^2}{\lambda_x^2}\frac{\partial W}{\partial II_2}, \tag{3.43}$$

where $\alpha = x$ or y and no summation on α and

$$T_{zz} = -p + 2\frac{\lambda_{xa}^2\lambda_{ya}^2}{\lambda_x^2\lambda_y^2}\frac{\partial W}{\partial I_2} - 2\frac{\lambda_x^2\lambda_y^2}{\lambda_{xa}^2\lambda_{ya}^2}\frac{\partial W}{\partial II_2}. \tag{3.44}$$

Using similar procedure previously used for $s \leq s_a$, the equilibrium equations and the boundary conditions lead to the following relations:

$$\sigma_\alpha = 2\left(\frac{\lambda_\alpha^2}{\lambda_{\alpha a}^2} - \frac{\lambda_{za}^2}{\lambda_z^2}\right)\left(\frac{\partial W}{\partial I_2} + \frac{\lambda_{\alpha a}^2\lambda_{za}^2}{\lambda_\alpha^2\lambda_z^2}\frac{\partial W}{\partial II_2}\right), \tag{3.45}$$

where $\alpha = x$ or y. We note that the last relation (3.45) can be obtained simply by removing the contribution of the first mechanism in the first term of (3.42).

3.2.2 A special case: equibiaxial extension

When both stretch ratios; λ_x and λ_y are maintained equal, so that $\lambda_x = \lambda_y = \lambda$ during the loading (equibiaxial extension), the relations (3.33),(3.42) and (3.45) are simplified. It should be clear from (3.33) that during equibiaxial loading, σ_x and σ_y become equal, say equal to σ, and the following relation is true:

$$\sigma = 2(\lambda^2 - \frac{1}{\lambda^4})(\frac{\partial W}{\partial I_1} + \lambda^2 \frac{\partial W}{\partial II_1}). \tag{3.46}$$

When λ is increased so that s, defined by (3.30) for $\lambda_x = \lambda_y = \lambda$, is equal to s_a, the second mechanism is activated. The body occupies configuration $\kappa_2 \in K_a$ where the value of the scalar parameter s is given by $\lambda = \lambda_a$ where $s(I_1(\lambda), II_1(\lambda)) = s_a$. Here, λ_a is a special case of the set of pairs of $\lambda_{xa}, \lambda_{ya}$ that have equal value.

Provided that $\lambda_{xa} = \lambda_{ya} = \lambda_a$, it's easy to see that in (3.42), (and of course in (3.45)), $\sigma_x = \sigma_y = \sigma$. When the loading is continued and s is increased, so that $s_a \leq s < s_b$, relation (3.42) therefore become

$$\sigma = 2(\lambda^2 - \frac{1}{\lambda^4})(\frac{\partial W}{\partial I_1} + \lambda^2 \frac{\partial W}{\partial II_1}) + 2(\frac{\lambda^2}{\lambda_a^2} - \frac{\lambda_a^4}{\lambda^4})(\frac{\partial W}{\partial I_2} + \frac{\lambda^2}{\lambda_a^2}\frac{\partial W}{\partial II_2}). \tag{3.47}$$

Moreover, it should follow that when λ is increased so that deactivation criterion $s = s_b$ is satisfied, the relation (3.45) becomes

$$\sigma = 2(\frac{\lambda^2}{\lambda_a^2} - \frac{\lambda_a^4}{\lambda^4})(\frac{\partial W}{\partial I_2} + \frac{\lambda^2}{\lambda_a^2}\frac{\partial W}{\partial II_2}). \tag{3.48}$$

3.2.3 Unloading

In this subsection, we will discuss the behavior of σ_x and σ_y during unloading for the general biaxial cases. We suppose that at some deformation level, say at $s = s^*$ given by $\lambda_x = \lambda_x^*$ and $\lambda_y = \lambda_y^*$, we decrease s to the zero stress state. As in the case of uniaxial extension, three cases of s^* must be considered; $s^* < s_a$, $s_a \leq s^* < s_b$ and $s_b \leq s^*$.

- Case 1: $s^* < s_a$

  In this case, the unloading starts before the recruitment of the new material. This is similar to unloading of an elastic material with a single mechanism. Therefore, during the unloading, the relations (3.33) are used. It can be seen from (3.33) that the zero stress will be achieved when $\lambda_x = \lambda_y = \lambda = 1$, corresponding to the original reference configuration κ_1.

- Case 2: $s_a \leq s^* < s_b$

  In this case, the unloading starts when the new material has been recruited but the original material is still load bearing. When s is decreased from s^* to $s = s_a$, both mechanisms are active and the strain energy is given by $W = W_1(I_1, II_1) + W_2(I_2, II_2)$. The relation in (3.42) are valid during the unloading process. The path of unloading doesn't have to be the same path used during loading from s_a to s^*. Hence, the configuration taken by the body when $s = s_a$ during unloading can be different from the configuration when $s = s_a$ during loading. So, λ_{xa} and λ_{ya} in (3.42) can differ from the one we used during loading. When the unloading proceeds so that $s < s_a$, the contribution of the second mechanism is ceased. We don't consider the possibility that the recruited material contributes compressive stress after it reaches zero stress and therefore the strain energy is given by $W = W_1(I_1, II_1)$ and the stresses versus stretch relations are given by (3.33). As in the previous unloading case, any unloading path will lead to the zero stress state corresponding to the reference configuration κ_1.

- Case 3: $s_b \leq s^*$

  In this last case, the unloading starts when the first material is deactivated permanently, that is $s_b \leq s^*$. When s is decreased from s^* to s_b, the relations (3.45) are valid. When the unloading is continued so that $s < s_b$, the deactivated material cannot be

recovered, therefore the strain energy is still given by $W = W_2(I_2, II_2)$ and the relations (3.45) are still used for σ_x and σ_y. We can see from (3.45) that the zero stress state corresponds to $\lambda_x = \lambda_{xa}$ and $\lambda_y = \lambda_{ya}$. Here, the values of λ_{xa} and λ_{ya}; as long as they satisfy $s(\lambda_{xa}, \lambda_{ya}) = s_a$, do not have to be the same as λ_{xa} and λ_{ya} during loading, since unloading can follow a different path from loading. The configuration taken by the body after unloading at zero stress is denoted by κ_2' and $\kappa_2' \in K_a$ and $\kappa_2' \neq \kappa_1$.

3.2.4 Summary

The analytical solutions for biaxial stretch of a dual mechanism slab for which each mechanism is an isotropic, incompressible, hyperelastic material have been presented in equations (3.33),(3.42), and (3.45). The analytical solutions for equibiaxial stretch are presented in equations (3.46),(3.47), and (3.48). Clearly, no specific strain energy function W is required to obtain the solutions.

Similar to the uniaxial stretch case, the relations between σ_α and λ_α, $\alpha = x$ or y, during loading and unloading can be summarized in a compact manner. The relation (3.33) can be seen as composition of a function of stretch ratios, denoted $E(\Lambda, \Gamma)$, defined as:

$$E(\Lambda, \Gamma) \equiv 2 * (\Lambda^2 - \Gamma^2) \tag{3.49}$$

and a response function, denoted $w_{1\alpha}$ (α is either x or y), as a function of λ_α and λ_z, defined as:

$$w_{1\alpha} \equiv (\frac{\partial W}{\partial I_1} + \frac{1}{\lambda_\alpha^2 \lambda_z^2} \frac{\partial W}{\partial II_1}). \tag{3.50}$$

Making use these definitions, (3.33) can be written as follows:

$$\sigma_\alpha = E(\lambda_\alpha, \lambda_z) w_{1\alpha}. \tag{3.51}$$

It can be seen that the function E is used in the second term of (3.42) and (3.45) with $\lambda_\alpha/\lambda_{\alpha a}$ as arguments. Another response function $w_{2\alpha}$ is introduced for (3.42) and (3.45) and it is defined as;

$$w_{2\alpha} \equiv (\frac{\partial W}{\partial I_2} + \frac{\lambda_{\alpha a}^2 \lambda_{za}^2}{\lambda_\alpha^2 \lambda_z^2} \frac{\partial W}{\partial II_2}). \tag{3.52}$$

Using the above definitions of E, $w_{1\alpha}$, and $w_{2\alpha}$, the relations between σ_α and λ_α (α is either

Table 6: The relations between σ_α and λ_α ($\alpha = x$ or y) during biaxial loading. The definitions of $E(\Lambda, \Gamma), w_{1\alpha}$ and $w_{2\alpha}$ are given by (3.49), (3.50), and (3.52), respectively.

Range of s	σ_α vs. λ_α
$1 \le s < s_a$	$\sigma_\alpha = E(\lambda_\alpha, \lambda_z) w_{1\alpha}$
$s_a < s \le s_b$	$\sigma_\alpha = E(\lambda_\alpha, \lambda_z) w_{1\alpha} + E(\frac{\lambda_\alpha}{\lambda_{\alpha a}}, \frac{\lambda_z}{\lambda_{za}}) w_{2\alpha}$
$s_b \le s$	$\sigma_\alpha = E(\frac{\lambda_\alpha}{\lambda_{\alpha a}}, \frac{\lambda_z}{\lambda_{za}}) w_{2\alpha}$

Table 7: The relations between σ_α and λ_α ($\alpha = x$ or y) during biaxial unloading for different maximum deformation level s^*. The definitions of $E(\Lambda, \Gamma), w_{1\alpha}$ and $w_{2\alpha}$ are given by (3.49), (3.50), and (3.52).

Location of s^*	Range of λ_α	σ_α vs. λ_α
$1 \le s^* < s_a$	$1 \le s < s_a$	$\sigma_\alpha = E(\lambda_\alpha, \lambda_z) w_{1\alpha}$
$s_a \le s^* < s_b$	$s_a < s \le s_b$	$\sigma_\alpha = E(\lambda_\alpha, \lambda_z) w_{1\alpha} + E(\frac{\lambda_\alpha}{\lambda_{\alpha a}}, \frac{\lambda_z}{\lambda_{za}}) w_{2\alpha}$
	$1 \le s < s_a$	$\sigma_\alpha = E(\lambda_\alpha, \lambda_z) w_{1\alpha}$
$s_b \le s^*$	$1 \le a$	$\sigma_\alpha = E(\frac{\lambda_\alpha}{\lambda_{\alpha a}}, \frac{\lambda_z}{\lambda_{za}}) w_{2\alpha}$

Table 8: Some examples of $w_{1\alpha}$ and $w_{2\alpha}$ for biaxial stretch. The definitions of $w_{1\alpha}$ and $w_{2\alpha}$ are given by (3.50) and (3.52), respectively.

Type of W	$w_{1\alpha}$	$w_{2\alpha}$
Neo Hookean	α_1	α_2
Mooney Rivlin	$\alpha_1 + \beta_1 \frac{1}{\lambda_\alpha^2 \lambda_z^2}$	$\alpha_2 + \beta_2 \frac{\lambda_{\alpha a}^2 \lambda_{za}^2}{\lambda_\alpha^2 \lambda_z^2}$
Exponential	$\alpha_1 e^{\gamma_1 (I_1 - 3)}$	$\alpha_2 e^{\gamma_2 (I_2 - 3)}$

x or y) during loading and unloading can be summarized in Tables 6 and 7, respectively. In Table 8, we display $w_{1\alpha}$ and $w_{2\alpha}$ for some specific strain energy functions: Neo Hookean, Mooney Rivlin and Exponential type strain energy function. The definition of each strain energy function can be seen in Table 3. In Table 8, α_1, β_1, and γ_1 are material parameters for the first mechanism, while α_2, β_2, and γ_2 are those of the second mechanism. The exponential type model contains the first invariants of the first and second mechanism, denoted I_1 and I_2, respectively, where I_1 is given by (3.30.1) and $I_2 = \lambda_x/\lambda_{xa} + \lambda_y/\lambda_{ya} + \lambda_{xa}\lambda_{ya}/\lambda_x\lambda_y$. As in the uniaxial case, the combinations of W_1 and W_2 in (3.33),(3.42), and (3.45) for biaxial case and in (3.46),(3.47), and (3.48) for equibiaxial case, do not have to be of the same type.

3.2.5 An example and discussion

As an example, we consider here the results of a slab made of the exponential type hyperelastic material given in (2.21) with its material parameters given in Table 5 that undergoes biaxial extension where λ_y and λ_x are maintained in the following relation:

$$(\lambda_y - 1) = \frac{2}{5}(\lambda_x - 1) \tag{3.53}$$

during loading and unloading. This biaxial ratio is also employed in Rajagopal and Wineman [104]. We suppose that the scalar parameter s depends solely on the first invariant of the first mechanism I_1 as is given in (3.34). Figure (15) depicts the $s = s_a = 1.4237$ curve (PQ curve) and $s = s_b = 3.4791$ curve (RS curve). In this figure, the loading path used in this example is represented by the straight line OC. The loading path OC crosses PQ curve at

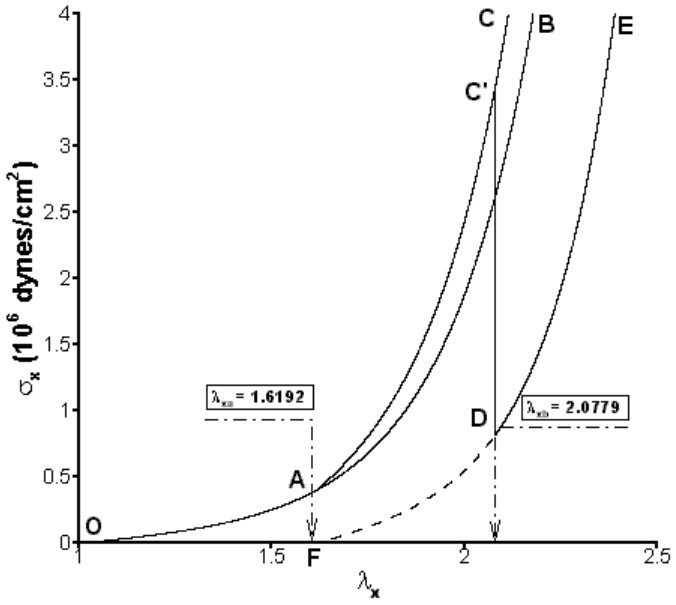

Figure 16: Resulting σ_x vs λ_x curves for biaxial stretch of a block with material parameters given in Table 5. Here, λ_{xa} and λ_{xb} correspond to s_a=1.4237 and s_b=3.4790, respectively.

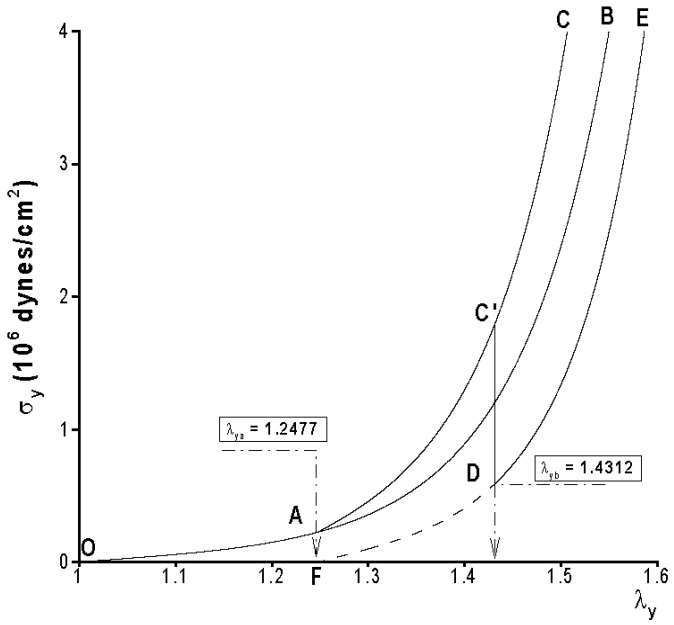

Figure 17: Resulting σ_y vs λ_y curves for biaxial stretch of a block with material parameters given in Table 5.Here, λ_{ya} and λ_{yb} correspond to s_a=1.4237 and s_b=3.4790, respectively.

A ($\lambda_{xa} = 1.6192$ and $\lambda_{ya} = 1.2477$), when the second mechanism is activated. Moreover, when the loading is continued, the loading path crosses the RS curve at B ($\lambda_{xb} = 2.0779$ and $\lambda_{yb} = 1.4312$) when the first mechanism is deactivated. We suppose that the loading stops at point C at which the unloading begins. This is the case where the unloading occurs after the deactivation of the first mechanism representing total elastin breakage.

The functions $\sigma_x(\lambda_x)$ and $\sigma_y(\lambda_y)$ during loading and unloading are given in Figure 16 and 17, respectively. In each figure the line OB represents the solution for the selected material without activating the second mechanism. So, curve OB represents a solution of a classical elastic material with the same material parameters. Curve OC in both Figures 16 and 17, display the results for the selected material when the second mechanism is activated at $s = s_a$. Here, we see that the material becomes slightly stiffer than before the activation. Lines OC'DE in both figures indicate the solution for our material experiencing both the activation of the second mechanism and the deactivation of the first mechanism. The deactivation of the first mechanism is indicated by the drop of the material response (stress values). As was seen in the uniaxial case, line EDF indicates the path of material response taken by an unloading case that occurs after deactivation. We suppose that the stretch ratios λ_x and λ_y during unloading take the relation (3.53) as well. This line EDF also indicates a new elastic regime of the material beside curve OB.

The unloading case for biaxial stretch suggests a possible improved experimental method for obtaining the parameters s_a and s_b associated with the activation criterion. While the uniaxial unloading may lead to the recovery of the activation stretch ratio λ_a, the biaxial loading and unloading can lead us to recover a specific functional form of s and corresponding critical value s_a. The process can be done by performing the unloading Case 3 in which the entire elastin is deactivated when the maximum s^* is attained. So in this case $s^* > s_b$. The value of s_b is also unknown, so *a priori* there is no certainty that loading causes total deactivation. One technique to overcome this is to perform loading and unloading for a specific loading path for increasing values of s^* *i.e* maximum λ_x and λ_y. According to our proposed theory, the slab will return to the reference configuration κ_1 when $s^* < s_b$ or otherwise to a new reference configuration, which corresponds to the activation state. Thus, the loading and unloading must be repeated until a permanent deformation is obtained. The

permanent deformation will correspond to some point in the λ_x vs. λ_y diagram as is shown in Figure 15. This procedure then is repeated for other loading paths to produce more points corresponding to different permanent deformation states. The resulting collection of points on the λ_x vs. λ_y diagram should form a curve of $s = s_a$ similar to that indicated by curve PQ in Figure 15. The resulting curve can be used to determine the formulation of s and the value of s_a. Note however that the proposed approach assumes that the different samples that are used for the loading and unloading procedure possess similar forms of s and values of s_a.

3.3 HOMOGENEOUS DEFORMATION: INFLATION OF A CYLINDRICAL MEMBRANE

3.3.1 Loading

In this section, we consider the idealized problem of inflation of a dual mechanism cylindrical membrane, for which both mechanisms are hyperelastic, isotropic, and incompressible. Uniform pressures P_i and P_o are applied on its inner and outer wall, respectively. In classical mechanics, the analytical solution for this problem is available and is very useful for material identification [137, 138]. Many experiments aimed at material identification of the arterial wall are performed using this idealized solution. The idealized solution considers cylindrical membrane of infinite length, constant wall thickness and constant radius along the length. In reality, the segment has finite fixed length and the radius along the sample segment may not be constant. In experiments, the pressure at the inner wall of the cylinder is produced by fluid perfusion. Here, investigators control the volume change of the intact segment and monitor the pressure that produces the changes.

The analytical solution of this problem for a dual mechanism cylindrical membrane for which both mechanism are hyperelastic, isotropic and incompressible will be presented in this section. We also consider specific strain energy functions for W_1 and W_2 and compare the results to available experimental data and obtain the material parameters for cerebral arterial and aneurysm walls. The data are extracted from experimental results presented

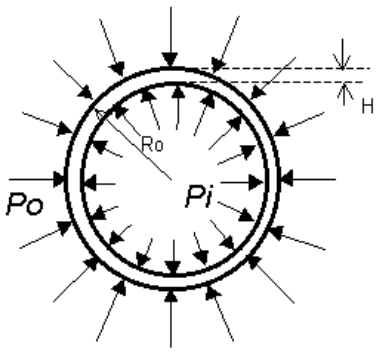

Figure 18: Inflation of a cylindrical membrane.

in Figure 5 in Scott *et al.*[79]. Exponential type functions will be employed to represent both the first and second mechanisms in (2.21). The Neo Hookean and Mooney Rivlin and their combinations were also evaluated but the results were not satisfactory. The regression analysis results for other strain energy functions are presented in Appendix B

With respect to the cylindrical coordinate system (R, Θ, Z), with Z axis aligned with the axis of the cylinder, the cylindrical membrane with length L, radius of midwall R_o and thickness H occupies the following domain in the undeformed configuration:

$$R \in [R_o - \frac{H}{2}, R_o + \frac{H}{2}], \qquad \Theta \in [-\frac{\pi}{2}, \frac{\pi}{2}], \qquad Z \in [0, L]. \tag{3.54}$$

Figure 18 shows the cylinder under consideration and its loading. The prescribed uniform pressures P_i and P_o at the inner and outer wall, respectively produce traction as follows:

$$\mathbf{t}|_{R=R_o-\frac{H}{2}} = +P_i\mathbf{e_r} \qquad \text{and} \qquad \mathbf{t}|_{R=R_o+\frac{H}{2}} = -P_o\mathbf{e_r}. \tag{3.55}$$

The thickness of the cylindrical membrane is assumed to be small; $H/R_o << 1$, so that the stress variation along the thickness can be neglected. In this case, the membrane approximation can be used to obtain the relation between uniform transmural pressure $\Delta p = P_i - P_o$ and λ [138, 139]. Here, the cylinder is regarded as a surface of revolution with radius R constant along the axis of revolution that is aligned with the axis Z.

In this problem, we look for the solution of a cylindrical membrane that inflates in a purely radial direction to become a deformed cylindrical membrane with larger radius r due to the pressure difference Δp. Let's denote λ as the ratio between the deformed radius r and the original radius R, so $\lambda = r/R$ and $\lambda \geq 1$ during inflation. Standard calculations using membrane approximations yield the deformation gradient $\mathbf{F_1}$ whose basis is given by the principle axis of the surface: parallel to the Z axis (longitudinal direction), in the circumferential direction of the cylinder, and in the normal direction to the surface as follows:

$$\mathbf{F_1} = \text{DIAG}[1, \lambda, \frac{1}{\lambda}]. \tag{3.56}$$

In the normal direction, as a result of the incompressibility restriction, the cylinder experiences thinning as it is enlarged. The deformed thickness h is given by:

$$h = \frac{1}{\lambda} H. \tag{3.57}$$

The corresponding Left Cauchy Green strain tensor and its inverse are:

$$\mathbf{B_1} = \text{DIAG}[1, \lambda^2, \frac{1}{\lambda^2}], \qquad \mathbf{B_1}^{-1} = \text{DIAG}[1, \frac{1}{\lambda^2}, \lambda^2]. \tag{3.58}$$

The first and second invariants of $\mathbf{B_1}$, I_1 and II_1 are equal and are given by:

$$I_1 = II_1 = 1 + \lambda^2 + \frac{1}{\lambda^2}. \tag{3.59}$$

In this case, λ serves as the only deformation parameter and therefore can be used to describe the changes in deformation level. As in the uniaxial case, the scalar function s defined in (2.4) then can be reduced to $s = \hat{s}(\lambda)$. Moreover, since s is a strictly monotonic function of the invariants and the invariants are strictly monotonic functions of λ for $\lambda \geq 1$, the relation of s to λ is also monotonic for $\lambda \geq 1$. The activation criterion (2.7) and deactivation criterion (2.14), can be reduced to $\lambda = \lambda_a$ and $\lambda = \lambda_b$, respectively, where λ_a and λ_b are the roots of (2.7) and (2.14), respectively.

Since λ doesn't depend on position, the values of the invariants (and also the strain and the Cauchy stress) are uniform throughout the body during the deformation history. Therefore when λ is increased so that $1 \leq \lambda < \lambda_a$, the entire body possesses only the first (or original material) and the strain energy function is given by $W = W_1(I_1, II_1)$ only. Following

(2.17),(2.18) for $s < s_a$, and (3.58), the nonzero Cauchy stress components $T_{zz}, T_{\theta\theta}$, and T_{rr} are:

$$T_{zz} = -p + 2\frac{\partial W_1}{\partial I_1} - 2\frac{\partial W_1}{\partial II_1} \tag{3.60}$$

$$T_{\theta\theta} = -p + 2\frac{\partial W_1}{\partial I_1}\lambda^2 - 2\frac{\partial W_1}{\partial II_1}\frac{1}{\lambda^2} \tag{3.61}$$

$$T_{rr} = -p + 2\frac{\partial W_1}{\partial I_1}\frac{1}{\lambda^2} - 2\frac{\partial W_1}{\partial II_1}\lambda^2. \tag{3.62}$$

The membrane equilibrium equations in the circumferential, longitudinal and normal to the surface are given respectively as follows (see in Green and Adkins [140]):

$$(\frac{1}{r^2}T_{\theta\theta}\lambda h)_{,\theta} = 0 \qquad (T_{zz}\lambda h)_{,z} = 0 \qquad -\frac{1}{r}T_{\theta\theta}\lambda + \Delta p = 0, \tag{3.63}$$

where all the shearing components of the Cauchy stress tensor are vanished. It's easy to see that the equilibrium equations in the longitudinal and circumferential directions are satisfied immediately.

The relation between $r\ \Delta p$ and λ when $\lambda \leq \lambda_a$ then can be obtained from (3.63.3) as follows:

$$r\ \Delta p = 2\frac{H}{\lambda}(\lambda^2 - \frac{1}{\lambda^2})(\frac{\partial W_1}{\partial I_1} + \frac{\partial W_1}{\partial II_1}), \tag{3.64}$$

where r is the current radius. Following the notation in Scott *et al.* [79], the product of the net pressure Δp and r later on will be referred to as 'tension'. When the deformation state reaches $\lambda = \lambda_a$, the body occupies configuration κ_a and the activation of the second mechanism occurs throughout the body. The deformation gradient of the second mechanism $\mathbf{F_2}$ relative to configuration κ_a of all the material points can be calculated using (2.12), where $t = t_2$ indicates the deformation state when $\kappa = \kappa_a$, as follows:

$$\mathbf{F_2} = \mathrm{DIAG}[\frac{\lambda_a}{\lambda}, \frac{\lambda}{\lambda_a}, 1]. \tag{3.65}$$

Using (3.65), the tensor $\mathbf{B}_2$ and its inverse can easily be obtained as follows:

$$\mathbf{B_2} = \mathrm{DIAG}[\frac{\lambda_a^2}{\lambda^2}, \frac{\lambda^2}{\lambda_a^2}, 1], \qquad \mathbf{B_2}^{-1} = \mathrm{DIAG}[\frac{\lambda^2}{\lambda_a^2}, \frac{\lambda_a^2}{\lambda^2}, 1]. \tag{3.66}$$

After recruitment of the second mechanism, the strain energy function is composed of two contributions: W_1 representing the original material and W_2 representing the recruited material. So, $W = W_1(I_1, II_1) + W_2(I_2, II_2)$, as is described in (2.18) for $s_a \leq s < s_b$. Following the same procedure as used for obtaining (3.64), we obtain the following relation for $\lambda_a \leq \lambda < \lambda_b$:

$$r\ \Delta p = 2\frac{H}{\lambda}[(\lambda^2 - \frac{1}{\lambda^2})(\frac{\partial W_1}{\partial I_1} + \frac{\partial W_1}{\partial II_1}) + (\frac{\lambda^2}{\lambda_a^2} - \frac{\lambda_a^2}{\lambda^2})(\frac{\partial W_2}{\partial I_2} + \frac{\partial W_2}{\partial II_2})]. \tag{3.67}$$

When the loading is increased so that $\lambda_b \leq \lambda$, (the first mechanism is deactivated when $s = s_b$ and therefore $\lambda = \lambda_b$) only the second mechanism contributes to the total mechanism, so that $W = W_2(I_2, II_2)$. The relation of tension versus λ for $\lambda_b \leq \lambda$ can be obtained simply by removing the first term of (3.67) and is given as follows:

$$r\ \Delta p = 2\frac{H}{\lambda}(\frac{\lambda^2}{\lambda_a^2} - \frac{\lambda_a^2}{\lambda^2})(\frac{\partial W_2}{\partial I_2} + \frac{\partial W_2}{\partial II_2}). \tag{3.68}$$

3.3.2 Unloading

We now suppose that at some chosen stretch $\lambda = \lambda^*$ the pressure is decreased (unloading). As is in previous homogeneous problems, for example in the uniaxial case, three cases of λ^* needs consideration: $\lambda^* < \lambda_a$, $\lambda_a \leq \lambda^* < \lambda_b$ and $\lambda_b \leq \lambda^*$.

- Case 1: $\lambda^* < \lambda_a$

  Here, the unloading begins before the recruitment occurs. Since the material is elastic, the unloading path will follow (3.64) with decreasing λ. As is expected, when no new mechanism takes place and no deactivation is initiated, the cylindrical membrane returns to its original undeformed configuration at the zero stress state.

- Case 2: $\lambda_a \leq \lambda^* < \lambda_b$

  In this case, the unloading begins after the second material is recruited. It should be clear that relation (3.67) holds when λ is reduced from λ^* to λ_a. When λ is decreased further, the contribution of the second mechanism or recruited material is ceased, since the second mechanism only participates when the activation criterion is satisfied $i.e\ \lambda \geq \lambda_a$. Thus, as

it is mentioned before, we suppose that during unloading the collagen fibers return to its crimped configuration and stop participating when it reaches its reference configuration. So, the relation of tension versus λ follows (3.64) when $\lambda < \lambda_a$. It is clear that in this case, the cylinder will return to the original reference configuration at the zero stress state.

- Case 3: $\lambda_b \leq \lambda^*$

  In the last case, the unloading begins after the first mechanism is deactivated. It should be clear that when λ is reduced from λ^* to λ_b, the relation (3.68) is used. However, when λ is reduced so that $\lambda < \lambda_b$, the first material that has been deactivated cannot be reactivated. So for this unloading case, the strain energy function W is always given by $W = W_2(I_2, II_2)$. The path of the unloading curve therefore cannot follow (3.67) nor (3.64), instead it will follow (3.68). It can be seen from (3.68) that the zero stress state corresponds to $\lambda = \lambda_a > 1$. This implies that the cylinder doesn't return to its original undeformed configuration but rather it obtains a new unloaded configuration. The new unloaded configuration corresponds to the reference configuration of the recruited material, κ_a.

3.3.3 Summary

The analytical solutions for inflation of a long cylindrical membrane composed of a dual mechanism material for which both mechanisms behave as incompressible, isotropic, hyperelastic materials were presented in (3.64),(3.67), and (3.68). Clearly, the solutions do not require specification of the strain energy function, W. As is in the previous two sections, (3.64) can be seen as a composition of a function of stretch denoted by $E(\lambda)$, and defined as:

$$E(\Lambda) \equiv (\Lambda^2 - \frac{1}{\Lambda^2}). \tag{3.69}$$

and a response function denoted by w_1, and defined as

$$w_1 \equiv (\frac{\partial W}{\partial I_1} + \frac{\partial W}{\partial II_1}). \tag{3.70}$$

Table 9: The relation between Tension and λ during inflation. The definitions of $E(\Lambda), w_1$ and w_2 are given by (3.69),(3.70) and (3.71), respectively. Here, H denotes the undeformed thickness.

Range of λ	Tension
$1 \leq \lambda < \lambda_a$	$2\ H/\lambda E(\lambda) w_1$
$\lambda_a < \lambda \leq \lambda_b$	$2\ H/\lambda(E(\lambda)w_1 + E(\frac{\lambda}{\lambda_a})w_2)$
$\lambda_b \leq \lambda$	$2H/\lambda E(\frac{\lambda}{\lambda_a})w_2$

A similar stretch function with a different argument, $\frac{\lambda}{\lambda_a}$ instead of λ, is used in the second term of equation (3.67) and in equation (3.68). The corresponding response function is defined as follows:

$$w_2 \equiv (\frac{\partial W}{\partial I_2} + \frac{\partial W}{\partial I I_2}). \tag{3.71}$$

The relations between tension and λ during loading and unloading therefore can be written using E, w_1 and w_2 and the undeformed thickness H. These relations are summarized in Tables (9) and (10).

3.3.4 Experimental data on the nonlinearity and inelasticity of cerebral arteries

In the following two sections we evaluate the performance of the proposed constitutive equation in capturing the mechanical behavior of real cerebral arterial segments. The results of experimental work on segments from human Circles of Willis published by Scott, Ferguson and Roach [79] are in particular interest. Scott *et al.* showed quantitatively the nonlinear inelastic behavior of anterior cerebral arteries (ACA) segments. Due to the importance of these results, for this work, the procedure of the experiment and the relevant results are described in this section. A regression analysis of the data as applied to the dual mechanism model will be described in the following section.

In their work, Scott *et al.* performed inflation tests on intact ACA segments *in vitro* using an experimental procedure developed by Nichol [141] and Roach and Burton [77]. In their works, the segment was attached to one end of a metal adapter using suture silk

Table 10: The relation between Tension and λ during unloading for possible cases of λ^*. The definitions of $E(\Lambda), w_1$ and w_2 are given by (3.69),(3.70) and (3.71), respectively (H is the undeformed thickness).

Location of λ^*	Range of λ	Tension
$1 \leq \lambda^* < \lambda_a$	$1 \leq \lambda < \lambda_a$	$2\ H/\lambda E(\lambda) w_1$
$\lambda_a \leq \lambda^* < \lambda_b$	$\lambda_a < \lambda \leq \lambda_b$	$2\ H/\lambda(E(\lambda)w_1 + E(\frac{\lambda}{\lambda_a})w_2)$
	$1 \leq \lambda < \lambda_a$	$2\ H/\lambda E(\lambda) w_1$
$\lambda_b \leq \lambda^*$	$1 \leq \lambda$	$2\ H/\lambda E(\frac{\lambda}{\lambda_a})w_2$

and closed with a glass plug at the other end. The inflation was produced by perfusion of the segment with dyed water using a syringe fit through the adapter. During the test, the segments were kept submerged in water contained in a glass chamber. A micrometer was attached to the syringe to control and to measure the delivery of perfusing fluid and therefore to measure volumetric changes of the lumen of the segments. Pressure changes due to perfusion were measured by a vertical mercury manometer. During the experiment, pressure and the corresponding luminal volume of the segment were recorded.

Changes in the segment's inner diameter were calculated from the measured luminal volumetric changes. This procedure can be done by assuming the segments maintained a cylindrical shape and length. However, since the ends were not fixed during inflation, the experimental procedure used by Scott *et al.* allowed axial contraction of the sample segment. This change in length was reported to be negligible for samples from patients over 30 years in age [49]. The mounting of the sample potentially also allowed the sample to bulge at high pressures resulting in a non-uniform or variation of radius along the segment. This effect was decreased by applying a large plug and adapter to hold the segment [77]. A procedure for measurements of the undeformed radius was suggested by Busby and Burton [49] who used similar apparatus. First, the segments were collapsed by applying a negative pressure. A small positive pressure then was applied to remove the collapse. The unloaded volume measured geometry, hence the undeformed circumference, was assumed to correspond to the state when visually the segments were no longer collapsed.

In this work, the term 'strain' was defined as the ratio of computed circumferential change to initial circumference. We will refer to this simply as strain and denote it by ϵ. Recall that the product of the applied pressure and the corresponding deformed radius is defined as tension. Scott *et al.* reported that the wall thickness of the segments were in the range from 100 to 200 μ.

In this experiment, Scott *et al.* subjected four ACA segments to slow cycles of loading and unloading though only results from the loading procedure were reported. Three samples were loaded up to 200 mm Hg and one control sample was loaded up to 100 mmHg. The experiments yielded significant results. The control segment was reported to show consistent curves of tension versus strain, ϵ, and tension versus deformed radius after six repetitions of loading and unloading.

The other three segments, on the other hand, were reported to behave differently from the control. It was reported that after three cycles of loading that produced three consistent distensibility curves similar to those of the control sample, the final six curves exhibited a measurable 'shifting'. These post shifting tension versus ϵ curves were reproducible. Similarly, the tension versus radius curves also showed a new series of consistent curves shifted from the first three curves. Significantly, the post shifting series displayed a larger unloaded radius implying that some form of permanent deformation had occurred. Scott *et al.* used the new reference radius to calculate ϵ after the shifting. The qualitative shape of the post shifting curves is also different from those before the shifting. The typical 'toe region' is not pronounced in the new or shifted curves. Scott *et al.* hypothesized that the shift of the curves was due to elastin breakage, however, they never performed a morphology study to investigate the fragments of the elastin. Nevertheless, Scott *et al.* found that the new curves of tension versus ϵ were more similar in shape to those from distensibility tests of aneurysm segments. Based on those similarities, they hypothesized that mechanical breakage of elastin may play a significant role in aneurysms formation [79].

In the following paragraph, we describe how the multi-mechanism equations can be used to model the nonlinear and inelastic response of the segments of human cerebral arterial walls reported by Scott *et al.* [79]. The proposed mechanisms experienced by the control segment and non control segments are described below.

We suppose that the initial stage of the first elastic regime, often referred as the 'toe region', corresponds to the mechanism produced by elastin load bearing or simply the first mechanism. As the deformation progresses, at some stretch level or configuration, say κ_a, collagen is recruited, initiating the second mechanism produced by recruited collagen fibers. We also suppose that the maximum perfusion of the control segment and the first two runs of the non control segments doesn't cause substantial breakage of elastin. This is supported by the repeatability of the loading curves. During unloading, the extended collagen fibers will be unstretched and return to their undeformed configuration, κ_a, at a nonzero transmural pressure. When the unloading continues, the collagen fibers become 'recrimped' and do not contribute to compression stress in the wall. At κ_a, the elastin is still stretched so when the unloading continues, the elastin will continue to contract more until the elastin reaches its reference configuration which corresponds to zero transmural pressure. When these loading and unloading paths are completed, the segment will return to its reference configuration. The control segment is reported to exhibit six consistent elastic tension/strain curves during the six loading cycles. The unloading curves are not reported, but there was no report that the control segment possesses new zero pressure radius after unloading. Assuming that material hysteresis is negligible, the response of the control segment therefore is elastic [1].

The three non control segments were exposed to larger maximum pressure (200 mmHg) than that experienced by the control (100 mmHg). We suppose that the maximum pressure of 200 mmHg for the first three loading doesn't cause the elastin to be totally damaged. As a result, the first series of distensibility curves resemble those produced by the control. On the fourth loading run, we suppose that the maximum perfusion is sufficiently large to produce total elastin breakage. We suppose that once the elastin breaks, it becomes inactive, unable to contribute to further loading and unloading. When the unloading is performed after elastin breakage, the collagen will return to its reference configuration, κ_a. Here, the unloading cannot continue since the elastin has been inactive and the collagen fibers have no mechanism for generating a force to contract further. So, the configuration κ_a now corresponds to zero transmural pressure. The segment possesses a new unloaded radius because the reference configuration κ_a does not coincide with the original unloaded

[1] The viscoelasticity effect was not shown in the experiment by Scott *et al.* so it will be ignored.

configuration. Here, the inelastic feature becomes pronounced. The non control segments now contain only collagen fibers as the active component. When the pressure is reapplied, collagen immediately is recruited since the zero pressure configuration corresponds to the configuration in which the collagen fibers is ready to be activated. The typical 'toe region' obviously disappear since the elastin that produced it has been deactivated. The new series of distensibility curves feature a modified elastic regime. This should be expected since the elastic regime before the shifting arose from elastin at the lower strain level and by both the elastin and recruited collagen at higher strain levels.

The non control segments exhibit two distinct series or regimes of elastic tension vs. strain curves and series of tension vs. radius curves implying that at least two mechanisms are involved. However, the new undeformed radius that clearly becomes the reference configuration for the post shifting runs, implies that the material doesn't 'switch' from one mechanism to another. In fact, the new reference configuration after the shifting supports the idea of having the second mechanism being initiated at some level of deformation during the pre shifting elastic response. We hypothesized that the pre shifting regime is produced by both mechanisms while the post shifting regime is produced by the second mechanism alone, since the first mechanism had been deactivated.

Furthermore, we suppose that the experimental work and results by Scott *et al.* can be described using the analytical solution for a problem involving an inflated cylindrical membrane composed of a dual mechanism material. Some assumptions regarding the deformation experienced by the segment and regarding the class of the materials used to model the segments must be made to reduce the complexity of the modeling. So, we suppose that the deformation is quasi-static as a result from slow loading and unloading. Scott *et al.* didn't report the rate of loading, however the interval of the data points suggest a pressure increment of 20 mmHg. Moreover, it is described by Busby and Burton [49] that, typically, data measurement was done in the interval of at least 20 seconds to allow the stress to be relaxed. We assume the arteries are incompressible. This assumption is not novel for biotissues and gains support from, for example, experimental results by Chuong and Fung [142] and Carew *et al.* [143]. The incompressibility of the material restricts the deformation to be volume preserving. Many researchers suggest cerebral arterial wall is anisotropic [144, 145].

The isotropic assumption of the apical region of the bifurcation, at which the aneurysms frequently occur, is particularly reasonable. Findlay *et al.* [54] have shown that in this specific region the collagen fibers are laid out in a multi directional configuration. This arrangement prevents the region from having a specific preferred material symmetry. We also assume that the walls of the segment are homogenous. This assumption is mainly due to the fact that the strain measurements of Scott *et al.*, are based on volume measurements of the artery, a bulk response which does not provide information about the spatial variation in material response. In addition, we emphasize in the current approach the wall is treated as a membrane. As a result we are not attempting to capture the effects of material inhomogeneity across the wall thickness.

3.3.5 Data interpretation and nonlinear regression analysis

Our goal in this section is to evaluate whether the dual mechanism model can be used to fit the nonlinear and inelastic behavior of real cerebral arterial segments. This can be done by quantitatively comparing the data of Scott *et al.* to the analytical results of cylindrical inflation of dual mechanism material that has been constructed in the beginning part of this section. The resulting experimental data from the previously described procedures will be used here.

The data of Scott *et al.* will be divided into multi sub data corresponding to one mechanism of the proposed multi mechanism constitutive equation. The data therefore needs to be interpreted so that the correspondence between it and the new equations can be constructed. A nonlinear regression analysis will be performed afterwards. In order to extract data points needed in the regression analysis, Figure 5 in Scott it et al. [79] was scanned and the resulting images were digitized using SigmaScan, an image processing package. The resulting data are presented in Table 25. Following Scott *et al.* we label the curves before and after the shifting as Run13 and Run49, respectively. According to our proposed mechanism for the nonlinearity of cerebral arterial walls, Run13 therefore includes the response before and after the collagen fibers recruitment. The distinction between the two regions is critical in the regression analysis. For simplicity, we denote the subregions before the recruitment as Run13A, while

after the recruitment as Run13B. So, the subregion R13A corresponds to elastin only load bearing and the subregion Run13B corresponds to load bearing of both collagen fibers and elastin. The proposed constitutive equation also assumes that elastin breakage is responsible for the inelastic behavior of human cerebral arterial walls. We assume that during the third run of the test by Scott *et al.* the elastin breakage occurs simultaneously throughout the arterial wall. Consequently, Run49 corresponds to the response due to collagen fibers only. It should be clear that Run13A, Run13B, and Run49 correspond to equations (3.64), (3.67) and (3.68), respectively. Note however that Run49 contains strain data that are calculated using the new undeformed radius obtained after elastin breakage.

Only tension versus ϵ data is needed in the regression analysis. The stretch ratio λ in the equations (3.64),(3.67) and (3.68), by definition, is equivalent to $\epsilon+1$. We denote $\epsilon_a = \lambda_a - 1$ and $\epsilon_b = \lambda_b - 1$ as the strain associated with the deformation levels of the collagen activation and elastin deactivation, respectively. Scott *et al.*, however, did not specifically report the values of ϵ_a. Also, the maximum transmural pressure does not necessarily correspond to a specific strain at which the elastin is damaged (ϵ_b). In the experiment by Scott *et al.*, it was not clear if only the last run before the shifting was performed up to 200 mmHg or all of the runs were performed up to the same value. The values of λ_a and λ_b that are needed for specifying the range of Run13A and Run13B are approximated as follows.

The tension, T, versus radius, r, curve after the 'shifting', which is hypothesized to be produced by collagen only, displays a larger reference radius than that of the series of pre shifting curves. As we have hypothesized, this post shifting reference radius should correspond to the reference configuration for the collagen fibers, κ_a. From the same figure we found that the post shifting zero tension radius is 0.58 cm and while the pre shifting undeformed radius is 0.33 cm. Obviously, the two reference radius give $\lambda_a = 1.7610$ that corresponds to ϵ_a=0.7610. In the case of λ_b, we decided to use the maximum strain value in tension versus ϵ curves, which corresponds to $\epsilon_b = 1.30$ and λ_b=2.30.

To determine the material parameters; $\alpha_1, \alpha_2, \gamma_1$, and γ_2, a nonlinear regression analysis must be performed. As is known, during the analysis, material parameters in a system of equations are determined by means of minimizing the sum of square of the deviation of measured or experimental tension to theoretical tension for all data points from all the

Table 11: Resulting material parameters and corresponding R^2 values for undeformed thickness $H = 100$ and 125 μ and fixed λ_a=1.761029.

	Undeformed thickness (H) in μ	
Material Parameters	100	125
λ_a	1.761029	1.761029
$\alpha_1(10^3 dynes/cm^2)$	89.03572	71.21986
γ_1	0.622428	0.622428
$\alpha_2(10^3 dynes/cm^2)$	390.872	312.6121
γ_2	1.867193	1.867605
R^2	0.9903374	0.9903374

three groups; Run13A, Run13B and Run49, simultaneously. We developed a code that employs RNLIN; a nonlinear regression analysis subroutine that is available in the Fortran IMSL STAT/Library. The minimization of the total summation of deviation or error was performed by the built-in subroutine RNLIN that uses a modified Levenberg-Marquardt method to generate a sequence of approximations to a minimum point. To measure the quality of the curve fitting, a pseudo R^2 value is used, where [146]:

$$R^2 = 1 - \frac{\sum(T_{data} - T_{theoretical})^2}{\sum(T_{data} - T_{mean})^2}. \tag{3.72}$$

Here, T_{mean} is the average values of tension, T, calculated for each group of data points, Run13A, Run13B and Run49, while $T_{theoretical}$ is tension, T, calculated from (3.64), (3.67) and (3.68), with W is given by (2.18).

Specific strain energy functions W_1 and W_2 must be selected for equations (3.64),(3.64) and (3.68). Here, we suppose that both the first and second mechanisms can be represented by exponential type strain energy functions in (2.18). The exponential type strain energy function is selected since it is typically useful in biological applications. Neo Hookean and Mooney Rivlin materials were evaluated but no satisfactory regression analysis was resulted (the nonlinear regression analysis results are presented in Appendix B).

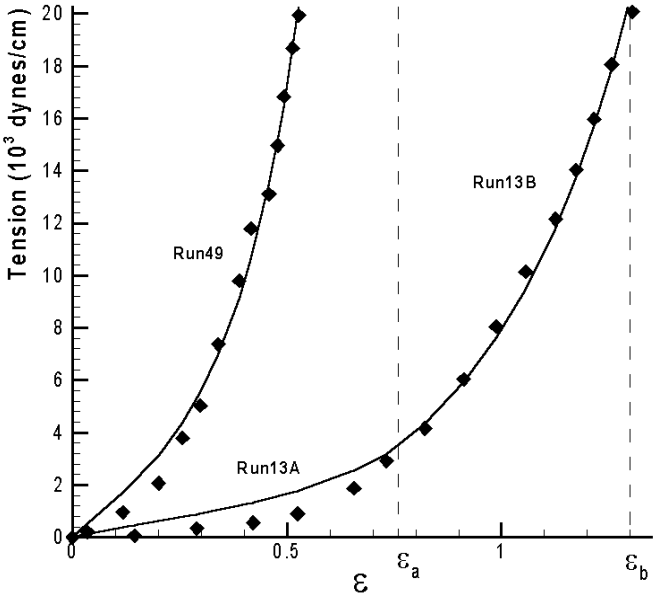

Figure 19: Resulting tension vs ϵ curves for inflation of cylindrical membrane with the material parameters given in Table 11 for $H = 125$ μ along with the experimental data points. The activation strain ϵ_a=0.7610 and the deactivation strain $\epsilon_b = 1.3$.

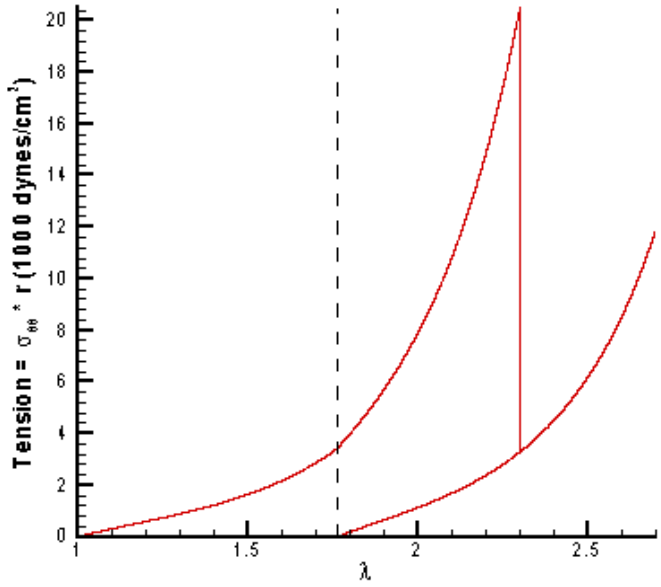

Figure 20: Resulting tension vs λ curves for inflation of cylindrical membrane with the material parameters given in Table 11 for $H = 125\ \mu$.

Recall that Scott *et al.* stated that the wall thickness H ranged from 100 to 200 μ but they did not specify a particular value of H for the experimental data points they used. The resulting material parameters for exponential type W_1 and W_2 for the two extreme thickness H are tabulated in Table 11. The values of the material parameters in the two columns indicate that they are insensitive to this range of membrane thickness. Although we can observe that the values of α_1 and α_2 for the two thickness are inversely proportional to the thickness. This should be expected from (3.64), (3.67), and (3.68) in which the tension are the product of thickness H and coefficients α_1 and α_2 and other terms. The values of R^2 for the two cases indicate that the theoretical curves very well fit the experimental data points. Therefore, at least for the deformation under discussion, the analytical solution can be used to describe the nonlinear and the inelastic behavior of human cerebral arterial segments.

It is expected that Neo Hookean and Mooney Rivlin materials produce qualitatively similar results since w_1 and w_2 for these two functions are simply constants. For Neo Hookean, the resulting material constants α_1 and α_2 are 293.08 $10^3 dynes/cm^2$ and 960.94 $10^3 dynes/cm^2$, respectively. For Mooney Rivlin, the resulting material constants $\alpha_1, \beta_1, \alpha_2$, and β_2 are (in $10^3 dynes/cm^2$) 78.21, 214.91, 462.83, and 498.08, respectively. These resulting constants are obtained for 125 μ thickness. The values of R^2 for these two functions are only 0.6565 indicating a poor fitting. Results of nonlinear regression analysis for Neo Hookean, Mooney Rivlin and the exponential type and their combinations for W_1 and W_2 are presented in Appendix B.

Plots of the relations (3.64),(3.67) and (3.68) with the resulting material parameters for $H = 125$ μ along with the data points are presented of in Figure 19. The resulting Tension vs. λ curves for $H = 125$ μ are displayed in Figure 20. Here, unlike in Figure 19, the curve after elastin breakage was not normalized to λ_a. The resulting material parameters displayed in Table 11 were obtained by fixing λ_a *a priori*. This value of λ_a was approximated from the tension vs. radius curves from Scott *et al.*. When such information is not available, λ_a then must become one of material parameters that needs to be determined via the nonlinear regression. A similar nonlinear regression analysis using equations (3.64),(3.67) and (3.68) was performed without fixing λ_a *a priori*. The material parameters obtained from this analysis are tabulated in Table 12.

Table 12: Resulting material parameters and corresponding R^2 values for undeformed thickness $H = 100$ and 125 μ and non fixed λ_a.

	Undeformed thickness (H) in μ	
Material Parameters	100	125
λ_a	1.596175	1.596258
$\alpha_1(10^3 dynes/cm^2)$	73.96133	59.16755
γ_1	0.590765	0.590855
$\alpha_2(10^3 dynes/cm^2)$	395.7232	316.598
γ_2	1.848324	1.848228
R^2	0.992577	0.992577

3.3.6 Nonlinear regression results for experimental data of the nonlinear elastic behavior of cerebral arteries

In the classical elastic sense, equation (3.64), which relates tension to circumferential strain in membrane cylindrical inflation, is valid for all $\lambda \geq 0$. Here, equation (3.64) is seen as a gross representation of the mechanical response by the cerebral arterial walls disregarding the individual behavior of both the elastin and the recruited collagen fibers. It will be shown in this chapter that the equation (3.64), which employs only the first mechanism part of the exponential type strain energy function given in (2.21.1), can be used to successfully describe the commonly known nonlinear elastic behavior of a variety of intracranial arteries from both humans and animals.

In this chapter we present the results of nonlinear regression analysis using equation (3.64) for experimental data on intracranial arteries that are obtained from the following sources:

- Data by Scott *et al.* [79] obtained from experiments on Anterior Cerebral Artery (ACA), Middle Cerebral Artery (MCA) and Posterior Cerebral Artery (PCA) of a 34-year old woman. The data are presented in Table 27.
- Data by Töth *et al.* [83] obtained from experiments on ACA of 11 aneurysm patients

Table 13: Resulting material parameters and corresponding R^2 values for experimental data by Scott *et al.* [79] obtained from segments of ACA, MCA and PCA of a young woman using equation (3.64).

	ACA	MCA	PCA
$\alpha_1(10^3 dynes/cm^2)$	38.7630	232.9863	95.5911
γ_1	0.4147	1.8614	0.3676
R^2	0.9922	0.9836	0.9789

and 16 patients with no cerebral artery disease. The data are presented in Table 26.

- Data by Nagasawa *et al.* [147] obtained from experiments on basilar segments of 25 treated and ten untreated mongrel dogs. The data are presented in Tables 28 and 29.

Note that only the average data value will be used in the regression analysis.

Scott *et al.* [79] investigated the variation of the mechanical behavior of arterial segments from different locations in the Circle of Willis. The mechanical tests were performed by inflating the cylindrical samples by fluid perfusion. A wide variation of behavior was found among samples from ACA, MCA and PCA from a young woman. The equation (3.64) that employs the first mechanism part of strain energy (2.21.1) gives satisfactory results for the three different arteries. Scott *et al.* reported that the thicknesses of the samples are between 100 to 200 μ but specifies are not given for individual experiments. Hence, here we set the undeformed thickness at 125 μ. The resulting material parameters and R^2 values are presented in Table 13. The highest R^2 value is obtained for the ACA. The curves that fit the experimental data, which are reproduced by manually scanning Figure 3 in Scott *et al.* [79], are presented along with the data in Figure 21. Töth *et al.* [83] investigated the mechanical behavior of ACA from aneurysm patients and normal human subjects (control). From the pressure vs. external radius curves, they concluded that the behavior of the ACA from the two groups do not differ. The representation of the data, which are reproduced from manually scanning Figure 1B in Töth et al. [83], in a tension vs. ϵ chart however reveals that ACA from aneurysm patients are stiffer than control arteries.

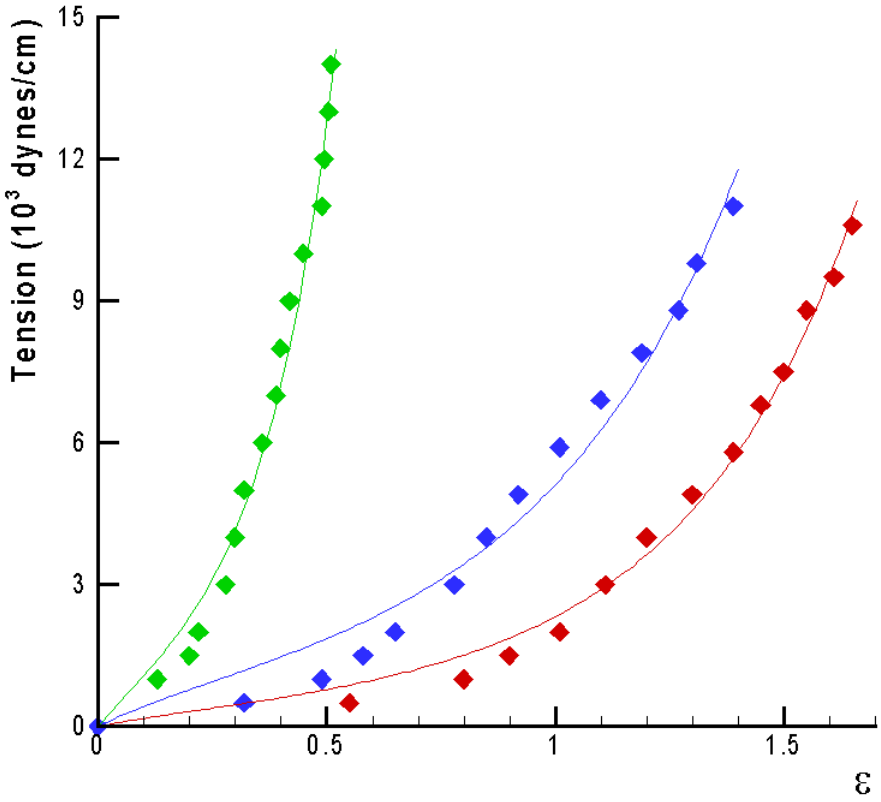

Figure 21: Resulting tension vs ϵ curves for inflation of cylindrical membrane and the experimental data (diamond symbols) for ACA (red color), MCA (green color), and PCA (blue color) shown in Table 13.

Table 14: Resulting material parameters and corresponding R^2 values for experimental data by Töth *et al.* [83] obtained from segments of Anterior Cerebral Artery (ACA) of aneurysm patients and normal patients using equation (3.64).

	Aneurysm patients	Control
$\alpha_1(10^3 dynes/cm^2)$	17.4962	18.5178
γ_1	1.9807	1.4234
R^2	0.9930	0.9916

The equation (3.64) again is employed in the regression analysis. The average thickness for ACA from aneurysm patients and human subjects with no cerebral artery disease, which are obtained from Fig. 1A in Töth *et al.* [83], are 280 μ and 210 μ, respectively. The resulting material parameters and R^2 values are displayed in Table 14. The R^2 values indicate that equation (3.64) gives satisfactory results. The resulting tension vs. ϵ curves and the experimental data are displayed in Figure 22. Nagasawa *et al.* [147] investigated the mechanical behavior of basilar segments of mongrel dogs with different collagen to elastin ratio (C/E). The variation of C/E is a product of replacing some cerebro spinal fluid with fresh blood in an attempt to produce vasospasm. The mid wall stress vs. strain data shown in Figure 4 in Nagasawa *et al.* [147] are transformed into tension vs. strain data for nonlinear regression analysis purpose. Tension data can be computed by factoring the tangential wall stress data with the corresponding deformed radius calculated from the strain data and the undeformed radius shown in Figure 3 of the same publication. The results of the nonlinear regression analysis using the equation (3.64) shows satisfactory results. The resulting material parameters for treated basilar and control segments are presented in Table 15. The resulting tension vs. ϵ curves and the experimental data (diamond symbols) for basilar segments with different C/E ratios are presented in Figure 23. The curves produced by basilar segments with high C/E ratios, which indicate high collagen content compare to elastin, indicate that these basilar are stiffer than those with the lowest C/E ratio.

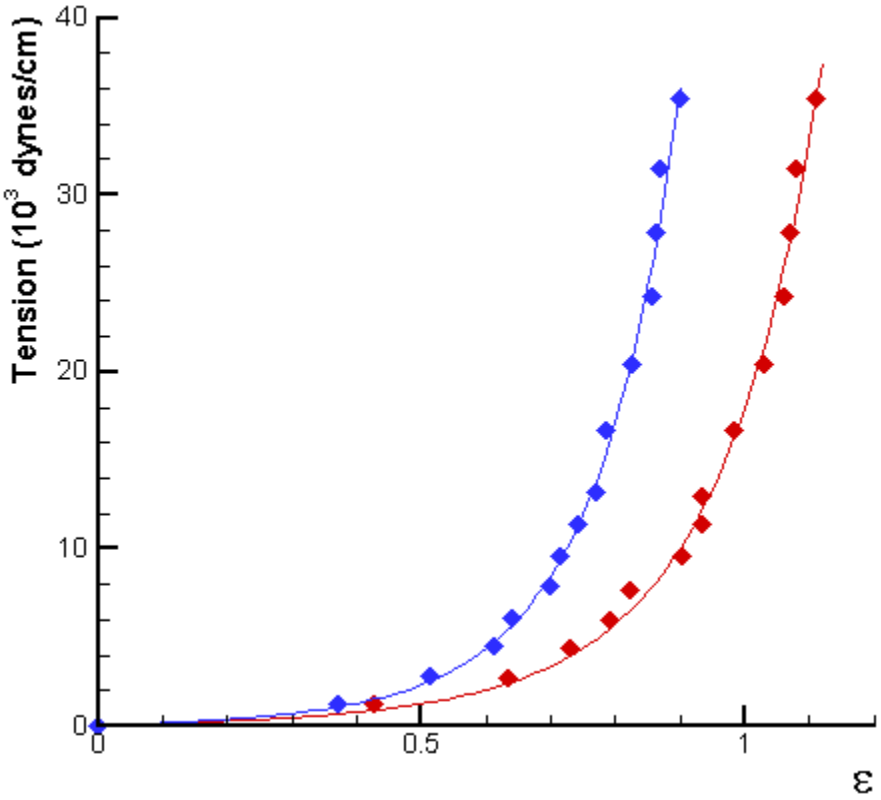

Figure 22: Resulting tension vs. ϵ curves for inflation of cylindrical membrane and the experimental data (diamond symbols) of ACA from aneurysm patients (blue color) and normal/control (red color) along with the corresponding data from Töth *et al.* [83].

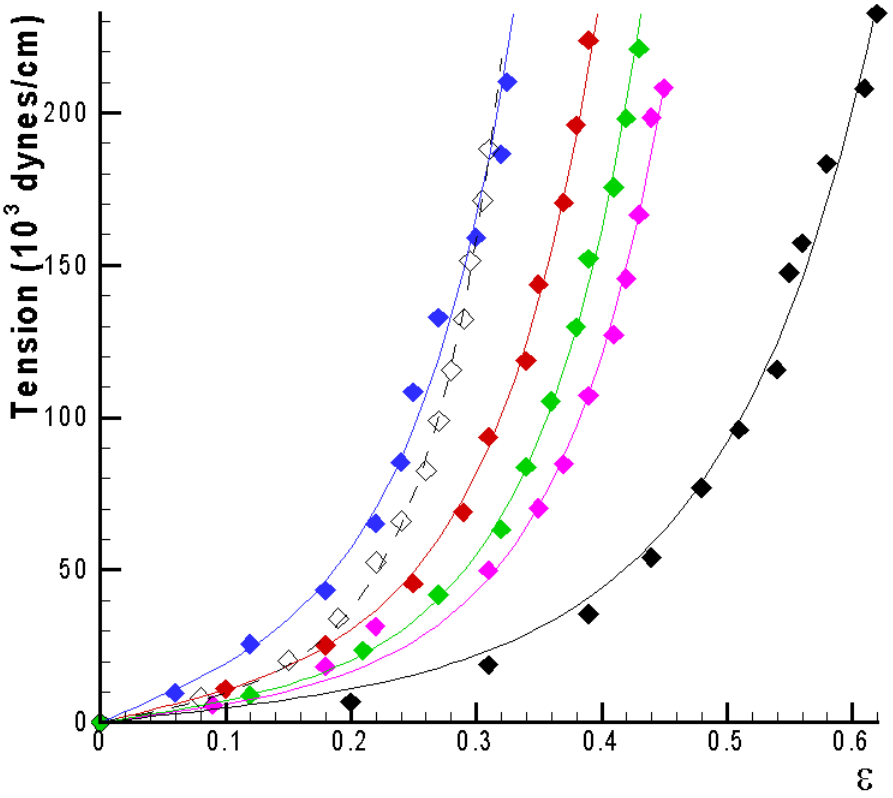

Figure 23: Resulting tension vs ϵ curves for inflation of cylindrical membrane of samples A (black color), B (red color), C (blue color), D (purple color), E (green color) and F (black dashed line) of which the material parameters shown in Table 15 along with the corresponding experimental data from Nagasawa *et al.* [147].

Table 15: Resulting material parameters and R^2 values for experimental data by Nagasawa *et al.* [147] on basilar segments of treated mongrel dogs using equation (3.64).

Labels	A	B	C	D	E	F
C/E contents:	1.6 ± 0.2	2.1 ± 0.3	2.7 ± 0.4	3.5 ± 0.5	4.3 ± 0.6	5.1 ± 0.9
$\alpha_1(10^3 dynes/cm^2)$	1004.208	2088.555	3698.864	1189.203	1406.443	1674.112
γ_1	2.5976	4.6615	5.1351	4.3772	4.6510	7.7963
R^2	0.9899	0.9956	0.9862	0.9941	0.9950	0.99833

3.4 NONHOMOGENEOUS DEFORMATION: INFLATION OF A THICK WALLED HOLLOW CYLINDER

In this section, we consider a thick walled dual mechanism cylinder where each mechanism is composed of an isotropic incompressible hyperelastic material that is radially inflated due to the transmural pressure $\Delta P = P_i - P_o$, where P_i and P_o are the uniform pressures acting at the inner and outer wall, respectively. The perfusion test of an intact arterial segment previously discussed can be modelled by this particular deformation when the arterial wall is considered thick and so the stress variation along the thickness is taken into account. In the work by Carroll [148], the behavior of the transmural pressure ΔP during loading was studied for various strain energy functions. A relevant work is provided by Demiray and Vito [125] in which using computational results of combined inflation and extension of exponential type thick walled cylinder identified segments of an artery. Unlike in those two studies, here we consider pure inflation of thick walled cylinder (without considering extension) and also some possible unloading cases in the context of the multi mechanism theory.

It will be seen that this problem serves as an example in which the resulting deformation is nonuniform throughout the body (inhomogeneous deformation). As a result, each of the activation and deactivation criteria is not simultaneously satisfied throughout the body. During loading, (provided that the deformation level is sufficiently large), the activation and deactivation criteria are first satisfied at the inner most layer of the wall. This implies that collagen fibers at the inner layers theoretically will be recruited earlier than those at the outer

layers and similarly the elastin at the inner layers will be damaged first. The first suggestion might be difficult to demonstrate since generally collagen fibers are not evenly distributed throughout the thickness of a cerebral arterial wall [149]. Nevertheless, observations on perfused segments of rabbit aorta show that when the pressure increases to 200 mmHg the collagen fibers in the media appear to loose their waviness while those in the adventitia remain in bundles [150]. Here, the collagen recruitment is measured indirectly by observing how the crimped collagen bundles transform into taut and oriented fibers. On the other hand, the later implication, on the location of elastin breakage, to the best of our knowledge, has not been demonstrated yet.

We will see as a result of inhomogeneity of the deformation the wall will contain one or more of the following regions: a region that is occupied by elastin only, a region that contains both elastin and collagen fibers and a region that contains only collagen fibers. In the unloading case, an 'empty' region with neither active elastin nor active collagen may develop.

Let the inner and outer radii of the undeformed cylinder denoted by R_i and R_o, respectively (see Figure 24). With respect to the cylindrical coordinates system (R, Θ, Z) with Z-axis aligned with the axis of the cylinder, the undeformed cylindrical shell occupies the following space:

$$R \in [R_i, R_o], \qquad \Theta \in [0, 2\pi], \qquad \text{and} \qquad Z \in [0, L]. \tag{3.73}$$

Let the configuration that is taken up by the undeformed body denoted by κ_1. We suppose that $P_i > P_o$, so that the cylinder experiences pure radial inflation (see Figure 24). It is assumed that the length of the undeformed cylinder L is sufficiently long so that the deformation can be regarded as plain strain and the ends effect can be neglected. In addition, the deformation is assumed to be axisymmetric. The inner and outer radii of the deformed cylinder are denoted as r_i and r_o, respectively. The pressures are introduced as applied surface traction that can be summarized as follows:

$$\mathbf{t} = -P_i \mathbf{e_r} \text{ on } r = r_i \qquad \text{and} \qquad \mathbf{t} = -P_o \mathbf{e_r} \text{ on } r = r_o. \tag{3.74}$$

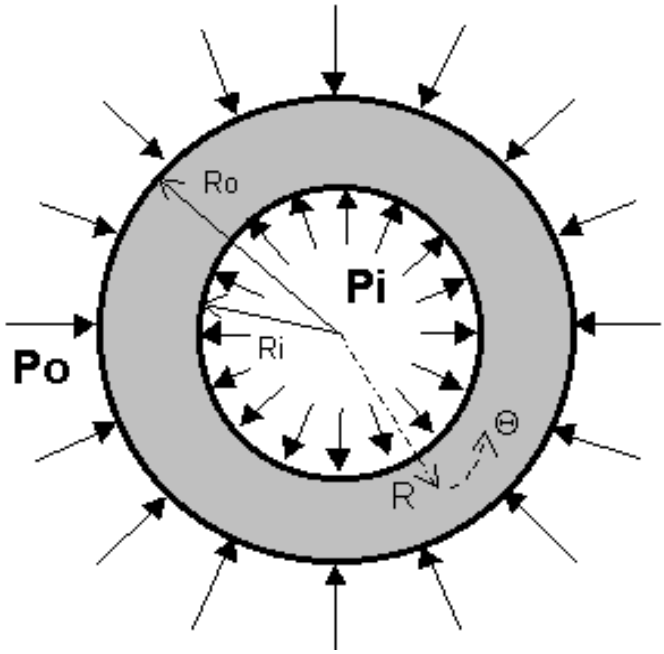

Figure 24: Inflation of a thick walled cylindrical shell.

As sufficiently low transmural pressure, the activation criterion of the second mechanism will not be satisfied anywhere in the body. In the cylindrical coordinate system, material points of original material at arbitrary position (R,Θ,Z) at reference configuration κ_1 will move to new radius r in the deformed or current configuration κ with no change to their circumferential or axial position. The deformation can be described as follows:

$$r = \sqrt{R^2 + C}, \qquad \theta = \Theta, \qquad \text{and} \qquad z = Z, \tag{3.75}$$

where C is a constant. The following deformation gradient as well as the corresponding Left Cauchy Green tensor and its inverse are derived from the motion described in (3.75) for all material points relative to the reference configuration κ_1,

$$\mathbf{F_1} = \text{DIAG}[\frac{1}{\lambda}, \lambda, 1], \qquad \mathbf{B_1} = \text{DIAG}[\frac{1}{\lambda^2}, \lambda^2, 1], \qquad \mathbf{B_1}^{-1} = \text{DIAG}[\lambda^2, \frac{1}{\lambda^2}, 1], \tag{3.76}$$

where the incompressibility restriction has been implemented. In (3.76), λ denotes the stretch ratio r/R, where r and R denote the deformed and undeformed radii, respectively, of a particle in the wall. A procedure given by Spencer [151] can be used to obtain $\mathbf{F_1}$

in (3.76.1). It will be seen that λ is dependent on spatial position. The first and second components of $\mathbf{F_1}$ represent the stretch ratios in the radial and circumferential directions, respectively. The third component is always unity implying that there is no stretch in the longitudinal direction. During inflation, *i.e* $\lambda > 1$, as the circumference enlarges, the wall thins to preserve the volume of the cylinder.

The first and second invariants of $\mathbf{B_1}$ are equal and denoted by I_1 and II_1 , respectively:

$$I_1 = II_1 = 1 + \lambda^2 + \frac{1}{\lambda^2}. \tag{3.77}$$

Since the activation criterion is not satisfied anywhere in the body, the non-zero Cauchy stress tensor components are given by (2.17) and (2.18) for $s < s_a$ with $\mathbf{B_1}$ and its inverse given by (3.76.2 and 3), respectively:

$$\begin{aligned} T_{rr} &= -p + 2\frac{\partial W_1}{\partial I_1}\frac{1}{\lambda^2} - 2\frac{\partial W_1}{\partial II_1}\lambda^2 \\ T_{\theta\theta} &= -p + 2\frac{\partial W_1}{\partial I_1}\lambda^2 - 2\frac{\partial W_1}{\partial II_1}\frac{1}{\lambda^2} \\ T_{zz} &= -p + 2\frac{\partial W_1}{\partial I_1} - 2\frac{\partial W_1}{\partial II_1}. \end{aligned} \tag{3.78}$$

The equilibrium equations in the cylindrical coordinates system are reduced to the following equations:

$$\frac{\partial T_{rr}}{\partial r} + \frac{T_{rr} - T_{\theta\theta}}{r} = 0, \qquad \frac{1}{r}\frac{\partial T_{\theta\theta}}{\partial \theta} = 0, \qquad \text{and,} \qquad \frac{\partial T_{zz}}{\partial z} = 0. \tag{3.79}$$

The equations (3.79.2 and 3) imply the dependency of the Cauchy stress on r only. The differential equations reduces to the integration of the stress difference $(T_{rr} - T_{\theta\theta})$ shown in (3.79.1). The integration of (3.79.1) across the wall thickness and the use of boundary conditions (3.74) results in the relation between the transmural pressure ΔP and the stress difference as follows:

$$T_{rr}(r_o) - T_{rr}(r_i) = \Delta P = \int_{r_i}^{r_o} \frac{T_{\theta\theta} - T_{rr}}{r} dr. \tag{3.80}$$

At this stage, one can rewrite the stress difference as a function of r instead of λ and perform the integration to obtain the expression of ΔP in terms of r_i and r_o. A method suggested by Carroll [148] results in more useful expression of ΔP in terms of nondimensional variable

λ_i, the stretch ratio at the inner radius. This however requires substitution of r with λ using the following relation between dr and $d\lambda$:

$$\frac{dr}{r} = -\frac{d\lambda}{\lambda(\lambda^2 - 1)}, \tag{3.81}$$

that can be derived from the following local incompressibility restriction:

$$r^2 - r_i^2 = R^2 - R_i^2. \tag{3.82}$$

After substituting (3.78.1 and 2) and (3.81) into (3.80) and replacing the limits of the integration with the corresponding values of λ, the following relation is obtained:

$$\Delta P = -\int_{\lambda_i}^{\lambda_o} 2(\frac{\partial W_1}{\partial I_1} + \frac{\partial W_1}{\partial I I_1})(\lambda^2 - \frac{1}{\lambda^2})\frac{d\lambda}{\lambda(\lambda^2 - 1)}, \tag{3.83}$$

where the upper and lower limits of the integration can be determined from the incompressibility restriction as follows:

$$\lambda_o = \lambda(R_o) = \sqrt{1 + (\lambda_i^2 - 1)(\frac{R_i}{R_o})^2}. \tag{3.84}$$

The relation (3.84) can be derived from (3.82) for $r = r_o$ and $R = R_o$, which is equivalent to imposing incompressibility for the entire volume of the cylinder. The generalization of (3.84) for any radius stretch ratios can be done by manipulating (3.82) to obtain the following important relation:

$$\lambda = \lambda(R) = \sqrt{1 + (\lambda_i^2 - 1)(\frac{R_i}{R})^2}. \tag{3.85}$$

The relations (3.84) and (3.85) demonstrate the inhomogeneity of the deformation that, for this particular deformation, is manifested as a monotonically decreasing stretch ratio λ from the innermost to the outermost layer of the wall for any inflated state. Moreover, the relation between λ_i and λ_o shown in (3.84) allows the deformation to be measured by one parameter. The stretch ratio of the inner radius, λ_i, commonly is selected as the parameter since it is always maximum. Since the deformation is now parameterized by a single variable, it follows that the activation (2.7) and deactivation criteria (2.14) can be reduced to

$$A_a = \lambda - \lambda_a \qquad \text{and} \qquad A_b = \lambda - \lambda_b, \tag{3.86}$$

respectively. Here, λ_a and λ_b are the critical stretch ratios of the activation of the second mechanism, representing collagen recruitment, and the deactivation of the first mechanism, representing elastin breakage, respectively. Here, we also assume that there is no spatial variation of values of the critical stretch ratios λ_b and λ_a and that $\lambda_b > \lambda_a$ all the time.

Since λ is always maximum at $r = r_i$, the activation and deactivation criteria are always satisfied at the innermost layer first. This means that the recruitment of collagen fibers and the breakage of the elastin will always occur at the innermost layer first.

We shall discuss briefly here the involvement of many reference configurations for the introduction of the second mechanism. This phenomenon must be distinguished from a similar one encountered in biaxial loading in which the collagen recruitment is associated with a set of reference configurations each of which represents a loading state with $s = s_a$ but from many different possible biaxial loading configurations *i.e* different λ_x to λ_y ratio. While in the biaxial loading case, once a biaxial loading path is selected, a loading history can only have one, among many others, reference configuration for the second mechanism, in the inflation of thick walled cylinder a loading history must employ multi reference configurations for the second mechanism.

We begin the discussion by considering the configuration occupied by the deformed body when the collagen fibers are activated at the innermost layer. So, in this configuration, say κ_{2a}, $\lambda_i = \lambda_a$ and hence $s(r = r_i) = s_a$. The mechanical response representing the active collagen contained in layer $r = r_i$ is called the second mechanism introduced at $r = r_i$. This second mechanism takes configuration κ_{2a} as the reference configuration. Note that when s at the innermost layer is equal to s_a, s values at neighboring layers are less than s_a since the stretch ratio at the innermost layer is always maximum. Therefore at κ_{2a} only collagen fibers contained in the innermost layer becomes active and not in other layers ($r > r_i$).

The situation changes when the loading continues. Following (3.85), the progression of λ_i causes the stretch ratios at the neighboring layers, $\lambda(r > r_i)$, to increase. However, for any inflated state, λ monotonically decrease toward the outer wall from its maximum at the inner wall. In other words, during loading, λ of each layer progresses from some degree less than to become equal to λ_a. This also means that for any configuration identified by some $\lambda_i > \lambda_a$ there is always one layer having $s = s_a$ marking the activation of collagen fibers contained

in that layer. The second mechanism representing the activated collagen fibers then pick up the corresponding configuration as its reference configuration. When λ_i is increased, more and more layers end up having $s = s_a$ and therefore more collagen fibers are activated and more configuration must be employed. This process is valid until $s(r = r_o)$ (the outermost layer) is equal to s_a when all layers in the wall contain active collagen fibers and no more collagen fibers can become activated. This particular inflated state, where $s(r = r_o) = s_a$, will be identified with $\lambda_i = \lambda_{ioa}$ which can be seen as the magnitude of λ_i ($\lambda(r = r_i)$) that causes $\lambda(r = r_o) = \lambda_o = \lambda_a$.

3.4.1 Loading

In this subsection, we study the behavior of the transmural pressure ΔP as the inner wall stretch ratio λ_i progresses. Due to the inhomogeneity of the deformation, we should expect that the collagen fibers will become activated throughout the wall in a gradual manner. The same expectation should be applied to the elastin breakage process. It will be seen that generally during the loading, λ_i will follow the progression path below:

$$1 \rightarrow \lambda_a \rightarrow \min(\lambda_{ioa}, \lambda_b) \rightarrow \max(\lambda_{ioa}, \lambda_b) \rightarrow \lambda_{iob}, \tag{3.87}$$

where λ_{ioa} and λ_{iob} denote the value of λ_i that causes the outer wall to satisfy the activation and deactivation criteria, respectively. The following loading states must be considered:

- Loading Case 1: $1 \leq \lambda_i < \lambda_a$

  The case when $\lambda_i < \lambda_a$ was discussed above. This is the loading range where the criteria are not met at the innermost layer (and therefore nowhere in the wall). Obviously, this case resembles inflation of the classical hyperelastic thick walled cylinder. In this case, the transmural pressure, ΔP, is given by (3.83), where λ_o is related to λ_i through (3.84), for $1 \leq \lambda_i < \lambda_a$.

- Loading Case 2: $\lambda_a \leq \lambda_i < \min(\lambda_{ioa}, \lambda_b)$

  We suppose that the loading process continues from Case 1 so that an inflated state where the innermost layer satisfies the activation criterion is reached. Note however that as the loading is continued, more and more layers next to the innermost radius will

become stretched and will satisfy the collagen activation criterion. Therefore, eventually as the loading progresses the wall will be completely filled with active collagen fibers in addition to elastin. This occurs when λ_o reaches λ_a (or equivalently when λ_i reaches λ_{ioa}). However, there is a chance that the innermost layer satisfies the elastin breakage criterion at some inflated state before the collagen fibers fully occupy the wall.

It follows that we should consider in this loading case, a loading range of λ_i from λ_a, when the innermost layer begins to activate the collagen fibers, until either λ_b, when the innermost layer begins to experience elastin damage, or λ_{ioa}, when the outermost layer satisfies the collagen recruitment criterion, depending on the values of λ_b relative to λ_{ioa}. The deformation gradients of the first and second mechanisms will be discussed next. The deformation gradient of the first mechanism relative to the reference configuration κ_1 however has been described earlier. The deformation gradient of the second mechanism will be described below. First we recall that at the early stage of this loading case, say when $\lambda_i = \lambda_a$, the deformation gradient of the material points at the innermost layer relative to the reference configuration κ_1 can be derived from (3.76.1) as follows;

$$\mathbf{F_1}(r = r_i) = \text{DIAG}[\frac{1}{\lambda_a}, \lambda_a, 1]. \tag{3.88}$$

Let the configuration that is occupied by the body at this stage be denoted as κ_{2a}. Then, as was discussed before, at configuration κ_{2a} the collagen fibers contained in the innermost layer begin to be activated. The second mechanism representing the activated collagen fibers takes configuration κ_{2a} as the reference configuration. Following (2.12) and (3.88), the deformation gradient of the second mechanism is given as follows:

$$\mathbf{F_{2a}}(r = r_i) = \text{DIAG}[\frac{\lambda_i}{\lambda_a}, \frac{\lambda_a}{\lambda_i}, 1] \tag{3.89}$$

with the corresponding Left Cauchy strain tensor and its inverse that are given as:

$$\mathbf{B_{2a}}(r = r_i) = \text{DIAG}[\frac{\lambda_a^2}{\lambda_i^2}, \frac{\lambda_i^2}{\lambda_a^2}, 1], \qquad \text{and} \qquad \mathbf{B_{2a}}^{-1}(r = r_i) = \text{DIAG}[\frac{\lambda_i^2}{\lambda_a^2}, \frac{\lambda_a^2}{\lambda_i^2}, 1]. \tag{3.90}$$

As λ_i progresses, the domain radii occupied by activated collagen fibers increases. At a particular inflated state $\lambda_i > \lambda_a$, the recruited collagen fibers occupy a region between r_i and, say, r_a, where r_a is given by:

$$r_a = \sqrt{\frac{(\lambda_i^2 - 1)}{(\lambda_a^2 - 1)}}\lambda_a R_i. \tag{3.91}$$

Simply speaking, $r = r_a$ represents the radius at which $s = s_a$. The relation (3.91) can be easily derived from (3.85) and by using the definition of $\lambda_a = r_a/R_a$. Moreover, (3.91) states that the region with recruited collagen grows, *i.e* r_a enlarges, as λ_i increases. On the other hand, the complimentary region ($r_a < r \leq r_o$) that contains active elastin only, shrinks as the loading progresses. The deformation gradient of the second mechanism of any r in the region bounded by $r_i \leq r \leq r_a$ can be generalized from (3.89) as follows:

$$\mathbf{F_2}(r) = \text{DIAG}[\frac{\lambda}{\lambda_a}, \frac{\lambda_a}{\lambda}, 1]. \tag{3.92}$$

Here, λ, or more precisely $\lambda(r)$, can be related to λ_i by (3.85). Of course, the value of λ_a in (3.92) generally can be set to be different from one layer to another. In the real situation in which the collagen fibers are not distributed uniformly and may be activated at different local stretch ratio, the situation can be modelled by setting different s_a or λ_a for each layer. Following (3.92), the Left Cauchy Green strain tensor and its inverse are given as follows:

$$\mathbf{B_2} = \text{DIAG}[\frac{\lambda_a^2}{\lambda^2}, \frac{\lambda^2}{\lambda_a^2}, 1], \qquad \text{and} \qquad \mathbf{B_2}^{-1} = \text{DIAG}[\frac{\lambda^2}{\lambda_a^2}, \frac{\lambda_a^2}{\lambda^2}, 1]. \tag{3.93}$$

The nonzero components of Cauchy stress tensor of material points in the region bounded by $r_i \leq r \leq r_a$, in which the activation criterion is satisfied, are given by (2.17) and (2.18) for $s_a \leq s < s_b$:

$$\begin{aligned}
T_{rr} &= -p + 2\frac{\partial W_1}{\partial I_1}\frac{1}{\lambda^2} - 2\frac{\partial W_1}{\partial II_1}\lambda^2 + 2\frac{\partial W_2}{\partial I_2}\frac{\lambda_a^2}{\lambda^2} - 2\frac{\partial W_2}{\partial II_2}\frac{\lambda^2}{\lambda_a^2} \\
T_{\theta\theta} &= -p + 2\frac{\partial W_1}{\partial I_1}\lambda^2 - 2\frac{\partial W_1}{\partial II_1}\frac{1}{\lambda^2} + 2\frac{\partial W_2}{\partial I_2}\frac{\lambda^2}{\lambda_a^2} - 2\frac{\partial W_2}{\partial II_2}\frac{\lambda_a^2}{\lambda^2} \\
T_{zz} &= -p + 2\frac{\partial W_1}{\partial I_1} - 2\frac{\partial W_1}{\partial II_1} + 2\frac{\partial W_2}{\partial I_2} - 2\frac{\partial W_2}{\partial II_2},
\end{aligned} \tag{3.94}$$

where tensors $\mathbf{B_1}$ and its inverse are still given by (3.76.2 and 3) and $\mathbf{B_2}$ and its inverse are given by (3.93). The nonzero components of Cauchy stress tensor of material points at the complimentary region defined by $r_a < r \leq r_o$ are given by (3.78). When (3.78.1 and 2) and (3.94.1 and 2) are substituted into (3.80) together with (3.81), the following relation is obtained:

$$\Delta P = E_1(\lambda_o) - E_1(\lambda_i) + E_2(\lambda_a) - E_2(\lambda_i), \tag{3.95}$$

where the useful notations $E_1(\Lambda)$ and $E_2(\Lambda)$ are defined as follows:

$$E_1(\Lambda) \equiv -\int_{\lambda}^{\Lambda} 2\left(\frac{\partial W_1}{\partial I_1} + \frac{\partial W_1}{\partial II_1}\right)\left(\lambda^2 - \frac{1}{\lambda^2}\right)\frac{d\lambda}{\lambda(\lambda^2-1)} \qquad \text{and}$$
$$E_2(\Lambda) \equiv -\int_{\lambda}^{\Lambda} 2\left(\frac{\partial W_2}{\partial I_2} + \frac{\partial W_2}{\partial II_2}\right)\left(\frac{\lambda^2}{\lambda_a^2} - \frac{\lambda_a^2}{\lambda^2}\right)\frac{d\lambda}{\lambda(\lambda^2-1)}. \tag{3.96}$$

It can be seen in the relation (3.95) that the contribution to the transmural pressure by the first mechanism is represented by $E_1(\Lambda)$s, and by the second mechanism is represented by $E_2(\Lambda)$. It is clear to see that the solution for a classical hyperelastic material is easily recovered by removing $E_2(\Lambda)$s from (3.95). The limits of integration for E_1 (maximum at λ_i and minimum at λ_o) dictate the participation of the elastin contained in the entire wall thickness for this particular loading case. However, the relation (3.95) rests on the assumptions that the first mechanism is homogeneous and isotropic material. On the other hand, the participation of collagen fibers are confined to the region between the inner wall to the layer having stretch ratio λ_a. It is clear therefore that $E_2(\Lambda)$ does not play a role when $\lambda_i \leq \lambda_a$.

The relation (3.95) is no longer valid when one of the following situations occurs. The first situation is when the collagen fibers are activated throughout the wall. As the loading increase, λ_i increases as well as the stretch ratios of the neighboring layers. The radius r_a of the layer having $\lambda = \lambda_a$, r_a also enlarges and eventually encompasses the outer wall, so that $r_a \geq r_o$. In this situation, λ_a cannot be the limit of integration $E_2(\Lambda)$ since r_a lies outside the wall. The limits of integration for $E_2(\Lambda)$ has to be λ_i and λ_o representing the inner and outer wall, respectively. The configuration at which the outer

wall satisfies the activation criterion will be identified with $\lambda_i = \lambda_{ioa}$. With the help of (3.84), λ_{ioa} can be obtained as follows:

$$\lambda_{ioa} = \sqrt{1 + (\lambda_a^2 - 1)\frac{R_o^2}{R_i^2}}. \tag{3.97}$$

The other scenario that violates (3.95) is when elastin breakage occurs. As was discussed, (3.95) is valid for elastin representation throughout the entire wall. When the stretch ratios at some inner layers become greater than λ_b, the elastin damage occurs there creating inactive elastin layers. The integration of $E_1(\Lambda)$s cannot be performed between the inner and outer walls, but must be done between the outer wall and some layer in the middle of wall thickness that separates the healthy from the deactivated wall region. The stretch ratio of the layer that is just about to experience damage obviously is λ_b. When this situation is met the limits of integration of E_1 must be changed to λ_o and λ_b.

- Loading Case 3A. $\lambda_b \leq \lambda_i < \lambda_{ioa}$

  We suppose that the loading is continued from Case 2. As was discussed in Case 2 and also according to (3.87), the next deformation level during loading depends on the value of λ_b relative to λ_{ioa}. We suppose that the breakage of elastin at the inner wall is achieved at an earlier deformation state than the collagen recruitment at the outer wall. In other words, $\lambda_b < \lambda_{ioa}$, which by (3.97) implies the following inequality must hold:

$$\frac{\lambda_a^2 - 1}{\lambda_b^2 - 1} > \frac{R_i^2}{R_o^2}. \tag{3.98}$$

  When $\lambda_i \geq \lambda_b$ the damaged elastin will occupy a region defined by $r_i \leq r \leq r_b$ where r_b is given by:

$$r_b = \sqrt{\frac{(\lambda_i^2 - 1)}{(\lambda_b^2 - 1)}}\lambda_b R_i. \tag{3.99}$$

  The radius $r = r_b$ represents the radius at which $s = s_b$. Moreover, the relation (3.99) can be easily derived from (3.85) and by using the definition of $\lambda_b = r_b/R_b$. It is clear that only collagen fibers are active in the region defined by $r_i \leq r \leq r_b$. The Cauchy stress therefore arises from the second mechanism only. The nonzero components of the

Cauchy stress tensor for material points in this region are given by (2.17) and (2.18) for $s_b \leq s$ are as follows:

$$\begin{aligned} T_{rr} &= -p + 2\frac{\partial W_2}{\partial I_2}\frac{\lambda_a^2}{\lambda^2} - 2\frac{\partial W_2}{\partial II_2}\frac{\lambda^2}{\lambda_a^2} \\ T_{\theta\theta} &= -p + 2\frac{\partial W_2}{\partial I_2}\frac{\lambda^2}{\lambda_a^2} - 2\frac{\partial W_2}{\partial II_2}\frac{\lambda_a^2}{\lambda^2} \\ T_{zz} &= -p + 2\frac{\partial W_2}{\partial I_2} - 2\frac{\partial W_2}{\partial II_2}, \end{aligned} \tag{3.100}$$

where $\mathbf{B_2}$ and its inverse given by (3.93). The region next to the damaged elastin region is occupied by both active elastin and collagen. The inner boundary of this middle region therefore is $r = r_b$. However, since the wall is only partially occupied by active collagen, the outer boundary of this region is the front of the collagen recruitment region given by the radius $r = r_a$. This middle region is defined by $r_b \leq r \leq r_a$. The nonzero components of the Cauchy stress tensor for material points in this region are given by (3.94). The outermost region in this loading case obviously is a region filled by elastin only and is defined by $r_a \leq r \leq r_o$. The nonzero components of Cauchy stress tensor for material points in this region are given by (3.78).

The computation of ΔP is obtained from substitution of (3.78), (3.94) and (3.101) into (3.80) together with (3.81). The result is:

$$\Delta P = E_1(\lambda_o) - E_1(\lambda_b) + E_2(\lambda_a) - E_2(\lambda_i), \tag{3.101}$$

where $E_1(\Lambda)$ and $E_2(\Lambda)$ are given by (3.96). As was discussed in Case 2, the difference between (3.101) and (3.95) is that the maximum limit of the integration for $E_1(\Lambda)$ is λ_b instead of λ_i.

- Loading Case 3B. $\lambda_{ioa} \leq \lambda_i < \lambda_{iob}$

  The previous loading case results in both collagen recruitment and elastin breakage in a region that only partially occupies the wall. The assumption that $\lambda_b > \lambda_a$ for all the inflated states however implies that, when the loading continues, the complete elastin breakage will not occur until the collagen recruitment fully occupies the wall. This progression path has been shown in (3.87). The complete collagen recruitment and complete elastin breakage are identified by $\lambda_i = \lambda_{ioa}$ and $\lambda_i = \lambda_{iob}$, respectively. The

current loading case deals with the states between a partial elastin breakage state and full collagen recruitment state ($\lambda_{ioa} \leq \lambda_i < \lambda_{iob}$).

The region of damaged elastin is still defined by $r_i \leq r \leq r_b$. In this case, the outer border of the region that is occupied by both active elastin and collagen has reached the outer wall and therefore the outer bound of the region is given by r_o instead of r_a. The Cauchy stress of material points in the region with damaged elastin is still given by (3.101), while those in the elastin and collagen region is given by (3.94). Following the procedure performed in previous cases, the transmural pressure ΔP in this case is given by:

$$\Delta P = E_1(\lambda_o) - E_1(\lambda_b) + E_2(\lambda_o) - E_2(\lambda_i), \tag{3.102}$$

where $E_1(\Lambda)$ and $E_2(\Lambda)$ are given by (3.96). The expression for ΔP in this case differs from those of Case 3A only in the minimum limit of the integration $E_2(\lambda)$ where we have here λ_o instead of λ_a.

- Loading Case 4A. $\lambda_{ioa} \leq \lambda_i < \lambda_b$

  An alternative loading path to Case 3A is provided by the situation where $\lambda_b > \lambda_{ioa}$. So, as opposed to (3.98), the following inequality must hold:

$$\frac{\lambda_a^2 - 1}{\lambda_b^2 - 1} < \frac{R_i^2}{R_o^2}. \tag{3.103}$$

  In this case, the innermost layer hasn't satisfied the elastin breakage criterion yet when the collagen recruitment reaches the outermost layer. Therefore, the entire wall is occupied by both active elastin and collagen fibers. The Cauchy stress components for material points throughout the wall are given by (3.94). The transmural pressure ΔP will be given by the following relation:

$$\Delta P = E_1(\lambda_o) - E_1(\lambda_i) + E_2(\lambda_o) - E_2(\lambda_i), \tag{3.104}$$

  where E_1 and E_2 are given by (3.96). It's easy to see that (3.104) demonstrates the participation of both mechanisms in the stress generation throughout the entire thickness.

- Loading Case 4B. $\lambda_b \leq \lambda_i < \lambda_{iob}$

  When the loading continues from Case 4A, λ_i is increased so that $\lambda_i \geq \lambda_b$ as is indicated by (3.87). Here, the elastin at the innermost layer is damaged and eventually a region with damaged elastin will develop as λ_i increases. The region with inactive elastin occupies radius r where $r_i < r \leq r_b$ and r_b is given by (3.99). The resulting regions of this case will be the same as those from Case 3B. The outcome of this case is the same as that described in loading Case 3B.

- Loading Case 5. $\lambda_{iob} \leq \lambda_i$

  We suppose that λ_i can be increased beyond that of Case 3B or Case 4B. As is indicated by (3.87), the outermost layer eventually will satisfy the deactivation criterion, *i.e* $\lambda_b \leq \lambda_o$. In this case the elastin in the entire wall will be deactivated, leaving only collagen as the mechanical source of bearing support. Replacing λ_a in (3.97) with λ_b, we can obtain λ_{iob}:

$$\lambda_{iob} = \sqrt{1 + (\lambda_b^2 - 1)\frac{R_o^2}{R_i^2}}. \tag{3.105}$$

  In this case, the Cauchy stress of the entire wall will be given by (3.101). The transmural pressure ΔP is given by:

$$\Delta P = E_2(\lambda_o) - E_2(\lambda_i), \tag{3.106}$$

  where E_2 is given by (3.96.2). The expression (3.106) clearly demonstrates the absence of the first mechanism in the stress generation.

3.4.2 Unloading

We also want to learn the behavior of the transmural pressure ΔP during unloading after a maximum deformation level is attained. We suppose that the maximum stretch ratios at the inner and outer walls obtained during loading be denoted by λ_i^* and λ_o^*, respectively. The behavior of ΔP will depend on the values of λ_i^* relative to λ_a and λ_b. Following the previously discussed loading cases, the unloading cases listed below will be considered.

- Unloading from case 1: $1 \leq \lambda_i^* < \lambda_a$

  Here, we consider the case when the unloading begins before any collagen recruitment.

Clearly, this case resembles the unloading of classical elastic materials in which only one mechanism is involved. During unloading the Cauchy stress will be given by (3.78) and the transmural pressure (3.83). It is easy to see that, in this case, the zero transmural pressure is obtained when $\lambda_i = \lambda_o = 1$, *i.e* the segment returns to its original reference configuration κ_1.

- Unloading from Case 2: $\lambda_a \leq \lambda_i^* < \min(\lambda_{ioa}, \lambda_b)$

  In this case, unloading begins at some deformation level after collagen recruitment begins but before either the elastin breakage as begun or collagen recruitment has been completed throughout the wall. At the beginning of the unloading process, the wall is divided into two regions: a region that is filled with elastin only at the outer side and an inner region that is occupied by both elastin and active collagen. The value of for particles inside the inner region is greater than s_a, while the value of s for particles inside the outer region is less than s_a. The radius of the interface between the two regions is given by $r = r_a$ at which $\lambda = \lambda_a$.

  During unloading, the amount of active collagen decreases and the inner region shrinks. As λ_i decreases, all $\lambda(r)$ and therefore all $s(r)$ along the radius decrease. The interface is no longer given by $r = r_a$ but somewhere at $r < r_a$. The value of s for layers in the inner region gradually become equal to and even less than s_a. Here, we suppose that when s reduces to s_a *i.e* λ reduces to λ_a, the stretched collagen fibers return to the unloaded length. Furthermore, in the layers where $\lambda < \lambda_a$, the collagen is recrimped and becomes inactive. Eventually, when $\lambda_i = \lambda_a$, all collagen fibers is inactive and the entire thickness is occupied solely by the elastin.

  In this unloading case, the process from $\lambda_i = \lambda_i^*$ to $\lambda_i = 1$ involves two ranges of λ_i: $\lambda_a \leq \lambda_i \leq \lambda_i^*$ and $1 \leq \lambda_i \leq \lambda_a$. In the first range, when λ_i reduces from λ_i^* to λ_a, the Cauchy stress of the particles in the inner region is given by (3.94), while of those in the outer region is given by (3.78). The transmural pressure, ΔP, is given by (3.95). During the second unloading stage, the inner region disappears and only elastin is active in the entire wall. This stage clearly is the same as the unloading case 1. The Cauchy stress then is given by (3.78). The transmural pressure, ΔP, will be given by (3.83) and becomes zero when the segment returns to the original reference configuration, κ_1.

- Unloading from case 4A: $\lambda_{ioa} \leq \lambda_i^* < \lambda_b$

  In this case, the unloading begins after the collagen is activated in the entire wall but before the elastin breakage occurs. So here, when $\lambda_i = \lambda_i^*$, the entire wall is filled with both active elastin and collagen. When λ_i is reduced from λ_i^*, both collagen and elastin are active throughout the thickness as long as the outermost layer is stretched beyond λ_a. Once this condition is ceases to be met, $\lambda_o < \lambda_a$, there is an outer region of the wall where collagen is inactive. At this deformation level, we return to the unloading process described in the previous case (unloading Case 2).

  Recalling that the deformation level at which $\lambda_o = \lambda_a$ is identified with $\lambda_i = \lambda_{ioa}$, it appears that the unloading process can be seen to involve three unloading stages; $\lambda_i^* > \lambda_i \geq \lambda_{ioa}$, $\lambda_{ioa} > \lambda_i \geq \lambda_a$, and $\lambda_a > \lambda_i \geq 1$. In the first stage, the Cauchy stress of all material points arise due to both mechanisms and is given by (3.94). The transmural pressure, ΔP, therefore is given by (3.104). When the unloading continues further so that $\lambda_i < \lambda_{ioa}$, the collagen fibers are active in only some part of the wall. The wall is divided into two regions, an elastin only region and an inner region filled with both elastin and collagen as was shown in the unloading for Case 2A. Clearly, further unloading situations can be described by the unloading of Case 2A.

- Unloading from Case 3A: $\lambda_b \leq \lambda_i^* < \lambda_{ioa}$

  In one case, the unloading may begin at some deformation level after some inner layers lost their elastin but before the collagen fibers completely occupy the entire thickness. So, here $\lambda_o^* < \lambda_b \leq \lambda_i^* < \lambda_{ioa}$, where λ_o^* is the corresponding outer wall stretch ratio when $\lambda_i = \lambda_i^*$. We suppose that the region in which the elastin is damaged occupies a region bounded by the inner radius r_i and the interface radius, say r_b^*, between the damaged region and the healthy region. The interface radius, r_b^*, is formulated as follows;

$$r_b^{*2} = \frac{(\lambda_i^{*2} - 1)}{(\lambda_b^2 - 1)} \lambda_b^2 R_i^2. \tag{3.107}$$

  The expression (3.107) is obtained by substituting λ_i^* for λ_i in (3.99). At the interface, $\lambda = \lambda_b$, when $\lambda_i = \lambda_i^*$. The Lagrangian description of these boundaries are given by the inner radius R_i and the interface radius R_b^* that is formulated as follows;

$$R_b^{*2} = \frac{(\lambda_i^{*2} - 1)}{(\lambda_b^2 - 1)} R_i^2. \tag{3.108}$$

The formulation is obtained from (3.107) and the definition of λ. As was discussed elsewhere, it is assumed that the damaged elastin is unrecoverable. The associated region, which is occupied by collagen only, is also unrepairable and is going to be unchanged throughout the unloading history. When λ of a damaged layer is decreased from some $\lambda > \lambda_b$ to $\lambda < \lambda_b$, the elastin contained in the layer cannot be reactivated.

The stress contribution by the first mechanism is generated from the region bounded by r_b^* and r_o only. The stretch ratios at this boundaries then must be defined. While λ_o can be easily calculated from (3.84), the stretch ratio at the boundary of damaged elastin region for a given λ_i is not defined yet. We denote the stretch ratio at $r = r_b^*$: or R_b^* in the reference configuration, with λ_{rb}. The value of λ_{rb} can be obtained with the help of (3.85) by substituting R with R_b^* obtained from (3.108) as follows:

$$\lambda_{rb}^2 = 1 + \frac{(\lambda_i^2 - 1)}{(\lambda_i^{*2} - 1)}(\lambda_b^2 - 1). \tag{3.109}$$

It can be verified that when $\lambda_i = \lambda_i^*$, $\lambda_{rb} = \lambda_b$ implying that at the maximum loading state $\lambda_{rb} = \lambda_b$. Moreover, when $\lambda_i = 1$, $\lambda_{rb} = 1$ implying that at the undeformed state, the interface layer must also be undeformed.

In this unloading case, the active collagen fibers occupy part of the wall bounded by r_i and r_a, where r_a is given by (3.91) and $r_a < r_o$. The elastin in the other hand occupies a region bounded by r_{rb} and r_o. It is easy to see that the transmural pressure ΔP is given as follows:

$$\Delta P = E_1(\lambda_o) - E_1(\lambda_{rb}) + E_2(\lambda_a) - E_2(\lambda_i). \tag{3.110}$$

In this unloading case, when the unloading begins, the wall is divided into three regions: a region with damaged elastin, *i.e* a region with only active collagen, that occupies region defined by $r_i < r \leq r_b^*$, a region filled by both active elastin and collagen that is bounded by r_b^* and r_a, where r_a is given by (3.91) and an elastin only region that occupies a region bounded by $r_a < r \leq r_o$.

During unloading, collagen fibers at $r = r_a$ are becoming inactive. The interface radius r_a therefore moves toward smaller radii. The composition of the wall is unchanged as

long as $r_a \geq r_b^*$. However, when λ_i is reduced such that r_a becomes smaller than r_b^* or when λ_i is in the range of:

$$\lambda_a \leq \lambda_i < \sqrt{1 + (\lambda_i^{*2} - 1)\frac{(\lambda_a^2 - 1)}{(\lambda_b^2 - 1)}\frac{\lambda_b^2}{\lambda_a^2}}, \tag{3.111}$$

the region filled with active collagen reduces and becomes smaller than the damaged elastin region ($r_a < r_b^*$). The wall composition is now provided by the following three regions; the inner region with only active collagen ($r_i \leq r \leq r_a$), an 'empty' region in the middle with no active elastin nor active collagen ($r_a < r \leq r_b^*$) and the outer region with active elastin only ($r_b^* < r \leq r_o$). Even though the composition is changed, basically the boundaries of the regions occupied by the elastin and collagen are not altered. Therefore, the transmural pressure ΔP is still given by (3.110).

The next stage of unloading is to reduce λ_i to λ_a. We can observe from (3.110) that the contribution of the second mechanism eventually vanishes when $\lambda_i = \lambda_a$. Basically, the negative contribution of the second mechanism when $\lambda_i < \lambda_a$ is not considered, since we assume that the collagen fibers do not introduce compression. So, when $1 < \lambda_i \leq \lambda_a$, the transmural pressure ΔP is given by:

$$\Delta P = E_1(\lambda_o) - E_1(\lambda_{rb}). \tag{3.112}$$

We can see from (3.112) that $\Delta P = 0$ corresponds to $\lambda_o = \lambda_{rb}$, which can be attained during undeformed state. This implies that the segment returns to the original reference configuration κ_1 as is in previous cases.

- Unloading from Case 3B or 4B: $\max(\lambda_{ioa}, \lambda_b) \leq \lambda_i^* < \lambda_{iob}$

  In this case, the loading ends when active collagen fibers occupy the entire wall and the elastin has been damaged in some layers near the inner radius. The wall is divided into only two regions: the inner region bounded by $r_i \leq r \leq r_b^*$ in which only collagen fibers are active and the outer region bounded by $r_b^* < r \leq r_o$ filled up by both active elastin and collagen fibers.

  Two unloading stages are considered for this case. The stages of λ_i are $\lambda_i^* \geq \lambda_i > \lambda_{ioa}$ and $\lambda_{ioa} \geq \lambda_i$. In the first stage of unloading, when λ_i is reduced from λ_i^* to λ_{ioa}, only $\lambda(r)$ for each of the layers are reduced. The wall composition remains unchanged. It's easy

to see that the transmural pressure ΔP during this first stage is given by the following relation:

$$\Delta P = E_1(\lambda_o) - E_1(\lambda_{rb}) + E_2(\lambda_o) - E_2(\lambda_i). \tag{3.113}$$

When the unloading is further done so that collagen contained in some outer layers become inactive *i.e* $\lambda_i < \lambda_{ioa}$ or $r_a < r_o$, the resulting case then can be described as is in the unloading case 3A. Clearly, in this case, as is in the previous case, when λ_i is further reduced, $\Delta P = 0$ corresponds to the initial reference configuration κ_1.

- Unloading from Case 5: $\lambda_{iob} \leq \lambda_i^*$

  In this case, at the beginning of the unloading, the elastin in the entire wall has been irreversibly damaged and so is inactive during the unloading process. The maximum loading in this case is $\lambda_i^* > \lambda_{iob}$, where λ_{iob} is defined by (3.105). Here, the entire wall consisted of a region with active collagen only and the Cauchy stress of the material points in the wall is given by (3.101). During unloading, the stretched collagen fibers return to their initial reference (unloaded) configuration. The fibers at the outermost layer are stretched less than the other and so will return to their reference configuration at earlier unloading stage compare to those at other layers. Once the outermost layer become inactive, the wall is partially occupied by collagen fibers and only this part of the wall needs to be included in the stress generation.

  It's clear that there are two unloading stages need to be considered; $\lambda_i^* > \lambda_i \geq \lambda_{ioa}$ $\lambda_{ioa} > \lambda_i \geq \lambda_a$. During the first unloading stage the active collagen fibers are bounded by the inner and outer radii of the wall, so the ΔP is given by;

$$\Delta P = E_2(\lambda_o) - E_2(\lambda_i). \tag{3.114}$$

  In the second unloading stage, the collagen fibers at the outer layers become recrimped and inactive. The transmural pressure ΔP is then contributed by collagen fibers in layers bounded by r_i and r_a, instead of r_o, and it is given by:

$$\Delta P = E_2(\lambda_a) - E_2(\lambda_i). \tag{3.115}$$

  We can see that in (3.115), ΔP vanishes as $\lambda_i = \lambda_a > 1$. Here, the unloading terminates, since there is no supporting active mechanical component below this level. Thus, in this

Table 16: Relations between ΔP and λ_i for inflation of a thick walled cylinder during loading. The definitions of $E_1(\Lambda)$ and $E_2(\Lambda)$ are given by (3.96).

Case no.	Range of λ_i	ΔP vs. λ_i
1	$1 \leq \lambda_i < \lambda_a$	$\Delta P = E_1(\lambda_o) - E_1(\lambda_i)$
2	$\lambda_a \leq \lambda_i < \min(\lambda_{ioa}, \lambda_b)$	$\Delta P = E_1(\lambda_o) - E_1(\lambda_i) + E_2(\lambda_a) - E_2(\lambda_i)$
3A	$\lambda_b \leq \lambda_i < \lambda_{ioa}$	$\Delta P = E_1(\lambda_o) - E_1(\lambda_b) + E_2(\lambda_a) - E_2(\lambda_i)$
3B	$\lambda_{ioa} \leq \lambda_i < \lambda_{iob}$	$\Delta P = E_1(\lambda_o) - E_1(\lambda_b) + E_2(\lambda_o) - E_2(\lambda_i)$
4A	$\lambda_{ioa} \leq \lambda_i < \lambda_b$	$\Delta P = E_1(\lambda_o) - E_1(\lambda_i) + E_2(\lambda_o) - E_2(\lambda_i)$
4B	$\lambda_b \leq \lambda_i < \lambda_{iob}$	$\Delta P = E_1(\lambda_o) - E_1(\lambda_b) + E_2(\lambda_o) - E_2(\lambda_i)$
5	$\lambda_{iob} \leq \lambda_i$	$\Delta P = E_2(\lambda_o) - E_2(\lambda_i)$

case, the segment doesn't return to its initial reference configuration κ_1 but instead the segment chooses configuration κ_{2a} as the new reference configuration.

3.4.3 Summary

The relations between ΔP and λ_i, during loading and unloading can be summarized in the Tables 16 and 17 displayed below. We also display part of the integrand of $E_1(\Lambda)$ and $E_2(\Lambda)$, say w_1 and w_2 respectively, from three specific strain energy functions: Neo Hookean, Mooney Rivlin and exponential type strain energy function in Table 18. The definitions of w_1 and w_2 are as follows:

$$w_1 \equiv \frac{\partial W_1}{\partial I_1} + \frac{\partial W_1}{\partial II_1} \qquad \text{and} \qquad w_2 \equiv \frac{\partial W_2}{\partial I_2} + \frac{\partial W_2}{\partial II_2}. \tag{3.116}$$

The first invariant of $\mathbf{B_2}$ (I_2) used in the formulation for exponential type strain energy function is given as follows:

$$I_2 = \frac{\lambda^2}{\lambda_a^2} + \frac{\lambda_a^2}{\lambda^2} + 1. \tag{3.117}$$

Table 17: Relations between ΔP and λ_i for inflation of a thick walled cylinder during unloading for different maximum loading λ_i^*. The definitions of $E_1(\Lambda)$ and $E_2(\Lambda)$ are given by (3.96).

Case no.	Location of λ_i^*	Range of λ_i	ΔP vs. λ_i (use case no. from Loading table)
1	$1 \le \lambda_i^* < \lambda_a$	$1 \le \lambda_i \le \lambda_i^*$	1
2	$\lambda_a \le \lambda_i^*$ $\le \min(\lambda_{ioa}, \lambda_b)$	$\lambda_a \le \lambda_i \le \lambda_i^*$ $1 \le \lambda_i < \lambda_a$	2 1
3A	$\lambda_b \le \lambda_i^* < \lambda_{ioa}$	$\lambda_a \le \lambda_i \le \lambda_i^*$ $1 \le \lambda_i < \lambda_a$	$\Delta P = E_1(\lambda_o) - E_1(\lambda_b^*) + E_2(\lambda_a) - E_2(\lambda_i)$ $\Delta P = E_1(\lambda_o) - E_1(\lambda_b^*)$
3B	$\lambda_{ioa} \le \lambda_i^* < \lambda_{iob}$	$\lambda_{ioa} \le \lambda_i \le \lambda_i^*$ $\lambda_a \le \lambda_i < \lambda_{ioa}$ $1 \le \lambda_i < \lambda_a$	$\Delta P = E_1(\lambda_o) - E_1(\lambda_b^*) + E_2(\lambda_o) - E_2(\lambda_i)$ $\Delta P = E_1(\lambda_o) - E_1(\lambda_b^*) + E_2(\lambda_a) - E_2(\lambda_i)$ $\Delta P = E_1(\lambda_o) - E_1(\lambda_b^*)$
4A	$\lambda_{ioa} \le \lambda_i^* < \lambda_b$	$\lambda_{ioa} \le \lambda_i \le \lambda_i^*$ $\lambda_a \le \lambda_i < \lambda_{ioa}$ $1 \le \lambda_i < \lambda_a$	$\Delta P = E_1(\lambda_o) - E_1(\lambda_i) + E_2(\lambda_o) - E_2(\lambda_i)$ 2 1
4B	$\lambda_b \le \lambda_i^* < \lambda_{iob}$	$\lambda_{ioa} \le \lambda_i \le \lambda_i^*$ $\lambda_a \le \lambda_i < \lambda_{ioa}$ $1 \le \lambda_i < \lambda_a$	$\Delta P = E_1(\lambda_o) - E_1(\lambda_b^*) + E_2(\lambda_o) - E_2(\lambda_i)$ $\Delta P = E_1(\lambda_o) - E_1(\lambda_b^*) + E_2(\lambda_a) - E_2(\lambda_i)$ $\Delta P = E_1(\lambda_o) - E_1(\lambda_b^*)$
5	$\lambda_{iob} \le \lambda_i^*$	$\lambda_{ioa} \le \lambda_i \le \lambda_i^*$ $\lambda_a \le \lambda_i \le \lambda_{ioa}$	$\Delta P = E_2(\lambda_o) - E_2(\lambda_i)$ $\Delta P = E_2(\lambda_a) - E_2(\lambda_i)$

Table 18: Some examples of w_1 and w_2 for inflation of a thick walled cylinder. The definitions of w_1 and w_2 are given by (3.116).

Type of Ws	w_1	w_2
Neo Hookean	α_1	α_2
Mooney Rivlin	$\alpha_1 + \beta_1$	$\alpha_2 + \beta_2$
Exponential	$\alpha_1 e^{\gamma_1(I_1-3)}$	$\alpha_2 e^{\gamma_2(I_2-3)}$

Table 19: Resulting material parameters obtained for fixed $\lambda_a = 1.761029$ using both finite thickness and membrane approximation.

Material Parameters	Finite Thickness (3D)		Membrane Approx.	
H (μ)	100	125	100	125
λ_a	1.761029	1.761029	1.761029	1.761029
$\alpha_1(10^3 dynes/cm^2)$	83.72267	67.68549	89.03572	71.21986
γ_1	0.6700442	0.6738098	0.6224279	0.6224279
$\alpha_2(10^3 dynes/cm^2)$	443.6744	361.6479	390.872	312.6121
γ_2	1.838987	1.850415	1.867193	1.867605
R^2	0.9928429	0.9928429	0.9903374	0.9903374

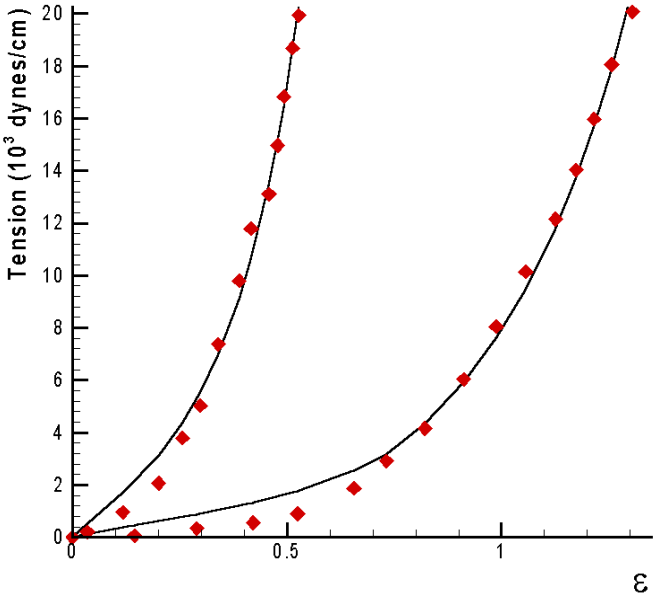

Figure 25: The resulting ΔP vs. λ_i curves for the exponential type material whose parameters are given in the second column of Table 19 for $H = 125\mu$.

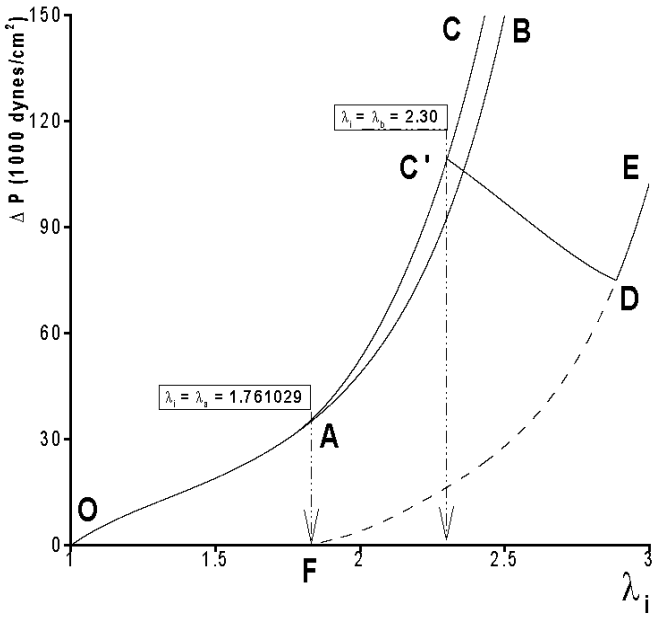

Figure 26: The resulting ΔP vs. λ_i curves for the same material as is used in Figure 25 but with $H = 1$ mm.

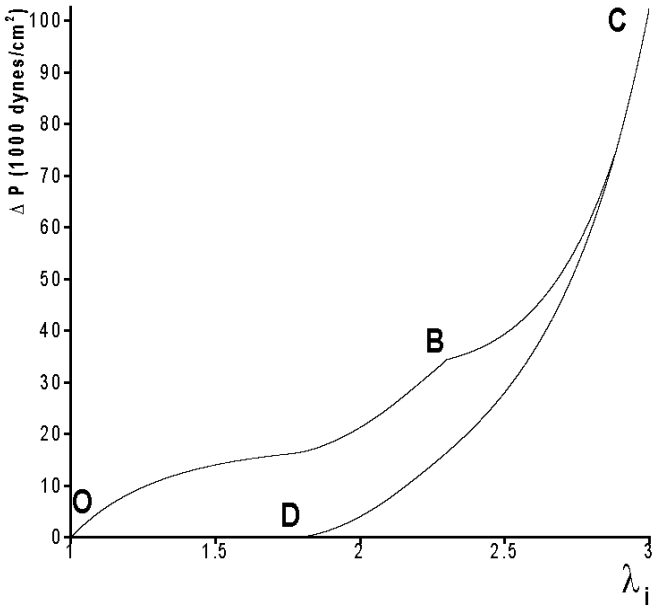

Figure 27: The resulting ΔP vs. λ_i curves for material with Neo Hookean as the first mechanism and exponential type as the second mechanism.

3.4.4 Examples and discussion

In order to obtain some meaningful illustration, the geometry of the cylinder and the strain energy functions, W_1 and W_2 must be specified. We consider in this section thick walled cylinders each of which has an inner radius of 0.3264 cm and other specifications as follows:

- A. Material parameters given in the first column of Table 19 and the undeformed thickness $(H) = 125\ \mu$.
- B. Similar material parameters as in A but using $H = 1$ mm.
- C. A material with the first and second mechanisms that are represented by Neo Hookean and exponential type functions, respectively. The parameters α_1, α_2, and γ_2 are 67.6855 dynes/cm^2, 361.6479 dynes/cm^2, and 1.8504, respectively. The critical stretch ratios, λ_a and λ_b, are adopted from examples A and B. The undeformed thickness H is 1 mm.

Material constants displayed in Table 19 are obtained from a nonlinear regression analysis of data provided by Scott *et al.* [79] using equations presented in Table 16 which are derived from a 3D theory. Here, a similar regression procedure to that described in Section 3.3 is employed. The activation and deactivation stretch ratios λ_a and λ_b both are set fixed and we suppose that these values are applicable to all layers. It can be observed in Table 19, the resulting constants do not demonstrate significant differences compared to material parameters obtained using membrane approximation. Clearly, for the thicknesses used in this case, the membrane approximation produces satisfactory results.

The resulting transmural pressure ΔP vs. λ_i curves for the example A for some possible cases are plotted in Figure 25. In the figure, the curve OAB illustrates the results when only the first mechanism is considered. Neither collagen recruitment nor elastin breakage are considered. The curve OAC depicts the resulting ΔP vs. λ_i when both elastin and active collagen recruitment are included. As was seen in other figures, here we can also see that the curve deviates from OAB at A when the collagen begins to be active. The wall becomes stiffer due to the additional material component. For both cases the unloading curves coincide with their corresponding loading curves. During unloading, the cylinder returns to the original reference configuration after complete unloading. The curve OAC'DE illustrates the case where both the collagen recruitment and elastin breakage are included in

the calculation. In this curve, point C' indicates that the elastin breakage begins to occur at the inner wall. Here, ΔP drops to the minimum value at D and then comes back (recovers) to point E. This last case corresponds to Loading Case 5 where the maximum loading λ_i^* exceeds λ_{iob} (the value of λ_i at which the elastin breakage reaches the outer wall). The relation between ΔP and λ_i during unloading for this case is described in Unloading from Case 5. The unloading curve EDF for this case is obtained using (3.114) and (3.115) and therefore does not coincide with the loading curve. It is seen from (3.115), the zero ΔP after complete unloading corresponds to $\lambda_i = \lambda_a$. This new unloaded configuration is different from the original reference configuration and in fact it is never occupied by the collagen only embedded body during loading.

The local minimum denoted by D corresponds to $\lambda_i = \lambda_{iob}$. When D is reached, all elastin is deactivated. When the loading continues, no more elastin degradation occurs so ΔP is recovered. Due to the inhomogeneity of the deformation, the local minimum D is achieved gradually not abruptly as happened in homogeneous deformations (see Figure 20 in the previous subsection). The value of λ_{iob} can be computed by substituting the inner and outer radii values and λ_b into formulation (3.105) to obtain $\lambda_{iob} = 2.371682$.

The gradual breakage is clearly illustrated in Figure 26 when a similar material was used but a much thicker wall was considered (material B). In the later example, the thickness of the wall is 1 mm, eight times thicker than the previous example. As is expected, the resulting transmural pressure is much higher than the previous case since the additional thickness causes the wall to be stiffer. Moreover, in the later case, the complete elastin breakage occurs at a much higher pressure than before. Here, $\lambda_{iob} = 2.8847$. This delay can be expected from (3.105) where the thickness factor R_o^2/R_i^2 plays role as the 'magnifying' factor for λ_{iob}. It can be seen that when the thickness is negligible, this factor approximates unity and λ_{iob} simply equals to λ_b. When the wall thickness increases, this factor is enlarged and $\lambda_{iob} > \lambda_b$.

The local minimum phenomenon seen in examples A and B (and also in previous cases of homogeneous deformation) in theory cannot be observed in a force-controlled experimental setting. The recovery zone will be simply 'skipped' or 'jumped over' when the transmural pressure is increased from the local maximum (C'). It is important therefore to consider a

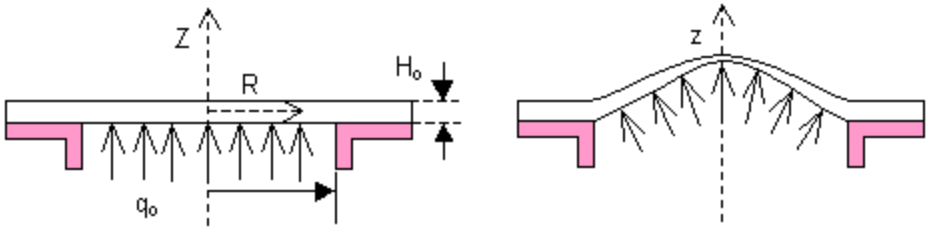

Figure 28: The undeformed and deformed states of an inflated clamped circular membrane.

strain-controlled experiments instead, so that the recovery zone can be identified. As an example, in the case of inflation of cylindrical segment, the volumetric change of the fluid that is used to perfuse the segment can be used as a control. The identification of this zone is essential since the critical deactivation stretch λ_b can only be detected in this zone.

The resulting ΔP vs. λ_i curve for material C is depicted in Figure 27. This example is intended to demonstrate that the deactivation of the first mechanism may not cause the transmural pressure to decrease during the inflation of cylindrical wall. So here, a local minimum is not produced.

3.5 NONHOMOGENEOUS DEFORMATION: INFLATION OF A CLAMPED CIRCULAR MEMBRANE

3.5.1 Loading

In this section, we consider an undeformed circular thin sheet that is clamped or fixed on its edge. The disc is made of a dual mechanism for which each mechanism is an isotropic incompressible homogenous hyperelastic material. A distributed pressure, q_o, is applied to the circular sheet or disc from below so that the disc axisymmetrically inflates. Figure 28 shows the side view of the undeformed and deformed disc.

The following motivations have directed the study of this particular model. First, we expect that the inflation of the flat disc can imitate the hypothesized initiation and development of cerebral saccular aneurysms. It has been hypothesized that an aneurysms sac

originates from a relatively flat arterial section that transforms into a 'bleb', a small outpounching formation, and progresses into a well developed saccular aneurysm with enlarged orifice [59]. The sketch of such a hypothesis is given in Figure 29.

The new constitutive equation can be used to simulate the aneurysms formation not only in a geometrical sense but also in a sense of the constituent of the sacs walls. The geometric progression hypothesized by Foutrakis *et al.* [59] certainly can be modelled as inflation of a clamped membrane made out of a classical elastic material (see the resulting profiles for examples in Adkins and Rivlin [139] and Crisp and Hart-Smith [152]). The medically observed fragmentation of elastin however cannot be explained using classical material that disregards alteration of the components of the body that may occur during the deformation. It will be seen later that elastin degradation is clearly captured in the modeling.

Note however, that some assumptions regarding the aneurysm orifice must be employed in this modeling. It is hypothesized by Foutrakis *et al.* [59] that the developing of aneurysms is accompanied by enlarging orifice. It is assumed here that the orifice is not enlarged during the deformation. However, it can be seen in the results the radial enlargement beyond the orifice size of the sac wall proximal to the edge. Furthermore, it was commonly believed that during their formation, aneurysms draw in the adjacent arterial wall from both branches and parent arteries [60, 46]. Here, it is assumed that the edge is fixed and therefore preventing tissue withdrawal from neighboring areas.

We consider here, the applied pressure at the inner wall that is either uniformly distributed or linearly varied with its maximum at the center of the circular membrane (the dome). In real biological situation, the distributed applied pressure can be considered as a representation of hemodynamics pressure produced by blood flow. The pressure distribution, in particular at the sac orifice, however is rarely reported in hemodynamics studies relevant to this subject. A 2D numerical hemodynamics study of saccular aneurysms reveals that fairly constant pressure distribution is observed both at the orifice of a well developed sac at a bifurcation and along the wall of another well developed sac at the outer wall a curved segment [59]. Similar 2D modeling of bifurcation without an aneurysm reveals that the linearly varying pressure distribution occurs at the apical region [153]. Secondly, this problem presents an inhomogeneous deformation case that involves two deformation parameters. The

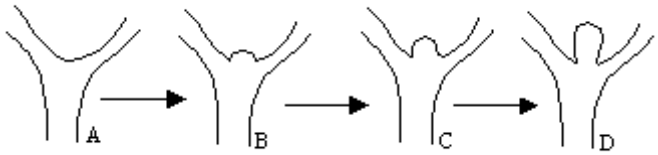

Figure 29: The hypothesized stages of aneurysms formation and development.

deformation level then must be measured with a scalar function of the deformation parameters. Here, we will consider a function, s, that depends on I_1 similar to the function s used in the 3D biaxial problem. The inhomogeneity of the deformation is demonstrated by the stretch ratios that monotonically decrease from a maximum at the dome to a minimum at the edge as was shown in the classical works by Adkins and Rivlin [139]. As will be shown later, this result is used as the basis for the assumption that the collagen recruitment and elastin breakage will always occur first at the dome.

Thirdly, this problem is studied since it can potentially be used for experiments directed at material identification. Such efforts have been performed by Treloar [136], Crisp and Hart-Smith [152], Wineman *et al.* [154] and Hsu *et al.* [155]. None of them however performed experiments in the context of multi mechanism constitutive theory.

We have to mention here too that Wineman and Huntley [105] have carried out a numerical computation of this problem in the case of multi mechanism material. They calculated the deformed state of membrane inflation made of Neo Hookean material that experienced damaged induced softening. The softening was regarded as a sequence of new mechanisms that continuously were born during deformation. This following work employs similar equations and adopts many numerical techniques used in Wineman and Huntley's calculation [105]. However, here the exponential type material will be used instead of Neo Hookean. Also in this discussion, as in earlier model problems, we consider a material with only two discrete mechanisms, the mechanism contributed by elastin and by recruited collagen fibers. As is in the previous problems, here the second mechanism is activated, to mimic the collagen recruitment, at some levels of deformation followed by the deactivation of the first

mechanism, to mimic the elastin breakage, at higher levels of deformation. The forms of the criteria that will be used in this problem also adopt the formulation used in the 3D biaxial case.

The undeformed disc has radius R_0 and thickness $2h_0$. We suppose that the origin of the cylindrical coordinate system with coordinates denoted by (R, Θ, Z) be placed at the center of the circular membrane sheet, so that the body will occupy the following region:

$$0 \leq R \leq R_0, \qquad 0 \leq \Theta \leq 2\pi, \qquad -h_0 \leq Z \leq h_0. \tag{3.118}$$

The disc's circular edge, along $R = R_0$ and $Z = 0$, serves as a fixed boundary. The surface $Z = h_0$ is traction free, while at the surface $Z = -h_0$ a uniformly distributed pressure q_0 is applied. The loaded profile is an axisymmetric inflated dome.

We suppose that the ratio of the thickness to the radius of the disk is very small ($h_0/R_0 \ll 1$). The disk then is assumed to be very thin and the variations of the kinematic quantities along the thickness of the disk can be neglected. Moreover, it is assumed that a straight fiber that is perpendicular to the middle surface ($Z = 0$) will remain straight during the deformation. This suggests that only the deformed state of the middle surface needs to be determined while those of the top and bottom surfaces can be calculated from middle surface results. In addition, we consider the variation of s only on the middle surface and not within the thickness. The activation and deactivation would occur not within the thickness but on the surface. Moreover, it is important to assume that those assumptions still hold after the introduction of the multi mechanism. Based on these assumptions, the relation between the pressure q_o and some measure of inflation can be computed using the membrane approximation.

It can be calculated and shown that the material points on the membrane surface locally experience biaxial stretch in the principal directions of the deformed membrane: the circumferential and meridional directions [105, 139]. We denote the stretch ratios in the meridional, circumferential and normal directions with λ_1, λ_2, and λ_3, respectively. Their definitions are as follows:

$$\lambda_1 = [(\frac{\partial r}{\partial R})^2 + (\frac{\partial z}{\partial R})^2]^{1/2}, \qquad \lambda_2 = \frac{r}{R}, \qquad \text{and,} \qquad \lambda_3 = \frac{1}{\lambda_2 \lambda_3}, \tag{3.119}$$

where r and R are radial position in the current and reference configuration, respectively, of a point in the middle surface and z is the ordinate of a deformed position. Here, it can be seen that due to the incompressibility restriction, the material point experiences compression in the normal direction when the tissue is being stretched.

Moreover, it is more convenient to write the kinematics of the membrane surface with a curvilinear coordinate system formed by the two principal directions of the inflated membrane and a direction normal to that surface. Generally, the components of Cauchy stress tensor of material points of a shell like body such as flat circular membrane are derived from a strain energy function that depends on 2D strain tensor and some measure of strain in the thickness direction. However, here we suppose that the components of the Cauchy stress tensor can be derived from a strain energy function W in a similar formulation as is shown in (2.17) and (2.18). Such an assumption is acceptable when the deformation in the normal direction of the surface is not taken into account [156]. Furthermore, we will consider here strain energy functions of the exponential type similar to those that are used in 3D model problems given by equations (2.21).

The deformation gradient, Left Cauchy Green tensor and its inverse, respectively, of the first mechanism are written as follows:

$$\mathbf{F_1} = \mathrm{DIAG}[\lambda_1, \lambda_2, \lambda_3], \qquad \mathbf{B_1} = \mathrm{DIAG}[\lambda_1^2, \lambda_2^2, \lambda_3^2], \qquad \mathbf{B_1}^{-1} = \mathrm{DIAG}[\frac{1}{\lambda_1^2}, \frac{1}{\lambda_2^2}, \frac{1}{\lambda_3^2}]. \quad (3.120)$$

It's easy to see that the first and second invariants of $\mathbf{B_1}$ are, respectively:

$$I_1 = \lambda_1^2 + \lambda_2^2 + \lambda_3^2, \qquad \text{and} \qquad II_1 = \frac{1}{\lambda_1^2} + \frac{1}{\lambda_2^2} + \frac{1}{\lambda_3^2}. \quad (3.121)$$

First we consider the deformation that is large but is not large enough to activate the second mechanism anywhere on the surface . In these loading stages, the components of the Cauchy stress tensor are derived from (2.17) using (2.18) for $0 \leq s < s_a$ and W_1 given by (2.21.1). Observing the (3.120.2 and 3), the only nonzero components of Cauchy stress tensor are T_{ii}, no sum on i, $i = 1..3$. Moreover, the membrane approximation assumes that the

middle surface is in the plane stress state, so $T_{33} = 0$ everywhere. The Lagrange multiplier p then can be obtained and can be used to obtain the following T_{11} and T_{22}:

$$T_{11} = 2(\lambda_1^2 - \lambda_3^2)\frac{\partial W}{\partial I_1} - 2(\frac{1}{\lambda_1^2} - \frac{1}{\lambda_3^2})\frac{\partial W}{\partial II_1}$$
$$T_{22} = 2(\lambda_2^2 - \lambda_3^2)\frac{\partial W}{\partial I_1} - 2(\frac{1}{\lambda_2^2} - \frac{1}{\lambda_3^2})\frac{\partial W}{\partial II_1}. \tag{3.122}$$

Denoting T_{11} and T_{22} as σ_1 and σ_2, respectively, the equilibrium equation in the meridional direction is as follows:

$$\frac{\partial(\lambda_3\sigma_1)}{\partial R} + \frac{\eta\lambda_3(\sigma_1 - \sigma_2)}{\lambda_2 R} = 0, \tag{3.123}$$

where

$$\eta = \frac{\partial r}{\partial R} \tag{3.124}$$

and equilibrium equation in the normal direction:

$$\kappa_1\lambda_3\sigma_1 + \kappa_2\lambda_3\sigma_2 = \frac{q_0}{h_0}, \tag{3.125}$$

where κ_1 and κ_2 are the curvatures in the meridional and circumferential directions and they are defined as follows:

$$\kappa_1 = \frac{\eta\frac{\partial\lambda_1}{\partial R} - \lambda_1\frac{\partial\eta}{\partial R}}{\lambda_1^2\sqrt{(\lambda_1^2 - \eta^2)}} \qquad \text{and} \qquad \kappa_2 = \frac{\sqrt{(\lambda_1^2 - \eta^2)}}{\lambda_1\lambda_2 R}. \tag{3.126}$$

The applied distributed pressure, which is denote by q_0, is defined as follows:

$$q_0 = q_{dome}\,(1 + C\;R/R_0), \tag{3.127}$$

where q_{dome} is the value of the pressure at the dome, R_0 is the undeformed radius of the membrane and C is the radial pressure gradient of q_o. So, when $C = 0.00$, the applied pressure is uniformly distributed. When $c < 0$, the maximum load is applied at the dome and when $C > 0$, the applied pressure at the dome becomes the minimum. In the study involving nonuniform pressure, we only apply the case in which the maximum pressure is at the dome.

Due to the axisymmetry of the deformation, the dome ($R = 0.00$) of the inflated disc experiences equibiaxial stretching. Denoting t for both the stretch ratios in the circumferential and meridional directions at the dome, Green and Adkins [140], Rivlin and Adkins [139] and Wineman and Huntley [105] assume the following conditions at the dome:

$$\lambda_1 = \lambda_2 = \eta = t \qquad \text{at} \qquad R = 0. \tag{3.128}$$

These assumption has been used and shown to work well with the classical elastic material [140] and multi mechanism based constitutive equations [105]. The assumption will be employed in this work and also t will be used as a measure of inflation.

It follows from (3.122.1 and 2) and (3.128), that at the dome, $\sigma_1 = \sigma_2$. Also, due to the symmetry at the dome, the curvatures in both directions are the same, so $\kappa_1 = \kappa_2$ for $R = 0$. It can be seen that at the dome, the equilibrium equation (3.125) becomes simply

$$2h_0\lambda_3\kappa_2\sigma_2 = q_0, \tag{3.129}$$

which after making use (3.126.2), we obtain the following important equation:

$$\eta = \pm\sqrt{(\lambda_1^2 - (\frac{\lambda_1^2\lambda_2^2 R q_0}{2h_0\sigma_1})^2)}. \tag{3.130}$$

Beside at the dome, another boundary condition must be satisfied at the edge of the membrane. There the circular membrane is clamped preventing stretching in the circumferential direction, thus

$$\lambda_2 = 1.00 \qquad \text{at} \qquad R = 1.00. \tag{3.131}$$

The differential equations (3.123) and (3.125) with the constitutive relations given by (3.122.1 and 2) involve three unknown variables: η, λ_1, and λ_2. Due to the axisymmetry of the inflated disc, the three unknown variables depend only on R. Following Wineman and Huntley [105], the system of differential equations will be solved numerically using the Runge Kutta method. The method requires explicit expressions of the derivatives of the unknown variables with respect to R: $\frac{\partial\lambda_1}{\partial R}$, $\frac{\partial\lambda_2}{\partial R}$ and $\frac{\partial\eta}{\partial R}$. The derivation process is briefly described in

the following section. The derivative of λ_2 is obtained by taking the derivative of (3.119.2) with respect to R and making use (3.124), yielding:

$$\frac{\partial \lambda_2}{\partial R} = \frac{\eta - \lambda_2}{R}. \tag{3.132}$$

The derivative of η can be obtained by substituting (3.126.1 and 2) into (3.125) to obtain:

$$\frac{\partial \eta}{\partial R} = \frac{\eta}{\lambda_1}\frac{\partial \lambda_1}{\partial R} + \frac{\lambda_3 \lambda_1 (\lambda_1^2 - \eta^2)}{R}\frac{\sigma_2}{\sigma_1} - \frac{q_0}{h_0}\frac{\lambda_1}{\lambda_3}\frac{(\lambda_1^2 - \eta^2)^{1/2}}{\sigma_1} \tag{3.133}$$

We make use the following useful identity that can be derived from (3.119.3):

$$\frac{\partial \lambda_3}{\partial R} = -\lambda_3 (\frac{1}{\lambda_1}\frac{\partial \lambda_1}{\partial R} + \frac{1}{\lambda_2}\frac{\partial \lambda_2}{\partial R}) \tag{3.134}$$

in the calculation of the derivative of λ_1. In this calculation we also need the derivative of σ_1 with respect to R. The explicit expression of $\frac{\partial \lambda_1}{\partial R}$ can be obtained by substituting (3.134), (3.132) and the derivative of σ_1 into (3.123) and rearranging the terms. The resulting expression is as follows:

$$\frac{\partial \lambda_1}{\partial R} = \frac{\lambda_1}{\lambda_2}\frac{\eta(\sigma_2 - \sigma_1) - (S_2\lambda_2 - \sigma_1)(\eta - \lambda_2)}{R(\lambda_1 S_1 - \sigma_1)}, \tag{3.135}$$

where S_1 and S_2 are functions of λ_1 and λ_2 and the expression of which depends on the form of the strain energy function being employed. In fact, S_1 and S_2 will also depend on s, since the value of s relatives to s_a and s_b determines mechanism components that must be included in the strain energy function. In this work, we'd like to confine our attention to the exponential type strain energy function that is given by (2.21). The complete expression of S_1 and S_2 will be given later.

In the following discussion, it is helpful to reformulate the governing equations previously introduced in a nondimensional form. The nondimensionalization is calculated using the following relations: $\hat{R} = \frac{R}{R_0}$, $\hat{r} = \frac{r}{R_0}$, $\hat{z} = \frac{z}{R_0}$, $\hat{\sigma}_\alpha = \frac{\sigma_\alpha}{\alpha_1}, \alpha = 1, 2$, where R_0 is the undeformed radius of the undeformed circular membrane and α_1 is the material parameter of the first mechanism shown in (2.21). When those relations are used, the following nondimensional equations will be obtained:

$$\eta = \pm\sqrt{(\lambda_1^2 - (\frac{\lambda_1^2 \lambda_2^2 Q R}{2\sigma_1})^2)}. \tag{3.136}$$

In (3.136), variable Q will be termed as the nondimensional pressure which can be linearly varied along the radius of the disc. The nondimensional relation of Q is as follows:

$$Q = \frac{q_0 R_0}{h_0 \alpha_1}$$

and

$$\frac{\partial \eta}{\partial R} = \frac{\eta}{\lambda_1}\frac{\partial \lambda_1}{\partial R} + \frac{\lambda_3 \lambda_1 (\lambda_1^2 - \eta^2)}{R}\frac{\sigma_2}{\sigma_1} - Q\frac{\lambda_1}{\lambda_3}\frac{(\lambda_1^2 - \eta^2)^{1/2}}{\sigma_1}. \tag{3.137}$$

Here, we have dropped the hat sign for convenience. As a result the expressions for the derivatives of λ_1 and λ_2 are still given by (3.135) and (3.132), respectively. From now on, equations (3.135) and (3.132) are understood to represent their nondimensional form. The formulations of σ_1, σ_2, S_1 and S_2 are given as follows:

$$\sigma_1 = M_1(\lambda_1^2 - \lambda_3^2) \qquad \text{and} \qquad \sigma_2 = M_1(\lambda_2^2 - \lambda_3^2) \tag{3.138}$$

and

$$S_1 = 2\frac{M_1}{\lambda_1}((\lambda_1^2+\lambda_2^2)+\gamma_1(\lambda_1^2-\lambda_2^2)^2) \qquad \text{and} \qquad S_2 = 2\frac{M_1}{\lambda_2}(\lambda_3^2+\gamma_1(\lambda_1^2-\lambda_2^2)(\lambda_1^2-\lambda_3^2)), \tag{3.139}$$

where $M_1 = e^{(\gamma_1(I_1-3))}$. Equations (3.135), (3.132), and (3.137) are to be used to numerically solve the system for $s < s_a$.

We consider now the condition where more than one mechanism is involved. First we will discuss variables that can be used to determine either the activation of the second mechanism or the deactivation of the first mechanism. Note that t globally cannot be used to indicate both the activation and the deactivation, since $t = \lambda_1 = \lambda_2$ is true only at the dome. In this problem, the stretch ratios λ_1 and λ_2 monotonically decrease from a maximum at the dome along the radius of membrane to a minimum at the edge [105, 139]. Note also that an equation that can either relate local λ_1 (or λ_2) to t or an relate λ_1 to λ_2 is not available. A scalar function, s, that depends on both λ_1 and λ_2 then must be employed to indicate both the activation of the second mechanism and the deactivation of the first mechanism. In this work, we use the function s given by (2.22) introduced in Chapter 2. The first invariant of $\mathbf{B}_1$ is given by (3.121.1). It will be seen that the stretch ratios λ_1 and λ_2 vary along R and

depend on the value of the stretch ratios at the dome, t. So, the scalar parameter s must depend on R and t through λ_1 and λ_2 as follows:

$$s = s(\lambda_1(R,t), \lambda_2(R,t)). \tag{3.140}$$

In this case, we also employ scalar values s_a and s_b to indicate the activation and the deactivation, respectively. We will suppose that both scalars are space independent and $s_a < s_b$. Moreover, the activation and deactivation criteria are given by (2.8) and (2.15), respectively.

At a particular value of t, as was mentioned earlier, λ_1 and λ_2 are both maximum at the dome. Hence, s is maximum at the dome for all inflated states and so the activation criterion (and later on also the deactivation) criterion is satisfied at the dome first. Here, we assume that the collagen recruitment occurs first at the inflated dome. Note however, that no supportive histological evidence of this result is available currently.

Moreover, λ_1 and λ_2 both monotonically decrease along the radius. It follows that s also monotonically decreases along the radius. Therefore when $s(R = 0) > s_a$, the activation criterion (2.8) is satisfied only at one material point along the radius. We denote R_a as the radius of that point relative to the dome. And we introduce λ_{1a} and λ_{2a} to denote the stretch ratios λ_1 and λ_2, respectively, satisfying the criterion (2.8) at R_a.

It immediately follows that when $s(R = 0) = s_a$, the activation occurs exactly at the dome ($R_a = 0$) and $\lambda_{1a} = \lambda_{2a}$. The corresponding value of t is denoted as t_a. So, t_a is a positive real root of the following relation:

$$s(\lambda_1(R = 0, t_a), \lambda_2(R = 0, t_a)) = s_a. \tag{3.141}$$

Moreover, when t is increased so that $s(R = 0.0) > s_a$, the activation is satisfied at a particular nonzero radius ($R_a > 0$) (provided that t is not large enough to produce value of s greater than s_a at all nodes other than the edge). It will be discussed later on (in the Appendix A in which we describe the numerical procedure employed in this work) that the radius R_a and the associated λ_{1a} and λ_{2a} can be computed from the following relation:

$$s(\lambda_{1a}(R_a, t), \lambda_{2a}(R_a, t)) = s_a. \tag{3.142}$$

As t is monotonically increased, s is increased everywhere and R_a is enlarged. The progression of t forms an enlarging circular area with radius R_a inside which the material points have their s progressively becoming greater than s_a implying a region with collagen recruitment in addition to the elastin. Obviously, outside this region is a region filled with elastin only.

The Cauchy stress tensor of the material points at which the collagen fibers are activated must include the contribution of the second mechanism represented by the collagen fibers mechanical response. As was discussed before, the second mechanism will take the configuration at which the activation criterion (2.8) is satisfied, say κ_2, as their reference configuration. The deformation gradient relative to κ_2 however can be written in terms of the deformation gradient relative to the reference configuration κ_1. Using (2.12), the deformation gradient $\mathbf{F_2}$ relative to κ_2 can be obtained as follows:

$$\mathbf{F_2} = \text{DIAG}[\frac{\lambda_1}{\lambda_{1a}}, \frac{\lambda_2}{\lambda_{2a}}, \frac{\lambda_3}{\lambda_{3a}}], \tag{3.143}$$

where due to incompressibility, $\lambda_{3a} = \lambda_{1a}/\lambda_{2a}$. The Left Cauchy Green strain tensor and its inverse are given, respectively, by

$$\mathbf{B_2} = \text{DIAG}[\frac{\lambda_1^2}{\lambda_{1a}^2}, \frac{\lambda_2^2}{\lambda_{2a}^2}, \frac{\lambda_3^2}{\lambda_{3a}^2}] \qquad \text{and} \qquad \mathbf{B_2}^{-1} = \text{DIAG}[\frac{\lambda_{1a}^2}{\lambda_1^2}, \frac{\lambda_{2a}^2}{\lambda_2^2}, \frac{\lambda_{3a}^2}{\lambda_3^2}]. \tag{3.144}$$

The first invariant of $\mathbf{B_2}$ is given by;

$$I_2 = \frac{\lambda_1^2}{\lambda_{1a}^2} + \frac{\lambda_2^2}{\lambda_{2a}^2} + \frac{\lambda_3^2}{\lambda_{3a}^2}.$$

Note however that different material points satisfy the activation criterion at different loading states, thus implying that more than one configuration of the body will be used as the reference configuration for the second mechanism.

At material points whose $s \geq s_a$, the equations for the stress components are given by (2.17) and (2.18) for $s_a \leq s < s_b$ with W given by (2.21). When the plane stress restriction is imposed, the resulting nonzero components σ_1 and σ_2 take the following form:

$$\begin{aligned}
\sigma_1 &= 2(\lambda_1^2 - \lambda_3^2)\frac{\partial W}{\partial I_1} - 2(\frac{1}{\lambda_1^2} - \frac{1}{\lambda_3^2})\frac{\partial W}{\partial II_1} + 2(\frac{\lambda_1^2}{\lambda_{1a}^2} - \frac{\lambda_3^2}{\lambda_{3a}^2})\frac{\partial W}{\partial I_2} - 2(\frac{\lambda_{1a}^2}{\lambda_1^2} - \frac{\lambda_{3a}^2}{\lambda_3^2})\frac{\partial W}{\partial II_2} \\
\sigma_2 &= 2(\lambda_2^2 - \lambda_3^2)\frac{\partial W}{\partial I_1} - 2(\frac{1}{\lambda_2^2} - \frac{1}{\lambda_3^2})\frac{\partial W}{\partial II_1} + 2(\frac{\lambda_2^2}{\lambda_{2a}^2} - \frac{\lambda_3^2}{\lambda_{3a}^2})\frac{\partial W}{\partial I_2} - 2(\frac{\lambda_{2a}^2}{\lambda_2^2} - \frac{\lambda_{3a}^2}{\lambda_3^2})\frac{\partial W}{\partial II_2}
\end{aligned} \tag{3.145}$$

After substituting (2.21) into (3.145) and using the nondimensional variable $\hat{\sigma}_\alpha, \alpha = 1, 2$, it follows that

$$\sigma_1 = M_1(\lambda_1^2 - \lambda_3^2) + M_2(\frac{\lambda_1^2}{\lambda_{1a}^2} - \frac{\lambda_3^2}{\lambda_{3a}^2}) \qquad \text{and} \qquad \sigma_2 = M_1(\lambda_2^2 - \lambda_3^2) + M_2(\frac{\lambda_2^2}{\lambda_{2a}^2} - \frac{\lambda_3^2}{\lambda_{3a}^2}), \quad (3.146)$$

where the hat sign has been removed for convenience and M_1 and M_2 are defined as follows;

$$M_1 = e^{(\gamma_1(I_1-3))} \qquad \text{and} \qquad M_2 = \frac{\alpha_2}{\alpha_1} e^{(\gamma_2(I_2-3))} \quad (3.147)$$

All of the nonzero stress components, whether evaluated at the material points satisfying the activation criterion or at other points, must satisfy the equilibrium equations given by (3.125) and (3.123). It can be shown that the expression for derivatives of η and λ_2 needed in the Runge Kutta method are given by (3.133) and (3.132), respectively. However, since σ_1 shown in (3.146.1) contains terms from the second mechanism, the derivative of λ_1 differs from (3.135). We skip the lengthy calculation for the derivative of λ_1 and only present the results below:

$$\frac{\partial \lambda_1}{\partial R} = \frac{\lambda_1}{\lambda_2} \frac{\eta(\sigma_2 - \sigma_1) - (S_2\lambda_2 - \sigma_1)(\eta - \lambda_2) - \lambda_2 R(Z_1 \frac{\partial \lambda_{1a}}{\partial R} + Z_2 \frac{\partial \lambda_{2a}}{\partial R})}{R(\lambda_1 S_1 - \sigma_1)}, \quad (3.148)$$

which is nondimensional and where S_1, S_2, Z_1 and Z_2 are given as follows:

$$\begin{aligned} S_1 &= 2\frac{M_1}{\lambda_1}((\lambda_1^2 + \lambda_3^2) + \gamma_1(\lambda_1^2 - \lambda_3^2)^2) + 2\frac{M_2}{\lambda_1}((\frac{\lambda_1^2}{\lambda_{1a}^2} + \frac{\lambda_3^2}{\lambda_{3a}^2}) + \gamma_2(\frac{\lambda_1^2}{\lambda_{1a}^2} - \frac{\lambda_3^2}{\lambda_{3a}^2})^2) \\ S_2 &= 2\frac{M_1}{\lambda_2}(\lambda_3^2 + \gamma_1(\lambda_1^2 - \lambda_3^2)(\lambda_2^2 - \lambda_3^2)) + 2\frac{M_2}{\lambda_2}(\frac{\lambda_3^2}{\lambda_{3a}^2} + \gamma_2(\frac{\lambda_1^2}{\lambda_{1a}^2} - \frac{\lambda_3^2}{\lambda_{3a}^2})(\frac{\lambda_2^2}{\lambda_{2a}^2} - \frac{\lambda_3^2}{\lambda_{3a}^2})) \end{aligned} \quad (3.149)$$

and

$$\begin{aligned} Z_1 &= -2\frac{M_2}{\lambda_{1a}}((\frac{\lambda_1^2}{\lambda_{1a}^2} + \frac{\lambda_3^2}{\lambda_{3a}^2}) + \gamma_2(\frac{\lambda_1^2}{\lambda_{1a}^2} - \frac{\lambda_3^2}{\lambda_{3a}^2})^2) \\ Z_2 &= -2\frac{M_2}{\lambda_{2a}}(\frac{\lambda_3^2}{\lambda_{3a}^2} + \gamma_2(\frac{\lambda_1^2}{\lambda_{1a}^2} - \frac{\lambda_3^2}{\lambda_{3a}^2})(\frac{\lambda_2^2}{\lambda_{2a}^2} - \frac{\lambda_3^2}{\lambda_{3a}^2})), \end{aligned} \quad (3.150)$$

and M_1 and M_2 were defined in (3.147). For completeness, the derivative of σ_1 given in (3.146.1) is presented below:

$$\frac{\partial \sigma_1}{\partial R} = S_1 \frac{\partial \lambda_1}{\partial R} + S_2 \frac{\partial \lambda_2}{\partial R} + Z_1 \frac{\partial \lambda_{1a}}{\partial R} + Z_2 \frac{\partial \lambda_{2a}}{\partial R}. \quad (3.151)$$

As for earlier examples, we would like to study, the behavior of the inflated clamped membrane when the elastin stops participating in the load bearing mechanism. We now consider the stage where the loading has been increased to the level where the deactivation criterion (2.15) is satisfied at the dome and its neighboring points. As with collagen recruitment, the elastin breakage is assumed to occur at the dome first. However, currently, it is not clearly understood where in aneurysms walls the elastin starts to fragment. As is for collagen recruitment, for a fixed $t \geq t_b$ the criterion (2.15) is satisfied only at one material point along the radius. We denote R_b as the radius of that point relative to the dome. The corresponding stretch ratios λ_1 and λ_2 that satisfy the deactivation criterion (2.15) are denoted as λ_{1b} and λ_{2b}, respectively.

When the inflated state is such that $s(R = 0.0) = s_a$, the deactivation occurs exactly at the dome ($R_b = 0.0$) and $\lambda_{1b} = \lambda_{2b}$. We denote these stretch ratios as t_b. Therefore, t_b is a positive real root of the following relation:

$$s(\lambda_1(R = 0, t_b), \lambda_2(R = 0, t_b)) = s_b. \tag{3.152}$$

As t monotonically increase, the stretch ratios λ_1 and λ_2, and hence the value of s, of the neighboring material points of the dome also monotonically increase. In fact, the following relation:

$$s(\lambda_{1b}(R_b, t), \lambda_{2b}(R_b, t)) = s_b \tag{3.153}$$

produces values of increasing R_b and a set of pairs of λ_{1b} and λ_{2b} for increasing t. The progression of t corresponds to an enlarging circular area with radius R_b inside of which $s \geq s_b$ for all the material points. Namely, this is a region with elastin breakage. The circular line with radius R_b therefore becomes the interface between an inner region filled with only collagen and an outer region filled with both recruited collagen and elastin. We assume that s_b is always larger than s_a implying that elastin breakage occurs only inside the region with recruited collagen.

At the points where $s \geq s_b$ the stresses are generated according to (2.17) and (2.18) for $s \geq s_b$ with W is given by (2.21). Similar procedures and restriction as in the recruitment are used to obtain the nonzero stresses σ_1 and σ_2. However, they can be easily deduced from

(3.146.1 and 2) by removing the term corresponding to the first mechanism. The resulting formulations are as follows:

$$\sigma_1 = M_2(\frac{\lambda_1^2}{\lambda_{1a}^2} - \frac{\lambda_3^2}{\lambda_{3a}^2}) \qquad \text{and} \qquad \sigma_2 = M_2(\frac{\lambda_2^2}{\lambda_{2a}^2} - \frac{\lambda_3^2}{\lambda_{3a}^2}), \tag{3.154}$$

where both σ_1 and σ_2 are nondimensional variables. These expression of σ_1 and σ_2 are to be used in the differential equations (3.133), (3.132) and (3.148). In these equations, S_1 and S_2, respectively, are:

$$\begin{aligned} S_1 &= 2\frac{M_2}{\lambda_1}((\frac{\lambda_1^2}{\lambda_{1a}^2} + \frac{\lambda_3^2}{\lambda_{3a}^2}) + \gamma_2(\frac{\lambda_1^2}{\lambda_{1a}^2} - \frac{\lambda_3^2}{\lambda_{3a}^2})^2) \\ S_2 &= 2\frac{M_2}{\lambda_2}(\frac{\lambda_3^2}{\lambda_{3a}^2} + \gamma_2(\frac{\lambda_1^2}{\lambda_{1a}^2} - \frac{\lambda_3^2}{\lambda_{3a}^2})(\frac{\lambda_2^2}{\lambda_{2a}^2} - \frac{\lambda_3^2}{\lambda_{3a}^2})) \end{aligned} \tag{3.155}$$

The expressions for Z_1 and Z_2 given in (3.150) are still valid. The resulting differential equations that must be solved are summarized and grouped according to their range of s in Table 20.

3.5.2 Unloading

We also want to study the unloading behavior of the inflated clamped membrane as Q is decreased after a maximum t, denoted as t^*, is achieved. As in previous model problems, several cases of t^* need consideration: $t^* < t_a$, $t_a \leq t^* < t_b$ and $t_b \leq t^*$.

- Case 1: $t^* < t_a$

  In this case, we suppose that the unloading begins before the collagen recruitment occurs at the dome. Since the second mechanism is not activated yet, it's easy to see that this case resembles an unloading case of classical elastic materials with only one mechanism involved. During unloading, the nondimensional components of Cauchy stress tensor are generated by (3.138.1 and 2) with $M_1 = e^{(\gamma_1(I_1-3))}$. The nondimensional differential equations that need to be solved are given by (3.135, 3.132 and 3.137) with S_1 and S_2 given by (3.139.1 and 2). These equations are given in the top box of Table (20). Clearly, the unloading returns the inflated circular sheet membrane into a flat membrane with stress free reference configuration.

Table 20: The nondimensional differential equations used in the numerical calculations of the inflation of circular clamped membrane.

Range of s: $0 < s < s_a$
$\frac{\partial \lambda_2}{\partial R} = \frac{\eta - \lambda_2}{R}$ $\frac{\partial \lambda_1}{\partial R} = \frac{\lambda_1}{\lambda_2} \frac{\eta(\sigma_2 - \sigma_1) - (S_2\lambda_2 - \sigma_1)(\eta - \lambda_2)}{R(\lambda_1 S_1 - \sigma_1)}$ $\frac{\partial \eta}{\partial R} = \frac{\eta}{\lambda_1} \frac{\partial \lambda_1}{\partial R} + \frac{\lambda_3 \lambda_1 (\lambda_1^2 - \eta^2)}{R} \frac{\sigma_2}{\sigma_1} - Q \frac{\lambda_1}{\lambda_3} \frac{(\lambda_1^2 - \eta^2)^{1/2}}{\sigma_1}$ $\sigma_1 = M_1(\lambda_1^2 - \lambda_3^2) \qquad \sigma_2 = M_1(\lambda_2^2 - \lambda_3^2)$ $S_1 = 2\frac{M_1}{\lambda_1}((\lambda_1^2 + \lambda_2^2) + \gamma_1(\lambda_1^2 - \lambda_2^2)^2)$ $S_2 = 2\frac{M_1}{\lambda_2}(\lambda_3^2 + \gamma_1(\lambda_1^2 - \lambda_2^2)(\lambda_1^2 - \lambda_3^2))$ $M_1 = e^{(\gamma_1(I_1 - 3))}$
Range of s: $s_a \leq s < s_b$
The expressions for $\frac{\partial \lambda_2}{\partial R}$ and $\frac{\partial \eta}{\partial R}$ are the same as those for range of $s \in [0, s_a]$ $\frac{\partial \lambda_1}{\partial R} = \frac{\lambda_1}{\lambda_2} \frac{\eta(\sigma_2 - \sigma_1) - (S_2\lambda_2 - \sigma_1)(\eta - \lambda_2) - \lambda_2 R(Z_1 \frac{\partial \lambda_{1a}}{\partial R} + Z_2 \frac{\partial \lambda_{2a}}{\partial R})}{R(\lambda_1 S_1 - \sigma_1)}$ $\sigma_1 = M_1(\lambda_1^2 - \lambda_3^2) + M_2(\frac{\lambda_1^2}{\lambda_{1a}^2} - \frac{\lambda_3^2}{\lambda_{3a}^2}) \qquad \sigma_2 = M_1(\lambda_2^2 - \lambda_3^2) + M_2(\frac{\lambda_2^2}{\lambda_{2a}^2} - \frac{\lambda_3^2}{\lambda_{3a}^2})$ $S_1 = 2\frac{M_1}{\lambda_1}((\lambda_1^2 + \lambda_3^2) + \gamma_1(\lambda_1^2 - \lambda_3^2)^2) + 2\frac{M_2}{\lambda_1}((\frac{\lambda_1^2}{\lambda_{1a}^2} + \frac{\lambda_3^2}{\lambda_{3a}^2}) + \gamma_2(\frac{\lambda_1^2}{\lambda_{1a}^2} - \frac{\lambda_3^2}{\lambda_{3a}^2})^2)$ $S_2 = 2\frac{M_1}{\lambda_2}(\lambda_3^2 + \gamma_1(\lambda_1^2 - \lambda_3^2)(\lambda_2^2 - \lambda_3^2)) + 2\frac{M_2}{\lambda_2}(\frac{\lambda_3^2}{\lambda_{3a}^2} + \gamma_2(\frac{\lambda_1^2}{\lambda_{1a}^2} - \frac{\lambda_3^2}{\lambda_{3a}^2})(\frac{\lambda_2^2}{\lambda_{2a}^2} - \frac{\lambda_3^2}{\lambda_{3a}^2}))$ $Z_1 = -2\frac{M_2}{\lambda_{1a}}((\frac{\lambda_1^2}{\lambda_{1a}^2} + \frac{\lambda_3^2}{\lambda_{3a}^2}) + \gamma_2(\frac{\lambda_1^2}{\lambda_{1a}^2} - \frac{\lambda_3^2}{\lambda_{3a}^2})^2)$ $Z_2 = -2\frac{M_2}{\lambda_{2a}}(\frac{\lambda_3^2}{\lambda_{3a}^2} + \gamma_2(\frac{\lambda_1^2}{\lambda_{1a}^2} - \frac{\lambda_3^2}{\lambda_{3a}^2})(\frac{\lambda_2^2}{\lambda_{2a}^2} - \frac{\lambda_3^2}{\lambda_{3a}^2}))$ $M_2 = \frac{\alpha_2}{\alpha_1} e^{(\gamma_2(I_2 - 3))}$
Range of s: $s_b \leq s$
The expressions for $\frac{\partial \lambda_2}{\partial R}$ and $\frac{\partial \eta}{\partial R}$ are the same as those for range of $s \in [0, s_a]$ The expression of $\frac{\partial \lambda_1}{\partial R}$ is the same as that for $s \in [s_a, s_b]$ $\sigma_1 = M_2(\frac{\lambda_1^2}{\lambda_{1a}^2} - \frac{\lambda_3^2}{\lambda_{3a}^2}) \qquad \sigma_2 = M_2(\frac{\lambda_2^2}{\lambda_{2a}^2} - \frac{\lambda_3^2}{\lambda_{3a}^2})$ $S_1 = 2\frac{M_2}{\lambda_1}((\frac{\lambda_1^2}{\lambda_{1a}^2} + \frac{\lambda_3^2}{\lambda_{3a}^2}) + \gamma_2(\frac{\lambda_1^2}{\lambda_{1a}^2} - \frac{\lambda_3^2}{\lambda_{3a}^2})^2)$ $S_2 = 2\frac{M_2}{\lambda_2}(\frac{\lambda_3^2}{\lambda_{3a}^2} + \gamma_2(\frac{\lambda_1^2}{\lambda_{1a}^2} - \frac{\lambda_3^2}{\lambda_{3a}^2})(\frac{\lambda_2^2}{\lambda_{2a}^2} - \frac{\lambda_3^2}{\lambda_{3a}^2}))$ The formulations of Z_1 and Z_2 are the same as those for $s \in [s_a, s_b]$
For all ranges, $Q = \frac{q_0 R_0}{h_0 \alpha_1}$

- Case 2: $t_a \leq t^* < t_b$

  In the second case, we suppose the sheet is unloaded after the collagen is recruited at the dome and its neighboring points, so, here $t_a \leq t^* < t_b$. As was discussed previously, the active collagen fibers contained in the deformed body will return to its stress free and unstretched reference configuration during unloading. Recall that, due to the inhomogeneity, an inner circular region with radius $R_a < 1.00$ is filled with active collagen fibers the stretch of that is maximum at the dome and minimum at $R = R_a$. The material points in the inner region possess $s \geq s_a$, with the maximum at the dome and minimum $(s = s_a)$ at $R = R_a$. So here, R_a denotes the radius of material point with $s = s_a$. The complementary region is filled with material points possessing only elastin. The s values in the complementary region are always less than s_a. During unloading, s in both regions monotonically decrease. The s value at $R = R_a$ reduces from $s = s_a$ to $s < s_a$ and s values at some $R < R_a$ reduce from some $s > s_a$ to $s = s_a$. The interface radius R_a decreases and the inner region shrinks while the outer region enlarges.

  During unloading, the stress generation of the points that were in the outer region before the unloading began obviously follows that of classical elastic materials, since the collagen is never activated there. The equations generating the stress and corresponding differential equations at these material points are those used in the first unloading case previously discussed.

  During unloading, some of the material points that possess both active collagen fibers and elastin at the maximum loading generally will loose the active collagen fibers due to unrecruitment and as a result will have only elastin. The stress generation at these points depends on their s values. The stress generation of the points with $s > s_a$ is given by (3.146.1 and 2) with M_1 and M_2 given by (3.147.1 and 2), respectively. The nondimensional differential equations are given by (3.148) with S_1 and S_2 given respectively by (3.149.1 and 2) and Z_1 and Z_2 given respectively by (3.150.1 and 2), (3.132) and (3.137) with Q as the nondimensional pressure. Furthermore, eventually the value of s decreases due to the unloading and become less than s_a. The stress generators and differential equations that are used by these points with $s < s_a$ admit those that are used in the first case of the unloading $(t^* < t_a)$.

More importantly, the unloading will reach a deformation level at which the whole region is occupied only by the elastin just as is in the first unloading case ($t^* < t_a$). Here, as is in the first case, the unloading will return the inflated sheet into a flat stress free membrane as the membrane was in the original reference configuration.

- Case 3: $t_b \leq t^*$

  This is the case when the unloading begins after some points at the dome and its neighboring region lost their elastin. As was assumed, the damaged elastin is unrepairable and therefore they cannot be reactivated by decreasing s below the breaking value s_b during the unloading. This differs from the collagen of which the activity is governed by the s values of the points possessing it, disregarding whether it is loading or unloading case.

  At the beginning of unloading, generally the inflated sheet is divided into three regions: the innermost region, which is the region with damaged elastin leaving collagen as the sole mechanical component, the middle region, which is occupied by both active elastin and collagen fibers and the outer region, which is filled with points possessing only active elastin. The s values in the innermost region is greater than s_b. In the middle region, the s values are $s_b > s > s_a$ and in the outermost region, $s \leq s_a$. When t is reduced, the s values in the three regions are reduced. Moreover, as was explained in the second case, the radius of the interface R_a is also reduced causing the middle region to shrink while the outermost region grows. The same logic however cannot be applied to the interface with radius R_b dividing the innermost region and the middle region. While in principal, during loading, R_b denotes the radius of material points with $s = s_b$ bounding a region with $s > s_b$. The radius R_b also denotes the radius bounding the region where the elastin is damaged. The two regions coincide during loading but not during unloading. Due to the unloading, the s values decrease causing the region with $s \geq s_b$ to shrink, however the region with damaged elastin remains. We suppose that R_b remains to denote the radius of material point with $s = s_b$. So, during the unloading, R_b also becomes smaller. We denote the radius of the fixed region filled with damaged elastin with R_b^*.

  In summary, the following regions are developed during the unloading process:

  - Region 1a. ($0 \leq R < R_b$): The innermost region filled only with active collagen.

– Region 1b. ($R_b \leq R < R_b^*$): Generally, this region is similar to the first region with the exception of the s values that are less than s_b.

– Region 2. ($R_b^* \leq R < R_a$): The middle region that is filled with both active collagen and elastin.

– Region 3. ($R_a \leq R < 1.00$): The outermost region that is filled with active elastin only.

The differential equations that are involved during the calculation are summarized below:

– Region 1a and 1b

In this region the first mechanism has been deactivated. The differential equations are given by (3.137),(3.148), and (3.132) with the definitions of σ_1 and σ_2 are given by (3.154.1 and 2), respectively with M_2 is given by (3.147.2). The definitions of S_1, S_2, Z_1, and Z_2 given by (3.156.1 and 2), (3.150.1 and 2), respectively.

– Region 2

In this region, both mechanisms are active. The differential equations and the stress generator that are involved in the calculation are the same as those that are used in the inner region of the second unloading case.

– Region 3

It is easy to see that this region resembles that of a classical elastic material. The differential equations of the first unloading case are used in this region.

It is very important to note that in this particular case, the fixed radius R_b^* and the decreasing radius R_a eventually will coincide. At this particular unloading stage, two regions remain: the collagen only region ($0 < R < R_b^* = R_a$) and the elastin only region ($R_b^* = R_a < R < 1.00$). Furthermore, when the unloading proceeds, theoretically R_a becomes smaller than R_b^* and basically an 'empty' region $R_a < R < R_b^*$, in which no elastin nor collagen are active, is developed. Technically, however, the numerical calculation never achieves this state of deformation since the algorithm cannot handle this 'empty' region. In fact, the unloading then ceases at some inflated membrane state and some nonzero nondimensional pressure Q. We do not know if the 'empty' region phenomenon can explain the inelastic behavior of saccular aneurysms. The mechanics of the inactive collagen fibers that are embedded in the deforming membrane, if any, is

also unknown. We also cannot predict the profiles of the membrane when Q continuous decreasing to a zero value. However, it will be shown in the next section the membrane profiles when Q is close to zero values.

3.5.3 Results

In this section we present results for inflation of circular clamped membranes composed of the dual mechanism material each of which is an exponential type material. Four materials are employed as examples: material A, B ,C and D. The material parameters are tabulated in Table (21). Basically these parameters are obtained through the nonlinear regression analysis presented in Section 3.3. The material parameters for A and B are obtained by having λ_a fixed during nonlinear regression analysis. Unlike materials A and B, material parameters C and D are obtained by having λ_a not fixed resulting in 'early' recruitment (small λ_a). The values of fixed λ_a=1.7610 and non fixed λ_a=1.5962 correspond to s_a=1.4237 and s_a=0.9407, respectively. Recall that for both cases, the value of λ_b is assumed to be 2.3 which corresponds to s_b = 3.4790. At the dome of inflated clamped membrane, s_a=1.4237, s_a=0.9407, and s_b = 3.4790 correspond to t_a = 1.4485, t_a = 1.3510, and t_b = 1.7862, respectively. Observe also that the thicknesses of materials A and C both are 100 μ, while those of materials B and D both are 125 μ.

We will see in this section, the resulting curves of Q_d (the value of non dimensional pressure Q at the dome) versus t (the dome stretch ratio) during loading and unloading for different material parameters, different pressure distribution and different maximum loading. We also will see the resulting profiles for different pressure distribution. Only linearly varying distribution with maximum pressure at the dome is considered in this section. The distribution of the pressure along the radius is measured by a parameter C. Uniform distribution corresponds to C = 0.00. The value of C = -G indicate that the local pressure at the edge (R=1.00) is (1-G) times those at the dome.

The resulting Q_d vs. t curves during loading with uniform pressure for materials A and B and C and D are depicted in Figures (30) and (31), respectively. In these figures, curves OAB represent the response given only by the first mechanism. Curves OAC'C represent

Table 21: The materials and their parameters used as examples in this section. The strain energy function of the material is given by (2.21).

Material Parameters	A	B	C	D
Undeformed thickness (H) (μ)	100	125	100	125
λ_a	1.76103	1.76103	1.5962	1.5963
$\alpha_1(10^3 dynes/cm^2)$	89.0357	71.2199	73.9613	59.1676
γ_1	0.6224	0.6224	0.5908	0.5909
$\alpha_2(10^3 dynes/cm^2)$	390.872	312.6121	395.723	316.598
γ_2	1.867193	1.867605	1.8483	1.8482
s_a	1.4237	1.4237	0.9407	0.9407
s_b	3.4790	3.4790	3.4790	3.4790
t_a	1.4485	1.4485	1.3510	1.3510
t_b	1.7862	1.7862	1.7862	1.7862

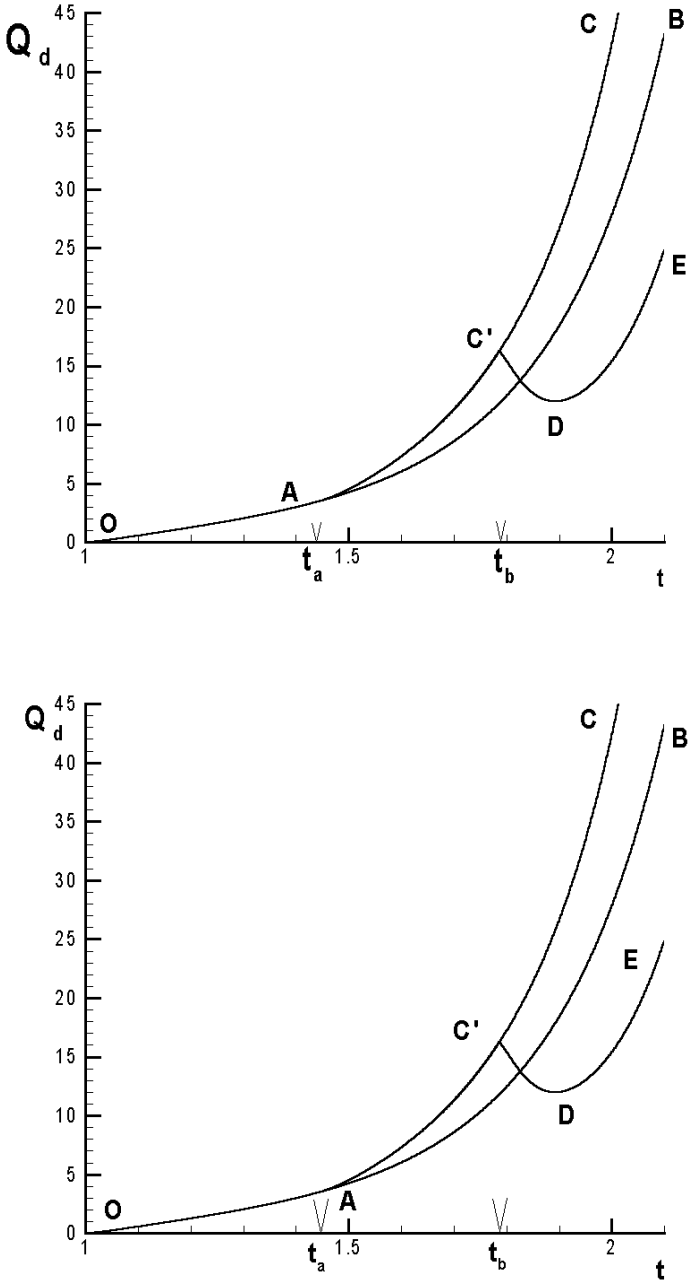

Figure 30: Resulting Q_d vs t curves corresponding to the materials A (top) and B (bottom) given in Table 21.

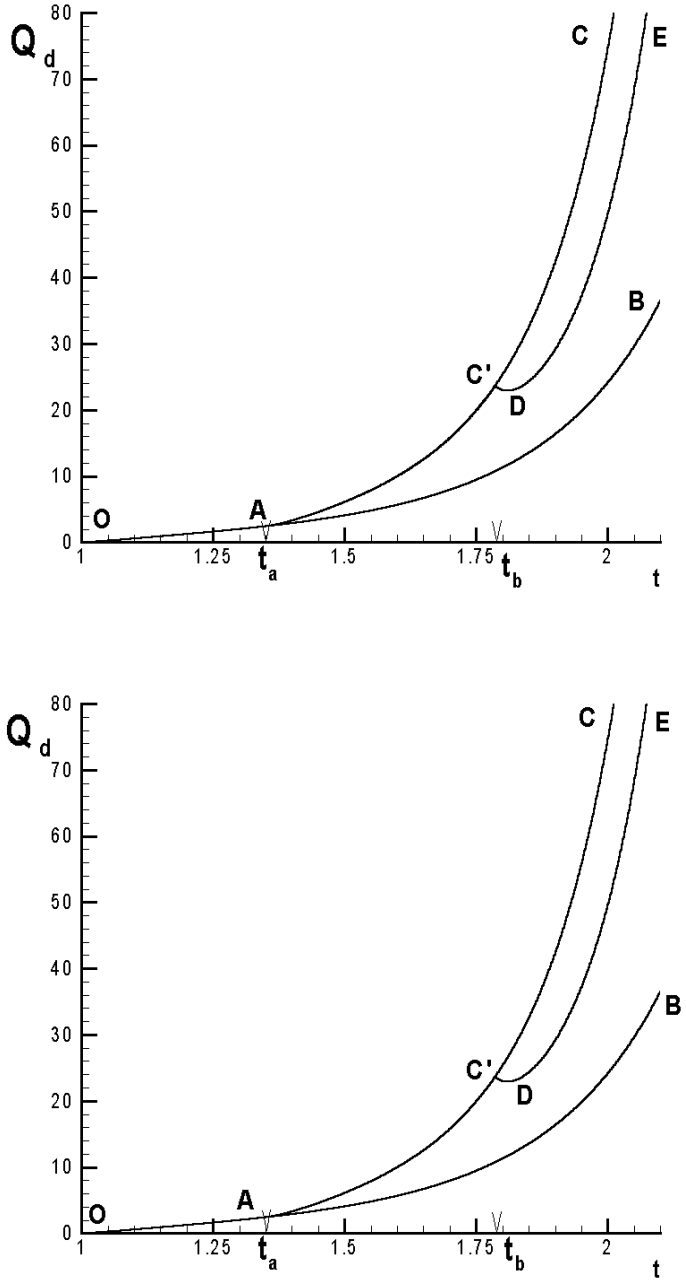

Figure 31: Resulting Q_d vs t curves corresponding to the materials C (top) and D (bottom) given in Table 21.

the response given by both first and second mechanism without elastin breakage. For both materials A and B, the second mechanism is activated at $t_a = 1.4485$, while for both materials C and D the second mechanism is activated at $t_a = 1.3510$. In all of these figures, at $t = t_a$ (indicated by point A) curves OAC deviate from curve OAB indicating material stiffening due to the additional mechanism. Curves OC'DE represent the response of a dual mechanism material that experiences elastin breakage. The breakage occurs at $t = t_b$ (indicated by point C') when the response shows local maximum. The values of t_b for all of the materials A, B, C, and D are 1.7862. At these local peaks, instead of having abrupt jumps as typically occur in homogenous deformation cases, the values of Q_d gradually decrease as the values of t increase. The values of Q_d reach local minimum D and recover. The recovery of materials C and D however appear to be 'faster' than those of materials A and B. The 'fast' recovery of materials C and D is probably due to the 'early' recruitment that allows a sufficient amount of the recruited material to be deposited at the dome and the neighboring area to compensate the weakening that is produced by the deactivation of the first mechanism.

The resulting Q_d vs. t curves for material A and B qualitatively are the same. Similarly, the resulting Q_d vs. t curves for material C and D qualitatively are also the same. These similarities should be expected since the equilibrium system is non dimensional. The ratios of the coefficients of the second mechanism materials to the coefficients of the first mechanism materials are more important than the individual values of the coefficients. The ratios of α_2 to α_1 for both materials A and B approximately are 4.39, while those for both materials C and D approximately are 5.35. Figure 32 shows the resulting Q_d versus t curves for material C during both loading (OBC and OB'C') and unloading (CD and C'D') cases. Curve OBCD is the response of material C when a uniform pressure Q is applied, while curve OB'C'D' is the response when a linearly varying Q is applied. In the later case, the value of Q_d at the dome is twice of that at the edge (so here C=-0.5). As is expected, a Q_d value to produce a particular value of t in the non uniform case is higher than that in the uniform case. For both pressure distribution cases, the maximum loading t^*=1.88 before unloading occurs after total elastin breakage. The path of unloading does not follow the loading path. The unloading for both cases are terminated at some nonzero Q_d (indicated by point D and D' for C=0.00 and C=-0.5, respectively).

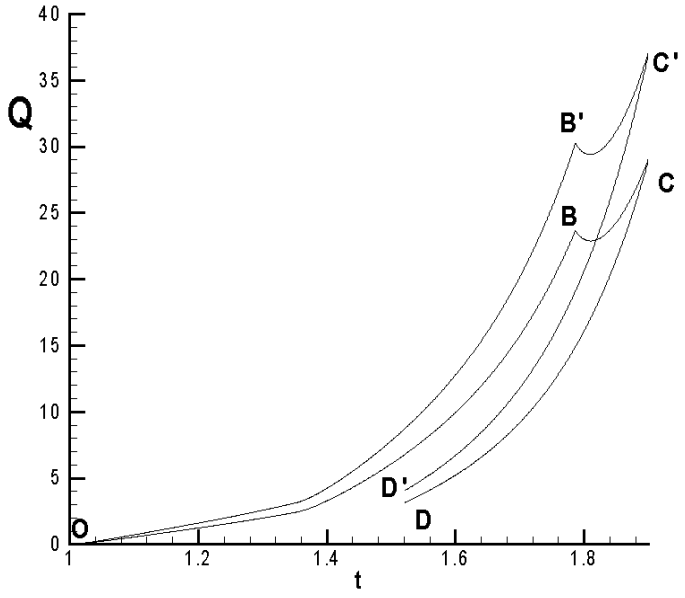

Figure 32: Resulting loading and unloading Q_d vs. t curves for both uniform and linearly varying Q corresponding to the material parameters C given in Table 21.

From the computation point of view the termination can be explained as follows. Recall that during loading a circular region of damaged elastin is enlarged along with the progression of t. If total elastin breakage is achieved, as occurs in the loading for these cases, then the entire circular membrane is left with only active collagen fibers. During unloading, the stretched collagen fibers return to their unstrained reference configurations. One might expect that the unloading will stop at $t = t_a$ (t_a=1.3510 in these two cases) below which all collagen fibers become inactive. However, $t = t_a$ corresponds to the collagen activation, or deactivation in the unloading case, only at the dome. In fact, the rest of collagen fibers have been deactivated when the inflated state reaches $t = t_a$. In the case of total breakage, $t = t_a$ is never obtained during unloading. The collagen fibers away from the dome are deactivated earlier than those at the dome (since s is always maximum at the dome). As is now, the computation cannot handle the case when neither elastin nor collagen is active at a particular node. In this situation the computation is terminated. In the cases under discussion, the terminal states after unloading, indicated by D and D', both correspond to t=1.56 corresponding to low values of $Q_d \approx 4.0$ and $Q_d \approx 3.0$ for C = 0.00 and C = -0.5, respectively. For the linearly varying pressure distribution, $Q_d = 4.0$ corresponds to local Q = 2.0 at the edge. Considering these significantly low values of Q_d, the terminal inflated states that are obtained here can be seen as near stress free states. Figure 33 demonstrates the effect of the variation of C values. In this case, material D is loaded with different pressure distribution and unloaded at t^*=1.8. Here we can see that as C values are decreased, Q_d required to produce the same amount of t are increase.

Figure 34 shows typical developing profiles of an inflated circular clamped membrane composed of dual mechanism for both cases: uniform and linearly varying pressure distribution. The numbers shown in the figure are values of applied t corresponding to the material C. These numbers vary from one material to other materials. In the figure, the wall thinning, especially at the dome, is well demonstrated. In the left figure, the values of t_a and t_b (in the figure are shown as λ_a and λ_b) are 1.35099 and 1.7862, respectively. At t=1.84 the profiles looks elongated in the Z direction . This is due to the elastin breakage that occurs first at the dome causing that area to be weaken. The right figure demonstrates that at t=1.90, the profile reaches its maximum height. When t progresses beyond the maximum height state,

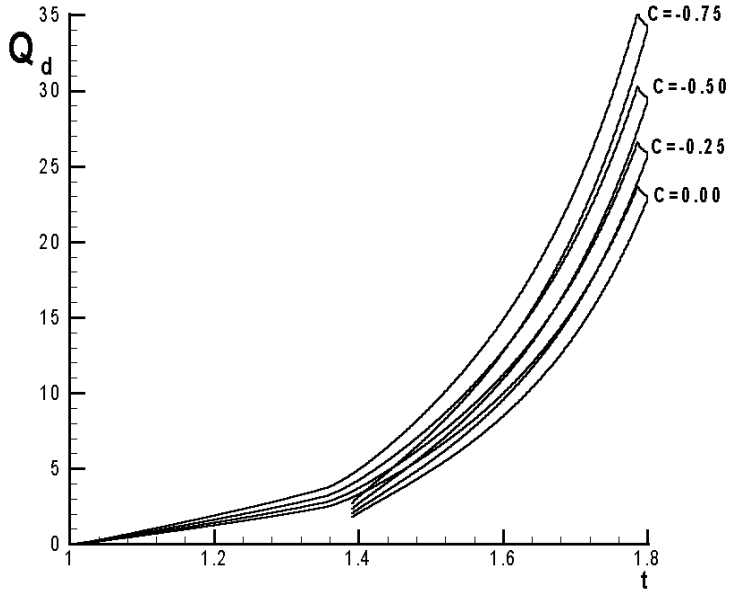

Figure 33: Resulting Q_d vs t curves corresponding to the material parameters D given in Table 21 during loading and unloading for different values of C. For the same amount of t values, Q_d values increase proportionally to the decrement of C.

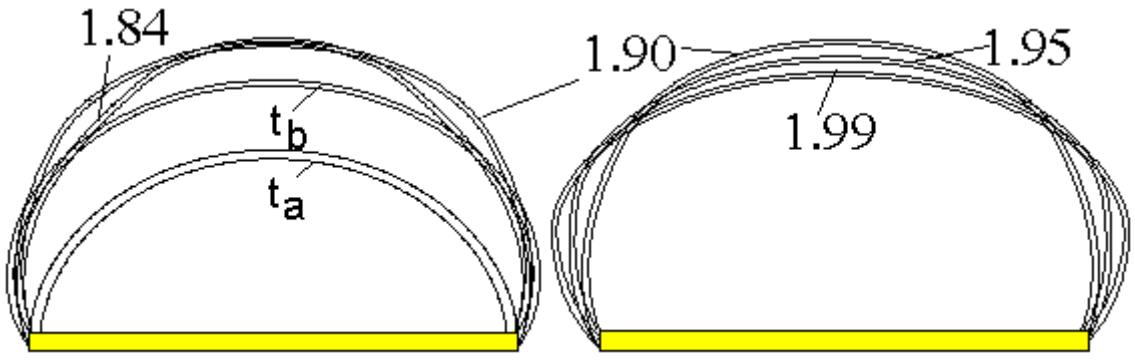

Figure 34: Representative resulting inflated membrane profiles.

the profiles develop in rather lateral direction (perpendicular to the Z axis). This is due to the built up of collagen fibers that has been recruited. The stiffness contributed by collagen fibers compensate the dome weakness created by elastin breakage. In fact, since the collagen is stiffer than elastin, the dome area stiffen and thus preventing the development in the axial direction (parallel to Z axis).

Figures 35 and 36 show the inflated profiles for different pressure distribution. The solid and dashed lines represent resulting profiles for C=0.00 and C=-0.50, respectively. Figures 35 top and bottom both show the resulting profiles for the two different pressure distribution but for the same amount of Q_d. The top and bottom figures correspond to $Q_d \approx 30.00$ and $Q_d \approx 51.10$, respectively. The profile resulted from C=-0.50 shows dome area that is more elongated in the Z axis direction rather than those resulted from C=0.00. Similarly, Figures 36 top and bottom both show the resulting profiles for the two different pressure distribution for the same amount of dome stretch ratios t. The top and bottom figures correspond to t =1.799 and t =1.965, respectively. Again here we can see that the linearly varying pressure distribution produces inflated profiles that are more elongated in the Z axis direction compare to those produced by uniform distributed pressure.

Figure 37 shows the effect of different maximum loading t^* on the final inflated profiles after unloading. Here the circular membrane made out of material D is loaded with uniform pressure distribution. The unloading is performed for several different maximum loading t^*. The resulting terminal inflated profiles after unloading for t^*=1.9 (solid line) and t^*=2.1 (dashed line) show that the later case appears to be flattened than the first case. Clearly, the amount of maximum loading in the later case provides more amount of recruited collagen fibers resulting in stronger stiffening at the dome compare to those provided by the first case.

The results for other maximum loading are tabulated in Table 22. In this table r_b^*, t_f, q_f indicate the final radius of the region occupied by elastin fragments, final t and final q after unloading, respectively. The corresponding maximum Q_d for each t^* is given by q_{max}. The maximum value of r_b^* therefore is 1.00. As is expected, the values of r_b^* are enlarged proportionally to the increment of the maximum loading t^*. The value of r_b^*=0.00 implies that the elastin breakage has not occurred yet when the unloading is initiated. An example of this case is when $t^* = 1.7 < t_b$. In this case the t_f value is approximately 1.00 and the

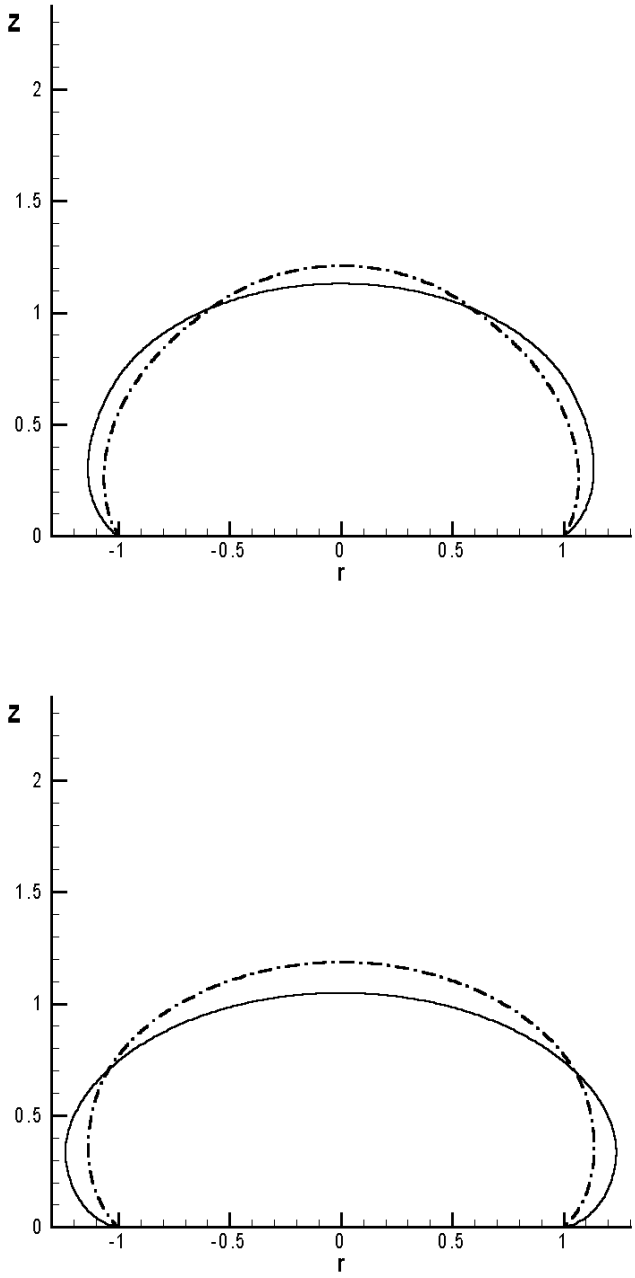

Figure 35: Resulting inflated profiles for material D at $Q_d \approx 30.0$ (top) and $Q_d \approx 51.1$ (bottom) for C=0.00 (solid line) and for C=-0.50 (dashed line). The figures clearly indicate that for the same amount of dome pressure Q_d, linearly varying pressure distribution ($C = -0.5$) produces a profile that is more elongated in the axial direction compare to those produced by uniformly distributed pressure (C=0.00).

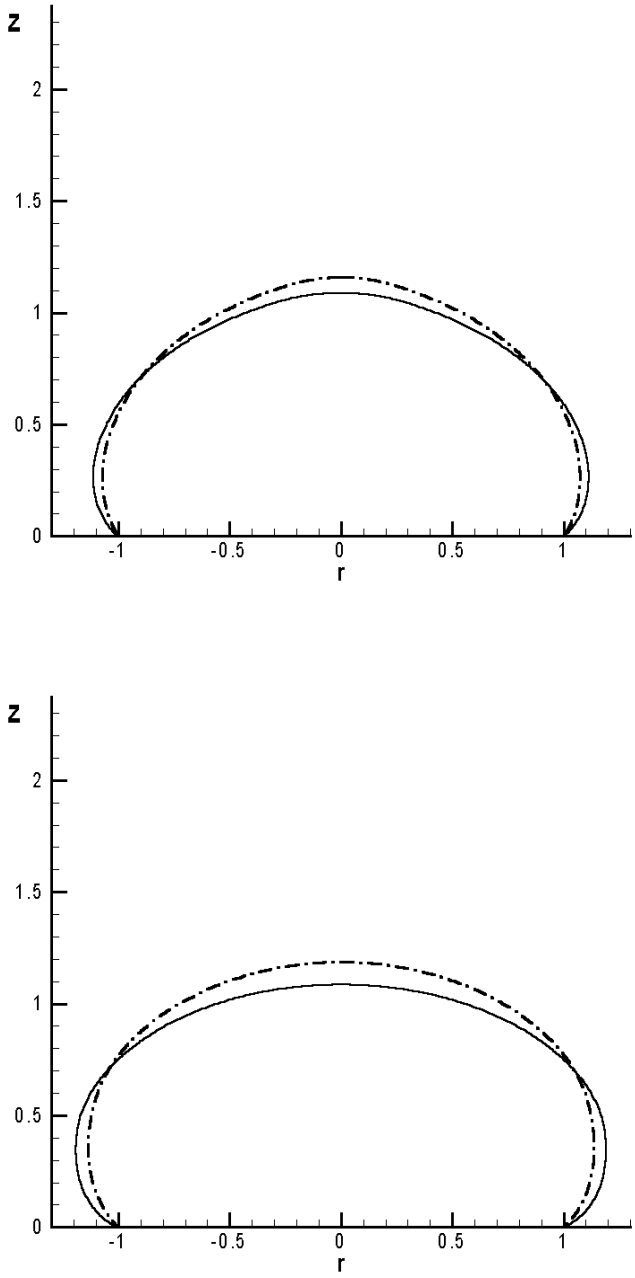

Figure 36: Resulting inflated profiles for material D at t=1.799 (top) and t=1.965 (bottom) for C=0.00 (solid line) and for C=-0.50 (dashed line). The figures clearly indicate that for the same amount of dome stretch ratio t, linearly varying pressure distribution (C=-0.50) produces a profile that is more elongated in the axial direction compare to those produced by uniformly distributed pressure (C=0.00).

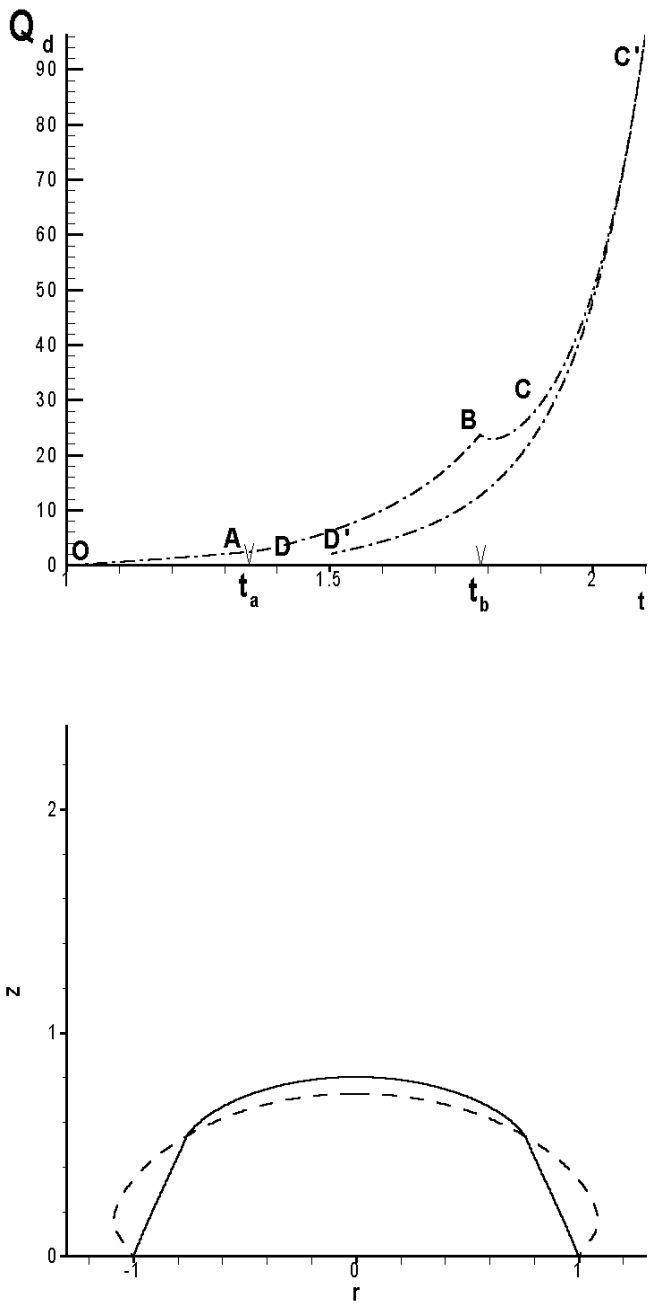

Figure 37: The top figure show the resulting Q_d vs t curves corresponding to the material parameters D given in Table 21 during loading and unloading for maximum loading t^*=2.1 (dot dashed lines) and t^*=1.9 (solid lines). The bottom figure shows the resulting terminal inflated states for both maximum loading cases: t^*=2.1 (dashed lines) and t^*=1.9 (solid lines).

Table 22: Results of different maximum loading t^* for material D. Here, q_{max}, r_b^*, t_f, q_f are the corresponding Q_d value for t^*, the radius of elastin fragments region, final t and final q after unloading.

Maximum loading t^*	q_{max}	r_b^*	t_f	q_f
1.7	15.8386	0.0000	1.0040	0.0000
1.8	22.9845	0.1809	1.3840	1.4977
1.9	29.2590	0.6015	1.4120	0.9081
2.1	96.2413	0.9030	1.5030	2.0236
2.2	204.547	0.9999	1.5850	3.7580

q_f value is close to zero indicating the membrane returns to its flat configuration. When t^*= 2.2, r_b^*= 0.999 indicating that the entire circular membrane has no active elastin during unloading. The t_f and q_f values in this case are 1.5850 and 3.750, respectively. The final inflated state is near stress free state. An improvement to the computation algorithm should be made so that q_f values that are close to zero can be obtained.

4.0 DISCUSSION

Aside from its promising results, the proposed constitutive equation has some limitations with respect to applications to cerebral arterial tissues. It will be seen that the limitations arise from either insufficient experimental data or inherent assumptions. In this chapter we also discuss future works to address these limitations.

4.1 LIMITATIONS OF THE PROPOSED CONSTITUTIVE EQUATION

The limitations in applications of the constitutive equation mostly arise from the assumptions employed in the constitutive equation that must be prescribed due to insufficient real data on the mechanics of cerebral arterial tissues, in particular the inelastic behavior. While the nonlinearity of cerebral arterial walls has been confirmed by several experimental results [82, 79, 83], the inelastic behavior, on the other hand, is seldom reported. The report by Scott, Ferguson and Roach [79] may be the only documentation regarding the inelastic behavior of cerebral arteries. Holzapfel *et al.* reported similar inelastic behavior of the media of extracerebral arteries [80]. The inelastic behavior that is hypothesized to be due to the damage of elastin [79] is an essential feature to be incorporated for cerebral aneurysm applications due the finding of fragmented elastin on the aneurysm walls [2, 55].

- It is assumed that all collagen fibers occupying a material point are recruited at the same deformed state. Busby and Burton [49] however hypothesized that the nonlinear appearance of the elastic curves of arteries are due to recruitment of collagen fibers in a gradual manner. Busby and Burton also assumed that the number of collagen fibers recruited during the deformation can be approximated by the second derivative of the

tension with respect to the circumferential stretch. No histological evidence however is offered to support this relation. The assumption of non gradual recruitment employed in this work therefore is taken due to lack of data on the recruitment rate.

- It is assumed that all elastin occupying a material point fragments at the same deformed state (local total breakage). One resulting consequence is that the loading and unloading cycles of a particular homogeneous deformation produce only two elastic curves: before and after the elastin breakage. Results from the experiments of Scott *et al.* [79] demonstrate more than two elastic curves prior to the inelastic deformation leading to a hypothesis that the elastin is fragmented rather gradually. However, their data does not include sufficient information to evaluate this hypothesis of gradual elastin fragmentation. Local total elastin breakage assumption therefore is taken due to insufficient data on the fragmentation rate.
- It is assumed in the equation that the damaged elastin are not regenerated. This assumption reflects the fact that currently there is no report of elastin rehabilitation at the aneurysm walls.
- It is assumed that the first and second mechanisms are isotropic with respect to reference configurations κ_1 and κ_2, respectively. The elastin embedded body generally can be regarded as an isotropic material. The apical region of an arterial bifurcation contains collagen fibers with no preferred orientation [54]. Yet experimental results confirming the material symmetry of this particular region are unavailable. The isotropy assumption for the second mechanism therefore is taken due to lack of experimental data.
- It is assumed in this work that the original body containing the elastin and collagen is homogeneous. The histology of arterial walls reveals that structurally an arterial segment can be considered uniform in the longitudinal and circumferential directions but not in the radial direction (across the wall thickness) [150, 157]. This is consistent with mechanical testing demonstrating that the material properties of arterial walls can be considered uniform in the longitudinal and the circumferential direction but not in the radial direction[158]. The assumption regarding the homogeneity across the thickness however is imposed since the small thickness of the cerebral arterial wall justifies the use of the membrane approximation theory for the deformations considered here.

4.2 FUTURE WORK

The aforementioned limitations immediately suggest future directions for this work that can be categorized into three groups: theoretical, experimental and numerical work.

4.2.1 Future theoretical work

- To consider collagen recruitment in a gradual manner

  The multi-mechanism constitutive equation is not restricted to the involvement of the new mechanisms in a discrete manner. A simple example of gradual involvement of new mechanisms can be seen in Rajagopal and Wineman [104]. The gradual recruitment can be thought of as continuous recruitment of fibers or groups of fibers at different configurations.

- To allow more than one mechanism representing more than one kind of collagen fiber

  Blood vessel walls contain four types of collagen: Type I, Type III, Type IV and Type V [70]. Deficiency of Type III collagen is hypothesized to play a role in the rupture of aneurysm [15]. Therefore the distinction between mechanisms representing response of bodies embedded with these different types of collagen therefore may be important when dealing with aneurysm rupture. In principal, multi-mechanism modeling does not limit the number of mechanisms that can be added in the equilibrium system. Technically, the consideration of other kinds of collagen fibers can be done easily by adding another (or other) strain energy function(s) for example in the current constitutive equation. The addition of the new component(s) certainly demands new material parameter identification.

- To consider gradual elastin breakage

  As was mentioned before, a non discrete microstructural change is not a novel application in multi-mechanism modeling (see an example in Rajagopal and Wineman [104]). The incorporation of gradual elastin breakage is an essential effort to more realistically mimic the elastin fragmentation process. The implementation of gradual breakage requires factors that can quantify the breaking rate of elastin.

- To allow elastin regeneration

  Elastin fragmentation has been hypothesized to play a role in aneurysm formation. Hence, it is possible that future prevention of aneurysm formation will include efforts to artificially introduce 'new' elastin. From a multi-mechanism modeling point of view, the introduction of 'new' or regenerated elastin technically can easily be done by considering mechanisms that are added at a specified deformed level. Experimental information regarding the material parameters of the newly generated elastin certainly are required.

- To construct a constitutive equation that incorporates anisotropy

  It has been commonly accepted that arterial walls are well modelled as cylindrically orthotropic[159, 160]. An isotropic assumption however sometimes is still used [125, 126]. Cerebral arterial walls however are anisotropic [161]. The degree of anisotropy of cerebral arterial walls however has not been explored yet and it likely depends on the local geometry. Recall that the apical region of an arterial bifurcation contains collagen fibers with no preferred orientation [54]. Therefore, the isotropic assumption is likely reasonable for modeling aneurysm development at bifurcations. The wall anisotropy however becomes an essential issue when one models the formation of saccular aneurysm at curved segments of arteries where the collagen fibers are more oriented and therefore may introduce anisotropy.

- To consider material inhomogeneity

  Recall that, as remarked by Patel and Vaishnav, the inhomogeneity in the radial direction may becomes an important issue for some types of deformations, such as bending, [158]. In these cases, it may be important to treat the individual contributions of wall constituents, such as collagen and elastin, as separate entities, occupying physically different radial positions. The incorporation of this type of inhomogeneity certainly can be done within the framework of multi-mechanism constitutive equations.

4.2.2 Future experimental work

Future experimental work can be directed at the following issues:

- To construct experimental protocols suitable for the proposed equation

  It's clear that the currently proposed approach demands new experimental procedures that differ from the traditional ones. As an example, we can see that both the recruitment and breakage criteria, certainly cannot be evaluated using commonly used experimental procedures. We have already made substantial progress in developing a suitable experimental protocol using real samples from cadavers. The experimental results will be presented in future publications.
- To run experiments on real tissue samples

  Once the desired protocol is established, experiments using real samples can be run to obtain data and material constants including the form of the function of deformation parameters $s(\mathbf{F}_1)$ and values of both the recruitment and breakage criteria s_b and s_b, respectively.
- To include morphology studies in particular regarding the elastin breakage

  The phenomenon of elastin breakage is fundamental to the current modeling due to the abundant evidence of elastin fragments in the aneurysm walls.

4.2.3 Future numerical work

The results presented in this work are mainly from geometrically simplified model problems that can be solved either analytically or numerically. When geometrically complex problems must be considered, complex numerical tools must be employed. Unfortunately, the concept of multi-mechanism constitutive equations is relatively new and therefore is not yet implemented in any commercial numerical tools.

Two possible directions therefore are open. One direction is to implement the dual mechanism concept in a commercial finite element or finite difference package. The other method is to construct a numerical tool based on either a finite element or finite difference method incorporating the proposed constitutive equation. Challenges will include modeling of geometrically complex bodies and fluid-structure interactions.

5.0 CONCLUSION

The conclusions of this work can be summarized below:

- A new constitutive equation for both cerebral arterial and aneurysm walls has been presented. The new constitutive relation can handle both the nonlinearity and inelasiticty exhibited by the tissues. More importantly, using the new contitutive equation, the two different entities, the arterial wall and aneurysm wall, can be related or coupled. The separation of the two entities that was commonly practiced becomes unnecessary.
- Results of the proposed dual mechanism used in some relevant model problems, including homogeneous and inhomogeneous deformations, 3D and 2D, and either single or multi parameter, have been presented. These examples are intended to show how to implement the new constitutive equation in some basic models and provide guidance for future experimental work.
- It has been shown that the proposed constitutive equation can capture the inelastic bevahior of cerebral arterial walls observed by Scott *et al.*[79]. The resulting regression analysis shows that exponential type strain energy functions serve very well for both mechanisms. It is very important to emphasize that the material identification is not intended to predict the material properties of collagen fibers and elastin sheet. It has to be understood that the identification is only a way to quantify the gross mechanical response produced by a body that is composed of either elastin only or by collagen only or by both collagen and elastin.
- Some suggested experimental methods for material identification of the proposed constitutive equation have also been given, in particular the determination of s and value of s_a.

- Finally, the proposed constitutive equation can model the early stages of aneurysms formation. The model can predict the elastin fragmentation observed inn the wall of aneurysms, wall thinning at the fundus, the inhomogeneity of the wall due to partial elastin breakage and collagen recruitment, and the sac-like behavior of the dome. The variation of sac shape due to the distribution of the applied pressure implies the importance of hemodynamic factors.
- It is expected that the new constitutive equation presented here can be used to incorporate various proposed mechanisms that may either precede aneurysm formation or favor aneurysm development. The generalisation from the classical constitutive equation, which is restricted to include only one mechanism, is expected to result in more realistic predicitions of both aneurysm formation and development in future application of this model.

APPENDIX A

NUMERICAL PROCEDURE OF SOLUTION FOR INFLATION OF CIRCULAR CLAMPED MEMBRANE

The set of differential equations presented in Table (20) is integrated using the well known numerical scheme Runge-Kutta (RK) method. The goal of the numerical process is to obtain the unknowns stretch ratios λ_1 and λ_2, η and the nondimensional pressure Q for a given inflated state identified by the dome stretch ratio t. This however does not imply that the numerical scheme can be used to solve the problem for any given t, independent from the history of t. As will be discussed below, the algorithm that handles the introduction of the second mechanism requires information from some preceding deformed states. The overall algorithm is lengthy and therefore only important numerical issues are discussed in this chapter. A full pictorial flowchart is presented in Appendix E.

The numerical procedure used here, particularly part of it that handles the multi-mechanism section, relies on the assumption that $s(R,t)$ monotonically decreases with R. Such a condition has been exhibited in the classical elastic material [140] as well as in the multi-mechanism based material [105]. Moreover, some important parts of the algorithm are inspired by the computational work by Wineman and Huntley[105].

Due to the problem's axisymmetry of the deformation, the circular membrane can be represented by material points or particles defined on the domain 0 to R_o. These particles form the computational domain of this problem. The radius line is nondimensionalized using the length of the circular membrane undeformed radius R_0. The material points then will be represented by some finite numbers of equally distanced nodes so that the numerical scheme

can be performed. The nodes are denoted by R_j, where $j = 1, 2, ...J$ and J is the number of nodes. The dome node $R = 0.00$ and the edge node $R = 1.00$ are denoted by R_1 and R_J, respectively. The distance between the nodes, ΔR, that leads to a convergent solution is found, by numerical experiments, to be either $\Delta R = 1.00/10$ or $\Delta R = 1.00/8$. In the RK method, the unknown values at node R_{k+1} are estimated by 'adding' incremental values to either computed or already known values at node R_k. The incremental values are calculated using the set of the differential equations displayed in Table (20) that employ values at node R_k. Generally, for a given inflated state identified by $t = \lambda_1(0, t) = \lambda_2(0, t)$, a an initial estimate for Q must be assigned first and modified later if the edge boundary condition (3.131) is not satisfied.

The rate of aneurysm development ranges from approximately 0.1 mm/year for nonsmokers aneurysms patients to 0.5 mm/year for smoker patients [14]. The formation and growth of the aneurysm therefore are considered to be sufficiently slow, the circular membrane can be considered to inflate in a quasi-static mode. No initial condition therefore is needed in the calculation process. With respect to the pulsating blood pressure, the quasi-static assumption however is far from realistic and needs to be improved in future modeling.

A.1 STAGES IN WHICH THE FIRST MECHANISM IS ACTIVE

We first discuss the numerical procedure for deformed states where only the first mechanism is active. By definition this means the dome stretch ratio t is less than t_a. These deformed states resemble those of classical single mechanism materials. In our discussion, these states will be referred to as no recruitment states. Due to the inhomogeneity of the deformation, the stretch ratios λ_α $(\alpha = 1, 2)$ monotonically decrease from its maximum at the dome to the minimum at the edge. The deformation parameter s is less than s_a everywhere in the computational domain for all $t < t_a$. It is clear that the value of s depends on the node radius R and the dome stretch ratios t, so $s(R, t) < s_a, R \in [0, 1]$ for $t < t_a$. For these deformed states, the nondimensional differential equations are given by (3.135,3.132 and 3.137) with S_1 and S_2 given by (3.139.1 and 2) and σ_1 and σ_2 respectively given by (3.138.1 and 2) with $M_1 = e^{(\gamma_1(I_1-3))}$. The details on how to implement the RK method for the

given system of differential equations will not be delivered here. Interested readers may find such information available from many sources, for example from Gerald and Wheatley [162]. Some special technical challenges derived from the boundary conditions of the problem and the introduction of the multi mechanism scheme however are not part of the RK method in general and they will be discussed in the following lines.

The first problem appears in the right hand sides of the system of differential equations (3.135,3.132 and 3.137) that are unbounded when the integration is initiated at $R = 0.00$ (R_1). A remedy for this problem, suggested by Green and Adkins [140] is to assume that at $R = 0.00$:

$$\frac{\partial \lambda_1}{\partial R} = \frac{\partial \lambda_2}{\partial R} = \frac{\partial \eta}{\partial R} = 0.00 \tag{A.1}$$

in order to obtain a bounded solution. However, the consequences is that the incremental values cannot be produced and the integration process fails to start. This problem is solved by supplying an alternative equation for η, (3.124) to reduce the system of differential equations to depend on two unknown variables: λ_1 and λ_2. The alternative equation provides estimation of η at R_2, while the reduced system provides the estimation of nonzero λ_1 and λ_2 there. Once the computed values at R_2 are obtained, the calculation of the values at the next nodes (at $R_3, R_4...$) can be achieved using the complete system of differential equations.

The next issue is the algorithm for an iterative procedure that is used to obtain the nondimensional pressure Q. As was discussed, an initial estimate Q must be supplied for each value of t in the integration process. The node-to-node calculation described above eventually will reach R_J, the edge node. The computed value $\lambda_2(R_J, t)$ must satisfy the boundary condition (3.131). A small tolerance is set to measure the closeness of the computed value to the required value. When the error is intolerable for the estimate value Q, a new estimate value of Q must be found and supplied in the next iteration. Observe however that the resulting $\lambda_2(R = 1.00, t)$ can be seen as a product of a function f of an initial estimate value Q for a fixed t as follows:

$$\lambda_2(R = 1.00, t) = f(Q). \tag{A.2}$$

The 'new' estimated Q can be found using the well known Secant iteration method [163] using the demanded boundary condition (3.131) as a target value for $\lambda_2(R = 1.00)$. Once

the new estimated Q is obtained, the node-to-node integration process can be repeated from R_1 toward R_J using this updated Q. The whole scheme, which includes the integration process, the checking of the edge condition and the updating of Q, is iterated until the error of $\lambda_2(1, t_i)$ is within some small tolerance indicating that the desired Q has been found for the given t_i.

A.2 STAGES IN WHICH BOTH THE FIRST AND SECOND MECHANISMS ARE ACTIVE

The numerical procedure involving the recruitment process is discussed next. We suppose that t increases such that the stretch ratios at the dome and its neighboring points are large enough to activate the collagen recruitment but not to initiate the elastin breakage at the dome ($t_a \leq t < t_b$). We shall refer these deformation states as the recruitment states. As was discussed earlier, during these recruitment states, a circular region with radius R_a that is occupied by both the elastin and recruited collagen is formed and is enlarged. In this region, both mechanisms, the first and the second, participate in the stress generation. In the complimentary region, as was discussed, only the first mechanism is active. Note however that the previous technical issues will still be encountered during these stages. In addition, more challenging issues due to the introduction of the second mechanism will be encountered during these stages.

First we will discuss the scheme that is used to obtain the stretch values λ_{1a} and λ_{2a} that appear in the second mechanism deformation gradients $\mathbf{F_2}$, which is employed in the stress generation of particles in the recruiting region (the corresponding λ_{3a} can be obtained easily from an incompressibility condition). Recall that the second mechanism is activated on particles that satisfy the collagen recruitment criterion. Each particle however satisfies the collagen recruitment criterion at different deformation levels. Clearly, the configuration of the deformed membrane corresponding to that activation phase becomes the reference configuration of the second mechanism for that particle. Eventually, every particle in the recruiting region employs a configuration once occupied by the deformed membrane as its second mechanism reference configuration. As a consequence, the second mechanism de-

formation gradient, $\mathbf{F_2}$, must be relative to the corresponding reference configuration. This dependency is demonstrated in $\mathbf{F_2}$ by the appearance of the stretch ratios λ_{1a} and λ_{2a}, which are λ_1 and λ_2, respectively, of a particle at R_k due to some $t \geq t_a$, say $t = \hat{t}$, that corresponds to a deformation level at which the collagen fibers of that particle begin to load bearing. Since the collagen fibers are activated when $s = s_a$ the following local relation, say at R_k, then must hold:

$$s(\lambda_{\alpha a}(R_k, \hat{t}(R_k))) = s_a \qquad \text{for} \qquad \alpha = 1, 2. \tag{A.3}$$

Here, since s monotonically decrease along R, the stretch ratios λ_{1a} and λ_{2a} are unique for each particle, say R_k, in the recruiting region. Moreover, each crown stretch ratio $\hat{t}$ is also unique for each recruiting particle, say R_k. The dome stretch ratios provide a good example. The dome stretch ratio t_a is t that satisfies the collagen activation criterion there and so $\lambda_{1a} = \lambda_{2a} = t_a$ for $R = 0.00$. Correspondingly, $\hat{t} = t_a$ for $R = 0.00$.

These values: $\lambda_{1a}, \lambda_{2a}, \hat{t}$, are *a priori* unknown and must be computed during the numerical process. Note that during the computational effort, t is increased incrementally by amount of Δt. If we suppose that the resulting s at R_k due to t_j is denoted by $s(k, j)$, then it is possible that when t progresses from t_j to t_{j+1}, s at R_k evolves from $s(k, j) < s_a$ to some $s(k, j+1) > s_a$. In this situation, we assume that s smoothly progresses with t, and so there exists $t_j < t = \hat{t} < t_{j+1}$ such that $s(k, t = \hat{t}) = s_a$. The following procedure to obtain $\hat{t}$ is adopted from the work by Wineman and Huntley [105]. The computation involves some deformation 'history'. We denote $\lambda_1(k, j)$ and $\lambda_2(k, j)$ as the stretch ratios of particle at radius R_k due to dome stretch ratio t_j as follows:

$$\lambda_\alpha(k, j) = \lambda_\alpha(R_k, t_j) \qquad \text{for} \qquad \alpha = 1, 2. \tag{A.4}$$

The set of $\lambda_\alpha(R_k, t_i)$ for $i = j, j-1, j-2$ describes the history of the stretch ratios of a particle at radius R_k. A second degree polynomial in t that is constructed by a Lagrange interpolation denoted by $P\lambda_\alpha(k, j)$ can be formed based on that history as follows:

$$\begin{aligned} P\lambda_\alpha(k) = \frac{(t - t_{j-1})(t - t_{j-2})}{(t_j - t_{j-1})(t_j - t_{j-2})}\lambda_\alpha(k, j) + \frac{(t - t_j)(t - t_{j-2})}{(t_{j-1} - t_j)(t_{j-1} - t_{j-2})}\lambda_\alpha(k, j-1) \\ + \frac{(t - t_j)(t - t_{j-1})}{(t_{j-2} - t_j)(t_{j-2} - t_{j-1})}\lambda_\alpha(k, j-2). \end{aligned} \tag{A.5}$$

So $P\lambda_\alpha(k)$ can be used to estimate the values of λ_α for a particle at radius R_k due to a given t that lays somewhere in between $t_{j-2}...t_{j+1}$. Moreover, an estimated value of s for R_k is easily given by:

$$Ps(k) = s(P\lambda_1(k), P\lambda_2(k)). \tag{A.6}$$

The formulation (A.6) that employs (A.5) can be considered as a function, say h, that produces s for a given, say τ, for t in (A.5) while keeping t_l and $\lambda_\alpha(k,l)$ for $l = j-2..j$ and $\alpha = 1,2$ fixed. The Secant method can be used here to approximate the value of $\tau = \hat{t}$ that gives $Ps(k) = s_a$. Furthermore, once $\hat{t}$ is obtained, it can be supplied to (A.5) to estimate $\lambda_{\alpha a}(k)$, for $\alpha = 1,2$, the stretch ratios λ_α at which the second mechanism begins to participate.

We now discuss the overall node-by-node procedure that must be followed when the second mechanism is introduced. The numerical scheme involving the multi-mechanism is initiated when $t \geq t_a$ *i.e* when the parameter s at the dome and some neighboring nodes become greater than s_a. The number of nodes with $s \geq s_a$ however cannot be known *a priori*. When $t \geq t_a$, and hence $s \geq s_a$, at the dome (R_1), the procedure assumes that s at the next node, say R_2, is also greater than s_a. Employing this assumption, the differential equations involving both mechanisms (see Table 20 for the range of s: $s_a \leq s < s_b$) are used to estimate the variables values at R_2. The resulting λ_1 and λ_2 and the resulting s of R_2, $s(R_2)$, is compared to s_a. If the resulting $s(R_2)$ is greater than s_a, the assumption then is accepted and the procedure moves on to the next node that is also assumed to have $s > s_a$. The process is stopped if either the edge node is reached or the resulting $s(R+\Delta R)$ is less than s_a.

Eventually, for an inflated state t, we would have a situation in which $s(R) > s_a$ but $s(R+\Delta R) < s_a$. Assuming that s monotonically decrease with R, there must exist $\Delta R_{cr} < \Delta R$ such that $s(R+\Delta R_{cr}) \approx s_a$ for fixed t and Q. We turn our attention now in searching for ΔR_{cr}. First, recall that the computation for values of $R+\Delta R$ employs variables values at R and also both t and Q. The resulting $s(R+\Delta R)$ then can be considered as a product of a function, say $g(\Delta R)$ while keeping fixed other variables values *i.e* $\lambda_1, \lambda_2, \eta, Q, t$ and R. It's important to note that the function g involves the multi-mechanism differential equations. A small $\delta < \Delta R$ can be supplied into g so that $g(\delta) = s(R+\delta)$. Having

the function g, an iteration method can be employed, here we use the Bisection method, to obtain ΔR_{cr} such that $g(\Delta R_{cr}) \approx s_a$. Once ΔR_{cr} is obtained, the resulting variables values at $R_c = R + \Delta R_{cr}$ can be calculated based on values at R using differential equations involving the dual mechanism.

Note that $s(R = R_c) \approx s_a$, so values at $R > R_c$ must be calculated using the values at $R = R_c$ and single mechanism differential equations. The stored values at R_c, for example, are used to calculate values at $R_c + \Delta R_{co}$ using single mechanism equations, where ΔR_{co} is the remaining distance to the next node from R_c, so $\Delta R_{co} = \Delta R - \Delta R_{cr}$. The single mechanism equations are used in further node-to-node computation until the edge node is reached.

When the variables values at the edge node are obtained, the boundary condition (3.131) must be satisfied. Otherwise, similar to the case where there is no recruitment, a new estimate Q must be searched using the secant method to be supplied for the next iteration. When a new Q is required, the above iteration must be performed again to produce new ΔR_{cr} that corresponds to the new Q.

A.3 STAGES IN WHICH THE FIRST MECHANISM IS DEACTIVATED

The numerical procedure that must be used when elastin breakage is involved will be discussed here. We suppose that t is increase such that the stretch ratios at the dome and its neighboring points are large enough to cause elastin breakage at the dome, *i.e* $t_b \leq t$. We shall to refer these deformation states as the breakage states. As was discussed in Section 3.5, during these states, a circular region with radius R_b that is occupied by active recruited collagen only is formed and is enlarged. In this region, the first mechanism is deactivated, while the second mechanism remains active in the stress generation.

Generally, the node-to-node computation goes as follows. When t of the dome is such that $t \geq t_b$, it is assumed that the next node, say R_2, is also having its $s > s_b$. As a consequence, the set of dual mechanism differential equations neglecting the first mechanism must be used here to estimate values at R_2. Technically, this is done simply by assigning a zero factor that eliminates the terms derived from the first mechanism. The dual mechanism

differential equations neglecting the first mechanism contribution can be viewed in Table 20 for range of s: $s_b \leq s$. Similar to what we did in the recruiting states, the value s at R_2 then is checked against s_b. The assumption is accepted when $s(R_2) > s_b$ and the computation using the same differential equations moves on to the next node assuming that the s at the next node also greater than s_b. Similar to that in the recruiting case, these computation is ceased if either the edge node is reached or the resulting $s(R + \Delta R)$ is less than s_b.

When the later case is met, a situation in which $s(R) > s_b$ but $s(R + \Delta R) < s_b$ for a fixed $t > t_b$ may occur. Assuming that s smoothly decreases with R for a fixed t, a similar technique employed before in the recruitment case can also be used here to obtain, say Δ_{crE}, so that $s(R + \Delta_{crE}) \approx s_b$. Note however, that the differential equations that are used to obtain Δ_{crE} must use the contribution of the second mechanism only. Once, Δ_{crE} is obtained, the same equations can be used to obtain values at $R_b = R + \Delta_{crE}$. Once values at R_b is obtained, we can calculate values at $R_b + \Delta_{coE}$, where Δ_{coE} is the remaining distance from R_b to the next node, so $\Delta_{coE} = \Delta R - \Delta_{crE}$. Since $s(R_b) = s_b$ and so $s(R > R_b) < s_b$, the computation for $R > R_b$ must use the full dual mechanism differential equations or the first mechanism differential equations. The calculation for $R_b + \Delta_{coE}$ uses both values at R_b and the dual mechanism differential equations. Due to the wide distance between s_a and s_b, most likely, $s(R_b + \Delta_{coE}) > s_a$. The computation using the full second mechanism differential equations can be continued for next nodes until a node with $s < s_a$ is encountered. Here, the procedure to obtain ΔR_{cr} as described above must be performed.

Similar to previous cases, when the edge is encountered, the RK computation is stopped and the edge boundary condition 3.131 is checked. When the condition is not satisfied for a certain degree, a new Q must be obtained. The new Q then is used in the next iteration and the above procedure is repeated until the edge condition is met.

A.4 UNLOADING STAGES

The following section explains the numerical procedure during unloading. As was discussed, generally three unloading cases will be encountered; $t^* < t_a, t_a \leq t^* < t_b$, and $t_b \leq t^*$, where t^* denotes the maximum dome stretch ratio during loading.

- Case 1: $t^* < t_a$

  The first case implies that the loading is maximized before the collagen recruitment begins. Clearly, this case resembles the unloading of classical single mechanism elastic materials. The procedure during unloading follows exactly those during loading with an obvious exception that t is applied in a decreasing manner from t^* to $t = 0.00$. If similar loading steps for t are used as before (Δt) is used in the unloading, the nondimensional pressure Q for each corresponding decreasing t can be restored. In doing so, no additional searching effort for the appropriate value of Q is needed for each given value of t.

- Case 2: $t_a \leq t^* < t_b$

  This case is encountered when the loading is maximized after the collagen recruitment occurs but before the dome experiences elastin breakage. As was described before here both the deformed collagen fibers and the deformed elastin will return to their own undeformed configuration. Intuitively, we should expect that the procedure that is used in unloading follows exactly that of the loading. This is true in general but the unloading process, benefiting by useful information stored during loading, requiring fewer iteration and less complex if-then-else logic step.

  As an example, we may consider the stretch ratios $\lambda_{\alpha a}$ ($\alpha = 1, 2$), which corresponds to the configuration in which the collagen fibers load bearing is initiated. The values of $\lambda_{\alpha a}$ are properties of the node. These values theoretically must never change since they reflect the information regarding the reference configuration of the recruited collagen fibers. The values of $\lambda_{\alpha\, a}$ for each node that were obtained and stored during loading can be restored and be used in the unloading process. The iteration process to obtain such values then can be avoided.

  For technical convenience, we use the same Δt that was used during loading in the unloading scheme. It follows immediately that the corresponding values of Q and the stretch ratios of each node due to each t can be restored from the results of loading. This leads to another technical convenience.

  Moreover, recall that after the collagen is recruited at the dome, a circular region filled with both active elastin and collagen with radius R_c is developed. It should be clear that the radius R_c is unique for each inflated state. The stored values of R_cs for each

corresponding inflated state (with $t > t_a$) can be restored and be used during unloading. The Bisection iteration for obtaining Δ_{cr} therefore can be avoided.

So generally, provided that the unloading step is the same Δt that was employed during loading, the node-to-node computation will follow that of loading but with decreasing t, instead of increasing t, to mimic the unloading process. Assumptions stating that $s > s_a$ at a node next to a node having $s > s_a$ are also imposed during unloading. Also, as was performed during loading, once the next node no longer has $s > s_a$ the scheme moves on to the next node using the single mechanism differential equations.

- Case 3: $t_b \leq t^*$

  This case is encountered when the maximum loading occurs after the elastin fragments at the dome. In this configuration, as was discussed, a circular region of radius R_b^*, filled with deactivated elastin, leaving only active collagen, is developed. During unloading, this circular region will not regain active elastin regardless of the decreasing values of s of the particles inside it. This implies that the computation of the nodes inside the breakage region must use only differential equations for the second mechanism at all the inflated states during unloading. To impose this restriction on every inflated state, a checking step is added to the scheme. When the radius of a computed node is less than R_b^*, a factor of 0.00 is assigned to eliminate the terms in the dual mechanism differential equations that are derived from the first mechanism. Due to the presence of this region, the corresponding Q and the stretch ratios of each node, which have been obtained during loading, must be recomputed for each inflated state t. In addition, the radius of the recruitment region R_c of an inflated state t during unloading is not expected to be the same as that of the same value of t in the loading process. This radius must also be recalculated for every inflated state t. The iteration technique that is used here follows the one that is used in the loading process. The 'memory' of stretch ratios that are employed to construct a Lagrange interpolation scheme similar to (A.5), however are obtained from 'higher' deformation levels (larger values of t). Note however that during the decrement of t, the radius R_c is decreasing and is approximating R_b^*. As was discussed, when both regions coincide and $R_b^* = R_c$ an 'empty region' is created in which none of the mechanisms is active.

APPENDIX B

REGRESSION ANALYSIS RESULTS FOR OTHER CHOICES OF STRAIN ENERGY FUNCTIONS

In principal, the first and second mechanism do not have to be represented by the same type of strain energy functions. The equation (2.18) implies that W_1 and W_2 can be of two different strain energy functions. This flexibility allows the incorporation of two material components possessing dissimilar behavior.

The choice of exponential type for both W_1 and W_2 given in (2.21) therefore is only one combination among many other possibilities. In this chapter, however, it will be shown that this choice is better than some other choices of strain energy functions for W_1 and W_2. Here, experimental data by Scott *et al.* [79] are again employed in a nonlinear regression analysis using the resulting equations (3.64),(3.67) and (3.68) from inflation of cylindrical membrane and W_1 and W_2 that are different from (2.21). The choices of W_1 and W_2 include the commonly used Neo Hookean and Mooney Rivlin hyperelastic models. The formulation for Neo Hookean and Mooney Rivlin can be seen in Table 3. The results are summarized in Table 23. The behavior of Mooney Rivlin materials and combinations with other functions are expected to be similar to the behavior of Neo Hookean materials and combinations with other functions. This is explained by the same resulting expression of response functions w_1 and w_2 of the two materials. The response functions w_1 and w_2 are defined by (3.70) and (3.71), respectively, and their values are proportional to tension as is described in equations (3.64),(3.67), and (3.68). The response functions for Neo Hookean and Mooney Rivlin materials are simply constants. Therefore, only Neo Hookean and its combinations are presented.

Table 23: Resulting material parameters and R^2 for Neo Hookean (NH), Mooney Rivlin (MR), Exponential (Exp) and their combinations for undeformed thickness H= 125 μ and fixed λ_a=1.761029.

Combination	A	B	C	D	E
W_1	NH	MR	NH	Exp	Exp
W_2	NH	MR	Exp	NH	Exp
$\alpha_1(10^3 dynes/cm^2)$	293.0811	78.2121	346.6768	52.1691	71.2198
$\alpha_2(10^3 dynes/cm^2)$	960.9422	462.8301	442.7509	922.0090	312.6121
γ_1	-	-	-	0.6605	0.6224
γ_2	-	-	1.3660	-	1.8676
$\beta_1(10^3 dynes/cm^2)$	-	214.9100	-	-	-
$\beta_2(10^3 dynes/cm^2)$	-	498.0802	-	-	-
R^2	0.6565	0.6565	0.77032	0.8144	0.9903

The resulting material parameters for all of the combinations of hyperelastic models and the corresponding R^2 values are tabulated in Table 23. The R^2 values clearly indicate that the choice given in (2.21) is the best at least among these particular group of combinations. Figure 38 depicts the resulting tension vs. strain curves compare to the experimental data by Scott *et al.* [79]. The poor fitting by either Neo Hookean or Mooney Rivlin model can be attributed to their natural characteristic, in particular, for inflation of cylindrical membrane case. It can be seen from the figure that parts of the tension vs. curves produced by employing Neo Hookean (or Mooney Rivlin) are always concave down instead of concave up as the experimental data tend to be. This should be expected since the second derivative of tension with respect to λ ($i.e$ ϵ) for $\lambda > 0$ for Neo Hookean or Mooney Rivlin are always negative.

Recalling the definition of tension given by (3.64) and (3.68), the tension contributed only by the first mechanism represented by Neo Hookean, say T_{1NH}, and tension contributed

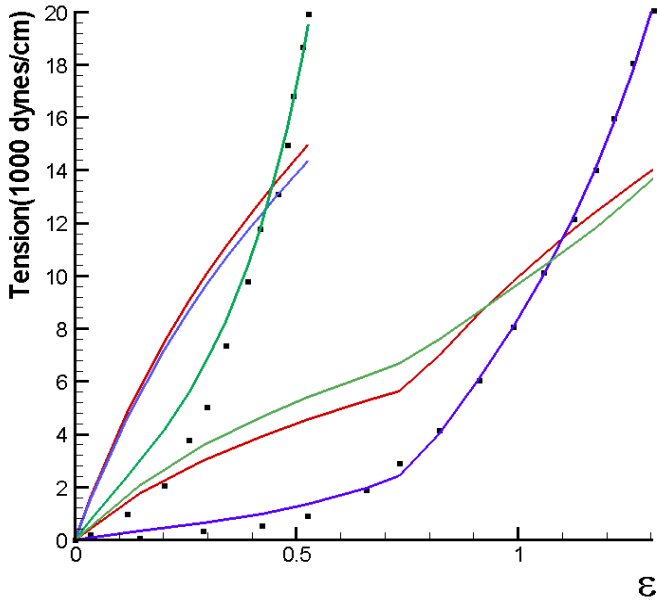

Figure 38: Resulting tension vs ϵ for inflation of cylindrical membrane for combinations of strain energy functions A (coincide with B, red line), C (green line), and D (blue line) shown in Table 23.

only by the second mechanism represented by Neo Hookean, say T_{2NH}, are given by:

$$T_{1NH} = 2\frac{H}{\lambda}(\lambda^2 - \frac{1}{\lambda^2})\alpha_1 \tag{B.1}$$

$$T_{2NH} = 2\frac{H}{\lambda}(\frac{\lambda^2}{\lambda_a^2} - \frac{\lambda_a^2}{\lambda^2})\alpha_2, \tag{B.2}$$

respectively, where λ_a is the activation stretch. The second derivatives of T_{1NH} and T_{2NH} with respect to λ are simply given by:

$$d^2T_{1NH}/d\lambda^2 = -24H/\lambda^5\alpha_1 \tag{B.3}$$

$$d^2T_{2NH}/d\lambda^2 = -24H\lambda_a^2/\lambda^5\alpha_2, \tag{B.4}$$

where H is the undeformed thickness. The values of (B.3) and (B.4) are always negative since $\lambda_a > 0$ and the range of λ are $0 < \lambda$.

APPENDIX C

REGRESSION ANALYSIS RESULTS FOR EXPERIMENTAL DATA ON THE NONLINEAR ELASTIC BEHAVIOR OF INTRACRANIAL ARTERIES

It is well known that cerebral arterial walls exhibit nonlinearity. The nonlinearity has been hypothesized to be due to the recruitment of collagen fibers at some deformed configuration [49]. It can be seen in Section 3.3.6 that the equation (3.64) alone can be used to describe this nonlinear characteristic. This approach disregards the individual contribution made by the response of elastin and collagen fibers. In this chapter it will be shown that an improvement can be obtained when we take into account the individual contribution made by the response of the cerebral arterial components, namely the elastin and collagen responses. We consider the strain energy functions (2.21) that employs two mechanisms to represent the two passive mechanical components.

We use here the experimental data by Scott *et al.* [79] on the inflation of PCA and ACA that were used in Section 3.3.6. The experimental data are presented in Table 27. We assume that the nonlinearity of PCA and ACA is due to both elastin and collagen fibers and is not due to collagen fibers only as a result of elastin damage. We employ the resulting equations of inflation of cylindrical membrane (3.64) and (3.67) to obtain the material parameters shown in (2.21). Since there is no information that can be used to obtain the recruitment stretch λ_a (used in equation (3.67)), the parameter λ_a is considered as part of the material parameters that must be obtained via nonlinear regression analysis.

The results of the nonlinear regression analysis using dual mechanism equations are tabulated in Table 24. The results are compared to the resulting material parameters and

Table 24: Resulting material parameters and corresponding R^2 for inflation of cylindrical membrane obtained from both single mechanism and dual mechanism approaches for the experimental data points of ACA and PCA by Scott *et al.* [79].

	Dual mechanism		Single mechanism	
Material Parameters	ACA	PCA	ACA	PCA
λ_a	1.8619	1.5566	-	-
$\alpha_1(10^3 dynes/cm^2)$	24.9874	50.0958	38.7630	95.5911
γ_1	0.4124	0.3225	0.4174	0.3676
$\alpha_2(10^3 dynes/cm^2)$	363.4576	447.3069	-	-
γ_2	0.6895	0.9967	-	-
R^2	0.9972	0.9967	0.9922	0.9789

R^2 obtained by the single mechanism approach. The R^2 values of the current results shows an improvement on the results produced by equation (3.64) alone. Figure 39 depicts the resulting curves for the single mechanism approach (dashed lines) and the dual mechanism approach (solid lines) along with the experimental data (reproduced from Figure 3 in Scott *et al.* [79]). It can be seen from the R^2 values in Table 24 that the dual mechanism equations produce better fitting compare to the single mechanism equation.

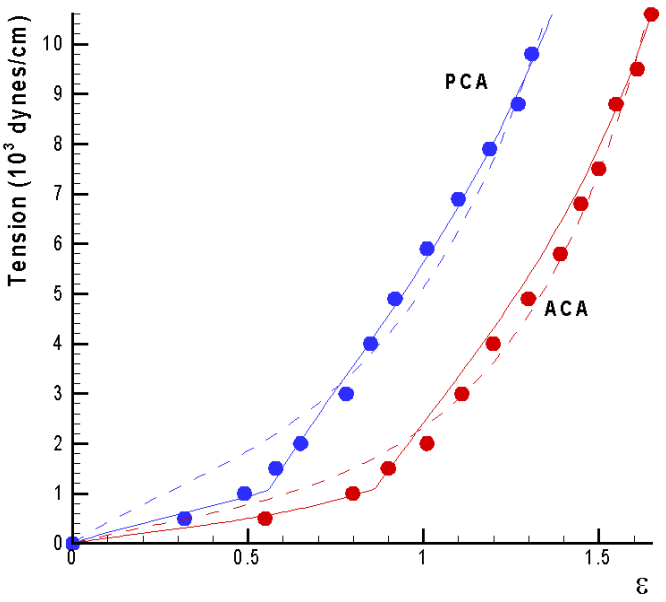

Figure 39: Resulting tension vs ϵ curves for inflation of cylindrical membrane obtained from single mechanism equation (dashed lines) and from dual mechanism equations (solid lines) along with the corresponding experimental data points of ACA (red color) and PCA (blue color) by Scott *et al.* [79].

APPENDIX D

EXPERIMENTAL DATA USED IN THE NONLINEAR REGRESSION ANALYSIS

In this Appendix the experimental data used in the nonlinear regression analysis are presented.

Table 25: Experimental data on a human ACA. The data are extracted from Figure 5B in Scott *et al.* [79].Strain and Tension are in the circumferential direction.

Before shifting (Run13)		After Shifting (Run34)	
Strain	Tension	Strain	Tension
	$(10^3 dynes/cm)$		$(10^3 dynes/cm)$
0	0.0	0	0.0
10	0.1	8	0.6
20	0.3	11	1.0
30	0.5	17	1.6
40	0.7	20	2.0
50	0.95	22	3.0
51	1.0	26	4.0
60	1.5	30	5.0
66	2.0	31	6.0
72	3.0	37	8.0
80	4.0	40	10.0
90	6.0	45	13.0
100	8.0	48	15.0
105	10.0	50	17.9
110	12.0	52	20.0
118	13.9		
121	15.9		
125	18.0		
130	20.0		

Table 26: Experimental data on ACA of aneurysm patients and normal subjects. The data are extracted from Figure 1B in Töth *et al.* [83].

Intraluminal	External Radius (mm)	
Pressure (mmHg)	Controls	Patients
0	0.63	0.70
10	0.90	0.96
20	1.03	1.06
30	1.09	1.13
40	1.13	1.15
50	1.15	1.19
60	1.20	1.20
70	1.22	1.22
80	1.22	1.24
100	1.25	1.25
120	1.28	1.28
140	1.30	1.30
160	1.305	1.305
180	1.31	1.31
200	1.33	1.33

Table 27: Experimental data of MCA, PCA, and ACA of a 34 year old woman. The data are extracted from Figure 3 in Scott *et al.* [79]. Strain and Tension are in the circumferential direction.

MCA		PCA		ACA	
Strain	Tension	Strain	Tension	Strain	Tension
	$(10^3 dynes/cm)$		$(10^3 dynes/cm)$		$(10^3 dynes/cm)$
0.00	0.0	0.00	0.0	0.00	0.0
0.13	1.0	0.32	0.5	0.55	0.5
0.20	1.5	0.49	1.0	0.80	1.0
0.22	2.0	0.58	1.5	0.90	1.5
0.28	3.0	0.65	2.0	1.01	2.0
0.30	4.0	0.78	3.0	1.11	3.0
0.32	5.0	0.85	4.0	1.20	4.0
0.36	6.0	0.92	4.9	1.30	4.9
0.39	7.0	1.01	5.9	1.39	5.8
0.40	8.0	1.10	6.9	1.45	6.8
0.42	9.0	1.19	7.9	1.50	7.5
0.45	10.0	1.27	8.8	1.55	8.8
0.49	11.0	1.31	9.8	1.61	9.5
0.495	12.0	1.39	11.0	1.65	10.6
0.505	13.0				
0.51	14.0				

Table 28: Experimental data on basilar arteris of treated mongrel dogs. The data are extracted from Figure 4 in Nagasawa *et al.* [147]. The number of days are the period of treatment. Stress and strain are in the circumferential direction.

2 Days		4 Days		7 Days	
Strain	Stress	Strain	Stress	Strain	Stress
	$(10^6 dynes/cm^2)$		$(10^6 dynes/cm^2)$		$(10^6 dynes/cm^2)$
0.00	0.00	0.00	0.00	0.00	0.00
0.20	0.14	0.10	0.20	0.06	0.18
0.31	0.36	0.18	0.43	0.12	0.45
0.39	0.64	0.25	0.73	0.18	0.72
0.44	0.94	0.29	1.07	0.22	1.05
0.48	1.30	0.31	1.43	0.24	1.35
0.51	1.59	0.34	1.77	0.25	1.70
0.54	1.88	0.35	2.13	0.27	2.05
0.55	2.38	0.37	2.49	0.3	2.40
0.56	2.52	0.38	2.84	0.32	2.77
0.58	2.90	0.39	3.22	0.325	3.11
0.61	3.23	0.40	3.59	0.33	3.50
0.62	3.59	0.41	3.66	0.335	3.89

Table 29: Experimental data on basilar arteris of treated mongrel dogs. The data are extracted from Figure 3 in Nagasawa *et al.* [147].The number of days are the period of treatment. Stress and strain are in the circumferential direction.

14 Days		28 Days		Control	
Strain	Stress	Strain	Stress	Strain	Stress
	$(10^6 dynes/cm^2)$		$(10^6 dynes/cm^2)$		$(10^6 dynes/cm^2)$
0.00	0.00	0.00	0.00	0.00	0.00
0.09	0.13	0.12	0.16	0.08	0.18
0.18	0.38	0.21	0.39	0.15	0.43
0.22	0.63	0.27	0.66	0.19	0.70
0.31	0.93	0.32	0.96	0.22	1.05
0.35	1.27	0.34	1.25	0.24	1.30
0.37	1.51	0.36	1.55	0.26	1.60
0.39	1.88	0.38	1.88	0.27	1.90
0.41	2.20	0.39	2.19	0.28	2.20
0.42	2.50	0.41	2.49	0.29	2.50
0.43	2.84	0.42	2.79	0.295	2.85
0.44	3.36	0.43	3.09	0.305	3.20
0.45	3.50	0.43	3.40	0.31	3.50

APPENDIX E

ALGORITHM FOR THE COMPUTATION OF THE INFLATION OF CIRCULAR CLAMPED MEMBRANE

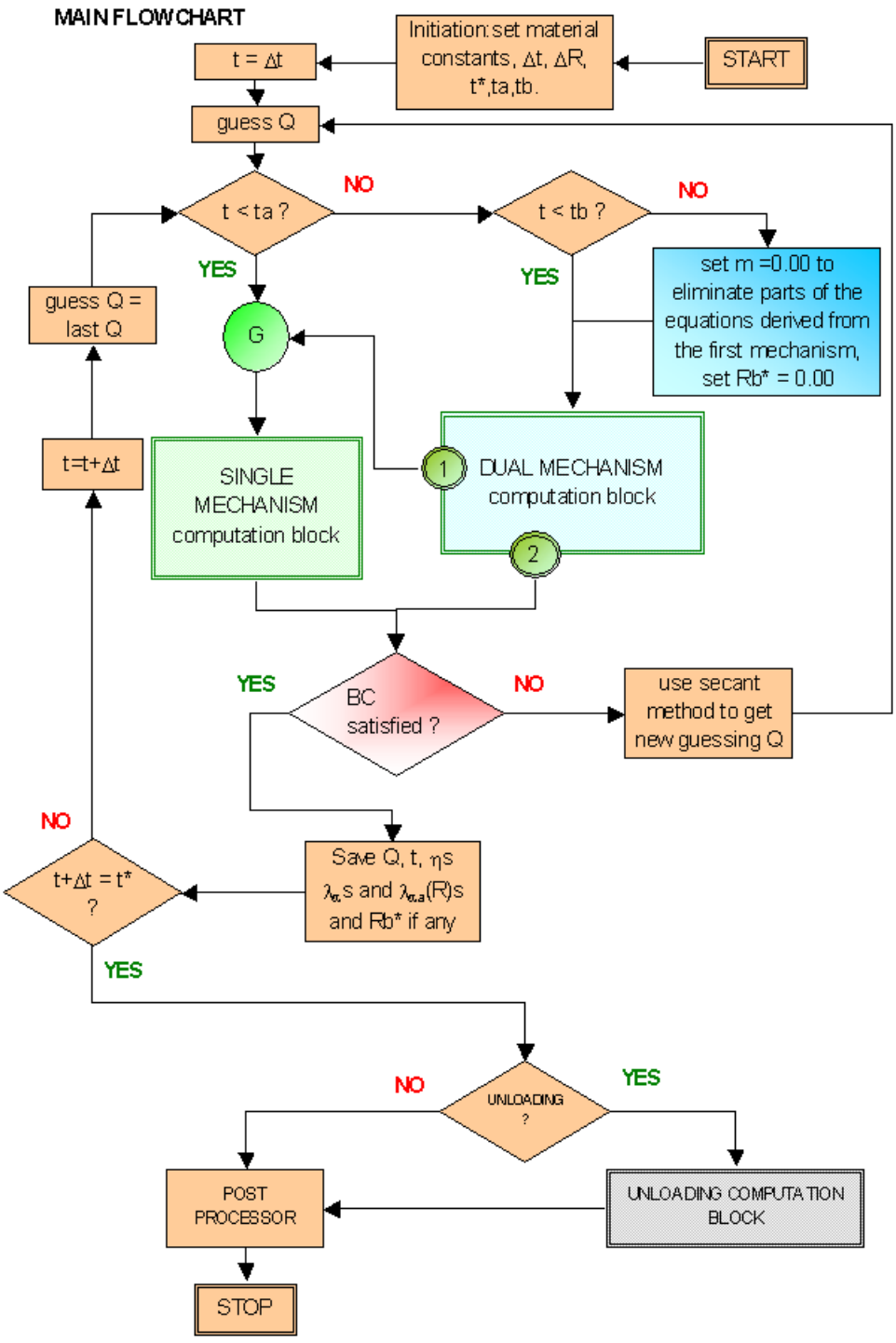

Figure 40: Flowchart of the main program.

Figure 41: Flowchart of the dual mechanism computation block used in the main program.

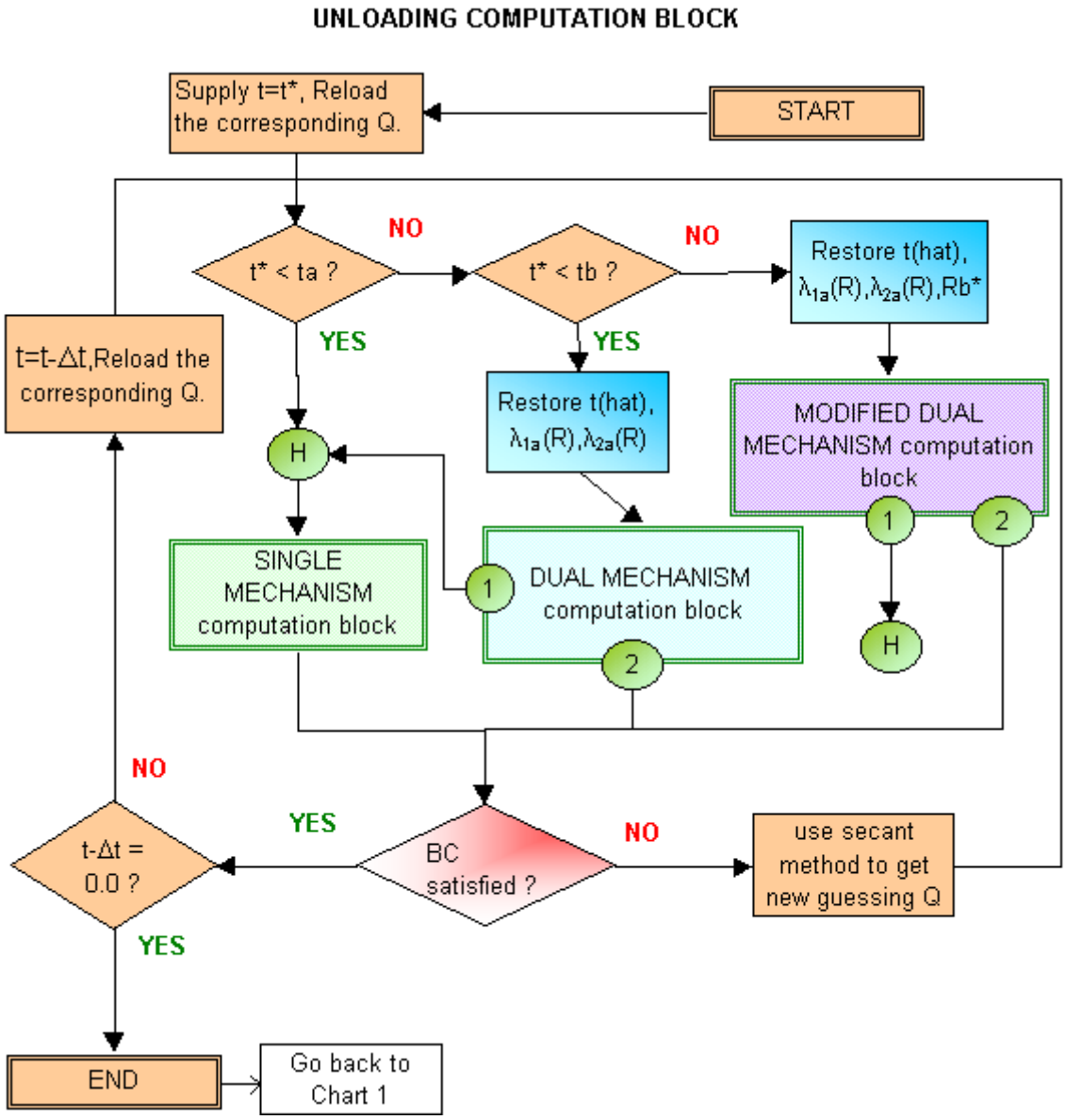

Figure 42: Flowchart of the unloading computational block used in the main program.

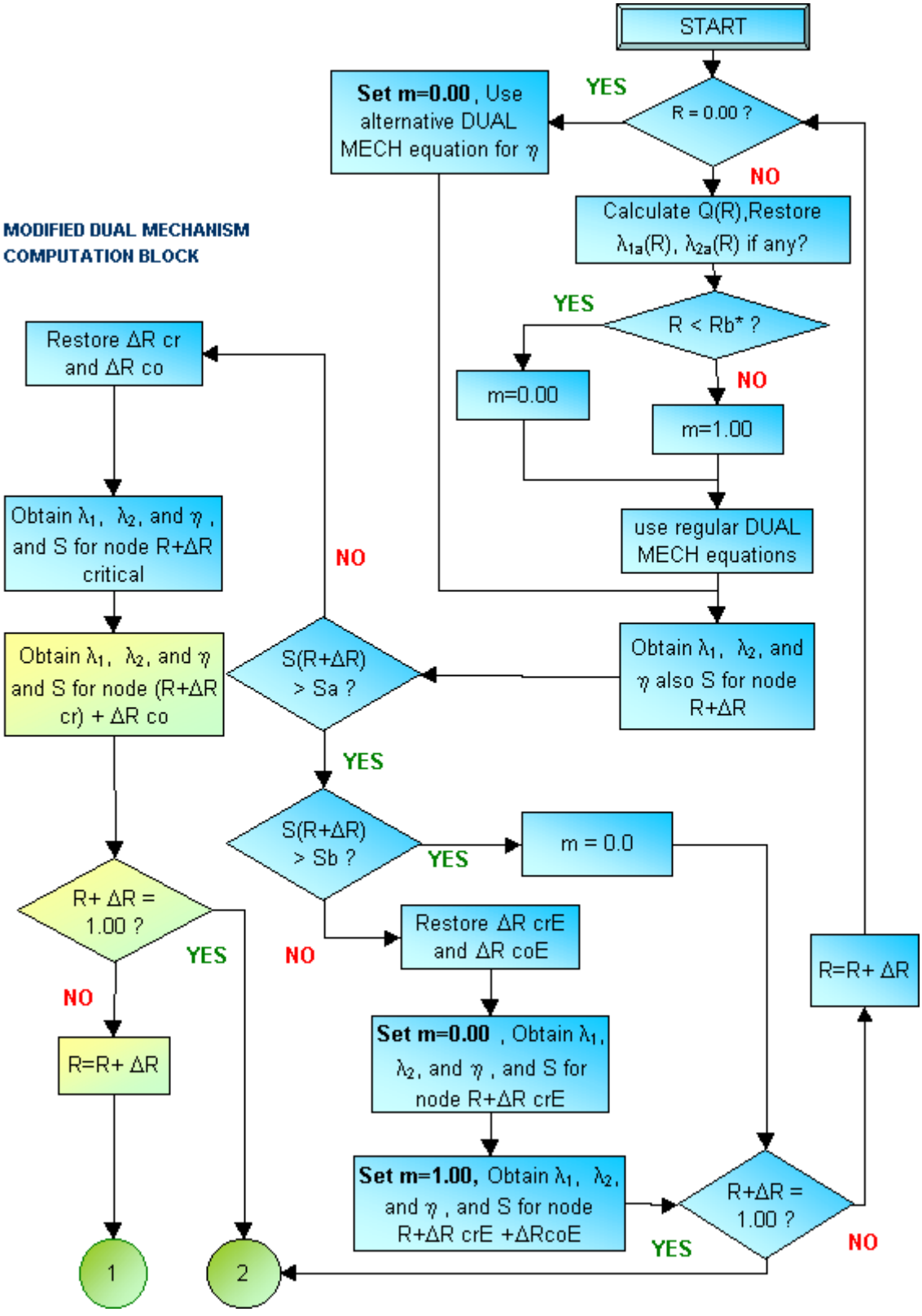

Figure 43: Flowchart of modified dual mechanism computational block used in the unloading computational block.

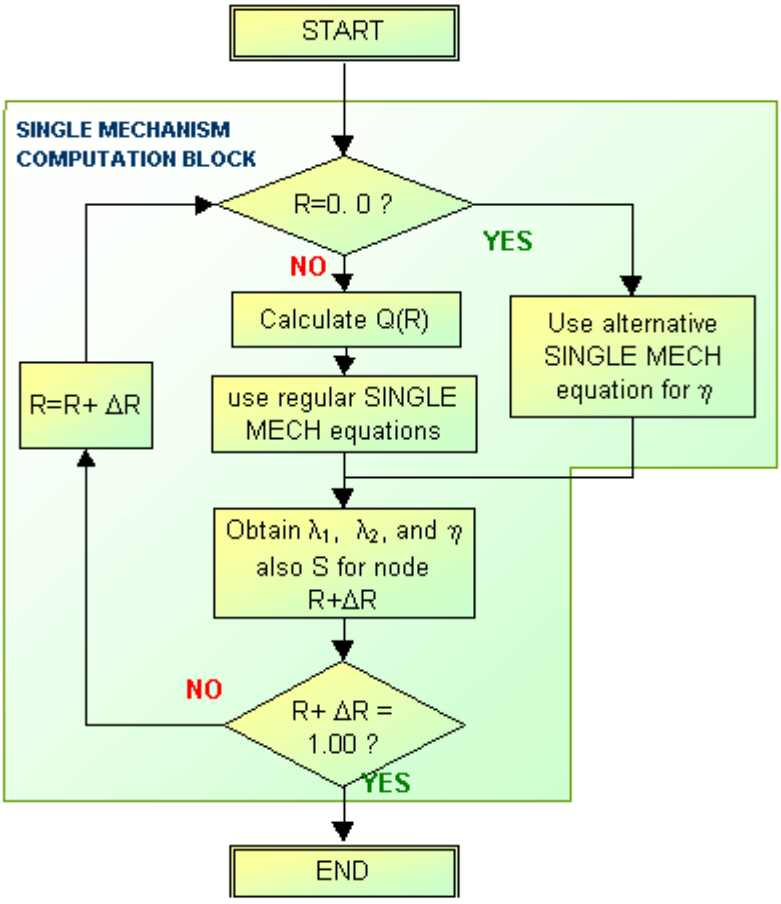

Figure 44: Flowchart of the single mechanism computational block used in the main program.

BIBLIOGRAPHY

[1] 'Abdullah Yusuf 'Ali. *The Meaning of the Holy Quran.* amana publications, Beltsville, Maryland, U.S.A, 1999.

[2] W. E. Stehbens. Aneurysms and anatomical variation of cerebral aneurysms. *Archs. Path.*, 75:45–64, 1963.

[3] Jr. A.L. Rhoton, K. Fujii, N. Saeki, D. Perlmutter, and A. Zeal. *Clinical Management of Intracranial Aneurysms*, chapter Microsurgical Anatomy of Intracranial Aneurysms, Part I, pages 201–213. Raven Press, 1982.

[4] P. J. Camarata, R. E. Latchaw, D. A. Rüfenacht, and R. C. Heros. Intracranial aneurysms. *Investigative Radiology*, 28:373 –382, 1992.

[5] H. Ujiie, K. Sato, H. Onda, A. Oikawa, M. Kagawa, K. Takakura, and N. Kobayashi. Clinical analysis of incidentally discovered unruptured aneurysms. *Stroke*, 24:1850–1856, 1993.

[6] H. B. Locksley. Report on the cooperative study of intracranial aneurysms and subarachnoid hemorrhage. sect v, part II. *J. Neurosurg.*, 25:321 –368, 1966.

[7] W. F. McCormick and Gaston J. Acosta-Rua. The size of intracranial saccular aneurysms: An autopsy study. *J. Neurosurg.*, 33:422 –427, 1970.

[8] N. F. Kassell and J. C. Torner. Size of intracranial aneurysms. *Neurosurgery*, 12(3):291–297, 1983.

[9] D. O. Wiebers, J. P. Whitsnant, T. M. Sundt, and W. N. O'Fallon. The significance of unruptured intracranial saccular aneurysms. *J. Neurosurger.*, 66:23 –29, 1987.

[10] T. Inagawa and A. Hirano. Autopsy study of unruptured incidental intracranial aneurysms. *Surg Neurol*, 34:361–365, 1990.

[11] R. M. Crowell. Aneurysms and arteriovenous malformations. *Neurologic Clinics*, 3:291 –312, 1985.

[12] R. A. Solomon, M. E. Fink, and J. Pile-Spellman. Surgical management of unruptured intracranial aneurysms. *J. Neurosurgery*, 80:440–446, 1994.

[13] E. S. Connolly Jr and R. A. Solomon. Management of symptomatic and asymptomatic unruptured aneurysms. *Neurosurgery Clinics of North America*, 9(3):509–524, July 1998.

[14] S. Juvela, K. Poussa, and M. Porras. Factors affecting formation and growth of intracranial aneurysms - a long-term follow-up study. *Stroke*, 32:485–491, 2001.

[15] G. Neil-Dwyer, J. R. Bartlett, A. C. Nicholls, P. Narcisi, and F. M. Pope. Collagen deficiency and ruptured cerebral aneurysms. *J. Neurosurgery*, 59:16–20, 1983.

[16] A. B. Chapman, D. Rubinstein, R. Hughes, J. C. Stears, M. P. Earnest, A.M. Johnson, P.A. Gabow, and W.D. Kaehny. Intracranial aneurysms in automosal dominant polycystic kidney disease. *The New England Journal of Medicine*, 327:916–920, 1992.

[17] P. M. Ruggieri, N. Poulos, T. M. Masaryk, J. S. Ross, N. A. Obuchowski, I. A. Awad, W. E. Braun, J. Nally, J. S. Lewin, and M. T. Modic. Occult intracranial aneurysms in polycystic kidney disease: Screening with MR angiography. *Neuroradiology*, 191:33–39, 1994.

[18] T. Wakabayashi, S. Fujita, Y. Ohbora, T. Suyama, N. Tamaki, and S. Matsumoto. Polycystic kidney disease and intracranial aneurysms. *J Neurosurg*, 58:488–491, 1983.

[19] W. I. Schievink, B. Mokri, and D. G. Piepgras. Angiographic frequency of saccular intracranial aneurysms in patients with spontaneous cervical artery dissection. *J. Neurosurg.*, 76:62 –6, 1992.

[20] J. Jakubowski and B. Kendall. Coincidental aneurysms with tumours of pituitary origin. *J Neurol. Neurosurg Psychiatry*, 41:972–979, 1978.

[21] S. Wakai, T. Fukushima, T. Furihata, and K. Sano. Association of cerebral aneuryms with pituitary adenoma. *Surg. Neurol.*, 12:503–507, 1979.

[22] K. Iwata, N. Misu, K. Terada, S. Kawai, M. Momose, and H. Nakagawa. Screening for unruptured asymptomatic intracranial aneurysms in patients undergoing coronary angiography. *J Neurosurg*, 75:52–55, 1991.

[23] P. D. Griffiths, S. Worthy, and A. Gholkar. Incidental intracranial vascular pathology in patients investigated for carotid stenosis. *Neuroradiology*, 38:25–30, 1996.

[24] M. Nagashima, M. Nemoto, H. Hadeishi, A. Suzuki, and N. Yasui. Unruptured aneurysms associated with ischaemic cerebrovascular diseases. Surgical Indication. *Acta Neurochir (Wien)*, 124:71–78, 1993.

[25] A. Ronkainen, M.I. Puranen, J.A. Hernesniemi, R.L. Vanninen, P.L. K. Partanen, J.T. Saari, P.A. Vainio, and M. Ryynanen. Intracranial aneurysms: MR angiographic screening in 400 asymptomatic individuals with increased familial risk. *Radiology*, 195:35–40, 1995.

[26] R. Leblanc, D. Melanson, D. Tampieri, and R.D. Guttman. Familial cerebral aneurysms: A study of 13 families. *Neurosurgery*, 37:633–639, 1995.

[27] V.V. Menghini, R.D. Brown, J.D. Sicks, W.M. O'Fallon, and D.O. Wiebers. Incidence and prevalence of intracranial aneurysms and hemorrhage in Olmsted County, Minnesota, 1965 to 1995. *Neurology*, 51:405–411, 1998.

[28] J. L. D. Atkinson, T. M. Sundt, O. W. Houser, and J.P. Whisnant. Angiography frequency of anterior circulation intracranial aneurysms. *J Neurosurg*, 70:551–555, 1989.

[29] E. M. Housepian and J. L. Pool. A systematic analysis of intracranial aneurysms from the autopsy file of the presbyterian hospital. *J. Neuropathol Exp Neurol*, 17(3):409–423, 1958.

[30] J. L. Chason and W. M. Hindman. Berry aneurysms of the Circle of Willis. *Neurology*, 8:41–44, 1958.

[31] W. F McCormick and J. D. Nofzinger. Saccular intracranial aneurysms: An autopsy study. *J. Neurosurgery*, 22:155–159, 1965.

[32] S. M. de la Monte, G. W. Moore, M. A. Monk, and G. M. Hutchins. Risk factors for development and rupture of intracranial berry aneurysms. *Am. J. Med.*, 78:957 –964, 1985.

[33] The International Study of Unruptured Intracranial Aneurysms Investigators. Unruptured intracranial aneurysms - risk of rupture and risks of surgical intervention. *The New England Journal of Medicine*, 339(24):1725–1733, December 1998.

[34] L.H. Phillips, J.P. Whisnant, W. M. O'Fallon, and T. M. Sundt. The unchanging pattern of subarachnoid hemorrhage in a community. *Neurology*, 30:1034 –1040, 1980.

[35] W. M. Garraway, J. P. Whisnant, and I. Drury. The continuing decline in the incidence of stroke. *Mayo Clin Proc*, 58:520–523, 1983.

[36] T. J. Ingall, J. P. Whisnant, D. O. Wiebers, and W. M. O'Fallon. Has there been a decline in subaracnoid hemorrhage mortality. *Stroke*, 20:718–724, 1989.

[37] J. P. Broderick, T. G. Brott, J. E. Duldner, T. Tomsick, and A. Leach. Initial and reccurent bleeding are the major causes of death following subarachnoid hemorrhage. *Stroke*, 25:1342–1347, 1994.

[38] R. L. Sacco, P. A. Wolf, N. E. Bharucha, S. L. Meeks, W. B. Kannel, L.J. Charette, P.M. McNamara, E. P. Palmer, and R. D'Agostino. Subarachnoid and intracerebral hemorrhage: Natural history, prognosis and percursive factors in the Framingham study. *Neurology*, 34:847–854, 1984.

[39] W. T. Longstreth, L. M. Nelson, T. D. Koepsell, and G. V. Belle. Clinical course of spontaneous subarachnoid hemorrhage: A population-based study in King County, Washington. *Neurology*, 43:712–718, April 1993.

[40] N.F. Kassell and C.G. Drake. Timing of aneurysm surgery. *Neurosurgery*, 10(4):514–519, 1982.

[41] D. O. Wiebers, J. C. Torner, and I. Meissner. Impact of unruptured intracranial aneurysms on public health in the United States. *Stroke*, 23:1416 –1419, 1992.

[42] D. Krex, H.K. Schackert, and G. Schackert. Genesis of cerebral aneurysms - an update. *Acta Neurochir (Wien)*, 143:429–449, 2001.

[43] W. E. Stehbens. *Structure and Function of the Circulation*, chapter Arterial structure at branches and bifurcations with reference to physiological and pathological processes, including aneurysm formation, pages 667–693. Plenum Press, 1981.

[44] A. L. Sahs. Observations on the pathology of saccular aneurysms. *J. Neurosurg.*, 24:792 –806, 1966.

[45] T. Crawford. Some observations on the pathogenesis and natural history of intracranial aneurysms. *J. Neurol. Neurosurg. Psychiat.*, 22:259 –266, 1959.

[46] W. E. Stehbens. Pathology and pathogenesis of intracranial berry aneurysms. *Neurol. Res.*, 12:29 –34, 1990.

[47] L. N. Sekhar and R. C. Heros. Origin, growth, and rupture of saccular aneurysms: A review. *Neurosurger.*, 8:248 –260, 1981.

[48] W. E. Stehbens. *Pathology of the Cerebral Blood Vessels*, chapter Structure and pathophysiology. C.V. Mosby Co., 1972.

[49] D. E. Busby and A. C. Burton. The effect of age on the elasticity of the major brain arteries. *Can. J. Physiol. Pharmacol.*, 43:185 –202, 1965.

[50] E. R. Lang and M. Kidd. Electron microscopy of human cerebral aneurysms. *J. Neurosurgery*, 20:554–562, 1963.

[51] D. Chyatte, J. Reilly, and M. D. Tilson. Morphometric analysis of reticular and elastin fibers in the cerebral arteries of patients with intracranial aneurysms. *Neurosurgery*, 26:939 –943, 1990.

[52] W. E. Stehbens. Focal intimal proliferation in the cerebral arteries. *Arch Path*, 36(3):289–301, 1960.

[53] W. E. Stehbens. Histopathology of cerebral aneurysms. *Arch. Neurol.*, 8:272–285, 1963.

[54] H. M. Finlay, P. Whittaker, and Peter B. Canham. Collagen organization in the branching region of human brain arteries. *Stroke*, 29:1595–1601, 1998.

[55] W. D. Forbus. On the origin of miliary aneurysms of the superficial cerebral arteries. *Bulletin of the Johns Hopkins Hospital*, 47:239 –284, 1930?

[56] W. E. Stehbens. *Pathology of the Cerebral Blood Vessels*, chapter Intracranial Arterial Aneurysms. C.V. Mosby Co., 1972.

[57] T. W. R. Macfarlane, P.B. Canham, and M. R. Roach. Shape changes at the apex of isolated human cerebral bifurcations with changes in transmural pressure. *Stroke*, 14:70–76, 1982.

[58] W. E. Stehbens. *Structure and Function of the Circulation*, chapter Intimal cushions (pads): Structure, location and functional significance, pages 603–635. Plenum Press, 1981.

[59] G. N. Foutrakis, H. Yonas, and R. J. Sclabassi. Saccular aneurysm formation in curved and bifurcating arteries. *American Journal of Neuroradiology*, 20:1309–1317, 1999.

[60] M. Sugai and M. Shoji. Pathogenesis of so-called congenital aneurysms of the brain. *Acta Path. Japan*, 18(2):139–160, 1968.

[61] R. Wulandana and A. M. Robertson. Use of a multi-mechanism constitutive model for inflation of cerebral arteries. In *Proceedings of the First Joint BMES/EMBS Conference, Atlanta, GA*, page 235, 1999.

[62] R. Wulandana and A. M. Robertson. A model of early stage aneurysm development. In *BED-Vol. 50, ASME 2001 Bioengineering Conference*, pages 419–420.

[63] M. Scanarini, S. Mingrino, M. Zuccarello, and G. Trincia. Scanning electron miscroscopy of biopsy specimens of ruptured intracranial saccular aneurysms. *Acta Neuropathol.*, 44:131 –134, 1978.

[64] S. Cajander and O. Hassler. Enzymatic destruction of the elastic lamella at the mouth of the cerebral berry aneurysm? *Acta Neruol. Scand.*, 53:171 –181, 1976.

[65] G. Ebhardt, R. Wüllenweber, and J. Cervós-Navarro. *The Cerebral Vessel Wall*, chapter The Ultrastructure of the Aneurysmatic Vessel Wall, pages 67–74. Raven Press, 1976.

[66] O. Hassler. Morphological studies on the large cerebral arteries with reference to the aetiology of subarachnoid haemorrhage. *Acta Neurol Scan. Suppl.*, 154, 1962.

[67] S. H. M. Nyström. Development of intracranial aneurysms as revealed by electron microscopy. *J. Neurosurg.*, 20:329 –337, 1963.

[68] R. R. Smith, Y. N. Subkov, and Y. Tarassoli. *Cerebral Aneurysms: Microvascular and Endovascular Management*. Springer-Verlag, 1994.

[69] J. Suzuki and H. Ohara. Clinicopathological study of cerebral aneurysms. *J Neurosurgery*, 48:505–514, 1978.

[70] Y. C. Fung. *Biomechanics: Mechanical Properties of Living Tissue*, chapter Mechanical Properties and Active Remodeling of Blood Vessels, pages 321–391. Springer-Verlag, 1993.

[71] K. Kataoka, M. Taneda, T. Asai, A. Kinoshita, M. Ito, and R. Kuroda. Structural fragility and inflammatory response of ruptured cerebral aneurysms : a comparative study between ruptured and unruptured cerebral aneurysms. *Stroke*, 30:1396–1401, 1999.

[72] M. R. Crompton. Mechanics of growth and rupture in cerebral berry aneurysms. *British Medical Journal*, 1:1138–1142, 1966.

[73] W. E. Stehbens. Etiology of intracranial berry aneurysms. *J. Neurosurger.*, 70:823 –831, 1989.

[74] W. I. Schievink. Genetics and aneurysm formation. *Neurosurgery Clinics of North America*, 9(3):485–495, July 1998.

[75] N. Hashimoto, H. Handa, and F. Hazama. Experimentally induced cerebral aneurysms in rats. *Surg. Neurol.*, 10:3–99, 1987.

[76] L. Miskolczi, L. R. Guterman, J. D. Flaherty, and L. N. Hopkins. Saccular aneurysm induction by elastase digestion of the artery wall: A new animal model. *Neurosurgery*, 43:595 –601, 1998.

[77] M. R. Roach and A. C. Burton. The reason for the shape of the distensibility curves of arteries. *Can. J. Biochem. Physiol.*, 35:681 –690, 1957.

[78] Z. J. Samila and S. A. Carter. The effect of age on the unfolding of elastin lamellae and collagen fibers with stretch in human carotid arteries. *Can. J. Physiol. Pharmacol.*, 59:1050–1057, 1981.

[79] S. Scott, G. Ferguson, and M. R. Roach. Comparison of the elastic properties of human intracranial arteries and aneurysms. *Canadian Journal of Physiology and Pharmacology*, 50:328 –332, 1972.

[80] G. A. Holzapfel, T. C. Gasser, and R. W. Ogden. A new constitutive framework for arterial wall mechanics and a comparative study of material models. *Journal of Elasticity*, 61:1–48, 2000.

[81] S. Nagasawa, H. Handa, A. Okumura, Y. Naruo, K. Moritake, and K. Hayashi. Mechanical properties of human cerebral arteries. Part 1: Effects of age and vascular smooth muscle activation. *Surg. Neurol.*, 12:297–304, 1979.

[82] K. Hayashi, S. Nagasawa, Y. Naruo, A. Okumura, K. Moritako, and H. Handa. Mechanical properties of human cerebral arteries. *Biorheology*, 17:211–218, 1980.

[83] M. Töth, G.L. Nádasy, I. Nyáry, T. Kerényi, and E. Monos. Are there systemic changes in the arterial biomechanics of intracranial aneurysm patients. *Eur.J. Physiol.*, 439:573–578, 2000.

[84] A. G. Hudetz, G. Mark, A. G. B. Kovach, T. Kerenyi, L. Fody, and E. Monos. Biomechanical properties of normal and fibrosclerotic human cerebral arteries. *Atherosclerosis*, 39:353–365, 1981.

[85] K. Hayashi. Experimental approaches on measuring the mechanical properties and constitutive laws of arterial walls. *ASME J. Biomechanical Engineering*, 115:481–488, 1980.

[86] W. C. P. M. Blondel, J. Didelon, G. Maurice, J-P. Carteaux, X. Wang, and J-F. Stoltz. Investigation of 3-d mechanical properties of blood vessels using a new *in vitro* tests systems: Results on sheep common carotid arteries. *IEEE Transactions on Biomedical Eng.*, 48(4):442–451, 2001.

[87] Y. C. Fung. Elasticity of soft tissue in simple elongation. *Am. J. Physiology*, 213:1532–1544, 1967.

[88] H. Demiray and R. P. Vito. A layered cylindrical shell model for an aorta. *Int. J. Engineering Science*, 29:47–54, 1991.

[89] R. N. Vaishnav, J. T. Young, J. S. Janicki, and D. J. Patel. Nonlinear anisotropic elastic properties of the canine aorta. *Biophysical Journal*, 12:1008–1027, 1972.

[90] K. Takamizawa and K. Hayashi. Strain energy density function and uniform strain hypothesis for arterial mechanics. *J Biomechanics*, 20(1):7–17, 1987.

[91] P. B. Canham and G. G. Ferguson. A mathematical model for the mechanics of saccular aneurysms. *J. Neurosurger.*, 17:291 –295, 1985.

[92] S. K. Kyriacou and J. D. Humphrey. Influence of size, shape and properties on the mechanics of axisymmetric saccular aneurysms. *J. Biomechanics*, 29:1015–1022, 1996.

[93] G. J. Hademenos, T. Massoud, D. Valentino, G. Duckwiler, and F. Vinuela. A nonlinear mathematical model for the development and rupture of intracranial saccular aneurysms. *Neurol. Res.*, 16:376–384, 1994.

[94] A.D. Shah and J.D. Humphrey. Finite strain elastodynamics of intracranial saccular aneurysms. *J. Biomechanics*, 32:593–599, 1999.

[95] E. J. Hung and M. R. Botwin. Mechanics of rupture of cerebral saccular aneurysms. *J. Biomechanics*, 8:385–392, 1975.

[96] K. Perkold, R. Peter, and M. Resch. Pulsatile non-newtonian blood flow simulation through a bifurcation with an aneurysm. *Biorheology*, 26:1011–1030, 1989.

[97] C. F. Gonzalez, Y.I. Cho, H. V. Ortega, and J. Moret. Intracranial aneurysms: Flow analysis and their origin and progression. *AJNR*, 13:181–188, 1992.

[98] M. Low, K. Perktold, and R. Raunig. Hemodynamics in rigid and distensible saccular aneursyms: A numerical study of pulsatile flow characteristics. *Biorheology*, 30:287 –298, 1993.

[99] K. Perkold. On the paths of fluid particles in an axisymmetrical aneurysm. *J. Biomechanics*, 20:311–317, 1987.

[100] S.M. Chitanvis, G. Hademenos, and W.J. Powers. Hemodynamic assessment of the development and rupture of intracranial aneurysms using computational simulations. *Neurological Research*, 17:426–434, 1995.

[101] J. D. Humphrey and F. C. P. Yin. A new constitutive formulation for characterizing the mechanical behavior of soft tissues. *Biophysical Journal*, 52:563–570, 1987.

[102] A.V. Tobolsky, I.B. Prettyman, and J.J. Dillon. Stress relaxation of natural and synthetic rubber stocks. *Journal of Applied Physics*, 15:380–395, 1944.

[103] A. S. Wineman and K. R. Rajagopal. On a constitutive theory for materials undergoing microstructural changes. *Arch. Mech.*, 42:53–75, 1990.

[104] K. R. Rajagopal and A. S. Wineman. A constitutive equation for nonlinear solids which undergo deformation induced microstructural changes. *International Journal of Plasticity*, 8:385–395, 1992.

[105] A. S. Wineman and H. E. Huntley. Numerical simulation of the effect of damaged induced softening on the inflation of a circular rubber membrane. *Int. J. Solids Structures*, 31:3295–3313, 1994.

[106] H. E. Huntley, A. S. Wineman, and K. R. Rajagopal. Chemorheologial relaxation, residual stress, and permanent set arising in radial deformation of elastomeric hollow spheres. *Mathematic and Mechanics of Solids*, 1:267–299, 1996.

[107] I. Lapczyk, K. R. Rajagopal, and A. R. Srinivasa. Deformation twinning during impact - numerical calculations using a constitutive theory based on multiple natural configurations. *Computational Mechanics*, 21:20–27, 1998.

[108] G. A. Johnson, K. R. Rajagopal, and S. L. Y Woo. A single integral finite strain (SIFS) model of ligaments and tendons. *Advances in Bioengineering*, 6:11 –23, 1992.

[109] G. A. Johnson, G. A. Livesay, S. L-Y Woo, and K. R. Rajagopal. A single integral finite strain viscoelastic model of ligaments and tendons. *ASME J. Biomechanical Engineering*, 118:221–226, 1996.

[110] K. R. Rajagopal and A. R. Srinivasa. On the thermomechanics of shape memory wires. *Z. angew. Math. Phys.*, 50:459–496, 1999.

[111] K. R. Rajagopal and A. R. Srinivasa. A thermodynamic frame work for rate type fluid models. *J. Non-Newtonian Fluid Mechanics*, 88:207–227, 2000.

[112] K. R. Rajagopal and A. R. Srinivasa. Modeling anisotropic fluids within the framework of bodies with multiple natural configurations. *J. Non-Newtonian Fluid Mechanics*, 99:109–124, 2001.

[113] C. K. Zarins and S. Glagov. *Aneurysms New Findings and Treatments*, chapter Atherosclerotic Process and Aneurysm Formation, pages 35–45. Appleton & Lange, 1994.

[114] Christopher K. Zarins, Arthur Runyon-Haas, Michale A. Zatina, Chien-Tai Lu, and Seymour Glagov. Increased collagenase activity in early aneurysimal dilatation. *J. Vasc. Surg.*, 3:238–248, 1986.

[115] D. Tilson and K. M. Newman. *Aneurysms New Findings and Treatments*, chapter Proteolytic Mechanisms in the Pathogenesis of Aortic Aneurysms, pages 3–10. Appleton & Lange, 1994.

[116] M. L. Raghavan, M. W. Webster, and D. A. Vorp. Ex vivo biomechanical behavior of abdominal aortic aneurysm: assesment using a new mathematical model. *Annal. Biomedical Engineering*, 24:573 –582, 1996.

[117] M. L. Raghavan and D. A. Vorp. Toward a biomechanical tool to evaluate rupture potential of abdominal aortic aneurysm: Identification of a finite strain constitutive model and evaluation of its applicability. *J. Biomechanics*, 33:475–482, 2000.

[118] D. H. J. Wang, M. Makaroun, M. W. Webster, and D. A. Vorp. Mechanical properties and microstructure of intraluminal thrombus from abdominal aortic aneurysm. *J. Biomechanical Engineering*, 123:536–539, 2001.

[119] Y. Lanir. A structural theory for the homogeneous biaxial stress-strain relationship in flat collageneous tissues. *J. Biomechanics*, 12:423–436, 1979.

[120] K. L. Billiar and M. S. Sacks. A method to quantify the fiber kinematics of planar tissues under biaxial stretch. *J. Biomechanics*, 30:753 –756, 1997.

[121] M. S. Sacks. Incorporation of experimentally-derived fiber orientation into a structural constitutive model for planar collagenous tissues. *Journal of Biomechanical Engineering*, 125:280–287, 2003.

[122] M. S. Sacks, David B. Smith, and Erik D. Hiester. A small angle light scattering device for plannar connective tissue microstructural analysis. *Annals of Biomedical Engineering*, 25:678–689, 1997.

[123] S. C. Ling and C. H. Chow. The mechanics of corrugated collagen fibrils in arteries. *J. Biomechanics*, 10:71–77, 1977.

[124] M. K. Kwan and Savio L-Y Woo. A structural model to describe the nonlinear stress-strain behavior for parallel-fibered collagenous tissues. *ASME J. Biomechanical Engineering*, 111:361–363, 1989.

[125] H. Demiray and R. P. Vito. Large deformation analysis of soft biomaterials. *Int. J. Engrng. Sci.*, 14:789–793, 1976.

[126] A. Delfino, N. Stergiopulos, J. E. Moore Jr., and J. J. Meister. Residual strain effects on the stress field in a thick wall finite element model of the human carotid bifurcation. *J. Biomechanics*, 30:777–786, 1997.

[127] Millard F. Beatty. Topics in finite elasticity: Hyperelasticity of rubber, elastomers, and biological tissues-with examples. *Appl. Mech. Rev.*, 40:1699–1734, 1987.

[128] D.C. Leigh. *Nonlinear Continuum Mechanics*, chapter Principles for Constitutive Equations, pages 139–149. McGraw Hill Book Company, 1968.

[129] A.C. Eringen. *Mechanics of Continua*, chapter Constitutive Equations, pages 142–185. John Wiley & Sons, Inc., 1967.

[130] G.A. Holzapfel. *Nonlinear Solid Mechanics - A Continuum Approach for Engineering*, chapter Some Aspects of Objectivity, pages 179–204. John Wiley & Sons, Ltd., 2000.

[131] C. Truesdell and W. Noll. *The Non-Linear Field Theories of Mechanics*, chapter Kinematics, pages 48–56. Springer-Verlag, 1992.

[132] L. E. Malvern. *Introduction to the Mechanics of a Continuous Medium*, chapter Constitutive Equations, pages 273–422. Prentice-Hall, Inc., 1969.

[133] G.P. Galdi. Theory of continuous media. Class Notes, 1998.

[134] R. S. Rivlin and D.W. Saunders. Large elastic deformations of isotropic materials :VII. experiments on the deformation of rubber. *Phil. Trans. A.*, 243:251–288, 1951.

[135] D.C. Leigh. *Nonlinear Continuum Mechanics*, chapter Elasticity, pages 174–188. McGraw Hill Book Company, 1968.

[136] L. R. G. Treloar. Strains in an inflated rubber sheet, and the mechanism of bursting. *Inst. Rubber Ind. Trans.*, 19:201–212, 1944.

[137] A. C. Pipkin. Integration of an equation in membrane theory. *J of Applied Mathematics and Physics (ZAMP)*, 19:818–819, 1968.

[138] A. J. M. Spencer. The static theory of finite elasticity. *J. Inst. maths. Applics.*, 6:164–200, 1970.

[139] J. E. Adkins and R. S. Rivlin. Large elastic deformations of isotropic materials : IX. The deformation of thin shells. *Phil. Trans. A.*, 244:505–531, 1952.

[140] A.E. Green and J.E. Adkins. *Large Elastic Deformations.* Oxford University Press, Oxford, 1960.

[141] J. T. Nichol. The effect of cholesterol feeding on the distensibility of the isolated thoracic aorta of the rabbit. *Canadian Journal of Biochemistry and Physiology*, 33(4):507–516, 1955.

[142] C. J. Chuong and Y. C. Fung. Compressibility and constitutive equation of the arterial wall in radial compression experiments. *J. Biomech.*, 17:35 –40, 1984.

[143] T. E. Carew, R. N. Vaishnav, and D. J. Patel. Compressibilty of the arterial wall. *Circulation Research*, 23:61–68, July 1968.

[144] Y. C. Fung, K. Fronek, and P. Patitucci. Pseudoelasticity of arteries and the choice of its mathematical expression. *Am. J. Physiol.*, 237:H620–H631, 1979.

[145] J. D. Humphrey and F. C. P. Yin. Biomechanical experiments on excised myocardium: Theoretical considerations. *J. Biomechanics*, 22:377–383, 1989.

[146] A. M. Brown. A step-by-step guide to nonlinear regression analysis of experimental data using a microsoft excel spreadsheet. *Computer Methods and Programs in Biomedicine*, 65:191–200, 2001.

[147] S. Nagasawa, H. Handa, Y. Naruo, K. Moritake, and K. Hayashi. Experimental cerebral vasospasm arterial wall mechanics and connective tissue composition. *Stroke*, 13(5):595–600, 1982.

[148] M.M. Carroll. Pressure maximum behavior in inflation of incompressible elastic hollow spheres and cylinders. *Quarterly of Applied Mathematics*, 45(1):141–154, 1987.

[149] D. A. Cope and M. R. Roach. A scanning electron microscope study of human cerebral arteries. *Can. J. Physiol. Pharmacol.*, 53:651–659, 1975.

[150] H. Wolinsky and S. Glagov. Structural basis for the static mechanical properties of the aortic media. *Circulation Research*, 14:400–413, 1964.

[151] A.J.M. Spencer. *Continuum Mechanics*, chapter Cylindrical and Spherical Polar Coordinates, pages 153–169. Longman Scientific and Technical, 1980.

[152] L.J.Hart-Smith and J.D.C.Crisp. Large elastic deformation of thin rubber membranes. *Int.J.Engrng.Science*, 5:1–24, 1967.

[153] G. N. Foutrakis, H. Yonas, and R. J. Sclabassi. Finite element methods in the simulation and analysis of intracranial blood flow. *Neurological Research*, 174-186, 1997.

[154] A. S. Wineman, D. Wilson, and J. W. Melvin. Material identification of soft tissue using membrane inflation. *J. Biomechanics*, 12:841–850, 1979.

[155] F. P. K. Hsu, C. Schwab, D. Rigamonti, and J. G. Humphrey. Identification of response funtions from axisymmetric membrane inflation tests : Implications for biomechanics. *Int.J.Solids Structures*, 31 No.24:3375–3386, 1994.

[156] M.B. Rubin. *Cosserat Theories: Shells, Rods and Points*, chapter Cosserat Shells, pages 73–190. Kluwer Academic Publishers, 2000.

[157] H. Wolinsky and S. Glagov. A lamellar unit of aortic medial structure and function in mammals. *Circulation Research*, 20:99–111, 1967.

[158] D.J. Patel and R. N. Vaishnav. *Cardiovascular Fluid Mechanics*, volume 2, chapter The Rheology of Large Blood Vessels, pages 1–64. Academic Press, 1972.

[159] D.J. Patel and R.N. Vaishnav. *Basic Hemodynamics and Its Role in Disease Processes*, chapter General Mechanical Properties of the Vascular Wall, pages 155–197. University Park Press, 1980.

[160] D. A. Vorp, K. R. Rajagopal, P. J. Smolinski, and H. S. Borovetz. Identification of elastic properties of homogeneous, orthotropic vascular segments in distension. *J. Biomechanics*, 28:501–512, 1995.

[161] M. Töth, G. L. Nádasy, I. Nyáry, T. Kerényi, M. Orosz, G. Molnárka, and E. Monos. Sterically inhomogeneous viscoelastic behavior of human saccular cerebral aneurysms. *Vascular Research*, 35:345–355, 1998.

[162] C. F. Gerald and P. O. Wheatley. *Applied Numerical Analysis*, chapter Numerical Solution of Ordinary Differential Equations, pages 393–466. Addison-Wesley Publishing Company, 1994.

[163] C. F. Gerald and P. O. Wheatley. *Applied Numerical Analysis*, chapter Solving Nonlinear Equations, pages 29–101. Addison-Wesley Publishing Company, 1994.